Planar Cell Polarity genes *prkl-1* and *dsh-1* polarize *C. elegans* motorneurons during organogenesis.

by

Leticia Sánchez-Alvarez

A thesis submitted to the Faculty of Graduate and Postdoctoral Studies

In partial fulfillment of the requirements for the Degree of

Doctor of Philosophy

Neuroscience Program

Department of Cellular and Molecular Medicine

Faculty of Medicine

University of Ottawa

ABSTRACT

The correct polarity of a neuron underlies its ability to integrate precise circuitries in the nervous system. The goal of my thesis was to investigate the pathways that establish and maintain neuron polarity/orientation *in vivo*. To accomplish this, I used bipolar VC4/5 motor neurons, which innervate the *C. elegans* egg-laying musculature, as a model system. Vulval proximal VC4/5 neurons extend axons in the left-right (LR) orientation, around the vulva; whereas vulval distal VC1-3,6 neurons extend axons along the anterior-posterior (AP) axis. A previous study showed that *vang-1*, a core planar cell polarity (PCP) gene, suppresses AP axon growth in VC4/5 neurons. In order to identify new components of this pathway we performed genetic screens for mutants with abnormal VC4/5 polarity/morphology. We isolated and mapped alleles of *farnesyl transferase β (fntb-1)* and of core PCP genes, *prickle-1* (*prkl-1*) and *dishevelled-1* (*dsh-1)*; all of which display tripolar VC4/5 neurons, similar to *vang-1 lof*. In *prkl-1* and *dsh-1* mutants, primary LR and ectopic AP VC4/5 axons are born simultaneously, suggesting an early role in establishing polarity. In addition, *prkl-1* and *dsh-1* act persistently to maintain neuron morphology/orientation. Genetic analysis of double mutants suggests that *prkl-1* interacts with *vang-1* in a common PCP pathway to prevent AP axon growth, while *dsh-1* also acts in a parallel pathway. Furthermore, *prkl-1* functions cell autonomously in neurons, whereas *dsh-1* acts both cell autonomously and cell non-autonomously in epithelial cells. Notably, *prkl-1* overexpression results in unipolar VC4/5 neurons, in a dose-dependent manner. In contrast, *dsh-1* overexpression in VC4/5 neurons results in a *lof* phenotype, similar to *vang-1 lof* and overexpression phenotype. Remarkably, *prkl-1* overexpression restores normal VC4/5 polarity in *dsh-1* and *vang-1* mutants, which is suggestive of a downstream role for *prkl-1*. Both PRKL-1 and DSH-1 are expressed in

uniformly distributed puncta at the plasma membrane of VC4/5, similar to VANG-1; suggesting that their asymmetric distribution is not critical for neuron polarity. Furthermore, we found that the vulva epithelium induces *prkl-1* expression in VC4/5; indicating a functional relationship between the egg-laying organ and neuron morphology. Moreover, a structure-function analysis of PRKL-1 revealed that the conserved PET domain and the C-terminal region are crucial to prevent AP axon growth, whereas the three LIM domains are dispensable for this role. In addition, we showed that *dsh-1* also regulates the morphology of AP-oriented PDE neurons. *dsh-1* promotes the formation of PDE posterior axons, contrary to its function in VC5 neurons; which indicates a context-dependent role for *dsh-1* in neuronal polarity. Altogether, this thesis implicates the PCP signalling pathway in a previously unknown role, in establishing and maintaining neuronal polarity, by controlling AP axon growth in response to organ-derived polarizing cues.

ACKNOWLEDGMENTS

This work was made possible by the contributions of many people who have helped me over the past many years:

I thank my supervisor Dr. Colavita, for allowing me to work in his laboratory in a fruitful project, and for offering suggestions to improve this dissertation.

I thank my advisory committee members Dr. Paul Albert, Dr. David S. Park and Dr. Hsiao Huei Chen, because their questions, suggestions and guidance helped shape this work.

I would like to express my gratitude to my lab mates, especially Janice Imai, Anna Su, Jiravat Visanuvimol, Carlos Edigio de Cavalho, Andrea McEwan and Nasrin Habibi for helpful discussions and assistance, and for their unbridled optimism and enjoyable company.

Also, I am very appreciative of the cooperative atmosphere at the Neuroscience Research Institute and of their people. Specially, I would like to thank members of Dr. Schlossmaher's lab, Dr. Albert's lab and Dr. Park's lab for their assistance with reagents, protocols, equipments and ideas. I also thank Dr. Charlie Thompson for my education on confocal microscopy.

I am indebted to Dr. Paul Albert, Dr Antoine Hakim and Dr Michael Schlossmaher for helping me navigate smoothly during the final stages of my PhD.

I thank NSERC, University of Ottawa and CIHR for funding my project, my attendance to conferences, or my living over the course of my studies.

I am also grateful for Paul Andre David's, Sylvie Deblois' and Nicole Trudel's secretarial support.

I thank my friends for their encouragement and help, especially Yasmilde. I also thank great teachers during my schooling in Cuba, Dr. Joaquin Diaz and Dr. Dámaris Fernandez, for what I learned from them it is still with me.

Most importantly, I express a heartfelt gratitude to my family: my parents Aurora and José, my husband Jean-Philippe and my precious little Sofia, for their love, constant encouragement, and immeasurable support over the years. To my family, I dedicate this work.

Here, I can not mention all, but I do value everyone that has assisted me in this pursue. Without all the help my dissertation would not be the same.

THESIS FORMAT

This Ph.D. thesis was written in accordance with the Guidelines for Thesis preparation from the Faculty of Graduate and Postdoctoral Studies of the University of Ottawa. I have written this thesis as a collection of three manuscripts. The three result chapters are preceded by a general literature review on neuronal polarity, and followed by a general discussion on the mayor findings of my work. This thesis has the following format:

CHAPTER I. General Introduction

CHAPTER II. Genetic screening and analysis of polarity mutants reveal a novel role for *fntb-1* and PCP genes *prkl-1* and *dsh-1* in suppressing AP ectopic axon outgrowth.

CHAPTER III. *prkl-1* regulates orientation and number of axons in *C. elegans* motorneurons during organogenesis.

CHAPTER IV. *C. elegans dsh-1* is required cell autonomously and cell non-autonomously to regulate neuron polarity.

CHAPTER V. General Discussion.

Each of the result chapters contains its own summary, introduction, materials and methods, results, and conclusions. Additionally, each chapter starts with a preface, a connecting text to logically bridge the manuscripts. References for chapters I to V can be found immediately after chapter V.

Some data from this thesis have been published as a co-first authorship publication with a fellow PhD student (Jiravat Visanuvimol) and summer student (Andrea McEwan). I have made explicit statement of who has contributed work to this thesis and to what extend in the section Contributions of Authors.

CONTRIBUTIONS OF AUTHORS

The candidate designed and performed the majority of the research described in this thesis, with supervision from Dr. Colavita. The contribution of other authors to this thesis is as follows:

In Chapter II, Lab technician Janice Imai provided technical assistance with EMS treatment of parental worms for both the forward and non-complementation screens described. She also performed an independent large-scale forward genetic screen from which she isolated the following mutants: *dsh-1(zy12)*, *vang-1(zy10)*, *prkl-1(zy17, zy18)*, *fntb-1(zy20, zy21, zy23, zy24)* which are listed in Table II-4. The candidate collaborated with Janice Imai to outcross and group all the lab's neuronal polarity mutants into non-complementation groups; results of which are presented in Table II-4. In addition, Janice identified the mutation in *vang-1(zy10)*. Lab technician Anna Su sequenced mutants: *fntb-1(zy21, zy23 and zy24)*. The candidate collaborated with fellow graduate student Jiravat Visanuvimol to collect data presented in Table II-5. Anna Su generated *gfp*-tagged genomic *prkl-1* and *dsh-1* constructs. **In chapter III**, summer student Andrea McEwan quantified VC4/5 morphology in wt and *prkl-1(zy11)* at L3 stage and took the images presented in Figure III-7B. Anna Su provided technical assistance to make *prkl-1* sense and antisense heat shock constructs. Jiravat quantified polarity defects in *vang-1(tm1422)* mutant, presented as a control datum in Figure III-11 and took pictures for Figure III-5C. **In chapter IV**, Andrea McEwan quantified VC4/5 morphology in wt and *dsh-1(ok1445)* at L3 stage and took the images for Figure IV-2B.

ORIGINAL CONTRIBUTIONS TO KNOWLEDGE

- Highly conserved farnesyl transferase β subunit (FNTB-1) suppresses AP ectopic axon growth in VC4 and VC5 motorneurons.
- Phylogenetically conserved, planar cell polarity (PCP) genes, *prickle-1* and *dishevelled-1* interact with *vang-1* in a PCP-like signalling pathway to regulate neuron morphology/polarity, by suppressing AP axon growth.
- Double mutant combinations *dsh-1;prkl-1* and *dsh-1;vang-1* result in a 90^{o} rotation in VC4/5 neurons orientation from left-right to AP, recapitulating the AP bipolar morphology in vulvaless mutants.
- PRKL-1 and DSH-1 are required throughout neuron development, to establish and to maintain neuron polarity by preventing AP axon growth.
- PRKL-1 functions cell autonomously in VC4 and VC5 motorneurons to regulate neuron morphology/polarity.
- *prkl-1 lof* results in tripolar VC4/5 neurons, while overexpression results in a *gof* phenotype, unipolar neurons; suggesting that *prkl-1* regulates both the number and orientation of neurites.
- PRKL-1 is expressed in VC4/5 and the vulva epithelia. Subcellularly in VC4/5, PRKL-1 is located in a punctuate pattern at the plasma membrane and smoothly in the nucleus.
- PRKL-1 expression in VC4/5 neurons is induced by the vulva epithelia.

- Ectopic expression of PRKL-1 in PDE neurons results in lack of or premature termination of anterior axons, suggesting that PRKL-1 plays an instructive role in preventing AP axon growth.

- PRKL-1 overexpression restores normal VC4/5 neuron morphology in *vang-1* and *dsh-1* mutants, suggesting that *prkl-1* overexpression circumvents the need for functional *vang-1* and *dsh-1* alleles, and that it is sufficient to regulate VC4/5 neuron polarity.

- The PET-domain-containing long PRKL-1 isoform is both necessary and sufficient to prevent AP axon growth, while the short PET-less isoform appears dispensable for this role.

- PRKL-1 C-terminal domain is critical, while the LIM domains are not required to prevent AP axon growth.

- DSH-1 is broadly expressed in *C. elegans* nervous system including the VNC, and in the vulva epithelia and muscles. Subcellularly in the VCs, DSH-1 is localized in symmetrically distributed puncta at the plasma membrane; it is also expressed smoothly in the cytosol while excluded from the nucleus.

- DSH-1 functions cell autonomously in the neurons and cell non-autonomously in the epithelia to prevent AP axon growth.

- DSH-1 overexpression in the VC4/5 neurons results in tripolar morphology, similar to *lof* phenotype, suggesting a permissive role in regulating neuron polarity.

- Both, *dsh-1 lof* and *dsh-1* overexpression in PDE neurons results in lack of or premature termination of posterior axons, suggesting a role for *dsh-1* in promoting

posterior axon outgrowth and/or extension to its defined destination. DSH-1 role in PDEs morphology is opposed to its role in VC4/5 neurons, suggesting that its function in neuron polarity is context-dependent.

LIST OF ABBREVIATIONS

AGE-1	age alteration, *C. elegans* ortholog of PI3K
AMP	adenosine Monophosphate
AMPK	AMP-activated protein kinase
AP	anterior-posterior orientation
aPKC	atypical protein kinase C
ATP	adenosine triphosphate
AVG	unipolar interneuron with cell body in the retrovesicular ganglion
AVM	anterior ventral microtubule cell, unipolar mechanosensory neuron
AWC	olfactory neuron
BDNF	brain-derived neurotrophic factor
BED	zinc finger, named after the *Drosophila* proteins BEAF and DREF
BiFC	bimolecular fluorescence complementation
CAM	Ror receptor tyrosine kinase
CamKII	Ca^{2+}-calmodulin-dependent protein kinase II
cAMP	cyclic AMP
CAT	abnormal catecholamine distribution
CAT-1	synaptic vesicular monoamine transporter required for the presence of dopamine and serotonin in nerve terminals
CB4856	Hawaiian *C.elegans* strain
CDC42	cell division cycle 42, Rho GTPase
CED-10	GTPase orthologous to human RAC1
CFZ	one of four *C. elegans* frizzled homologs
cGMP	cyclic GMP
COL-10	collagen protein, expressed exclusively in hypodermal cells
CRMP-2	collapsing response mediator protein 2
DAF-18	*C. elegans* ortholog of PTEN
DAAM1	dishevelled associated activator of morphogenesis 1. A formin protein
DEP	acronym for dishevelled, egl-10, pleckstrin, DSH/DVL conserved motif
Df	deficiency
DIC	differential interference contrast
DIX	for *disheveled* and Axin, DSH/DVL conserved motif
DNA	deoxyribonucleic acid
DNC	dorsal nerve cord
DPY	dumpy
DPY-20	BED zinc finger protein, no homologs in other species
DS	dashous
DSH/DVL	dishevelled
dsRNAi	double stranded ribonucleic acid interference
DTC	distal tip cell

DV	dorsal-ventral orientation
EGL	egg laying defective
EGL-20	Member of the WNT family
ELISA	enzyme-linked immunosorbent assay
EMS	ethyl methanesulfonate
ERK	extracellular signal-regulated kinase
FHL2	four and a half LIM domains protein 2
FJ	four-jointed, a Golgi associated-kinase
FMI	flamingo
FNTB	farnesyltransferase, beta subunit
FT	fat
FZ	frizzled
GABA	γ–Aminobutyric acid
GEF	guanosine nucleotide exchange factors
Gene CATCHR	method of generating reporter constructs that exploits YHR
GF-URA3-FP	targetted tag for gene CATCHR
GSK-3β	glycogen synthase 3β
GTP	guanosine-5'-triphosphate
GTPase	enzyme that binds and hydrolyze GTP
HIM	high incidence of males
HSN	hermafrodite specific neuron
IDAX	inhibitor of Dishevelled and Axin
KAR-1	mutant yeast with defects in a gene required for normal karyogamy (nuclear fusion) during mating
LAR	leukocyte antigen-related protein tyrosine phosphatase, regulator of insulin receptor signalling
LEF	lymphoid-enhancer factor
LG	linkage group
LGL	lethal giant larvae
LIM	acronym for Lin-11, Isl-1, Mec-3; a cysteine-histidine rich zinc-coordinating domain
LIN	lineage defective
LIN-17	one of four *C. elegans* frizzled homologs
LIN-18	member of the Ryk/Derailed family of tyrosine kinase-related receptors
LKB-1	acronym for liver kinase B1, master T/S kinase inactivated in Peutz-Jeghers Syndrome
LR	left-right orientation
MAP	microtubule associated protein
MAPK	MAP kinase
MAQgene	sotware tool to analyze *C. elegans* whole genome sequencing
MARK	mitogen-activated protein kinase
MF	microfilaments

MIG	migration defective
MIG-1	one of four *C. elegans* frizzled homologs
MIG-10	*C. elegans* orthologous of lamellipodin
MINK	Misshapen Nck-interacting ser/thr kinase
ML	medial – lateral orientation
MO25	protein cofactor, with S/T kinase activator activity,
MOM-5	one of four *C. elegans* frizzled homologs
MT	microtubule
MYO	myosin
N2	English *C. elegans* strain
ORF	open reading frame
PAR	partitioning defective
PAR-1	MARK-2 homolog
PAR-2	RING finger-containing protein, which acts in the uniquitination pathway
PAR-3	PDZ –containing protein scaffold
PAR-4	LKB-1 homolog
PAR-5	14-3-3, chaperone which binds phosphorylated S/T on polarity proteins
PAR-6	PDZ –containing protein scaffold
PCR	polymerase chain reaction
PDE4	cAMP-specific phosphodiesterase
PDK1	phosphoinositide-dependent kinase-1
PDZ	acronym for synaptic density protein (PSD95), *Drosophila* disc large tumor suppressor (Dlg1), and zonula occludens-1 protein (zo-1)
PET	conserved domain found in PRICKLE, ESPINAS, TESTIN proteins
PH	pleckstrin homology domain
PI3K	phosphoinositide 3-kinase
PIP2	phosphatidylinositol-3,4-phosphate
PIP3	phosphatidylinositol-3,4,5-phosphate
PLM	posterior lateral microtubule cell, mechanosensory neuron
PNS	peripheral nervous system
PKC	protein kinase C
PRKL	prickle protein
PTEN	phosphatase and tensin homologue
PVM	posterior ventral microtubule cell, mechanosensory neuron
PVP	posterior lateral microtubule cell, mechanosensory neuron
PVQ	interneuron, PVQL pioneers the left hand ventral cord
RAC-1	ras-related C3 botulinum toxin substrate 1, GTPase
ROL-6	roller mutant, gene encoding a cuticle collagen
RYK/DERAILED	receptor tyrosine kinase which acts as co-receptor with Frizzled for Wnt signalling
SAD	synapses of the amphid defective kinase
SLT-1	the sole C. elegans homolog of *Drosophila* Split, ligand to Sax-3/Robo

	receptor
snipSNP	restriction-fragment length SNP
SNP	single nucleotide polymorphism
SPLE	*Drosophila* PRICKLE - spiny legs isoform
STEF	acronym for SIF and Tiam 1-like GEF
STRAD	cofactor, STE20-like pseudokinase
SYD-2	Member of liprin family of proteins, LAR interacting proteins
TAG-15	a.k.a lim-9, *C. elegans* homolog to *Drosophila* LIMPET and vertebrate FHL2
TAG-224	a.ka. tes-1, *C. elegans* homolog to *Drosophila* CG6522-PA and of human LMCD1 and TESTIN
TCF	T-cell transcription factor
TES-1	tumor suppressor testin, protein found in focal adhesions and thought to play a role in cell motility
TGD	terminal differentiation genes
TMB	3,3′,5,5′-Tetramethylbenzidine, substrate to horseradish peroxydase
TrkB	tyrosine kinase receptor, a.k.a BDNF/NT-3 growth factors receptor or neurotrophic tyrosine kinase, receptor, type 2
UNC	uncoordinated
UNC-4	homeodomain protein required for the identity of A class motorneurons
UNC-6	*C. elegans* homolog of Netrin
UNC-34	the sole C. elegans Enabled/VASP homolog
UNC-40	*C. elegans* homolog of DCC (Deleted in Colorectal Cancer)
UNC-73	Protein with DH and PH domains, with potential GEF activity, which may activate Rho GTPases.
UNC-104	neuron-specific monomeric motor, member of kinesin 3 family.
UTR	untranslated region
VA	VNC motorneuron
VAB-8	variable abnormal morphology, kinesin related protein, upstream regulator of UNC-40
VANG	Van Gogh/strabismus planar polarity protein homolog
VC	hermaphrodite specific ventral cord motor neurons
VNC	ventral nerve cord
VPC	vulval precursor cells
WGS	whole genome sequencing
WNT	wingless, ligand to frizzled receptor
YAC	yeast artificial chromosome
YHR	yeast homologous recombination

TABLE OF CONTENTS

LIST OF FIGURES

LIST OF TABLES

CHAPTER I - GENERAL INTRODUCTION

Understanding how nerve cells reach and maintain their morphology is an important step towards formulating effective therapies for human neurological diseases and for acute brain and spinal cord injury. This thesis is a modest attempt at answering a fundamental question in Neuroscience, how do neurons polarize?

1.1 Neuron Polarity, Neuron Morphology, Neuron Orientation.

1.1.1 Overview on neuron polarity.

Virtually every living cell exhibits polarity (Nelson, 2003). The term polarity in cell biology refers to the **asymmetric** distribution of regulatory molecules and structural components between opposite poles of a cell, with the concomitant formation of morphologically and physiologically distinct compartments (Bradke and Dotti, 2000;Li and Gundersen, 2008). The acquisition of different cellular morphologies is critical to development of specialized functions. For example, epithelial cells polarize into apical and basolateral domains, providing barriers between different milieus, to regulate ionic homeostasis and the transport of selected molecules (van der Wouden et al., 2003); and migrating cells polarize into front and rear domains, each with distinctive signalling networks that orient the migrating cell toward attractive cues (Manes et al., 1999).

Similarly, neurons are highly polarized cells. They extend two distinct subcellular compartments, axons with presynaptic terminals and dendrites with postsynaptic densities; which are essential to receive, process and transmit information to target destinations (Arimura and Kaibuchi, 2005). The correct polarization of a neuron underlies its ability to

integrate precise circuitries in the nervous system. Importantly, neuronal circuitries are progressively formed during development and persistently maintained throughout life (Aurelio et al., 2002;Hobert and Bulow, 2003). Consequently, the correct functioning of the nervous system depends on the activity of molecular mechanisms to establish and also to subsequently maintain polarity in individual neurons.

A neuron's morphology/polarity can be described by the type, number, and orientation of processes it projects. While the morphology of a typical vertebrate neuron, meticulously described by Santiago Ramon y Cajal, comprises a single axon and several dendrites arising from the cell body (Andres-Barquin, 2001); invertebrate neurons may extend processes with mixed axonal and dendritic identities (Sanchez-Soriano et al., 2005;Rolls, 2011). Deviations from a neuron's wild type shape and orientation, including: 1) lack of axon (Jiang et al., 2005;Barnes et al., 2007), 2) supernumerary axons (Inagaki et al., 2001;Barnes et al., 2007), 3) supernumerary dendrites (Barnes et al., 2007) or 4) wrong orientation of neurites (Hilliard and Bargmann, 2006; Prasad and Clark, 2006), are all considered neuronal polarity defects. 1 and 2 are also referred to as axon outgrowth defects.

The initial event in establishing neuronal polarity is the specification of a single axon and dendrites (see 1.1.3 and 1.1.4). This is followed by polarized outgrowth and stabilization of axons and dendrites, involving selective trafficking and segregation of molecular and structural components into both compartments via cytoskeleton motors (see 1.1.2). Lastly, the structural and functional polarization is maintained via vesicle sorting, directed transport and selective retention of molecules within axonal and dendritic compartments (Szu-Yu and Rasband, 2011).

The initial polarization of postmitotic neurons may be triggered by 1) a stochastic asymmetric accumulation of cellular determinants (demonstrated *in vitro*, see 1.1.3); by 2) extracellular polarizing signals (demonstrated *in vivo*, see 1.1.4 and 1.1.5); or by 3) intrinsic asymmetry originated during the last mitotic division of the neural progenitor (de Anda et al., 2005).

Overall, the coordinated asymmetric distribution of cellular determinants, including cytoskeleton and associated proteins (see 1.1.2), polarizing complexes (see 1.1.3), signalling molecules (see 1.1.5), and membrane receptors (see 1.1.5) to axonal and dendritic compartments underlies the specification, acquisition and maintenance of neuronal morphology/polarity.

1.1.2 Polarized distribution of cytoskeleton, cytoskeleton-associated proteins, small GTPases and second messengers in axons and dendrites.

The **cytoskeleton** is a dynamic, polar lattice; a protein scaffold upon which the internal organization of every cell is built, which supports essential cellular functions such as division, **polarity**, directed trafficking of molecules and vesicles, cell migration and fusion (Li and Gundersen, 2008). Three kinds of cytoskeleton support neuron structure and function, microfilaments (MFs), neurofilaments (NFs) and microtubules (MTs) (Brady, 1993; Mandell and Banker, 1995). MFs are polymers of globular actin monomers (G-actin) and MTs are polymers of α- and β-tubulin heterodimers; which bind and hydrolyse ATP and GTP, respectively, following head to tail polymerization (Li and Gundersen, 2008). NFs are neuron-specific intermediate filaments made up of protein units containing a central α-helical "rod" domain with conserved secondary structure, and amino- and carboxy-terminal domains

of varying size and physico-chemical properties (Steinert and Roop, 1988). MFs and MTs possess intrinsic structural polarity, with all subunits uniformly aligned in the same direction. Accordingly, the two ends of the polymers differ structurally. Thus, while actin filaments contain a barbed and a pointed end, MTs contain a plus and a minus end (Li and Gundersen, 2008).

Furthermore, actin and MT cytoskeleton not only support the overall cell structure but also underlie dynamic morphological changes within subcellular compartments; such as in the growth cone of emerging axons, a structure that is critical to axon formation, the cytoskeleton promptly reorganizes in response to polarizing cues, thus transforming molecular signals into structural changes that regulate cell morphology. Ultimately, the net growth of the polymers, and consequently a cell's shape depends on signalling that is favourable to polymerization and on the specific concentration of free subunits (Li and Gundersen, 2008). Thus, repeated cycles of growth and retraction, and changes in direction of the growth cone in response to guidance molecules depends on cytoskeleton remodelling; that is, dynamic polymerization and de-polymerization of both actin and MT cytoskeleton (Lin et al., 1994; Tanaka and Sabry, 1995).

In addition, axons and dendrites contain a distinct cytoskeleton including different microtubule polarity patterns. For instance, in vertebrate neurons, microtubules are bundled along the long axis of the cell (*i.e.* soma-axon), in a plus-end-distal arrangement (Baas et al., 1988). However, dendrites contain non-uniformly oriented microtubules, with approximately half plus-end-distal and half minus-end-distal (Kwan et al., 2008;Baas and Lin, 2010). The

uniform orientation of axonal MT forms a unidirectional vector for the polarized transport of components required for axonal growth (Baas and Lin, 2010).

Several classes of **cytoskeleton-associated proteins** influence axon/dendrite specification, including microtubule associated proteins (**MAPs**), **motor proteins** and **small GTPases**. MAPs are MT-regulating proteins. There are two classes of **MAPs**, structural MAPs that modulate the stability of the cytoskeleton, and the MAPs that affect the dynamics of the MT cytoskeleton (Tahirovic and Bradke, 2009). Some of the structural MAPs have the ability to interact with actin filaments and MTs, such as MAP1B and MAP2 (Tahirovic and Bradke, 2009), while others are preferentially associated with one type of cytoskeleton. For instance, tau and collapsing response mediator protein 2 (CRMP-2) are associated with axonal MTs (Tahirovic and Bradke, 2009). Also, while most MAPs bind MT polymers directly, CRMP promotes MT polymerization through binding tubulin heterodimers (Fukata et al., 2002). In addition, it has been shown that CRMP overexpression results in multiple axons, while inhibition prevents axon formation in cultured neurons (Inagaki et al., 2001). Finally, certain MAPs are preferentially enriched in axons or dendrites, thus supporting their use as markers. For instance, tau and MAP2 are axonal and dendritic markers, respectively (Li and Gundersen, 2008).

Interestingly, cytoskeletal polymers serve as railways to **motor proteins** for polarized trafficking of cargo molecules and organelles to specific subcellular locations, including the incipient axon or dendrites (Li and Gundersen, 2008). Motor proteins are a family of mechanochemical enzymes that propel themselves with their cargo along the cytoskeleton, by cycling between conformations while using the energy from ATP hydrolysis (Li and

Gundersen, 2008). MFs and MTs use different motors. While, myosin is an actin specific motor, kinesins and dyneins are specific to MTs. The intrinsic polarity of cytoskeletal lattices is critical to the unidirectional movement of motors so that kinesins move towards the MT plus end whereas dyneins, towards the MT minus end (Li and Gundersen, 2008). Since motors can distinguish between the two ends of MT assemblies, they possess the ability to sort organelles and molecules to different compartments inside the cell (Bornens, 2008). Accordingly, distinct motors contribute to building axonal and dendritic compartments, for instance plus end kinesins transport axonal membrane proteins (Hirokawa and Takemura, 2005). Similarly, polarity protein PAR3 (see next section) is transported by a plus-end kinesin (KIF3A) to the growing end of axons, thus continuously keeping its asymmetric distribution during axon extension (Nishimura et al., 2004). In addition, kinesins also transport second messengers such as PIP3 to the emerging axon (Horiguchi et al., 2006).

Another family of proteins functionally linked to the cytoskeleton, **Rho small GTPases**, are major regulators of MFs and MTs that regulate cell polarity and mediate axon/dendrite specification (Yoshimura et al., 2006). Rho GTPases are low molecular weight guanine nucleotide binding proteins including Cdc42, Rac-1 and RhoA. They are molecular switches that cycle between active GTP-bound state to inactive GDP-bound state, by the actions of GTPase activating proteins (GAPs) which promotes hydrolysis of GTP to GDP, and guanine nucleotide exchange factor (GEFs) that promotes exchange of GDP to GTP (Etienne-Manneville and Hall, 2002). Binding of GTP to RhoGTPases induces an allosteric change that allows binding of downstream effectors which subsequently promotes cytoskeleton remodelling (Etienne-Manneville and Hall, 2002). For instance, GTP-bound small GTPase Ras has been shown to be a potent activator of PI3K (Rodriguez-Viciana et al.,

1994; Yoshimura et al., 2006b), a kinase that is important for localizing the PAR complex and CDC42 at the tip of the emerging axons and it is hence critical to axon formation (see later in this section and 1.1.3) (Shi et al., 2003). Also, it has been proposed that competition for a limited pool of Ras among neurites is essential to growing a single axon (Rodriguez-Viciana et al., 1994). Additionally, small GTPases cooperate with **formins**, a family of cytoskeleton-associated proteins which exist in an autoinhibited state in the cytoplasm, to nucleate actin or MT bundles (Goode and Eck, 2007). That is, membrane bound Rho GTPases bind the N-terminal GTPase binding domain of formins releasing the protein from autoinhibition, which results in formin activation and their availability to nucleate the cytoskeleton (Goode and Eck, 2007). Notably, while most formins promote the assembly of actin bundles, others associate with MTs (Goode and Eck, 2007; Bartolini et al., 2008; Li and Gundersen, 2008). The latter may hint at a role for formins in mediating the complex interplay between MTs and actin filaments during neurite specification and growth.

Recently, it has been shown how cytoplasmic enzymes such as nucleotide cyclases, kinases and phosphatases provide preferential axon- or dendrite- interpretations of extrinsic polarizing signals and/or the intrinsic state of neurons, by becoming asymmetrically activated in future axons or dendrites. Thus, **second messengers** generated by these enzymes become preferentially enriched in one type of process over the other and subsequently trigger distinct downstream effectors. For instance, cyclic adenosine monophosphate (**cAMP**) and cyclic guanosine monophosphate (**cGMP**), synthesized by enzymes **adenylyl cyclase** and **guanylyl cyclase**, respectively; have antagonistic activities in the differentiation of axons and dendrites (Shelly et al., 2010). Specifically, local up regulation of cAMP levels in an immature neurite promotes axon formation, whereas high levels of cGMP suppresses axon formation (Shelly et

al., 2010). The opposite is true for dendritic development; instead, local elevation of cGMP levels in an immature neurite supports dendrite differentiation (Shelly et al., 2010). Consistent with this, guanylyl cyclase was found to be asymmetrically localized to the apical dendrite in developing cortical pyramidal neurons (Polleux et al., 2000). Similarly, asymmetric changes in the local concentration of **phospholipids** in certain plasma membrane domains, affect the localization of Cdc42 GTPase and consequently, axon/dendrite polarization. Specifically, local concentrations of phosphoinositide(PI)-phosphates which result from the relative enzymatic activities of phosphoinositide 3-kinase (**PI3K**) and phosphatase and tensin homologue (**PTEN**), affect the fate of immature neurites (Maehama and Dixon, 1998; Menager et al., 2004). PI3K phosphorylates PI to generate phosphatidylinositol-3,4,5-phosphate (**PIP3)**, while PTEN removes the 5' phosphate to generate phosphatidylinositol-3,4-phosphate (**PIP2**) (Maehama and Dixon, 1998). Thus, higher levels of PIP2 and PIP3 have been linked to dendrite and axon differentiation, respectively. For instance, allosteric activation of PI3K by cAMP results in increased local concentration of PIP3 at the tip of the undifferentiated neurite that subsequently becomes an axon, whereas PI3K inhibition causes lack of axon differentiation (Shi et al., 2003; Menager et al., 2004). Consistently, PTEN overexpression inhibits axon formation (Jiang et al., 2005). Notably, although cAMP and PIP3 may have been activated through parallel signalling pathways they do converge on common downstream effectors to promote axon outgrowth and differentiation.

In summary, the polar nature of the cytoskeleton and associated proteins and the asymmetric distribution of enzymes and second messengers lay at the core of cell polarization. The specification of an axon elicits the sustained growth of the inherently polar

lattice inside a symmetrical sphere (immature neuron), which will break the sphere symmetry. This naturally evolves into cytoplasmic and membrane asymmetry (*i.e.* axon outgrowth) towards the specified site, in response to polarizing cues. Similarly, dendrites are specified by exclusion, on the remaining immature processes. It has been shown how axon and dendrites result from different interpretations to many of the same growth and guidance signals, suggesting that the decision axon *vs* dendrite does not lay solely on distinct extracellular cues but there is a significant contribution of intrinsic components as well (McAllister et al., 1995; Polleux et al., 2000; Xu et al., 2000). This section brings about more questions. *What are the signals that trigger axon vs dendrite specification? Which signalling pathways act on cytoskeleton components that accelerate neurite growth on the axon-to-be neurite, and how?* ***How is the number of axons controlled in vivo? How are axons oriented with respect to the target organ and the body plane?*** *I will discuss some of the current knowledge in the coming sections. I will begin by describing some of highly conserved polarizing protein complexes which become asymmetrically distributed in response to polarizing cues. Bolded questions are experimentally addressed in this thesis (see result chapters II-IV).*

1.1.3 Polarizing complexes.

The great diversity of cell shapes in multicellular organisms may suggest that different cell types use different mechanisms to attain polarity. However, in recent years, it has become evident that evolutionary conserved signalling pathways, which regulate polarity in *C. elegans* embryo and mammalian epithelial cells, also play a crucial role in polarizing neurons. For instance, the PAR (partitioning defective) signalling pathway induces

polarization in single cells and tissues in different species (Goldstein and Macara, 2007). *Par* genes were originally identified in a genetic screen for regulators of cytoplasmic partitioning in early *C. elegans* embryos (Kemphues et al., 1988). In the wild type nematode, the first division of the one-cell embryo is asymmetric, giving rise to two daughter cells with distinct cytoplasmic volume, content and developmental potential (Kemphues et al., 1988). Notably, while in the wild type two-cell *C. elegans* embryo the anterior daughter cell is significantly larger than the posterior; in *Par* mutants, however, both descendants appear symmetric (Kemphues et al., 1988). Altogether, phenotypic and functional analysis of *Par* genes have implicated PAR proteins in two facets of cell polarity: asymmetric localization of a set of proteins and RNA determinants that are essential for cell fate specification; and the asymmetric positioning of the mitotic spindle, that results in asymmetric cell division (Kemphues, 2000).

Five of the six *Par* genes isolated by Kemphues *et al*, as well as their protein products and associated functions, are highly conserved across species (Kemphues et al., 1988). These comprise serine-threonine kinases Par-1 and Par-4, PDZ-domain-containing signalling scaffolds Par-3 and Par-6, and a member of the 14-3-3 family of proteins Par-5, which binds phosphorylated serine and threonines on other polarity proteins (Goldstein and Macara, 2007). Par-2, on the other hand, encodes a nematode-specific protein with a RING finger domain that may act in the ubiquitination pathway (Goldstein and Macara, 2007).

In addition, PAR-4 like its mammalian counterpart LKB-1 is an early determinant of cell polarization in a variety of cells and tissues (Shelly and Poo, 2011). LKB-1/PAR-4 is a master kinase that becomes activated in response to both spontaneous intrinsic asymmetries

in cytosolic activity or to stimulation by extracellular polarizing cues (Shelly et al., 2007; Barnes et al., 2007). Once active, PAR-4 may phosphorylate at least 12 other downstream kinases (Shelly and Poo, 2011). Most significantly, LKB-1/PAR-4 phosphorylates and activates MARK/PAR-1 and SAD kinases which are essential regulators of MT stability during axon specification and outgrowth and AMPK which is a sensor of cellular energy (Shelly and Poo, 2011). Microtubule affinity-regulating kinases (MARK) are the closest mammalian homolog of PAR-1. Besides, Synapses of the Amphid Defective (SAD) kinases A and B, contain the conserved kinase domain of PAR-1. Both MARK and SAD phosphorylate MAPs, which reduce the affinity of MAPs to microtubules, thus increasing MT instability (Insolera et al., 2011).

Two excellent examples of the role of PAR in polarity are the establishment of the Anterior-Posterior (AP) axis in *C. elegans* and *Drosophila*. The AP axis in *C. elegans* is established shortly after fertilization, triggered by the entry of sperm; whereas in *D. melanogaster* the AP polarity axis is specified during oogenesis, triggered by womb specific cues (Goldstein and Macara, 2007). The AP axis is similarly defined in both cells by complex epistatic relationships among the Par family members; with LKB-1/PAR-4 residing at the top of a signalling cascade (Goldstein and Macara, 2007). This results in the asymmetric localization of PAR proteins to opposing cortical hemispheres of the nematode zygote and the fly oocyte (Goldstein and Macara, 2007). Thus, PAR-3 and PAR-6 become selectively enriched at the anterior cortex, forming a multiprotein polarity complex with atypical protein kinase C (aPKC) and specific GTPases; while PAR-1 is enriched at the posterior cortex (Goldstein and Macara, 2007). PAR-5 however, localizes symmetrically to both domains (Goldstein and Macara, 2007). In the *C. elegans* one-cell embryo, PAR-2

becomes concentrated in the posterior cortex (Goldstein and Macara, 2007). Collectively, PAR proteins define the anterior and posterior cellular domains, while simultaneously creating an asymmetric patterning of polarity determinants including proteins, RNA and cytoskeleton (Goldstein and Macara, 2007).

In addition, this core PAR multiprotein complex (PAR-3/PAR-6/aPKC) intersects with numerous other pathways in diverse ways. For instance, PAR complex interacts functionally with two other polarity complexes (Scribble and Crumbs) to polarize epithelial cells (Goldstein and Macara, 2007). Scribble is composed of lethal giant larvae (LGL) and discs large (DLG) while Crumbs is composed of the PDZ-domain-containing proteins PALS-1 and PATJ (PALS-1-associated tight-junction protein) (Goldstein and Macara, 2007). These three complexes mutually regulate the localization and activity of each other, such that the PAR and CRUMB complexes are localized to and define the identity of the apical membrane, while the SCRIBBLE complex regulates the identity of the basolateral membrane (Tanentzapf and Tepass, 2003;Nance and Zallen, 2011). Protein kinases dynamically recruit or exclude polarity proteins from the apical and/or basolateral domains. For instance aPKC phosphorylates Lgl and Par-1 causing their dissociation from the apical cortex and relocalization to the basolateral membrane (Nance and Zallen, 2011). However Par-1 phosphorylation of Baz/Par3 has an opposite effect, preventing it from localizing to the basolateral domain (Nance and Zallen, 2011).

Finally, pioneering studies of Dotti and Simons, carried out over 20 years ago, proposed the homology between the axonal and somatodendritic subcellular domains in neurons, to the apical and basolateral compartments in epithelial cells, respectively, in both

molecular composition and polarization mechanisms (Dotti and Simons 1990). More specifically, PAR proteins and other molecules that localize to the apical domain of epithelial cells are also found in dendrites, whereas PAR proteins and molecules located at the basolateral domain of epithelial cells are specifically enriched in axons. *This finding implied that the PAR family of proteins constitutes a polarizing multiprotein complex common to a diversity of cell types. Thus, the role of the PAR complex in neuron polarity will be detailed in the coming section.*

1.1.4 Breaking of symmetry in differentiating neurons. Mechanisms of neuron polarization *in vitro*.

The nerve growth factor (NGF) was the first molecule shown to trigger axon outgrowth (Levi-Montalcini, 1952; Levi-Montalcini et al., 1954). In the early 50s, Rita Levi-Montalcini *et al* discovered that a diffussible neurotrophic agent produced by mouse sarcomas elicited a potent growth of nerve fibers in cultured sensory and sympathetic ganglia (Levi-Montalcini et al., 1954). This factor was later isolated, christened NGF, and characterized (Cohen et al., 1954; Cohen, 1960). For the discovery of NGF, Rita Levi-Montalcini was awarded the 1986 Nobel Prize in Physiology and Medicine (Montalcini, 1986). This work paved the way for the identification of other neurotrophic factors such as the brain-derived neurotrophic factor (BDNF) (Barde et al., 1982; Lindsay et al., 1985). In addition, these discoveries laid the foundation for studying the mechanisms underlying neuron polarity/morphology. Much more research was needed to uncover the signalling pathways activated downstream of neurotrophins, that trigger axonal growth.

Most knowledge on neuronal polarity has been gained using cultured pyramidal neurons from rodent hippocampus and cortex as a model system (Dotti *et al*, 1988). Dissociated hippocampal and cortical neurons from rodent embryos (prior to axonogenesis) follow a stereotypical pattern of differentiation in culture. This process has been divided into 5 stages, based on the transient and evolving morphology of the polarizing neuron. Briefly, plated neurons initially display several equivalent short neurites (stage 2), then symmetry breaks (24 h after plating) when one neurite elongates faster to become the axon (stage 3) while the others remain short and become dendrites. 4) then after several days, the remaining neurites acquire characteristics of dendrites and 5) axon and dendrites reach maturation and form synapses (Wiggin et al., 2005).

What are the signals that allow only one neurite to grow rapidly at stage 3? See Figure I-1 for schematics on the current paradigm of axon specification *in vitro*. Briefly, stochastic stimulation of receptor tyrosine kinase (TrkB) by neurothrophins (such as NGF and BDNF), on one neurite, is followed by local accumulation of axon specifying components such as PI3P and cAMP, resulting in simultaneous activation of both PKA and PI3K pathways (Shi et al., 2003;Shelly et al., 2007). Local accumulation of PIP3 recruits a complex formed by PAR3, PAR6 and atypical protein kinase C (aPKC) at the tip of the committed neurite (Shi et al., 2003). By stage 3, PAR3 and PAR6 become restricted to the fast growing axon (Wiggin et al., 2005). Also, active Cdc42-GTP joins the PAR complex by direct binding to PAR6 and locally regulates actin dynamics (Shi et al., 2003). PAR3 directly binds to STEF/Tiam (guanosine nucleotide exchange factor) and activates Rac. Since Rac then activates PI3K, the signal initiated by PI3K terminates in PI3K itself. This positive feedback loop may be a driving force for axon specification (Nishimura et al., 2005). Moreover, PI3K phosphorylates

and activates serine/threonine kinase PKB/Akt via PI3P. PKB phosphorylates and inhibits GSK-3β (Inagaki et al., 2001; Yoshimura et al., 2006b). GSK-3β is constitutively active in all neurites at stage 2 and inhibits important regulators of axon outgrowth, such as CRMP2 and Tau (Inagaki et al., 2001; Yoshimura et al., 2005). Thus, phosphorylation by PKB selectively inactivates GSK-3β at the site of axon outgrowth which consequently releases the inhibitory tone over microtubule remodelling (Jiang et al., 2005; Li, 2005; Yoshimura et al., 2005; Yoshimura et al., 2006b). Simultaneously, BDNF activates ERK, which inhibits PDE-4 resulting in local accumulation of cAMP at the tip of the specified neurite (Gao et al., 2003). Increased cAMP levels leads to PKA activation which then phosphorylates and activates LKB1/PAR4 kinase which in a complex with cofactors (STRADα, MO25) phosphorylates and activates SAD-A,B kinases (Shelly et al., 2007; Barnes et al., 2007). SAD kinases promote tubulin polymerization and axon outgrowth (Barnes et al., 2007). To date, only SAD and LKB1 kinases have been shown to be required for neuronal polarity *in vivo* (Kishi et al., 2005; Barnes et al., 2007). In this model the dynamic PAR complex comprising PAR3 and PAR6 was found to be critical to axon specification (Wiggin et al., 2005). While at stage 2, the PAR complex is localized at the cell body and at tip of all nascent neurites, by stage 3, it is restricted to the cell body and the growth cone of the developing axon, while it is lost from the remaining processes (Wiggin et al., 2005). Thus, a higher order PAR complex, also including atypical protein kinase C (aPKC), Rac, Cdc42 and guanine nucleotide exchange factors (GEF), such as Tiam1, becomes selectively enriched at the soon-to-become axon tip, following localized activation of phosphatidylinositol 3' kinase (PI3K) and increased levels of PIP3. This phospholipid recruits PH domain containing proteins like PDK1, which activates aPKC which in turn activates the Rho family of

GTPases such as Cdc42 and Rac 1 (Wiggin et al., 2005; Nishimura et al., 2005). Thus, the cytoskeleton gets instructed as to which neurite will develop as an axon.

Studying the polarization of hippocampal and cortical neurons in culture is a convenient way to examine the intrinsic mechanisms governing axon specification and dendritic identity. However, this system does not recapitulate all aspects of neuronal polarization *in vivo*, where asymmetric extrinsic signals from neighbouring tissues likely play a major role in axon specification. *Yet, these findings suggest that other proteins with conserved roles in cell/tissue polarity may also act to establish normal neuronal morphology. In vivo models are required to investigate precisely the intrinsic and extrinsic signals that specify axon outgrowth.*

Figure I-1. Mechanisms of axon specification *in vitro*. Growth cone of differentiating rodent pyramidal neurons in culture. This diagram was made based on the references cited in section 1.1.4.

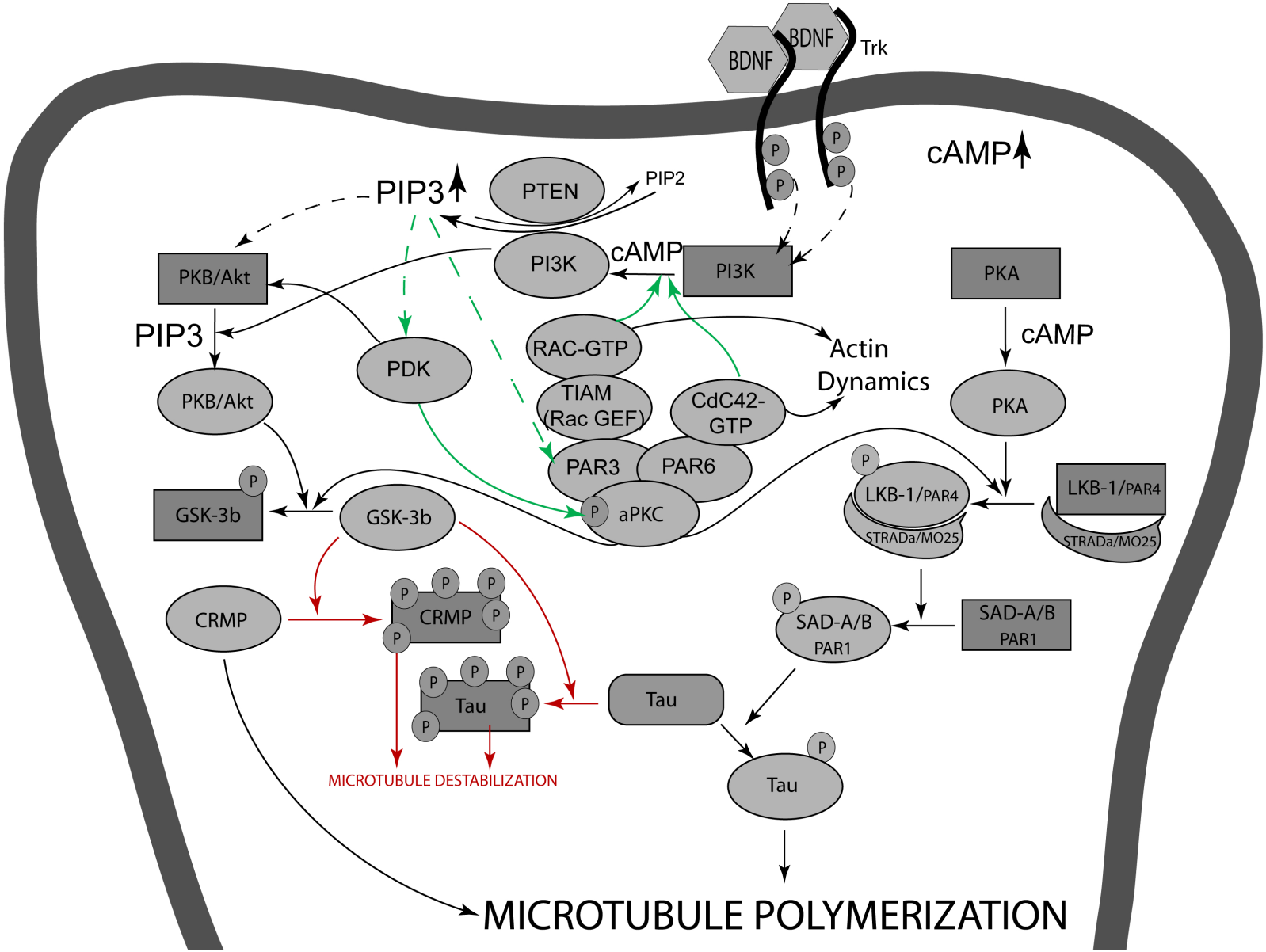
BDNF
BDNF
Trk
cAMP
PIP3
PTEN
PIP2
PI3K
cAMP
PI3K
PKB/Akt
PIP3
PDK
RAC-GTP
Actin
Dynamics
TIAM
(Rac GEF)
CdC42-
GTP
PAR3
PAR6
aPKC
PKA
cAMP
PKA
PKB/Akt
GSK-3b
GSK-3b
LKB-1/PAR4
STRADa/MO25
LKB-1/PAR4
STRADa/MO25
CRMP
CRMP
SAD-A/B
PAR1
SAD-A/B
PAR1
Tau
Tau
Tau
MICROTUBULE DESTABILIZATION
MICROTUBULE POLYMERIZATION

1.1.5 Mechanisms of neuron polarization *in vivo*.

Although neuronal polarization mechanisms *in vitro* and *in vivo* have fundamental differences, the worth of *in vitro* models has been validated by the demonstration that some genes first found *in vitro* also play a role *in vivo* (*e.g.* GSK-3β). However, the number of signalling pathways that have been shown to polarize neurons *in vivo* is scarce. One of them, the LKB-1_SAD/MARK pathway was reported simultaneously by two groups (Shelly et al., 2007; Barnes et al., 2007). As discussed earlier, LKB-1, an upstream regulator of PAR proteins is a master kinase that phosphorylates at least 12 other kinases including SAD-A and B (Shelly and Poo, 2011). Both groups showed that LKB-1 and downstream kinases SAD-A and -B are required for polarization of the mouse cerebral cortex (Shelly et al., 2007;Barnes et al., 2007). Briefly, it was shown that a conditional dorsal telencephalic LKB-1 KO displayed axonless cortical neurons that were defective in axon initiation; whereas simultaneous overexpression of LKB-1 and cofactor STRADα resulted in formation of supernumerary axons (Shelly et al., 2007). A previous *in vivo* study had shown that SAD kinases regulate neuronal polarity in cortical neurons at least in part by phosphorylating MAP Tau which has an effect on microtubule organization and is required for axon specification (Kishi et al., 2005), which closed the link between LKB-1 to the cytoskeleton. Finally, it has been suggested that gradients of extrinsic factors (*e.g.* growth factors) may act on developing cortical neurons *in vivo* to polarize intrinsic determinants such as LKB-1 that specify the direction of axon outgrowth (Shelly and Poo, 2011).

1.1.6 Role of guidance molecules and their receptors in neuronal polarity.

Recently, it has been shown that neurons' ability to attain the correct morphology and orientation *in vivo* depends on the cell's proper response to guidance signals that establish an internal axis of asymmetry. Guidance molecules polarize developing neurons by specifying the site of axon/dendrite outgrowth. Clearly, this function is prior to guiding the growing axon toward specific targets. Some examples of classic axon guidance molecules with an additional role in neuronal polarity are Semaphorin 3A which promotes dendrite formation in vertebrate cortical neurons (Polleux et al., 1998;Shelly et al., 2011); and Netrin/UNC-6 which specifies the site of axon outgrowth in the pair of HSN neurons in *C. elegans* (Adler et al., 2006).

Each of the HSN motorneurons, symmetrically located on both sides of the *C. elegans* egg-laying organ, extends an axon ventrally to the ventral nerve cord and then anteriorly to the head (White et al., 1986). UNC-6/Netrin defines the initial polarization in immature HSN neurons (Adler et al., 2006). Briefly, a gradient of attractive UNC-6/netrin, emanating from the VNC, promotes leading edge formation by inducing the asymmetric distribution of netrin receptor UNC-40 along the ventral membrane of morphologically unpolarized HSN neurons (Adler et al., 2006). UNC-40 then activates actin-regulator UNC-34/Ena and promotes an asymmetric increase in PIP2 levels along the ventral membrane (Adler et al., 2006). Consequently, the downstream effector MIG-10/Lamellipodin, which is a PH-domain-containing protein that specifically binds PIP2 phospholipids, becomes ventrally recruited (Adler et al., 2006). Hence, sustained asymmetric lipid signalling from AGE-1/PI3K_DAF-18/PTEN resulting in higher ventral levels of PIP2, and the subsequent enrichment of MIG-10 which recruits the active form of CED-10/Rac, cooperatively promote cytoskeleton

reorganization that induces the breaking of HSN spherical symmetry with the growth of a ventral axon (Adler et al., 2006). Importantly, even though the ventral-dorsal guidance in *unc-6* mutants is disrupted, HSN neurons ultimately extend an axon, although misguided anteriorly, suggesting that UNC-6 is required for neuron polarization and not for axon extension (Adler et al., 2006). Similarly, attractive Netrin, cooperatively with a gradient of repulsive guidance signal SLT-1/Slit, polarize unipolar mechanosensory neurons AVM and PVM (morphologically similar to HSNs) to grow a ventral axon (Quinn et al., 2006).

1.1.7 Concluding remarks on neuron polarization and general questions this thesis is aimed at studying.

Although the role of some individual neuronal polarity genes and pathways has been described, the mechanisms that establish or maintain neuronal polarity *in vivo* are still largely unknown. The use of multicellular organisms with a nervous system, both invertebrates (*e.g. D. melanogaster* and *C. elegans*) and vertebrates (*e.g. D. rerio*) have already probed useful in studying several aspects of nervous system development. For instance, studies of *C. elegans* nervous system have made important contributions in the understanding of axon guidance (Colavita et al., 1998), olfaction mechanisms (Bargmann et al., 1993;L'Etoile and Bargmann, 2000;Wes and Bargmann, 2001) and "the gene regulatory logic of dopamine neuron differentiation" (Flames and Hobert, 2009), to name a few. Accordingly, the nematode *C. elegans* may be indeed, an excellent tool to study how neurons polarize and adopt their final morphology within a living creature. My thesis uses the worm to explore two fundamental questions in the field of neuronal polarity: 1) **how is the number of axons controlled** and 2) **what genes and/or pathways regulate axon orientation?** *In the following section, I will*

describe the assets of C. elegans as a suitable model organism to study neuronal polarity questions, and more specifically the polarization of the VC4 and VC5 motorneuron pair, that innervate the egg-laying system, within the context of the developing organ.

1.2 *C. elegans* as a model system to study nervous system development.

1.2.1 Amenability of C elegans as a model organism

Caenorhabditis elegans (*Caeno*, Greek for recent; *rhabditis*, Greek for rod-like; *elegans*, Latin for elegant) is a small (~ 1 mm long as an adult), free-living, non-parasitic soil nematode that was first used as a model organism in 1967 (Brenner, 1974; Brenner, 2009). *C elegans* is a multicellular organism with musculature, digestive tract, sexual reproductive organs and a nervous system. Sydney Brenner selected this worm for his studies on nervous system development, because of its simplicity, rapid life cycle and easy of genetic manipulation (Brenner, 1974). Interestingly, one of Brenner's earliest and most satisfying realizations was that genetic transmission of traits in the worm followed the classic Mendelian proportion of 1:3; thus confirming the discovery of classical genetics made by Mendel and continued by Morgan, in other species (Mendel, 1865; Morgan, 1910; Brenner, 2009).

The awareness of *C. elegans'* value as a research tool has since grown rapidly, which prompted the development of a solid knowledge infrastructure. For instance, the detailed worm anatomy was described through reconstruction of serial electron micrographs, with the nervous system resolved at the level of the synapse (White et al., 1986). This method allowed the assembly of the complete wiring diagram of *C elegans* nervous system (White et al., 1986). Moreover, the postembryonic and embryonic cell lineages of the nematode were

completed and found to be remarkably invariant from one animal to the other (Sulston, 1976; Sulston and Horvitz, 1977; Sulston et al., 1983). Conveniently, the knowledge of which cells are derived from which provided the foundation for correlating genetic mutations with developmental processes. Moreover, knowing the cell lineage facilitates laser cell-ablation studies, thus allowing for a more precise assessment of cell-cell interactions during normal and aberrant development (Sulston and White, 1980; Chalfie et al., 1983; Thomas et al., 1990).

At the same time, the material infrastructure for *C. elegans* research has grown exponentially. For instance, thousands of *C. elegans* stocks are readily available from the *Caenorhabditis* Genetic Center (CGC, *http://www.cbs.umn.edu/CGC*), which banks and distributes mutant and transgenic strains created by laboratories worldwide and by the *C. elegans* gene knockout consortium (*http://celeganskoconsortium.omrf.org*), which generates mutant strains on demand. Also, a battery of invaluable *C. elegans* expression vectors, that virtually every worm laboratory owns, was created by Andrew Fire's laboratory.

In addition, *C. elegans* possesses numerous attributes that make it amenable for genetic work and consequently a successful research tool. The worm is inexpensive to cultivate in the laboratory, since it is easily grown in large numbers, on agar plates or liquid media containing *E coli*, usually OP50, as the source of food. In addition, worm stocks can be efficiently cryopreserved at -80^{o}C or $N_{(l)}$, with significant viability, which saves strains and labour (Sulston and Brenner, 1974). Furthermore, *C elegans* has a short life span of approximately 2-3 weeks. Also, a complete life cycle (from egg to adult) takes 3.5 days at room temperature, during which the worm goes through four larval stages (L1-4) (Brenner,

1974). Moreover, *C. elegans* exists as two sexes, hermaphrodites (with 959 somatic cells) and males (only 0.1 - 2 % occurrence, with 1031 somatic cells) (Corsi, 2006). Hermaphrodites are self-fertilizing females that produce and store sperm, before producing oocytes (Corsi, 2006). A single hermaphrodite is able to generate a brood of ~ 300 progeny within 3 days, which is useful to propagate strains and to generate homozygous mutations. In addition, the sexual dimorphism of *C. elegans* makes inbreeding and the control of genetic variants very simple. Also, mating males with hermaphrodites allows two or more mutations and/or genetic markers to be placed together in a single organism, which is important when mapping unknown mutations.

Furthermore, *C. elegans* has a relatively small genome of ~ 100 Mb, compared to the human genome which is estimated to consist of ~ 3000 Mb (Waterston et al., 1997; Hillier et al., 2005). Moreover, the worm's DNA content, which is condensed into just six chromosomes, has been fully sequenced, making genetic manipulation and analysis feasible (The *C. elegans* Genome Sequencing Consortium 1998). Although the *C elegans* genome is only ~ $1/30^{th}$ of that of human, it contains a relatively large number (19,735) of predicted protein-coding genes, 35 % of which are conserved in humans (Hillier et al., 2005). Consequently, some proteins and signalling pathways first discovered in worms have turned out to be highly conserved between worms and human. Two examples of the above are, 1) the discovery of the apoptotic pathway, first described in *C. elegans* and for which Dr. Horvitz shared a Nobel Price in 2003 (Horvitz, 2003) and 2) the discovery of RNA interference, for which Dr. Fire and Dr. Mello were awarded a Nobel Prize in 2006 (Fire, 2007; Mello, 2007). Hence, research in *C. elegans* is expected to shed more light into human physiology and disease.

Another advantage of *C. elegans* is that transgenic animals can be generated with relative ease, in less than two weeks, by injecting DNA into the luminal arms of the gonads and performing a few rounds of cloning the worms expressing the reporter marker (*e.g.* rolling locomotion, GFP or RFP fluorescence) (Evans, 2006). In brief, a gene/DNA of interest is introduced together with a reporter DNA, consisting of a fluorescent protein coding gene or a gene carrying a dominant mutation such as *rol-6(su1006),* that results in a reporter phenotype to identify transgenic animals. Injected DNA then forms concatamers that are segregated to the progeny. Extrachromosomal arrays can be stably transmitted for several generations. However, for long term use of the strains it is wise to integrate the arrays using any of the various strategies available, in order to gain on transgene stability and consistency of results.

Remarkably, the worm is transparent throughout its life cycle, which facilitates the observation of its cells and structures with regular Normaski optics. More notably, with the advent of Green Fluorescent Protein (GFP) as a marker for gene expression and the development of fluorescence and confocal microscopy, the nematode transparency became a paramount asset, because developmental processes could then be unequivocally followed in real time in the living organism (Chalfie et al., 1994). The use of GFP in the worm has become a powerful and indispensable tool for neuroscience, in a plethora of applications including to 1) perform manual and automated **genetic screenings** for genes involved in neuron development (lineage specification, differentiation, migration), 2) **examine gene expression** and protein localization at different stages of the living nematode, 3) understand the **regulatory mechanisms of gene expression** that instruct terminal identity in a neuron, 4)

track growth cone motility and guidance, 5) **study axon outgrowth and orientation**, and 6) decipher the mechanisms governing axon regeneration in real time.

1.2.2 Forward and reverse genetics to study nervous system development and function.

Genetic studies of *C. elegans* nervous system development and function has been routinely performed using **forward genetics**; that is by isolating and analyzing nematodes displaying a neuronal phenotype of interest, following treatment with a mutagen (*e.g.* EMS) (Brenner, 1974). Simple forward genetic screening, and modifier variations such as enhancer and suppressor screens, have permitted the elucidation of genetic pathways that are critical to the proper functioning of the nervous system, such as axon pathfinding (Zallen et al., 1999) (Colavita and Culotti, 1998) and olfactory sensation (L'Etoile et al., 2002).

Once mutants causing neuronal phenotype of interests are isolated from a screen, the mutated gene must be identified so that gene function can be correlated to the phenotype. An important first step is mapping/identifying the phenotype-causing genetic lesion which has been traditionally conducted via single nucleotide polymorphism (SNP) analysis, alone or in combination with two-point mapping (Fay and Bender, 2006) and/or complementation tests with deficiencies (Fay, 2006). SNP mapping is based on the large number of DNA polymorphisms, in general with no associated phenotype, that exist between Hawaiian and Bristol (N2) *C. elegans* strains. These DNA variations are listed online at [*www.wormbase.org*]. More attractive experimentally, are the SNPs (SNP/snip) which contain the recognition site of a retriction endonuclease. By examining genetic linkage to chosen SNPs, the mutation is first mapped to one of the six chromosomes, followed by locating the mutation to an interval between two SNPs, and then it is finely mapped to the

gene in question through iterative use of SNP mapping (Wicks et al., 2001). Mapping a mutation with this technique could often become an extraordinary challenge and it may take more than 6 months of work to complete, if successful. For instance, SNP/snip mapping could become difficult if the gene is linked to the integrated array that serves as neuron marker (See Chapter II), or if the mutation is lethal and requires a balancer, or if the gene displays maternal effects, or if the defective phenotype is not highly penetrant, or if the isolate is actually a double mutant that can not be segregated because of linkage or lethality. These, often tedious and prolonged, mapping strategies are slowly becoming a thing of the past, as a new approach, whole genome sequencing (WGS), first applied to worms in Dr. Hobert's laboratory at Columbia University, to circumvent altogether or complement traditional SNP/snip mapping strategies, is becoming increasingly available (Doitsidou et al., 2010; Hobert, 2010b). This procedure is based on automated genome sequencing of the mutant worm DNA. About 2 dozens sequence iterations are performed, followed by data processing with a software (MAQgene) designed to spot persistent polymorphism variants found in all trials, which are absent from the DNA of the non-mutagenized parental strain (Bigelow et al., 2009). Discerning the phenotype-causing mutation from other genetic variants introduced by mutagenesis, is yet more efficient by sequencing two alleles of the same locus. Although, phenotype-causing mutations can be identified with this technique in about 3 days, it is currently too costly to be used routinely in most labs.

Alternatively, a faster way to decipher genetic pathways would be to examine the phenotype generated by disrupting a candidate gene's function, via genetic analysis of available mutant alleles (from CGC or *C. elegans* KO consortium) or by down-regulating gene expression via double-stranded RNA. This approach is known as **reverse genetics**.

Many genetic pathways have been elucidated by examining the phenotype of candidate genes (Zwaal et al 1993), such as neuron polarization induced by guidance molecules (Adler et al., 2006), maintenance of axon position (Benard et al., 2009) and anterior-posterior axon orientation (Hilliard and Bargmann, 2006). DsRNA can be administered to the worms by either injecting it into the gonads, soaking the animals in a dsRNA solution or by feeding the animals with bacteria harbouring plasmids with dsRNA to a gene of interest. Feeding dsRNA is the simpler choice when a large number of genes are to be screened. Conveniently, a genome-wide feeding dsRNA library is commercially available,

(www.geneservice.co.uk/products/rnai).

Innovative strategies to screen for genes involved in development, maintenance, and repair of the nervous system are continuously devised. For instance, an exciting technique developed by Yanik MF *et al*, in 2004 (Yanik et al., 2004), based on a femtosecond infrared laser microsurgery to precisely dissect axons (axotomy), provided the foundation for screens to uncover the genetic basis of axon repair *in* vivo (Yanik et al., 2004). About 54 % of operated axons regenerated structurally and functionally (recovered connections), within 12-24 hours post-surgery (Yanik et al., 2004). This technique was successfully employed in a large-scale **reverse genetic** screen (using RNAi of candidate genes), which uncovered a MAP kinase pathway involved in axon regeneration (Hammarlund et al., 2009); and in several "robotic" high-throughput **forward genetic** screens coupled with digital imaging and worm sorters, whereby surgery is automatically performed in worms immobilized in microfluidic devices and their repair is tracked digitally (Guo et al., 2008). The simple anatomy and transparency of the worm, represent advantages over other genetic models

currently used to study axon repair, since dissecting fluorescent-labelled axons *in vivo* and following their real time regeneration can be performed at a single-axon resolution (Ghosh-Roy and Chisholm, 2010). Finally, unlimited creative potential can be applied to the worm as a genetic model in order to answer fundamental questions in Neuroscience.

During the course of my research, I have used gfp-labelled C. elegans VC motorneurons as a model system to study neuronal polarity. Specifically, I have performed forward genetic screens and genetic analysis of candidate genes in a quest for regulators of the establishment and maintenance of neuronal polarity, and also to map a mutant displaying defective VC polarity (See Chapter II). In the coming sections, I will describe the lineage, neurotransmitter identity, target innervations and function of the VC motorneurons within the context of the whole nematode's nervous system and the organ they innervate. Other neurons analyzed in this thesis (i.e. PDE) will be duly introduced in the individual result chapters.

1.2.3 Overview of *C. elegans* Nervous System.

1.2.3.1 Lineage of *C. elegans* neurons, with emphasis on the origin of VC motorneurons.

Most *C. elegans* neurons are generated non-clonally from various lineages (Hobert, 2010a). However, there are a few examples of clonal sub-branches which generate neurons exclusively; yet sisters or cousin neurons within that lineage sub-branch may not share much else, but a lineage history (Hobert, 2010a). Moreover, in a number of cases, decisions between neuronal *vs* non-neuronal fates are only made late in the lineage. Accordingly, some neurons are born from sub-branches that produce mainly muscle cells or hypodermal/epidermal cells and *vice versa* (Hobert, 2010a). The opposite is also true, as

there is no correlation between the terminal features of neuron types (*e.g.* neurotransmitter, morphology) and lineage history. For example, even though the eight dopaminergic neurons share neurotransmitter identity, their lineage roots are very diverse (Hobert, 2010a). Moreover, bilaterally symmetric neuron pairs, with similar morphologies, often do not share a left/right symmetric lineage. Furthermore, neighbour neurons may not share a lineage relationship, their proximity may result from substantial migrations during embryonic development (Hobert, 2010a). Likewise, neurons that are synaptic partners may not have common lineage history, such as HSN and VCs.

Although similar neurons may have very distinct lineage history, there are examples of similar neuron types that are generated by similar patterns of cell divisions (known as "repeated sub-lineages") (Hobert, 2010a). Repetitive patterns produce the same group of neuron types. For example, the generation of five postembryonic subtypes (VA, VB, **VC**, AS and VD) of Ventral Cord Motorneurons (VNC) follows a prototype of cell divisions (Hobert, 2010a). A few of the blasts cells (P[3-8]) that give rise to these specific sub-lineages are distant in origin, while others are quite close; for instance, pairs of progenitors P3-P4, P3-P6 and P3-P8 are each separated by 13 cell divisions, while pairs P3-P5 (sister blast cells) and P3-P7 (cousin blast cells) are separated by one and three cell divisions, respectively. In addition, the origin of three of the progenitors is traced to the anterior branch of the blastomere Ab.p, while the other three arise from the posterior [see complete neuronal lineage at (Sulston, 1983;Hobert, 2010a)]. Overall, the pattern to their formation can be better estimated by a quick glance at their lineage:

P3(AB.p.a.a.p.p.a.a.a), P4(AB.p.**p**.a.p.p.a.a.a),
P5(AB.p.a.a.p.p.a.a.**p**), P6(AB.p.**p**.a.p.p.a.a.**p**)
P7(AB.p.a.a.p.p.a.**p**.**p**) P8(AB.p.**p**.a.p.p.a.**p**.**p**).

Albeit the blast cells that initiate the repeated sub-lineages may have divergent ancestry, they implement a common and synchronized developmental program, which gives rise to the specific array of motorneurons. At the first cell division of the multipotent P[3-8] blast cells, a cell fate decision neuron *vs* epithelium is made (Figure I-2). As a result, the anterior daughters of P[3-8], neuroblasts P[3-8].a give rise to VC1-6 and other ventral motorneuron subtypes in a similar repetitive manner; while the posterior daughters, ectoblasts P[5-7].p give rise to vulval precursor cells that give rise to the vulva via morphogenesis (discussed later). Interestingly, almost all neurons in the worm are born through asymmetric cell divisions (Hobert, 2010a). For instance, neuropotent VC sister cells, divide once to generate two distinct daughters, motorneurons Vas and VBs subtypes. Although, sisters VA and VB share the cholinergic identity, have similar morphologies and co-express some genes, they have distinctive gene expression profiles and connect to different synaptic partners. Differential expression of genes and transcription factors underlie decisions at every juncture in the lineage. For instance, VA-VB diversifying pathway is led by the *unc-4* homeobox transcription factor; *i.e*. in the absence of *unc-4,* VA subtype adopts a VB fate (Hobert, 2010a).

Figure I-2. Repeated sublineages give rise to VC motorneurons and vulval precursor cells. P lineage in the *C. elegans* hermaphrodite. Schematics of the lineages of the complete array of motorneurons derived from the neuron subbranches of P[3-8].a; and the lineage of the 22 epithelial vulva precursor cells (VPCs) from sister branches of P[5-7].a which are generated through mirror-image patterns of cell division, initially via anterior-posterior divisions and terminally, via left-right divisions. Repeated sub-lineages that generate the six VC motorneurons are circled. Adapted with permission from (Sulston and Horvitz, 1977).

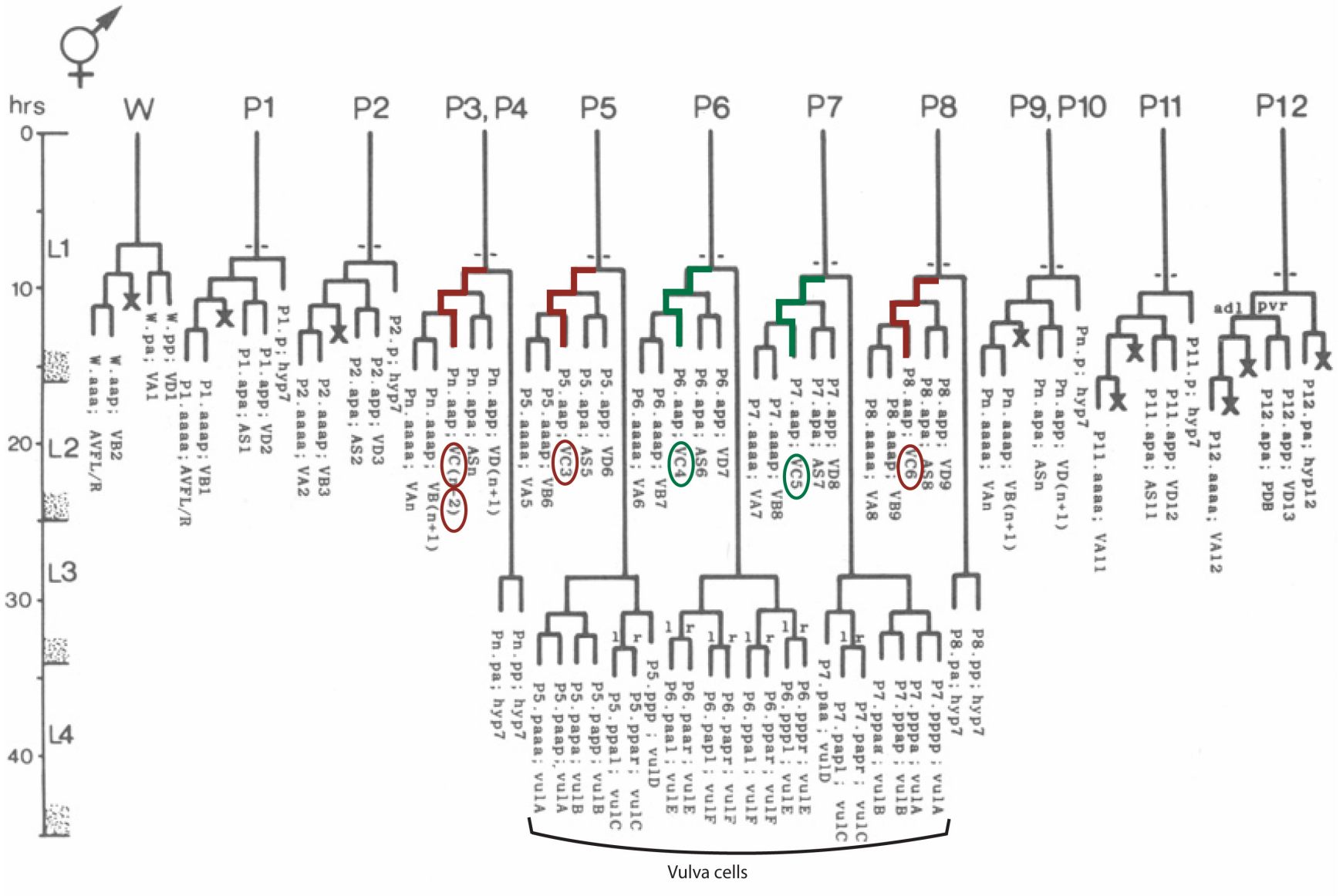
hrs
0
10
20
30
40
L1
L2
L3
L4
W
P1
P2
P3, P4
P5
P6
P7
P8
P9, P10
P11
P12
W.aap; VB2
W.aaa; AVFL/R
W.pp; VD1
W.pa; VA1
P1.aaap; VB1
P1.aaaa; AVFL/R
P1.p; hyp7
P1.app; VD2
P1.apa; AS1
P2.aaap; VB3
P2.aaaa; VA2
P2.p; hyp7
P2.app; VD3
P2.apa; AS2
Pn.aaap; VB(n+1)
Pn.aaaa; VAn
Pn.app; VD(n+1)
Pn.apa; ASn
P5.aaap; VB6
P5.aaaa; VA5
P5.app; VD6
P5.apa; AS5
P6.aaap; VB7
P6.aaaa; VA6
P6.app; VD7
P6.apa; AS6
P7.aaap; VB8
P7.aaaa; VA7
P7.app; VD8
P7.apa; AS7
P8.aaap; VB9
P8.aaaa; VA8
P8.app; VD9
P8.apa; AS8
Pn.p; hyp7
P11.aaaa; VA11
P11.p; hyp7
P11.app; VD12
P11.apa; AS11
P12.aaaa; VA12
P12.pa; hyp12
P12.app; VD13
P12.apa; PDB
adl
pvr
Pn.pp; hyp7
Pn.pa; hyp7
P5.paaa; vulA
P5.paap; vulA
P5.papa; vulB
P5.papp; vulB
P5.ppal; vulC
P5.ppar; vulC
P6.paal; vulE
P6.paar; vulE
P6.papl; vulF
P6.papr; vulF
P6.ppal; vulF
P6.ppar; vulF
P6.pppl; vulE
P6.pppr; vulE
P7.paa; vulD
P7.papl; vulC
P7.papr; vulC
P7.ppaa; vulB
P7.ppap; vulB
P7.pppa; vulA
P7.pppp; vulA
P8.pp; hyp7
P8.pa; hyp7
Vulva cells

1.2.3.2 Morphology and terminal differentiation of *C. elegans* neurons

Neuron processes in *C. elegans*, like in other invertebrates such as *D. melanogaster*, may contain both axonal (presynaptic) and dendritic (postsynaptic) specializations along their lengths (Rolls et al., 2007;Feinberg et al., 2008;Rolls, 2011). Thus, contrasting with vertebrate neurons where dendrites typically arise directly from the cell body (Andres-Barquin, 2001), processes in *C. elegans* neurons have mixed functions and dendrites usually emerge from a primary neurite [*www.wormatlas.org*]. For example, unipolar HSN neurons and bipolar VC neurons project one and two primary processes from the soma, respectively, which contain both pre and postsynaptic terminals. Other morphological variants of *C. elegans* neurons exist. For instance, bilaterally symmetric PLM neurons extend two functionally distinct processes directly from the cell body; a longer anterior neurite with a ventral branch which makes all synapses and form gap junctions; and a shorter posterior process with no branches and synapses (Hilliard and Bargmann, 2006).

Despite the morphological simplicity of *C. elegans* neurons, relative to vertebrate neurons, their gene expression profile and regulatory mechanisms are extraordinarily complex and found to be phylogenetically conserved. In this line, studies in *C. elegans* have revealed much of the regulatory logic of gene expression that define and maintain mature differentiated neurons. That is, while some genes are only expressed transiently during neuron development, such as axon pathfinding cues/receptors; terminal differentiation genes (TDG) are persistently expressed throughout the life of a neuron (Hobert et al., 2010). Expression of TDGs define and maintain neuron morphology, neurotransmitter identity, electrical properties, synapses and the overall function of a mature, terminally differentiated

neuron. Consistently, neurons that share neurotransmitter phenotype express a functionally related terminal gene battery (TGB) that encodes the set enzymes that synthesize, pack, transport and reuptake the neurotransmitter (Hobert, 2010a). Studies in *C. elegans* have shown that neuron-type specific TGBs are usually co-regulated by combinations of synergistically acting transcription factors (terminal selectors) (Hobert et al., 2010). Terminal selectors also need to be persistently expressed throughout the life of a neuron to maintain the neuron-type commitment. For instance, experimental removal of terminal selectors resulted in the loss of the differentiated state of dopaminergic neurons (Flames and Hobert, 2009). Terminal selectors are transcription factors which regulate gene expression through conserved *cis*-regulatory elements found in TDGs. For example, the terminal phenotype of the AIY interneuron, required to process thermosensory information, is determined by two homeodomain transcription factors, whose expression exclusively overlap in AIY neurons, and that simultaneously bind a specific *cis*-regulatory element (AIY motif), found in five terminal differentiation genes that define AIY neuron identity (Hobert et al., 2010). The AIY motif is necessary and sufficient to define the identity of the AIY interneuron class. Similar shared motifs control the fate of other neuron classes. For instance, even though their lineage is diverse, all dopaminergic neurons in the worm share the same transcriptional control mechanism (Flames and Hobert, 2009). The dopaminergic phenotype is regulated by a common neuron-type *cis* motif. Thus, the terminal selector AST-1 controls the dopaminergic identity through binding to a conserved *cis* regulatory element present in all dopamine pathway genes, that are involved in synthesis and transport of dopamine (Flames and Hobert, 2009).

1.2.3.3 Composition and anatomy of *C. elegans* nervous system.

The *C. elegans* nervous system is evolutionarily simple, yet it is the most complex tissue in the worm, with the largest number of cells and cellular diversity. This nematode is wired with 302 neurons making approximately 7000 synapses and contains 56 glial cells (White et al., 1986;Hobert, 2010a); contrasting with the complexity of more evolved nervous systems, including *D. melanogaster* with ~10^5 neurons (Weiner, 2012), and *H. sapiens* with ~86 x 10^9 neurons only in the brain (Herculano-Houzel, 2009). Based on their ultrastructural analysis of the nervous system, White and collaborators defined 118 different neuron classes, mostly distinguished by their position, and common axodendritic projections and synaptic patterns (White et al., 1986).

The *C. elegans* nervous system is mainly structured into several ganglia in the head (a.k.a. "brain or mind") and in the tail; and into a spinal cord-like ventral nerve cord (VNC) (White et al., 1986) (Figure I-3). In *C. elegans*, most neurons and their axons are bundled in the nerve ring that encircles the pharynx (180 nerve cells, ~ 60 % of all neurons) and in the VNC (Zallen et al., 1999) (Figure I-3).

In the adult hermaphrodite, the VNC consists of an asymmetric pair of axon bundles that extend parallel to each other from head to tail, along the ventral midline (Wightman et al., 1997) (Figure I-3). A large bundle of approximately 40 axons, on the right side, is separated from a smaller bundle of 3-5 axons, on the left side, by a bulge of ventral epithelium, also known as hypodermal ridge (White et al., 1986;Wightman et al., 1997).

During embryonic development, specific growth cones in the primordial VNC, navigate along neuroglia while creating an axon scaffold that supports the growth of follower

axons (Wightman et al., 1997). AVG and PVPR growth cones pioneer the right and left VNC bundles, respectively; and provide cues that guide follower growth cones. For instance, PVPR is required for the selective pathfinding of PVQL, AVKR and HSNL growth cones along the left VNC bundle (Wightman et al., 1997). Consistently, laser-ablation of PVPR results in the absence of a left VNC bundle, with the left axons running ectopically along the right bundle. Within VNC nerve bundles, adjacent axons make synapses between them; keeping neighbour axons joint in fascicles. Maintenance of nerve fascicles is essential to the proper functioning of the nervous system (Benard and Hobert).

According to function and connectivity, worm neurons can be grouped as sensory, interneurons and motorneurons or combinations thereof (Chalfie and White, 1988). Most sensory neurons and interneurons are bilaterally symmetric pairs, with homologues on the left and the right sides (Bargmann and Kaplan, 1998) for instance, the left and right AWC olfactory neurons. Moreover, the number of neurons along the VNC of the newly hatched larvae is 15; while the adult VNC is made of 57 motoneurons, including processes from head and tail interneurons, processes from neurons located on lateral positions, and processes from sensory ganglia in the head and tail (White et al., 1976;Sulston, 1976).

Eight classes of VNC motorneurons (DA, DB, DD, VA, VB, **VC**, AS and VD) control muscle contractions and movement by forming neuromuscular junctions with body muscles (White et al., 1986). Three subtypes (DA, DB and DD) are added to the VNC during embryonic development, whereas five postembryonic subtypes (VA, VB, **VC**, AS and VD) are incorporated during larval stage 1 (Sulston and Horvitz, 1977;Sulston, 1983;Sulston et al., 1983). VNC motorneurons are grouped and named on the basis of anatomical features (A, B,

C and D, see wormatlas for details), common neurotransmitter identity (*e.g.* type D is GABAergic, serotonergic; while A and B, are cholinergic), and presynaptic specificity (*e.g.* VA, VB and VC innervate ventral body wall muscles while DA, DB and AS innervate dorsal wall muscles; and VCs also innervate egg-laying muscles on the ventral side) (White et al., 1986). Five classes of VNC motorneurons (DA, DB, DD, VD and AS) extend axons as commissures to the dorsal midline, where they turn longitudinally to establish the dorsal nerve cord (DNC) and to make synapses with dorsal body wall muscles (White et al., 1986).

Even simple nervous systems display vast anatomical complexity, which is put in place by the interplay of molecular mechanisms that govern 1) the precise positioning of neuronal cell bodies, 2) neuron differentiation, 3) axon outgrowth and guidance, 4) axon branching, and 5) dendrite formation and synapses. Thus, nervous system architecture is precisely and consistently built and maintained in every organism within the species. Also, despite significant differences in the nervous systems among species, some of the operating mechanisms are phylogenetically conserved.

Altogether, *C. elegans*, like the fruit fly and the mouse, has become a standardized tool to study neuronal development. Since its introduction by Sydney Brenner, *C. elegans* has been productively used to study a broad spectrum of nervous system questions including axon guidance (Colavita et al., 1998;Zallen et al., 1999), neuron orientation (Hilliard and Bargmann, 2006), synaptogenesis (Patel et al., 2006;Colon-Ramos et al., 2007) and behaviour (Bendesky et al., 2011) .

Most *C. elegans* neurons exhibit simple unipolar or bipolar morphologies, extending processes along the anterior-posterior (AP) and dorsal-ventral (DV) body axes (Altun and

Hall, 2011) (Figure I-3). VC4 and VC5 neurons are exceptions as they polarize medial-laterally (ML), sending one axon to the right and one to the left, forming a circular tract around the vulva (Figure I-4). Hence, VC4/5 anatomy is distinct from the vulval distal VCs and from all neurons whose cell bodies are born by the ventral nerve cord. In addition, most *C. elegans* neurons are unbranched, with a few exceptions including VC4/5 and HSN motorneurons, which make several simple synapses with the egg laying muscles; and the pairs of PVD and FLP neurons, which make abundant synapses with their target muscles; and other highly branched neurons located at the preanal ganglion (Altun and Hall, 2011).

Figure I-3. The structure of the *C. elegans* nervous system. Inverted fluorescent image of *C. elegans* nervous system at larval stage 1, using a pan-neuronal *gfp* reporter. Adapted from [http://www.sfu.ca/biology/faculty/hutter/hutterlab/research/Ce_nervous_system.html] with permission from Dr. Harald Hutter.

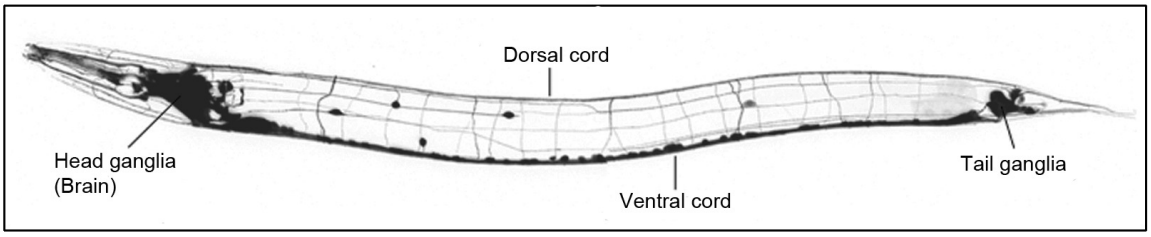

Figure I-4. Ventral Nerve Cord (VNC) motorneurons. VC4 and VC5 polarize medial-laterally concomitantly with vulva organogenesis. A) Schematic diagram of *C. elegans* hermaphrodite (lateral view) showing the positions of the VNC motor neurons cell bodies, between retrovesicular ganglion (RVG) and preanal ganglion (PAG). Adapted from (Altun and Hall, 2011). VC cell bodies are highlighted in green (4, 5) and maroon (1-3, 6). **B)** Ventral view schematics of VC1-6 polarity and positioning relative to the vulva and HSN motor neurons in wild type (Top) and vulvaless animals (Bottom). **C)** Ventral view schematics depicting VC4, VC5 and vulva development from stage L3 to Adulthood. **D)** Confocal images of VC4, VC5 and vulva development from stage L3 to Adulthood (Top); and their corresponding Normaski images (Bottom). VC4 and VC5 were visualized with *Punc-4::gfp* (L3 and early L4) and *Pcat-1::gfp* reporter (mid, late L4 and adult). VC4 is located at the left bottom quadrant of each image. **E)** Representative images of VC4 and VC5 (green) and subsets of vulval precursor cells (blue) at late-L3, early-L4 and mid-L4 stages. VC4 and VC5 and vulval precursor cells were visualized with the *Punc-4::GFP* transgene *cyIs3* and the *Pegl-17::CFP* transgene *syIs59* respectively. Scale bar, 10 μm

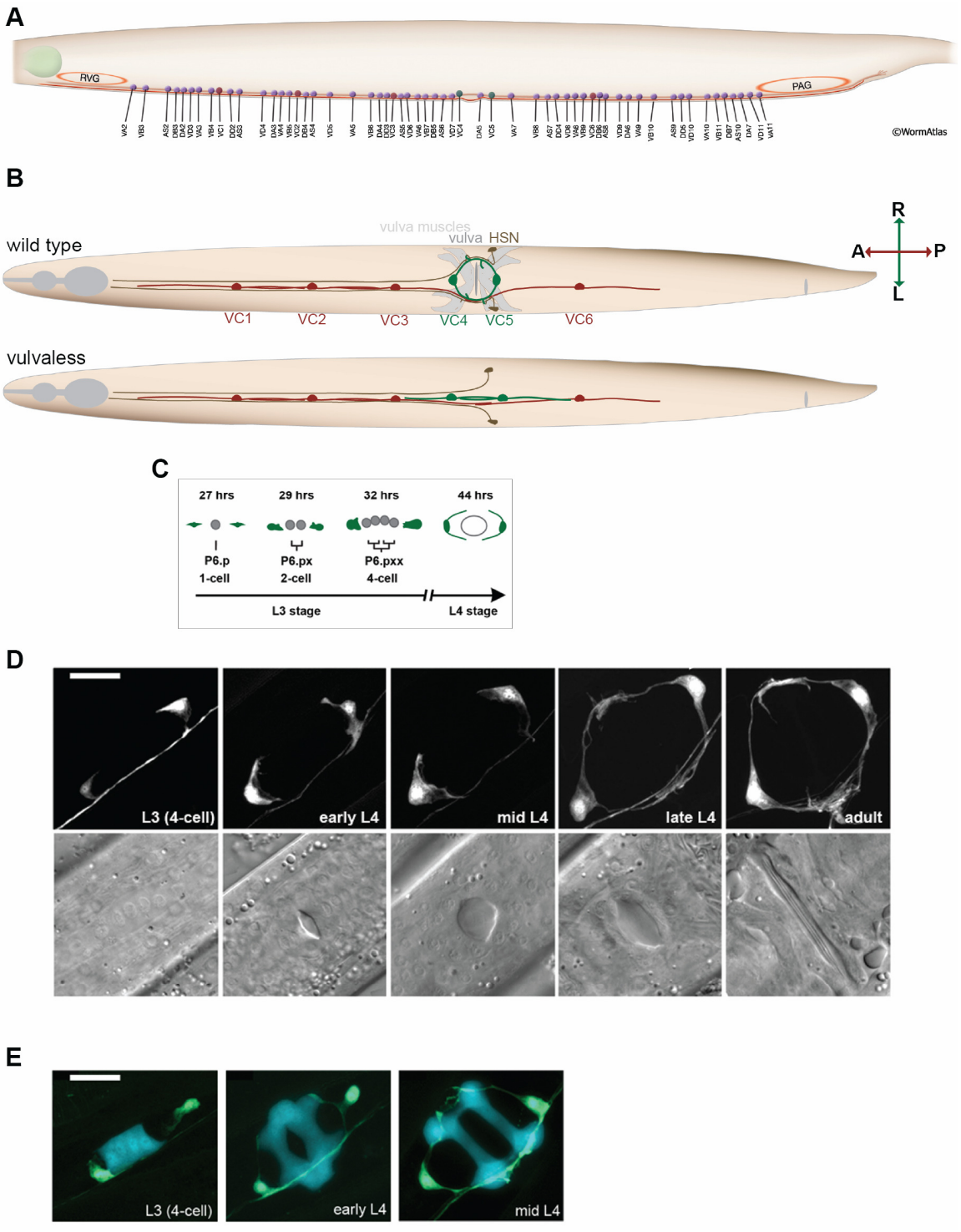
A
RVG
PAG
©WormAtlas
B
wild type
vulva muscles
vulva
HSN
R
A
P
L
VC1
VC2
VC3
VC4
VC5
VC6
vulvaless
C
27 hrs
29 hrs
32 hrs
44 hrs
P6.p
1-cell
P6.px
2-cell
P6.pxx
4-cell
L3 stage
L4 stage
D
L3 (4-cell)
early L4
mid L4
late L4
adult
E
L3 (4-cell)
early L4
mid L4

As mentioned, VC motorneurons make synapses with egg-laying muscles and the HSN motorneurons to control egg-laying behaviour. In the coming section, I will introduce the coordinated development of C. elegans' egg-laying organ and the VCs, which will be followed by a discussion of the preliminary work that gave rise to this thesis' hypothesis

1.2.4 *C. elegans* egg-laying system.

1.2.4.1 Components of the egg-laying organ and role of cell-cell interactions during development.

C. elegans egg-laying requires the coordinated functioning of the gonad, vulva, egg-laying musculature and the innervating neurons. Fertilized eggs, stored in the uterus, are expelled from the gonads through the vulva by contractions of the vulval and uterine muscles (Sulston and Horvitz, 1977). The components of the egg-laying system, including vulva, HSN and VC4/5 motorneurons, and the vulval and uterine muscles, are illustrated in Figure I-4B. Below, I provide an integrative understanding of the individual components and their interactions during development.

The **gonad** primordium consists of four cell types, Z1 and Z4 that generate the somatic gonad, and Z2 and Z3 that generates the germline (Li and Chalfie, 1990). At birth, the gonad is formed by two of each cell types. Microlaser ablation studies and genetic analysis of mutants with misplaced gonads have revealed that the somatic gonad primordium is essential to orchestrate the development of the egg-laying system via cell-cell interactions (Thomas et al., 1990). For example, a specialized anchor cell (AC), descendant of either Z1.pp or Z4.aa granddaughters, secretes a morphogen (epidermal-like growth factor) that promotes vulva formation. In addition, the somatic gonad serves as guideposts to direct the final positioning

of the egg-laying muscles. The AC has yet another crucial morphogenetic role in connecting the uterus and the developing vulva through a cell invasion event (Sharma-Kishore et al., 1999;Sherwood and Sternberg, 2003). AC-induced vulval precursor cells (VPC), descendants of P6.p with a 1^{o} fate, produce a diffusible attractive signal that stimulates AC invasive response (Sherwood and Sternberg, 2003). Briefly, at the P6.p one-cell stage (early to mid L3) the AC is located directly over the P6.p cell and does not cross the basement membrane that separates the gonad and VPCs (Sherwood and Sternberg, 2003). By the P6.p four-cell stage (mid to late L3) the basement membrane becomes interrupted just below the AC cell; and the basolateral side of the AC extend a process that crosses the opening in the basement membrane and through the inner P6.p granddaughters. The membrane process continues to expand during the six-cell stage while the vulva starts to invaginate. By the P6.p eight-cell stage (early L4) the AC has finished invasion and moved to the apex of the vulva. Finally, the AC fuses to the apex while its apical side rests at the uterine lumen (Sherwood and Sternberg, 2003).

The **vulva** forms over a period of 20 hours. Vulva morphogenesis has been extensively characterized, with the time frame of all events described in details (Sharma-Kishore et al., 1999). Consequently, stages of vulva formation constitute hallmark based on which the developmental age of the nematode can be determined. Briefly, the vulva is derived from a row of 12 ventral hypodermal cells (P[1-12].p) that are born during the first larval stage (Sulston and Horvitz, 1977). Six of these (P[3-8].p) are the vulval precursor cells (VPCs), which are equipotent to generate vulva cells (Sulston and White, 1980). During late L2 stage, the anchor cell of the somatic gonad primordium, releases a growth factor (LIN-3) that promotes vulval fate specification (Hill and Sternberg, 1992). VPCs respond to a gradient of

LIN-3 in a dose-dependent manner; inducing the nearest VPCs P[5-7].p to undergo 1^o and 2^o lineages (Kimble, 1981). During L3 stage, cells expressing 1^o and 2^o fates divide to generate vulva cells, while the remaining VPCs P[3,4,8].p, that are more distal from AC, express 3^o fate and their nonvulval daughters fuse with the hypodermal syncytium hyp7 (Kimble, 1981). In the absence of the signal from the AC, all six Pn.p cells adopt the 3^o fate and the animal becomes vulvaless (Kimble, 1981). The LIN-3 factor binds to and activates LET-23, a receptor tyrosine kinase on the surface of the VPCs, which triggers a signal transduction cascade involving Ras (LET-60) and MPK-1 MAP kinase (MAPK) (Sharma-Kishore et al., 1999). MAPK and downstream targets are involved in the decision between vulval and epidermal fates (Greenwald, 1997). Upon induction, P[5-7].p cells undergo a maximum of three longitudinal or transversal cell divisions to generate 22 descendants (Sharma-Kishore et al., 1999). These cells are organized in a row of cells comprising six cell fates (A, B, C, D, F), in a palindromic sequence (Sharma-Kishore et al., 1999). The induction pathway, originated in the AC, works simultaneously with a lateral signalling pathway among the vulval cells that stabilizes their fates (Greenwald, 1997). During L4 stage, the 22 cells form the vulva via morphogenesis/organogenesis, a process that involves a series of cell migrations (toward the center of the vulval primordium) and cell fusions, which results in the formation of a stack of 7 toroids (VulA to VulF) organized at the midline (Sharma-Kishore et al., 1999). More fusions between rings and reorganizing of the tubular structure happen before the vulva reaches a final morphology that connects the uterus with the outside environment (Sharma-Kishore et al., 1999).

The **egg-laying musculature** includes uterine and vulval muscles which are derived from two sex myoblasts (SMs) (Thomas et al., 1990). SMs are born at the end of L1 stage, at

the posterior ventral muscle quadrants, one on each side of the animal (Thomas et al., 1990). During L2, the somatic gonad primordium induces the SMs to migrate anteriorly until they reach the center of the developing gonad (Thomas et al., 1990). During L3, each SMs undergo three cycles of cell division, to generate a total of 16 egg-laying muscle cells that are innervated and regulated by the HSN and VC motorneurons (Thomas et al., 1990). Eight of these are uterine muscle cells, attached circumferentially around the uterus, that contract to expel the eggs from the gonad; and the rest, eight vulval muscle cells that attach to and contract the vulva, creating an opening to lay eggs (Sulston and Horvitz, 1977;Thomas et al., 1990;Garriga et al., 1993). The extensive presence of gap junctions interconnecting the uterine and vulva muscles is thought to cause the musculature to contract synchronously (Garriga et al., 1993).

Predominantly serotonergic **HSNs** and predominantly cholinergic **VCs motorneurons** synapse directly and form a neuronal circuitry that stimulate the contractions of the egg-laying muscles (Garriga et al., 1993). The two **HSNs** are a pair of bilaterally symmetric neurons (right and left) that are born during embryogenesis, in the tail of the embryo, and then migrate anteriorly to a lateral position, posterior to the center of the gonad (Thomas et al., 1990;Garriga et al., 1993). The HSNs extend axons postembryonically. During early L4, each neuron grows an axon ventrally that enters the ventral nerve cord (VNC) and then extends anteriorly to the nerve ring. HSNs axons run parallel to each other, along the ipsilateral VNC bundle, with a brief defasciculation at the vulva (Garriga et al., 1993). The **VCs** is a set of six bipolar postembryonic neurons (VC1-6), born during the first larval stage, and whose cell bodies lay on the VNC. VC1-3 and 6 axons are oriented in the anterior-posterior axis along the length of the worm. However, VC4 and VC5 cell bodies flank both

sides of the vulva and extend axons that are polarized medial-laterally, forming a circular nerve tract around the egg-laying organ (Colavita and Tessier-Lavigne, 2003).

Both classes of motorneurons contain multiple neurotransmitters. The HSNs contain at least three: serotonin, acetylcholine and FMRFamide related neuropeptide (Waggoner et al., 1998); similarly, the VCs contain acetyl choline, FMRFamide related neuropeptides and possibly also serotonin (Waggoner et al., 1998). Although, VC4 and VC5 contain the vesicular monoamine transporter CAT-1, that transports serotonin, they don't express the serotonin biosynthetic enzyme tryptophane hydroxylase (HERE + schafer 2006). Yet, VC4 and VC5 stain weakly for serotonin, which could enter the neurons by reuptake from neuromuscular junctions (Schafer, 2006).

Both HSNs and VC4/5 synapse extensively with the egg-laying muscles (White et al., 1986). In comparison with VC4 and VC5, vulval-distal VCs (VC1-3 & 6) make fewer synapses with the egg-laying musculature than VC4 and VC5 (Schafer, 2005). Additionally, HSNs also synapse with VC4/5 (White et al., 1986). Thus, the egg-laying circuitry comprised of HSNs and VC4/5 is connected and possibly also synchronized. Importantly, elimination of HSNs either by mutation or laser ablation results in egg-laying defective animals (*egl*), which retain developing eggs and become severely bloated; by contrast hermaphrodites lacking the VC4/5 neurons displayed no obvious egg-laying defects (Sulston and Horvitz, 1981;Trent et al., 1983;Desai et al., 1988;Desai and Horvitz, 1989). In other words, while the HSNs have been known to be necessary for egg-laying, the role of VC4/5 in this behaviour had remain unclear (Garriga et al., 1993), until more recently when Waggoner *et al* performed a more accurate assessment of the role of VCs in egg-laying (Waggoner et al., 1998). First they

complemented previous studies. When the authors ablated both neuron types, HSNs and VC4/5 simultaneously, thus removing the entire egg-laying circuitry, they found that the severity of the *Egl* phenotype was significantly increased compared to animals lacking only HSNs (Waggoner et al., 1998). Double HSNs/VC4,5 ablated animals failed to lay eggs even in the presence of exogenous serotonin, contrasting with serotonin egg-laying stimulating effects on HSN-only ablated nematodes (Waggoner et al., 1998). These results hinted at a role for VCs in egg-laying behaviour and suggested that acetylcholine, a neurotransmitter produced by both types VC4/5 and HSNs motorneurons, played a critical role (Waggoner et al., 1998). Waggoner *et al* characterized the behavioural pattern of egg-laying in wild type animals; concluding that animals alternate between an active phase (eggs laid in clusters) and an inactive phase (eggs retained in uterus). They established a model that accurately describes egg-laying behaviour, which allowed them to finely quantify differences between temporal patterns of egg-laying in nematodes with mutations or neuronal ablations (Waggoner et al., 1998). While assessing the egg-laying parameters in HSNs ablated animals, they observed that HSNs were dispensable for efficient egg-laying during the active phase; instead they found an increased rate of egg-laying during this phase. In essence, in HSN-ablated worms, eggs were still laid in clusters similarly to wild type; however the inactive phase was significantly longer, which accounted for the severe Egl phenotype (Waggoner et al., 1998). Since the most significant neurons beside the HSNs to innervate the egg-laying musculature are VC4/5, they hypothesized that VC4 and VC5 did indeed play a role (Waggoner et al., 1998). They found that VC4/5-ablation resulted in a small but significantly rise in the time between clusters, and similarly to HSNs-ablation, in an increased rate of egg-laying during the active phase. Finally, by conducting these neuron

ablation experiments together and some pharmacological studies, they concluded that serotonin induces the active phase while acetylcholine triggers individual egg-laying events (Waggoner et al., 1998). To summarize, they proposed a comprehensive model which explains how HSNs and VC4/5 cooperate to control egg-laying (Waggoner et al., 1998) (Figure I-5).

Figure I-5. **Model of neuronal and pharmacological control of egg-laying in *C. elegans*.** Serotonin released mostly by HSNs triggers the onset of the active phase through binding to serotonin receptors in the muscles. Acetylcholine released by both HSNs and VC4/5 trigger individual muscle contractions and consequently egg-laying events during the active phase through binding to nicotinic receptors on the egg-laying muscles. Image taken, with permission, from (Waggoner et al., 1998).

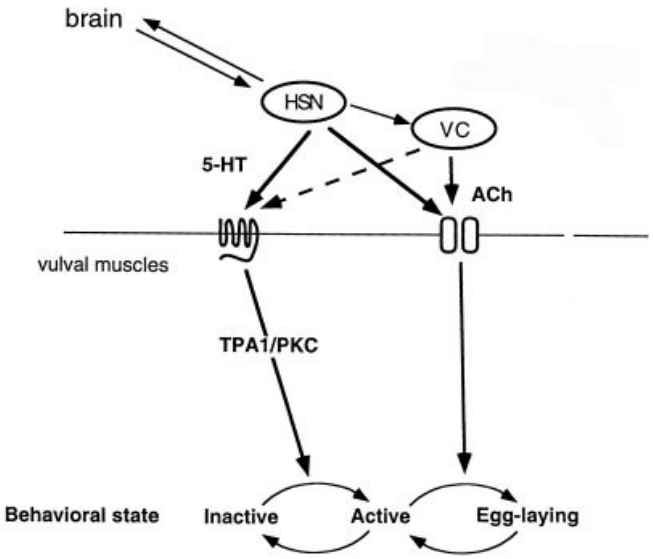

In summary, the vulva-innervating motorneurons, VC4 and VC5, represent an exciting model in which to study neuronal polarity. VC4 and VC5 are uniquely attractive as they extend processes, which are orthogonal to the orientation of the VNC neurons including that of the vulval-distal VCs, in response to organ-derived polarizing cues (Li and Chalfie, 1990). See coming section.

1.2.4.2 VC4 and VC5 motorneurons innervate the vulva during organogenesis

Although VC motorneurons and vulva epithelia share a common ancestor in ventral Pn blast cells, their birth is spaced in time by a few developmental stages. VCs are born during the L1 stage, while the VPCs are born during L3 to early L4. However, since the VCs and vulva tight physiological relationship is concurrent with a connected lineage (both discussed previously), it is no surprise that the onset of VC4/5 terminal differentiation is delayed to match the timing of vulva morphogenesis (Li and Chalfie, 1990), with a remarkably conserved sequence of events. In other words, VC4 and VC5 polarization is coordinated with vulva morphogenesis, as the neurons' orientation is dependent on polarizing cues from the vulva (Li and Chalfie, 1990). Briefly, during L1 stage, prior to vulva development, VC4 and VC5 are born. Early in the L3 stage (~ 30 hours post-hatching), primary VPC P6.p (1-cell stage) divides once producing two daughter cells (2-cell stage), while the VC4/5 neurons exhibit anterior-posterior protrusions (Sanchez-Alvarez et al., 2011). Presumably VC4/5 "wait" to receive a polarizing cue from the to-be-innervated organ. By 34 hours, the two primary VPC cells divide to generate four granddaughter cells (4-cell stage) (Sanchez-Alvarez et al., 2011). In wild type nematodes, VC4 and VC5 motorneurons are generally flanking these four VPC cells. At the four cell stage VC4/5 display protrusions that are

oriented towards the four granddaughters of P6.p. The early L4 stage is marked by a small invagination in the incipient lumen of the vulva, just at the time when VC4/5 growth cones are largely resolving into axons, that project along the new medial-lateral axis created by the vulval primordium (Sharma-Kishore et al., 1999). During mid L4 stage ~40 hours, characterized by the Christmas tree morphology of the vulva, VC4/5 axons continue to extend around the developing organ. Finally, by the young adult stage ~ 44-50 hours, when the vulva slit is formed (Sulston and Horvitz, 1977), VC4/5 have formed a complete circular tract that branch at the vulval muscles and connect with the HSN neurons via synapses (Garriga et al., 1993), creating a neural circuit that controls egg-laying muscles to assist egg-laying behaviour. P6.p and its progeny can be used to assign an approximate developmental age of a nematode. During vulva organogenesis, VC4/5 and the vulval primordium are in close physical contact. For instance, in Figure I-4E, the growth cones of VC4/5 emerging axons appear to be “hugging” the vulva cells. This intimate contact may hint to the existence of axon guiding cues on the surface of VPCs.

1.2.4.3 The vulva is a source of polarizing signals for VC neurons.

Previous studies addressing the biological relationship between the vulva and development of innervating neurons (VC4/5 and HSNs), have shown that the vulva epithelium plays a pivotal guidepost role in the formation and assembly of the egg laying neural circuit, particularly in neurite orientation and branching (Li and Chalfie, 1990). Cell interactions between VPCs and developing VC4/5 are particularly important in instructing neuron morphology and maturation (Li and Chalfie, 1990). For instance, in vulva-ablated animals, VC4 and VC5 axons orient antero-posteriorly instead of medial-laterally (right-left),

similar to the remaining VCs, and exhibit no branches; while in multivulva specimens the closest VCs to the ectopic vulva exhibit medial-lateral orientation and branches, just like wild type VC4/5 neurons (Li and Chalfie, 1990). These results suggested that the vulva region regulates neuron orientation and induces branching. Accordingly, to uncover the source of VC4/5 neuron branching and polarizing cues, a series of genetic studies and laser microsurgery was performed to assess the contribution of the individual components of the egg-laying system. Three components were examined, vulva epithelium, vulval muscles, and innervating neurons. This study showed that both, target egg-laying muscles (demonstrated by ablating the M progenitor cell) and the nearby HSNs (demonstrated by using *egl-1* mutant) had no detectable effect on VC4/5 polarity and or branching. However, the vulva epithelium (demonstrated by ablating the AC cell) was found to instruct neuron morphology and were deemed to be the source of branch-inducing signals and axon orientation. The unique medial-lateral orientation of VC4/5 neurons compared to the other VCs, and the equipotency of all VCs to acquire ML or AP orientations depending on the proximity to vulva epithelia, represents an exceptional context in which to study the establishment and maintenance of neuronal polarity.

In our laboratory, we use VC4 and VC5 neurons of *C. elegans* as a simple developmental model to study the mechanisms involved in the establishment and maintenance of neuronal morphology/polarity. To visualize the development of VC4/5 neurons and follow up the formation of their processes we mainly use two reporter strains, *cyIs3* [*Punc-4::gfp*, *rol-6*] (active from early larval stages to adult) that labels all VCs; and *cyIs4* [*Pcat-1::gfp*, *rol-6*] (ON from early L4 to adult) in which both VC4/5 are specifically GFP-labelled, but not the remaining VCs (1-3, 6). *cat-1* encodes a vesicular monoamine

transporter (Colavita and Tessier-Lavigne, 2003). Throughout this thesis, worm stages have been determined by specific traits of vulva development.

1.2.4.4 PCP gene *vang-1* mutants display ectopic axon outgrowth in VC4 and VC5 motorneurons.

Previously in our laboratory, two mutant alleles (*zy1* and *zy2*) of *C. elegans* homolog of *strabismus/Van Gogh* (*vang-1*), displaying VC4 and VC5 polarity defects, were isolated during a forward genetic screen using the *cyIs4* parental strain. Mutations in the *vang-1* gene disrupted the bipolar morphology of VC4/5, resulting in the extension of ectopic axons along the AP axis (tripolar phenotype). This result hinted at a role for *vang-1* in suppressing ectopic AP axon outgrowth. Genetic analysis of the *vang-1* deletion mutant *tm1422*, a predicted null (Hoffmann et al., 2010), later confirmed this result (Sanchez-Alvarez et al., 2011). Strabismus is a core gene in the Planar Cell Polarity (PCP) signalling pathway, which has been shown to interact genetically and physically with other core PCP components (see next section). Accordingly, in a quest for other genes involved in the same phenotype, our laboratory performed an RNAi screen including homologues to several PCP players, which revealed that downregulation of *prkl-1* and *dsh-1* phenocopied the *vang-1* mutant tripolar phenotype (J. Visanuvimol and A. Su, unpublished data). At the same time, I was mapping a mutant with the same tripolar phenotype, the identity of which I will reveal in Chapter I with a discussion of potential links to PCP.

Altogether, these results suggest a novel outcome for the PCP pathway in **neuron polarity**. Accordingly, this thesis started with 1) the need for genetic analysis to confirm that these individual PCP components were signalling in a PCP-like pathway to regulate VC4/5

polarity, 2) the need for genetic screenings to search for new mutants with a similar phenotype, and 3) the need to explore the mechanism by which PCP signalling, specifically *prkl-1* and *dsh-1* suppressed ectopic AP axon formation.

As discussed, defective expression of three PCP genes individually disrupts the normal left-right bipolar orientation of VC4 and VC5 neurons. This may suggest that PCP signalling may underlie their ability to polarize medial-laterally instead of anterior-posteriorly. In the coming section, I will introduce the conserved PCP pathway in different species and contexts. I will discuss the players (with emphasis on prickle, dishevelled and direct interacting partners) (see 1.3.1), distinct read-out phenotypes of PCP signalling and molecular mechanisms (see 1.3.2-1.3.6), and I will finalize discussing the link between PCP and neurological disease in humans (see 1.3.7). The following section will delineate rationale, hypothesis and objectives of this thesis.

1.3 Mechanisms of tissue polarization │ Planar Cell Polarity (PCP) pathway.

1.3.1 PCP concept and core players.

The Planar Cell Polarity pathway has been cleverly termed "the developing cell's compass" (Vladar et al., 2009) based on its ability to orient and inform cells of their position in three dimensions (Simons and Mlodzik, 2008). Thus, the term PCP is used to explain the coordinated orientation of cells and cellular structures within the planar dimension of an epithelial surface, which is orthogonal to the apical-basolateral axis of epithelial cells (McNeill, 2010); and also to describe the polarized migration of masses of cells during embryonic development (Wallingford et al., 2002). PCP was first acknowledged in *Drosophila* following observations of the disrupted patterning of cuticular structures (*i.e.*

wing hairs and body bristles) and the compound eye displayed by *dishevelled* and *frizzled* mutants (Fahmy and Fahmy, 1959); (Gubb and Garcia-Bellido, 1982; Adler and Lee, 2001) (Figure I-6). Yet, it wasn't until late 80's when the first PCP genes were cloned and PCP research took momentum (Vinson et al., 1989;Klein and Mlodzik, 2005). Extensive research has since uncovered a phylogenetically conserved PCP signalling pathway that is essential for numerous developmental processes, including accurate vision and hearing (see 1.3.2 and 1.3.3), neural tube and eyelid closure (see 1.3.4) and axon formation and orientation (see 1.3.5). Accordingly, disruption of PCP signalling has been linked to developmental anomalies including spina bifida (see 1.3.9) and polycystic kidney disease (Fischer et al., 2006).

Molecular and genetic studies have identified several "core" PCP genes. They encode proteins of different molecular nature, including multidomain cytoplasmic proteins Dishevelled (Dsh/ Dvl) (Klingensmith et al., 1989;Gubb et al., 1999a), Prickle (Prkl/ Pk) (Gubb et al., 1999b), and the ankyrin repeat protein Diego (Dgo) (Feiguin et al., 2001;Das et al., 2004); and membrane proteins Van Gogh (Vang/ Vangl, a.k.a. Strabismus) with four transmembrane domains (Wolff and Rubin, 1998; Taylor et al., 1998); and Frizzled (Fz) (Vinson et al., 1989) and atypical cadherin Flamingo (Fmi, a.k.a. Starry night/ Stan) (Usui et al., 1999), both with seven transmembrane domains. It has been shown that core PCP proteins become asymmetrically localized in the cell before any overt evidence of morphological polarization, which is a critical step in the establishment of PCP (Vladar et al., 2009) (Figure I-6). Unlike Wnt, Fz, Vang and Dsh, which are known to function in PCP (non canonical) and β-catenin (canonical) pathways (Wallingford et al., 2000; Park and Moon, 2002; Wang and Wynshaw-Boris, 2004; Wallingford and Habas, 2005), Prkl has been

exclusively associated with PCP signalling (Jenny et al., 2003; Deans et al., 2007; Mapp et al., 2011; Daulat et al., 2012).

VAN GOGH/Strabismus encodes a membrane protein containing a serine-rich N terminal cytoplasmic region, four transmembrane domains, and a large intracellular C terminus with two Strabismus-homology domains (STH1 and STH2) that are highly conserved between (Katoh, 2002). STH2 consists of the last 17 amino acids including a C-terminal PDZ domain binding motif (PBM, Ser/Thr-X-Val) that has been implicated in binding with DVL proteins (Katoh, 2002).

PRICKLE is a modular protein with a PET domain (for **P**rickle, **E**spinas, **T**estin), that is only found in Prickle like proteins (Bach, 2000), and has 3 LIM domains (for **L**in-11, **I**sl-1, **M**ec-3) (Bach, 2000). PRKL also contains a C-terminal CAAX consensus motif which suggests that it may be post-translationally modified by farnesylation and that this domain may be important for membrane localization (Bach, 2000). The biological function of the PET domain remains elusive. The LIM domain is a conserved cysteine-histidine rich, zinc-coordinating domain, consisting of two tandemly repeated zinc fingers (Bach, 2000). Unlike GATA type zinc fingers, LIM domains do not appear to bind DNA. Instead, they have been implicated in protein-protein interactions and in assembling multiprotein complexes (Bach, 2000).

DISHEVELLED is a multifunctional protein composed of an N-terminal DIX domain (involved in the canonical pathway (Pan et al., 2004), a central PDZ domain, and a C-terminal DEP domain (crucial for PCP signalling (Wang et al., 2006a). Dishevelled lays at the crossroads of Fz signalling. In brief, upstream of both canonical and non canonical

pathways, the Frizzled receptor is bound by the Wingless (Wnt) ligand at the cell surface; the signals are then transduced via Dishevelled (Wallingford and Habas, 2005). Depending on the context and developmental stage of the cell, this interaction would result in activation of the canonical pathway leading to cell fate specification or activation of the PCP/non-canonical pathway leading to cell polarization; through distinct downstream effectors (Wallingford and Habas, 2005).

A different group of PCP proteins that are essential for planar polarity in every *Drosophila* tissue do not become asymmetrically localized within the cell; rather their levels are graded across the tissue (Simons and Mlodzik, 2008). This group includes two very large cadherins, **Fat** (Ft) and **Dashous** (Ds), and a Golgi associated-kinase **Four-jointed** (Fj); which form the Ft/Ds/Fj polarity cassette (Simons and Mlodzik, 2008). Also known as the "global module", Ft/Ds/Fj coordinates PCP globally in all the cells of the tissue, by translating tissue-wide gradients of signals and transmitting the polarity information downstream into core PCP proteins; which then amplify and stabilize subcellular asymmetries (Axelrod, 2009).

1.3.2 Role of PCP signalling in orienting epithelial hairs and cilia.

PCP has been best illustrated by the development of an actin-based **hair** on the fly wing (Fanto and McNeill, 2004). Thus, each epithelial cell produces a single hair located at the distal cell edges (Fanto and McNeill, 2004). All hairs align along the proximal-distal axis, pointing uniformly towards the distal end of the wing (Fanto and McNeill, 2004). This organized pattern is disrupted in PCP mutants, while the cells retain their apical-basolateral polarity (Fanto and McNeill, 2004) (Figure I-6). PCP genes control the subcellular

localization, the orientation and the number of hairs extended by each cell. Fz is thought to receive the polarizing cue and transduce the signal (Saburi and McNeill, 2005).

An important step towards understanding the PCP mechanism was reached with the discovery that PCP proteins become asymmetrically localized during establishment of polarity (Fanto and McNeill, 2004). While FZ, its adaptor DSH, and DGO accumulate in the apical distal membrane of the hair cell, PRKL and STBM localize to the apical proximal side (Fanto and McNeill, 2004). However, FMI concentrates in both proximal and distal borders, where it is thought to coordinate polarity by providing intercellular communication (Saburi and McNeill, 2005). Moreover, STBM and PRKL interact physically. Initially, STBM recruits PRKL to the membrane and PRKL promotes clustering of STBM. Both proteins mutually influence their subcellular localization (Jenny et al., 2003). Similarly, FZ and DSH form a complex. It has been proposed that PRKL could block the recruitment of DSH to FZ, thereby antagonizing FZ signalling (Jenny et al., 2003). However, the asymmetric distribution of polarity proteins does not take place in all cell types where PCP establishes polarity, for instance PRKL and DSH do not localize asymmetrically in elongating myocytes (Gros et al., 2009). Moreover, the global module acting upstream of core PCP proteins is not asymmetrically distributed within individual cells. Instead, DS and FJ are expressed in gradients over the tissue. While FT is expressed evenly in the tissue; DS and FJ are graded in opposing directions (McNeill, 2010). Thus, DS is expressed at high levels at proximal regions in the wing and fades away towards the distal edge; whereas FJ expression is higher at distal regions and declines towards the proximal border (McNeill, 2010). Furthermore, DS and FT form asymmetric heterodimers which bridge cell borders and provide spatial cues to orient the planar polarity of the cells (McNeill, 2010).

A well studied example of PCP signalling in vertebrate is displayed by the sensory epithelia in the mouse inner ear (Deans et al., 2007). The apical surface of each sensory epithelial cell has a set of actin-based stereo**cilia** uniformly oriented relative to a single microtubule-based kinocilium (Uemura and Shimada, 2003). The precise alignment of this arrangement is coordinated by the PCP pathway and is critical for proper hearing and balance (Wang and Nathans, 2007;Deans et al., 2007).

1.3.3 Role of PCP signalling pathway in polarized orientation of the ommatidia in *Drosophila*'s compound eye.

While the basic unit of polarity in the wing is a single epithelial cell, the eye has a stereotypically arranged cluster of cells named ommatidium. Each ommatidium contains 8 photoreceptors (R1-R8) and several accessory cells (Fanto and McNeill, 2004). There are two PCP fields in the eye disc (dorsal and ventral) that are divided by a midline. PCP is established during the larval stage when ommatidia preclusters rotate 90^{o} clockwise on the dorsal side (resulting in ommatidia that point up) and counterclockwise in the ventral side (resulting in ommatidia that point down) (Fanto and McNeill, 2004) (Figure I-6). As a result, dorsal and ventral ommatidia have opposite orientations. After rotation, symmetry breaks within the cluster resulting in ommatidia with different chiralities on the dorsal and ventral fields. This organized pattern of ommatidia in the eye is essential for accurate vision (Fanto and McNeill, 2004). PCP signalling specifies both the direction of ommatidia rotation and the chirality (Fanto and McNeill, 2004). Interestingly, both loss- and gain-of-function of core PCP genes result in similar disruption of this organized pattern (Fanto and McNeill, 2004). In addition, PCP proteins accumulate asymmetrically at the R3/R4 interface (Axelrod, 2001;

Bastock et al., 2003; Jenny et al., 2003). Similar to the hair cells, in the eye, STBM and PRKL interaction is important for their confinement to their specific membrane locations and also for regulating FZ/DSH signalling activity (Jenny et al., 2005).

How is the Fz/PCP signal transduced downstream, to the cytoskeleton, in order to arrange such a complex cluster of cells? Although FZ is a seven-pass membrane protein with extracellular N terminus and intracellular C terminus, a serpentine structure reminiscent of classical G Protein Coupled Receptors, trimeric G proteins were shown to transduce Fz PCP signalling in the compound eye only a few years ago (Katanaev et al., 2005). Genetic and pharmacological evidence implicated $G\alpha_0$ including 1) pertussis toxin suppresses the Fz overexpression phenotype and 2) loss- and gain-of-function G_0 mutations disrupt PCP signalling in *Drosophila* eyes (Katanaev et al., 2005).

Figure I-6. PCP outcomes in *Drosophila*. A) Images of phalloidin-stained pupal wing epithelium in wt (top) and PCP mutant (bottom). The organized patterning of the wing hair is disrupted in PCP mutants. **B)** Thorax in wt (left) and PCP mutant (right). The uniform orientation of bristles and hairs is disrupted in *vang-1* mutants. **C)** Ommatidia in wt (left) and PCP mutant (right). Below, black and red arrows indicate the orientation of ommatidia above and below the equator (yellow line), respectively. The arrangement of photoreceptors in each ommatidium and the arrangement of the ommatidia with respect to the whole eye is disrupted in PCP mutants. **D)** Some PCP proteins are asymmetrically distributed in the apical membrane of wing hair cells. STBM recruits PK to the proximal membrane whereas Fz recruits DSH to the distal membrane. FMI is evenly distributed to both ends. **E)** Logic of asymmetric localization. Apical view of two hair cells undergoing PCP. FMI forms homotypic complexes on both ends of the membrane; whereas STBM/PK complexes and FZ/DSH/DGO complexes engage in mutually exclusive protein-protein interactions to maintain polarized distribution. DGO antagonizes the inhibitory action of PK on FZ/PCP signalling. Images taken with permission from (Vladar et al., 2009) [A, D], (Heisenberg, 2002) [B], (Jenny et al., 2003)[C] and (Seifert and Mlodzik, 2007) [E].

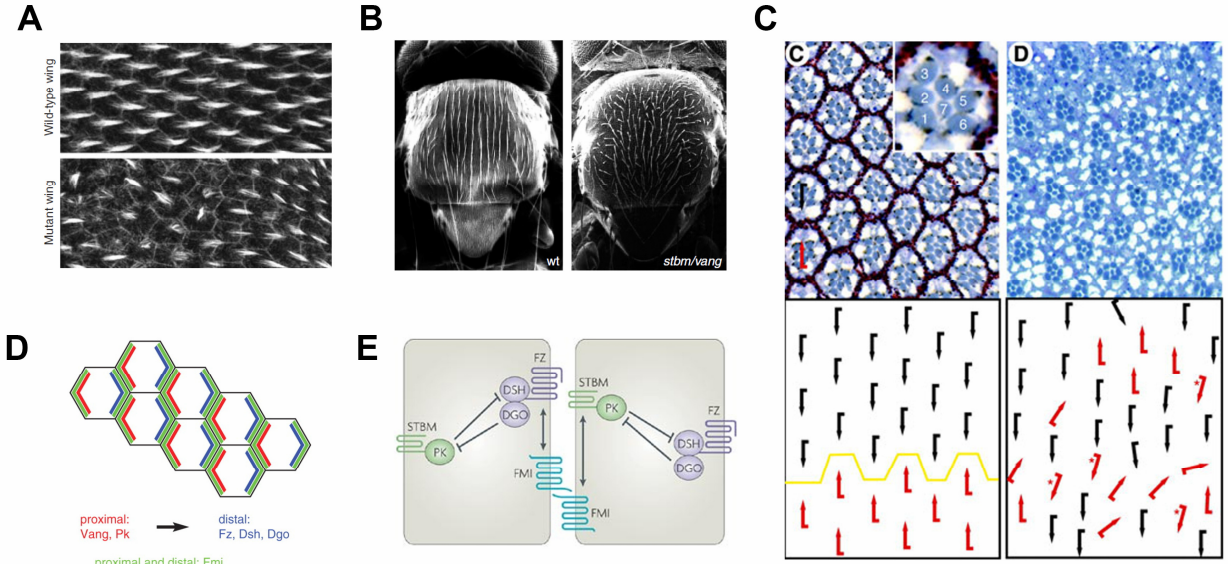

1.3.4 Role of PCP signalling in regulating convergent extension during gastrulation and neurulation in vertebrates.

During **gastrulation**, mesenchymal cells elongate laterally and move directionally to intercalate with neighbouring cells, resulting in convergence in one plane and extension in the perpendicular direction. This process, called **Convergent Extension** (CE), is the basis for the lengthening and narrowing of the embryonic axis and neural plate. CE can be disrupted in zebrafish by mutations in *Prkl* (Veeman et al., 2003;Carreira-Barbosa et al., 2003;Takeuchi et al., 2003) and in *Vangl-2* (*trilobite*) (Jessen et al., 2002); in Xenopus by mutations in *prkl* (Takeuchi et al., 2003) and by interfering with *Dvl* (Wallingford and Harland, 2001;Copp et al., 2003a) and *Stbm* function (Kibar et al., 2001). In mice, *Vangl2* mutants (Kibar et al., 2001;Murdoch et al., 2001); *Celsr1* mutants (*flamingo*) and double KO mutants $dvl1^{-/-};dvl2^{-/-}$ (Wang et al., 2006a) and $fz3^{-/-};fz6^{-/-}$ (Wang et al., 2006b) all have shortened and wider embryos caused by deficient CE. Interestingly, $fz3^{-/-};fz6^{-/-}$, $dvl1^{-/-};dvl2^{-/-}$ and $vangl2^{-/-}$ PCP mutants show severe **Neural tube closure** (NTC) defects in which the entire neural tube from mid-brain to tail fails to close, a congenital condition known as craniorachischisis in humans (Wang et al., 2006a). Closure of the neural tube involves precise morphogenetic cell movements within the neural plate and neighbouring tissues which resemble CE. An elongated neural plate develops a U-shaped groove in which the folds in the dorsal walls eventually fuse at the midline to create the neural tube (Wang and Nathans, 2007). Additionally, many of the PCP mutant mice also display **eyelid closure** defect. Eyelid closure, like NTC, occurs around E16 in the mouse and involves a medial convergence of a pair of flanking epithelial sheets (Wang et al., 2006a).

1.3.5 Role of PCP signalling in axon extension and orientation.

PCP has also been shown to play a role in the developing nervous system of the mouse and *C. elegans*. From a structural point of view, an axon is a long microtubule-filled membrane. Thus, it seems reasonable that PCP signalling would control **axon extension** and **orientation** in a similar way it does microtubule-filled kinocilia. Accordingly, inactivation of either *Fz3* or *Celsr3* (*fmi*) in the mouse caused a very dramatic axon-less phenotype (Wang et al., 2002;Tissir et al., 2005). Lack of either *Fz3* or *Celsr3* eliminates the major axon tracts that connect the thalamus and the cortex (Wang et al., 2002;Tissir et al., 2005). Proliferation and migration of cortical neurons were largely unaffected. In addition, dendrites were able to reach maturity. Interestingly, the expression patterns of their transcripts are overlapping in the CP of the cerebral cortex (Tissir et al., 2005). Thus, the similar phenotype of the KOs and the overlapping expression profiles in the cortex suggest that Celsr3 and Fz3 are interacting in a PCP like pathway which controls axon formation in cortical neurons (Tissir and Goffinet, 2006). Coincidently, Dvl3 transcripts are also present in postmitotic neurons and absent from zones of proliferation (Tissir and Goffinet, 2006) which may hint at a role for Dvl3 in the same pathway.

Besides, some PCP genes have been shown to orient *C. elegans* neurons within the anterior-posterior (AP) axis (Hilliard and Bargmann, 2006). Many *C. elegans* neurons extend anterior-posterior processes, including the left and right PLM bipolar motorneurons (White et al., 1986). PLM neurons, whose cell bodies inhabit the posterior lumbar ganglion, extend one long anterior process to the middle of the body and a short posterior process (White et al., 1986). PLM orientation, however, was inverted in *Wnt* mutant *lin-44* and *Frizzled* mutant *lin-17* (Hilliard and Bargmann, 2006). In addition, LIN-44 wild type expression at a location

posterior to PLM cell body is required for the asymmetric localization of LIN-17 to the posterior process (Hilliard and Bargmann, 2006). Thus, LIN-44 triggers PCP signalling through LIN-17, to translate the directional cue into PLM polarity (Hilliard and Bargmann, 2006).

1.3.6 Role of VANG, DSH and PRKL in human neurological disease, in particular neural tube defect and epilepsy.

An unprecedented study led by P. Gros from McGill University, recently established a causative link between mutations in the human ***vangl-1*** gene and **neural tube defects** in humans (Kibar et al., 2007). Neural tube defects (NTDs) such as anencephaly and spina bifida are the second most common birth defect in humans, affecting 1 to 2 infants per 1000 births (Copp et al., 2003). All infants with anencephaly eventually die, whereas infants with spina bifida survive with severe disabilities (Copp et al., 2003). Based on the role of PCP in neurulation in other vertebrates (see previous section), Kibar, Z *et al,* hypothesized that mutations in VANGL-1 and/or VANGL-2 were linked to NTDs in humans (Kibar et al., 2007). Thus, the authors analyzed the coding regions to both *vangl* genes of a large group of patients with neural tube defects, including familial and sporadic cases and identified three variants of VANGL-1 linked to this phenotype (Kibar et al., 2007). A protein alignment of the regions flanking each VANGL-1_NTD linked mutation, which included sequences of nine species from *C. elegans* to Human, revealed that the three mutated positions were highly conserved throughout evolution; in particular V239 was identical in every single species and part of an invariant "VLLE" motif (Kibar et al., 2007). Significantly, the V239I missense mutation introduces a bulky group at a functional cost, as it abrogates VANGL-1 interaction with the three human DVL/DSH proteins (Kibar et al., 2007). The disrupted protein-protein

interaction likely prevents DVL recruitment to the plasma membrane which affects subsequent downstream signalling leading to neural-tube closure (Kibar et al., 2007). Interestingly, a finding that both gain-of-function and loss-of-function of Xenopus *prkl* resulted in embryos with spina bifida (Takeuchi et al., 2003), may suggest a similar link between PRKL and NTD.

More recently, it was published that mutations in *prkl* orthologs result in epileptic seizures in human, mice and flies (Bassuk et al., 2008;Tao et al., 2011). Epilepsy is a debilitating chronic disease characterized by recurrent seizures that affects 1% of the population (Frankel, 2009). In a previous report Bassuk *et al* described a homozygous recessive mutation in PRKL-1 present in families with myoclonus epilepsy (Bassuk et al., 2008). Consequently, they hypothesized that there is an association between PRKL function and epilepsy (Tao et al., 2011). Since the link between PRKL-1 and PRKL-2 had not been established, Tao, H *et al* sequenced the open reading frame and the intron-exon boundaries of *prkl-1* and *prkl-2* genes, from a large group of unrelated patients with myoclonus epilepsy (Tao et al., 2011). The authors found two missense mutations in PRKL-1 (in addition to the one from the first report), two missense mutations in PRKL-2 and a chromosomal deletion encompassing the *prkl-2* gene that were all linked to the disease (Tao et al., 2011). Interestingly, the four patients with missense mutations were heterozygous for the variants (Tao et al., 2011). Since both, heterozygous and homozygous *prkl* mutations, in humans and other organisms, cause myoclonus epilepsy, it is reasonable to conclude that PRKL dosage is critical to normal brain function (Tao et al., 2011). Moreover, the authors were able to reproduce some of these mutations in flies and mouse, which recapitulated the human

seizures phenotype and further confirmed the link between PRKL and epilepsy (Tao et al., 2011).

Without a doubt, these studies are a major breakthrough in understanding human neurological diseases. The study by Kibar, Z *et al* implicated VANG and DSH as risk factors in human neural tube defects; and the study by Tao, H *et al* implicated PRKl as risk factor in devastating epileptic conditions. These results are the natural progression of significant research that started in model organisms, which validates the necessity to better understand the role of PCP in the nervous system, using a variety of model systems. In the light of these findings, investigating the role of PCP genes, specifically PRKL and DSH in nerve cells polarization during development will likely translate into relevant data to the physiology and disease of the human nervous system. This is the long term goal of my thesis.

1.4 Rationale, Hypothesis and Objectives

C. elegans vang-1 mutants exhibit polarity defective VC4 and VC5 motorneurons (*i.e.* tripolar neurons with ectopic AP axons). This result together with a preliminary finding showing that RNAi-mediated downregulation of *prkl-1* and *dsh-1* resulted in mild tripolar neurons, similar to *vang-1 lof*, suggested that *prkl-1* and *dsh-1* are also involved in regulating VC4/5 morphology/orientation. These results laid the foundation for my thesis hypothesis.

Hypothesis

PCP genes *prkl-1* and *dsh-1* regulate neuronal polarity/orientation by preventing ectopic anterior-posterior axon outgrowth during organogenesis.

Objectives

1. To isolate and characterize *prkl-1* mutants and other neuronal polarity mutants with ectopic axon outgrowth defects. To map a mutant, with no assigned locus, displaying VC4/5 tripolar neurons (*zy7*). To group mutants into non-complementation groups and to characterize their molecular lesions. To perform reverse genetic analysis to identify other genes. To study genetic interactions of polarity genes involved in the morphology of VC4/5 neurons. In Chapter II.

2. To study the role of *prkl-1* in neuronal polarity/orientation during vulva morphogenesis. In Chapter III.

3. To characterize the role of *dsh-1* in neuronal polarity/orientation. In Chapter IV.

CHAPTER II

Genetic screening and analysis of polarity mutants reveal a novel role for *fntb-1* and PCP genes *prkl-1* and *dsh-1* in suppressing AP ectopic axon outgrowth.

Preface

Previous to our work, the role of the planar cell polarity pathway in organizing actin and/or microtubule-based structures in epithelia and in the oriented migration of mesenchymal cells during gastrulation had been extensively characterized in several model organisms. However, no role for PCP in neurons had been reported. Our laboratory found that *vang-1 lof* resulted in neurons with ectopic AP axons, hinting at a new outcome for the PCP pathway in neuron polarity. Prior to my project, there was no *prkl-1* mutant available with which to carry out genetic studies. In order to isolate *prkl-1* alleles and to uncover other genes controlling the wild type medial-lateral orientation of VC4/5 motorneurons we embarked on genetic screens to isolate new mutants with defective VC4/5 morphology, mapped their phenotype-causing mutations, performed genetic analysis of existing mutants and studied their genetic interactions. Chapter II presents evidence for the first genetic study on a new read out for PCP genes *prkl-1* and *dsh-1* in regulating neuron morphology/orientation. Importantly, this study also led to uncovering a new role for *fntb-1* in suppressing AP axon growth.

ABSTRACT

Neurons are highly polarized cells, yet the mechanisms by which they acquire and maintain their morphologies during development remain largely unknown. Planar Cell Polarity signalling regulates a variety of developmental processes in epithelial and mesenchymal tissues, including organized orientation of hairs and cilia in the mouse and the fly, patterned orientation of ommatidia in the fly eyes and convergent extension during gastrulation. The common factor in all of these functions is the ability of PCP genes/proteins to organize the cells' cytoskeleton within the planar dimension of the tissue they inhabit. Here we present evidence for a novel outcome to the PCP pathway in the context of *C. elegans* vulval-proximal VC4/5 motorneurons, which innervate the egg-laying muscles to modulate egg-laying behaviour. In *prkl-1* and *dsh-1* mutants VC4/5 display tripolar morphology. In addition, we mapped and identified a molecular lesion in the *fntb-1(zy7)* mutant with tripolar VC4/5 neurons; thus uncovering a new role for farnesyl transferase β subunit in preventing AP axon growth. FNTB-1 could potentially function by adding a farnesyl moiety to the CaaX motif of PCP protein PRKL-1 for membrane targeting. In addition, we describe the isolation and characterization of the *prkl-1(zy11)* allele, a mutant displaying a highly penentrant tripolar phenotype, which confirmed that *prkl-1* plays a role in VC4/5 neuron polarity. Also, we describe the isolation of two additional mutants, *zy19* and zy22, with tripolar neurons. Moreover, we mapped a total of 12 mutants with VC4/5 defective polarity to four complementation groups, *i.e.* four alleles of *prkl-1*, one of *dsh-1*, six of *fntb-1* and one of *vang-1*. Analysis of genetic interactions between PCP mutants revealed that *prkl-1* and *vang-1* function in a common pathway to prevent AP axon growth.

Moreover, both *prkl-1* and *vang-1* genetically interact with *dsh-1* in the same and/or parallel pathways to regulate the ML orientation of VC4/5 motorneurons.

INTRODUCTION

The genetic pathways underlying neuronal polarization *in vivo* are largely unknown. We use *C. elegans* as a model organism to study how neurons reach and maintain their morphologies in vivo. Most neurons in *C. elegans* polarize along the anterior-posterior (AP) and the dorsal-ventral (DV) body axes. We focus on two of six bipolar hermaphrodite-specific ventral cord neurons (VCs), vulval-proximal VC4 and VC5. This pair of neurons acquire a unique morphology as they polarize medial-laterally (ML), extending two axons in the left-right orientation, which encircle the egg-laying organ; whereas vulval-distal VCs extend processes along the anterior-posterior (AP) axis of the worm. The goal of this chapter was to isolate, map and characterize mutants with defective VC4/5 morphology and to identify the genes and pathways regulating the morphology/polarity of VC4/5 motorneurons.

To visualize VC4 and VC5 we used *cyIs4* (*Pcat-1::gfp; rol-6(su1006)* as a reporter line, which labels dopaminergic neurons including VC4/5, HSNs and PDEs (Duerr et al., 1999). Although VCs are born during L1, it is not until late L3 that morphological changes to the neuron's soma start to occur, in synchrony with vulva morphogenesis (Li and Chalfie, 1990). Hence, patterns in VC4/5 development can be correlated to stages in vulva maturation. Briefly, VC4/5 neuronal symmetry breaks at late L3/early L4 stage, when incipient left-right neurites emerge towards the developmentally active vulva epithelium; and by late L4 the neurons have completed a circular tract around the vulva (Li and Chalfie, 1990). In the adult, VC4/5 neurons form branches and make connections with HSN and VC

neurons and with the vulva muscles. The functional relationship between vulva and VC4/5 polarity was first demonstrated in a seminal experiment by C. Li and M. Chalfie (Li and Chalfie, 1990). They showed that VC4/5 adopt an AP orientation in vulva-ablated animals, signifying that the vulva is a source of polarizing cues necessary for the left-right orientation of VC4/5 neurons and that AP is the default orientation of all six VC neurons.

The bipolar ML morphology of VC4/5 neurons is disrupted in *vang-1* mutants and in nematodes with downregulated *prkl-1* and *dsh-1* activities; instead of wt ML orientation, neurons display a tripolar morphology, with ectopic AP axons. *vang-1*, *prkl-1* and *dsh-1* are core elements of the Planar Cell Polarity (PCP) signalling pathway. This finding suggested that PCP pathway may play a role in VC4/5 morphology/orientation. The PCP pathway is highly conserved across species, from invertebrates to humans, and is defined as the orientation of cells and cellular structures along an axis which is orthogonal to the plane of the tissue they inhabit (McNeill, 2010). The PCP pathway is important in a diverse spectrum of developmental functions; including convergent extension during gastrulation in *Xenopus* (Wallingford and Harland, 2001; Darken et al., 2002) and mouse (Wang et al., 2006a), neural tube closure in the mouse (Murdoch et al., 2001; Hamblet et al., 2002; Curtin et al., 2003) and human (Kibar et al., 2007), patterning of the stereocilia in the mouse inner ear (Deans et al., 2007), planar polarity of the *Drosophila* wing epithelia (Strutt, 2001; Strutt and Strutt, 2007) and patterning of the *Drosophila* compound eye (Rawls and Wolff, 2003). The involvement of core PCP genes *prkl-1*, *dsh-1* and *vang-1* in VC4/5 medial-lateral orientation with respect to the AP body axis, vulval distal VCs, and vulva epithelia (guideposts cells), could be regarded as a new outcome for the PCP pathway.

Here, we isolated mutants and characterize a novel function for *prkl-1*, *dsh-1* and *fntb-1* in regulating the morphology of VC4/5 neurons. In addition, we showed that *prkl-1* and *vang-1* function in a common pathway to prevent AP axon growth and that *dsh-1* acts in a parallel signalling which is also involved in promoting ML axon growth. Further studying this pathway has the potential to improve our understanding on how neurons polarize *in vivo.*

MATERIALS AND METHODS

C. elegans strains.

Strains were manipulated and maintained using standard procedures (Brenner, 1974). Some nematode strains used in this work were provided by the Caenorhabditis Genetics Center, which is funded by the NIH National Center for Research Resources (NCRR).

Wild type C. elegans

N2 (Bristol isolate) and CB4856 (Hawaiian isolate)

cyIs4 is N2 wild type strain containing integrated array [*Pcat-1::gfp, rol-6(su1006*]V (Colavita and Tessier-Lavigne, 2003). *cat-1* encodes a synaptic vesicular monoamine transporter. *Pcat-1* labels dopaminergic neurons, including VC4 and VC5 and HSN motorneurons. *rol-6(su1006)* encodes a mutant collagen protein that induces a dominant roller phenotype (Kramer et al., 1990;Mello et al., 1991).

Table II-1. Mutant strains used in this study.

Chrom.	Gene	Mutant allele	Strain	Mutation
LGI	Frizzled	*lin-17(n677)*	-	Nonsense W320Stop
		mig-1(n687)	-	Nonsense Q77Stop
		mom-5(or57)	EU311	Tc1 transposon-induced lesion
	Lim-9*	*tag-15(gk106)*	VC209	597 bp deletion
	Wnt	*lin-44(n1792)*	MT5383	Nonsense W100Stop
LGII	Dishevelled	*dsh-1(ok1445)*	RB1328	1132 bp deletion
		dsh-2(or302)	NG3124	458 bp-exon 6 deletion
		mig-5(tm2639)	-	811 bp deletion + 5 bp insertion
	ROR tyr kinase receptor	*cam-1(gm122)*	NG2615	Nonsense Q253Stop
LGIV	BED Zinc finger	*dpy-20(e1282)*	CB1282	Missense P354L
	Prickle-1	*prkl-1(ok3182)*	RB2346	649 bp deletion
	Tes-1**	*tag-224(ok1036)*	VC696	581 bp deletion
	Wnt	*egl-20(n585)*	-	Missense C99S
	Zim-1/-3_like	*him-8(e1489)*	CB1489	Missense G259R
LGV	Farnesyl-transferase	*fntb-1(ok1232)*	RB1188	~ 1600 bp deletion
		fntb-1(ok590)	VC399	1237 bp deletion
	Flamingo (Cadherin-like)	*fmi-1(tm306)*	-	822 bp deletion
	Frizzled	*cfz-2(ok1201)*	RB1162	1174 bp deletion
LGX	β-catenin	*bar-1(ga80)*	EW15	Nonsense Q97Stop
	Ryk tyr kinase receptor	*lin-18(e620)*	CB620	Nonsense Q71Stop
	Van Gogh	*vang-1(tm1422)*	-	596 bp deletion

* encodes PRKL-like protein with 1xPET and 6xLIM, orthologous to *Drosophila* LIMPET and vertebrate FHL2.

** encodes PRKL-like protein with 1xPET and 3xLIM, orthologous to *Drosophila* CG6522-PA and human LMCD1 and TESTIN.

For phenotypic analysis, these strains were crossed into *cyIs4* genetic background.

vang-1(tm1422) and *fmi-1(tm306)* were gifts from Shohei Mitani, Tokyo Women's Medical College, Tokyo, Japan.

More details on the nature of the mutations and overall mutant's phenotype can be found at www.wormbase.org. To genotype mutant alleles, genomic DNA was isolated from each strain and the mutant locus was PCR-amplified and diagnosed either by 1) DNA sequencing, and/or 2) restriction digest, and/or 3) size of deletion.

Construction of double mutants.

dsh-1(ok1445); prkl-1(zy11)

dsh-1(ok1445); cyIs4 hermaphrodites were mated with N2 males. Heterozygous roller males were then crossed with homozygous *prkl-1(zy11).* Roller crossprogeny, each with one allele of *zy11* and 50% probability of carrying *ok1445* allele, were cloned into new plates and allowed to self. F2 progeny was examined under the fluorescent scope and worms with ectopic AP axons were singled out and allowed to self. The F3 generation was genotyped for *dsh-1(ok1445)* by PCR using primers 5'gaacgacacgattgctcatagc3' and 5' aacactgtcaccagagtactggc3'. Wild type *dsh-1* species result in 1.8kb band, while homozygous deletion mutants render a 0.7kb band. Heterozygous amplified both bands. *Prkl-1(zy11)* was genotyped as described in results section. Positive double mutants were cloned again and the genotyping was confirmed in the F4 generation.

dsh-1(ok1445); vang-1(tm1422)

vang-1(tm1422) worms were mated with N2 males. Heterozygous *vang-1* males were then crossed with late L4 homozygous *dsh-1(ok1445); cyIs4* hermaphrodites. Potential crossprogeny hermaphrodites, GFP+ but non rollers (with only one allele of *cyIs4*), were cloned into individual plates and allowed to self. Crossprogeny contained one allele of *ok1445* and one allele of *tm1422* (since *vang-1* is located in LGX). F2 plates with mixed roller and non-roller worms were kept as crossprogeny and the rest discarded. F2 nematodes were then examined under the fluorescent scope and worms displaying VC4/5 with ectopic AP axons were singled out, then allowed to self and were subsequently genotyped. F3 worms were genotyped using PCR for *dsh-1(ok1445)* as described above, and for deletion allele

vang-1(tm1422) using primers 5'aaaatgtcataaacgccgagtc3' and 5'ttttagggtacctagcttgtgc3'. Wild type *vang-1* results in 0.8kb band while *vang-1(tm1422)* mutant results in a 0.2kb band. The genotype of double mutant was confirmed again in the F4 generation.

prkl-1(zy11); vang-1(tm1422)

Heterozygous *vang-1(tm1422); cyIs4* males were mated with homozygous *prkl-1(zy11)* hermaphrodites. F1 (crossprogeny) hermaphrodites contained one allele of *tm1422* and one of *zy11*. Rollers F1 were then cloned into new plates. Plates segregating rollers and non rollers were kept as crossprogeny. F2 nematodes with ectopic AP axons were cloned into new plates and allowed to self. The F3 generation was genotyped for both alleles as described above. Double mutants were confirmed in the F4 generation.

prkl-1(ok3182); vang-1(tm1422)

Heterozygous *vang-1(tm1422)*; *F4* males were mated with *prkl-1(ok3182)* homozygous hermaphrodites. Several F1 crossprogeny, containing one allele of *ok3182* and one allele of *vang-1(tm1422)*, were cloned into new plates and allowed to self. F2 nematodes displaying VC4/5 with ectopic axons were placed in individual plates. The F3 generation was genotyped for *vang-1(tm1422)* as described above, and for *prkl-1(ok3181)* using primers 5'ccatggatttccacagatttg3' and 5'cgaaggctatctgctgagtcc3'. Wild type nematodes generate a 3.3kb and while a *prkl-1(ok3182)* mutant band is 2kb. Double mutants were confirmed in the F4 generation.

Quantification of polarity defects.

Neurites were visualized with *cyIs4* reporter using an AxioplanII/Apotome (Zeiss) or LSM510 confocal microscope (Zeiss). Neurites were scored as axons if they were at least one VC cell diameter in length (~5 µm) at early and mid L4 stages and at least 3x VC cell diameters (~15 µm) at adult stage or when the ectopic neurite is at least equal in length to a primary neurite.

Positional cloning of *zy7* mutant.

To map the phenotype-causing mutation in *zy7* allele, a combination of approaches including SNP mapping, RNAi reverse genetics and complementation tests with chromosomal deficiencies and canonical mutants was used. Before mapping, the mutant strain was outcrossed 3x with N2 wild type, seeking to eliminate other lesions in the genome. While mating *zy7*, we learned that the mutation was tightly linked to the integrated reporter *cyIs4* in the basic line.

Single nucleotide polymorphism (SNP) mapping was first used to identify the Linkage Group (LG) and then iteratively to narrow down the mutation-containing interval between two SNPs, following standard procedures (Wicks et al., 2001). Briefly, polymorphic Hawaiian males were mated with *zy7, cyIs4* hermaphrodites to produce heterozygous F1, which were then cloned into individual plates and allowed to self. F2 plates that segregated only rollers were presumed self progeny and discarded. Approximately, 60% of worms carrying a single copy of *cyIs4* are rollers. Plates with crossprogeny, (*i.e.* containing a mix of rollers and non rollers), were further used. Thus rollers and non rollers *cyIs4* positive were screened under the fluorescence microscope for polarity defects in VC4/5. About 100 F2 worms displaying the mutant phenotype were singled onto fresh plates and kept for SNP

mapping. Some wt F2 nematodes were kept to obtain positional information on the breakpoint of chromosomal recombination between N2 and CB4856. Genomic DNA was isolated from the progeny of the individual F2 plates and the relative distribution of Hawaiian/N2 SNPs was analyzed using PCR-restriction digest or PCR-sequencing. Iterations of SNP mapping allowed us to position the mutation on the chromosome relative to the SNPs, based on linkage of the phenotype to the chosen genetic markers. A list of SNPs for each chromosome is available in www.wormbase.org. When it was not possible to use SNP mapping to narrow the physical location of the mutation any further, other approaches were used, including feeding RNA interference (RNAi) using strain *eri-1; lin-15b* (to make neurons sensitive to RNAi) (Sieburth et al., 2005), cosmid/plasmid transgenic rescue experiments (Fire, 1986) and complementation tests using chromosomal deficiencies or candidate mutants (Yook, 2005).

Complementation tests with chromosomal deficiencies.

Deficiencies (*Dfs*) lack specific regions within chromosomes (Fay, 2006). Many deficiencies lack multiple genes including some necessary for embryonic development and consequently are embryonic lethal (Fay, 2006). These *Dfs* require a balancer chromosome to survive, which usually carries a genetic marker for identification (Fay, 2006). *Dfs* are very useful in mapping mutations; by mating the mutant strain with the *Df* and examining the F1 progeny for the phenotype of interest. Thus, placing a recessive mutation *in trans t*o a deficiency can result in two possible outcomes, 1) it fails to complement the mutant's phenotype, suggesting the *Df* deletes the gene of interest, and the mutant allele is then hemizygous on the opposite chromosome or 2) it complements/rescues the phenotype

suggesting the gene of interest is not included in the *Df*. See Table II-1 for the list and description of the *Dfs* used in this Chapter. These deficiencies were used to obtain a mutant allele of *prkl-1* via non-complementation screen (*nDf41*), or to map the mutated locus in *zy7* allele (*nDf42*, *yDf8*, *yDf11* and *yDf4*).

Table II-2. Chromosomal deficiencies used in this study.

Strain	Genotype	Genetic pos. (cM)	Genomic pos. (~Mb)
MT5734	***nDf41*** IV/nT1[unc-?(n754) let-?](IV;V)	1.69 to 3.42	5.5 to 7.7
MT5813	***nDf42*** V/nT1[unc-?(n754) let-?](IV;V)	3.53 to 6.73	11.9 to 14.7
TY1470	***yDf8*** V/nT1[unc-?(n754) let-?](IV;V)	6.18 to 10.32	14.1 to 16.5
TY1313	***yDf11*** V/nT1[let-?(m435)](IV;V)	*	~14.7 to 15.0
TY832	***yDf4***/dpy-11(e224) unc-76(e911)V	10.32 to 14.10	16.5 to 18.1

* Genetic/genomic position not specified in Wormbase. ~ Approximate genomic location deducted from mapping data reported by (Rogalski et al., 2000)

Non-complementation genetic screen to isolate *prkl-1* alleles.

In order to specifically isolate *prkl-1* alleles we designed a non-complementation genetic screen which involved the use of *him-8(e1489)*IV mutants as a source of male worms. *him-8*(e1489) hermaphrodites produce a high proportion of male progeny (20 - 40 %)

due to defects in meiotic segregation of the X chromosome (Hodgkin et al., 1979). Briefly, germ cells of *him-8* (high incidence of males); *cyIs4* males were mutagenized with EMS following standard procedures (Brenner, 1974). EMS-treated *him-8(e1489);cyIs4* males were then mated with *nDf41* (chromosomal deficiency which lacks the *prkl-1* locus) hermaphrodites. F1 crossprogeny was screened for the presence of AP axons in VC4/5 neurons. *Prkl-1* alleles were selected on the basis of their failure to complement *nDf41* polarity defects in VC4/5 neurons. Potential mutants were then picked into new plates and the self progeny examined for phenotypic confirmation in the F2 generation and genotyping.

Forward genetic screen.

cyIs4 hermaphrodites were mutagenized with EMS following standard procedures (Brenner, 1974). The F2 progeny was screened for VC4 and VC5 with polarity defects. F2 worms displaying neurons with bipolar AP, tripolar or unipolar morphology were picked onto separate plates and allowed to self reproduce. The phenotype was again analyzed in the F3 generation to identify and only maintain true mutants. To discern how many genes and which genetic loci we were dealing with, we mapped all the new mutants with ectopic AP axons. Thus, gene assignment was performed using a combination of snip SNP mapping to identify the LG and complementation tests as described previously (Brenner, 1974).

***prkl-1* and *dsh-1 gfp*-tagged genomic constructs.**

We generated N-terminal GFP translational fusions of PRKL-1 and DSH-1 via yeast homologous recombination (YHR) using the Gene CATCHR cloning procedure as described (Sassi et al., 2005). This procedure preserves the integrity of the gene (*i.e.* exons, introns, promoter and 3'UTR regions), which is essential to generate physiologically significant data.

In essence, ~15 kb of *prkl-1* (5'-tgcattcttcgg…ttcgtaatgccc-3'), and ~15.8 kb of *dsh-1* (5'-gatcaatcgtgg…tttgcttctgcc-3') containing genomic regions were recombined from Yeast Artificial Chromosomes (YAC) strains Y40D6 and Y54E1 (gifts from A. Coulson), respectively, into a carrier vector. A GFP cassette was then inserted in-frame following the ATG start codons of *prkl-1* (isoform A) and *dsh-1* (isoform C) to generate *genomic prkl-1(+)*, and *genomic dsh-1(+)* respectively. A schematic representation of the procedure can be found in (Sassi et al., 2005) and the primers used are listed in Table II-3. In more detail, up and down cloning linkers to *prkl-1* and *dsh-1* were PCR amplified from cosmids ZK381 and C34F11, respectively. Transformation reactions were plated on SC-HIS and positive clones were then patched onto SC-HIS plus 5-Fluoro-orotic acid to select only yeast cells that carry the correct plasmid (successful YHR) and lost the YAC. For gfp-tagging, yeast bearing the pCATCHR 4 target clone were co-transformed with GF-URA3-FP targeted-tag vector (gfp is flanked by targeting sequences homologous to the insertion site in *prkl-1* and *dsh-1*, respectively). A subsequent round of selection on SC-HIS-URA plates allowed the growth of yeast colonies containing both tagged and untagged genes. Finally, to isolate yeast cells containing only the tagged plasmids, the latter yeast colonies were mated to a *kar-1* recipient strain and further selection steps were carried out. Finally, GFP-tagged genomic *prkl-1* and *dsh-1* constructs were injected into the gonads of *prkl-1* and *dsh-1* mutants, respectively, to obtain trangenic strains using standard methods. The constructs were injected at a final concentration of 1ng/µL or 10ng/µL together with 40ng/µL of *Podr-1::dsRed* as co-transformation marker into their respective *prkl-1(zy11)*, or *dsh-1(ok1445)* mutant backgrounds to generate the extrachromosomal arrays named [*prkl-1(+)*] and [*dsh-1(+)*], respectively.

Table II-3. Primers used to generate gfp-tagged *prkl-1* and *dsh-1* genomic constructs.

Cloning primers	Sequence 5'- 3'
pPrklup.F	atccgtcctaagaaaccattattatcatgacagcggccgctgcattcttcggcaacacagccaac
pPrklup.R	tacagttctggagttgtcagacttg
pPrkldown.F	tgatgatgtcgggaggcggtgttcg
pPrkldown.R	aagcgtggtgcactctcagtacaatctgctctgcggccgcgggcattacgaagaagaataaggac
pDsh1up.F	atccgtcctaagaaaccattattatcatgacagcggccgcgatcaatcgtggagcacatcatccg
pDsh1up.R	caccaagacgaatgagagggcactc
pDsh1down.F	cgccgccttcttaattcttgtcgcg
pDsh1down.R	aagcgtggtgcactctcagtacaatctgctctgcggccgcggcagaagcaaaaccgtccatagac

Diagnostic primers	Sequence 5'- 3'
pPrklupDiag.R	tctcttcccatcatcatcattcttc
pPrkldownDiag.F	agttccagatgtacagtatcttg
pDsh1upDiag.R	ttggaagaagaagaagacaaggg
pDsh1downDiag.F	tggcaactggacaaagatacgag
pCATCHUpDiag.F	aacacagagtaaattcccaaattattcc
pCATCHDownDiag.R	aagtagtcatcaaacaggtttcgg
GFPtagDiag.F	ggcagacaaacaaaagaatgg
GFPloopoutDiag.F	gcactactggaaaactacctg
GFPppsDiag.F	cgttccttatatgtagctttcg

RESULTS

Mutation in Farnesyl transferase β subunit (*fntb-1*) locus results in ectopic AP axon outgrowth in VC4 and VC5 motorneurons.

Previously, our laboratory had isolated a VC4/5 polarity defective mutant *zy7* from a forward genetic screen. VC4 and VC5 neurons in *zy7* mutants display a highly penetrant (~ 80 %) ectopic axon outgrowth phenotype along the AP axis, whereby LR bipolar neurons become tripolar (Figure II-1). While *zy7* displayed a similar polarity phenotype to *vang-1(tm1422)*, it was not allelic to *vang-1*. However, the similar VC4/5 phenotype to *vang-1* mutants, suggested two possibilities, 1) that *zy7* contained a DNA lesion on a different PCP gene or a novel gene functioning with *vang-1* in a PCP-like pathway, or 2) or a lesion in a novel gene functioning in an alternative pathway to control a common phenotype.

By the time I started my PhD studies, the identity of *zy7* was unknown. To understand the role of this gene in VC4/5 polarity we first needed to map the phenotype-causing mutation in *zy7,* in the hope of uncovering a gene whose involvement on VC4/5 morphology would provide insight into how this polarity pathway is orchestrated. The overall strategy used to identify the phenotype-causing DNA lesion in *zy7* mutant is schematically depicted in Figure II-1. First, *zy7*; *cyIs4* hermaphrodites in N2 background were mated with the polymorphic Hawaiian strain CB4856. Then, more than 100 F2 progeny displaying tripolar VC4/5 were singled out into fresh plates and allowed to self-reproduce. Each of these F2 worms represents a recombinant in which Bristol chromosomes have recombined with Hawaiian chromosomes. Genomic DNA was then isolated from the F3+ progeny in order to assess linkage of the mutation to selected SNPs (Figure II-1). Interestingly, while outcrossing

the *zy7* strain we noticed that the reporter *cyIs4* could not be segregated away from a *zy7* allele into an N2 wild type background, suggesting that *zy7* gene is located on chromosome V and is linked to the integration site of *cyIs4*. By that time, we had already mapped *cyIs4* to the right arm of chromosome V, but the exact location had not been finely determined. This tight linkage to the *cyIs4* reporter somewhat limits the use of the alleles, since the *cyIs4* array can't be replaced with a reporter of more interest. We reasoned that genomic regions close to *zy7* would contain a decreased incidence of Hawaiian SNPs while unlinked DNA regions would contain ~ 50 % representation of both Hawaiian and Bristol SNPs. Thus, we started out examining SNPs located over the length of Chromosome V. We found the mutation was positioned to the right arm partially linked to SNPs R11D1 and F57G8. Through subsequent iterative SNP analysis we were able locate the mutation down to a region of 2Mb between SNPs CE5-217 and T09F5. Unfortunately, not enough Hawaiian-Bristol recombination events appeared to happen within this 2 Mb region in *zy7, cyIs4* mutants, and the usefulness of SNP mapping came to an end. Consequently, in order to map the mutation further we performed complementation tests with partially overlapping deficiencies: *nDf42*, *yDf8*, *yDf11* and *yDf4*, which provided a good coverage of the right arm of LGIV (Figure II-1). Interestingly, we found that *nDf42*, *yDf8* failed to complement the defects in *zy7* mutant, suggesting that the mutated allele was hemizygous, in *trans* with both deletions (Figure II-1). In other words, the mutation was located within the overlapping region between both deficiencies. *nDf42* and *yDf8* overlap from 14.1 to 14.7 Mb which places the mutation in a span of 0.6 Mb. Next, we aimed at rescuing the phenotype with cosmid injections, reasoning that a rescuing cosmid will contribute a wild type copy of the mutated gene. Of the injected cosmids, only C53A5 rendered lines, which failed to rescue; suggesting that C53A5 cosmid

does not contain the gene mutated in *zy7* strain. Similarly, PCRed R11H6.2, a candidate gene within C53A5 cosmid, did not rescue *zy7* polarity defects. These attempts were followed by reverse genetics using a candidate gene approach, including complementation tests with canonical mutants and RNAi of candidate genes (Figure II-1). Ultimately, we found that mutant strains VC399 and RB1188 containing deletions in F23B12.6 locus, failed to complement *zy7, cyIs4*. This finding suggested that the phenotype-causing mutation was located in the F23B12.6 locus. This gene encodes the sole **farnesyl transferase β subunit-1** (FNTB-1) protein of the worm. *fntb-1* is located between genomic positions 14447630 bp – 14449570 bp, and encodes a relatively small enzyme, 401 residues long. In effect, DNA sequencing of *fntb-1* locus in *zy7* allele revealed a G>A transition, resulting in E321L missense mutation (Figure II-1 and Table II-4).

Figure II-1. Neuronal polarity defective *zy7* mutant maps to the farnesyl transferase β subunit (*fntb-1*) locus. A) Confocal picture of *zy7* mutant displaying VC4/5 with ectopic AP axon outgrowth. **B)** Quantification of the AP ectopic axon. **C)** Strategy used to map zy7 mutant. Briefly, using SNIP mapping *zy7* DNA lesion was found to be genetically linked to LGV. With iterative SNIP mapping the region was narrowed down to a span of 15.2 Mb. Further mapping was achieved by performing complementation tests with chromosomal deficiencies by which the area was reduced to 0.6 Mb. Then a failing-to-rescue cosmid injection further narrowed the area to 500 kb. From then on reverse genetics, a candidate gene approach using RNAi and complementation tests with available mutant *fntb-1(ok590)*, allowed the identification of the mutated locus, *fntb-1*. DNA sequencing revealed an E321K mutation. **D)** Top) schematic representation of the *fntb-1* locus, with annotations for *fntb-1(ok590)*, the deletion allele that identified the *zy7* locus in a non complementation test. Bottom) sequence change in the *fntb-1(zy7)* allele.

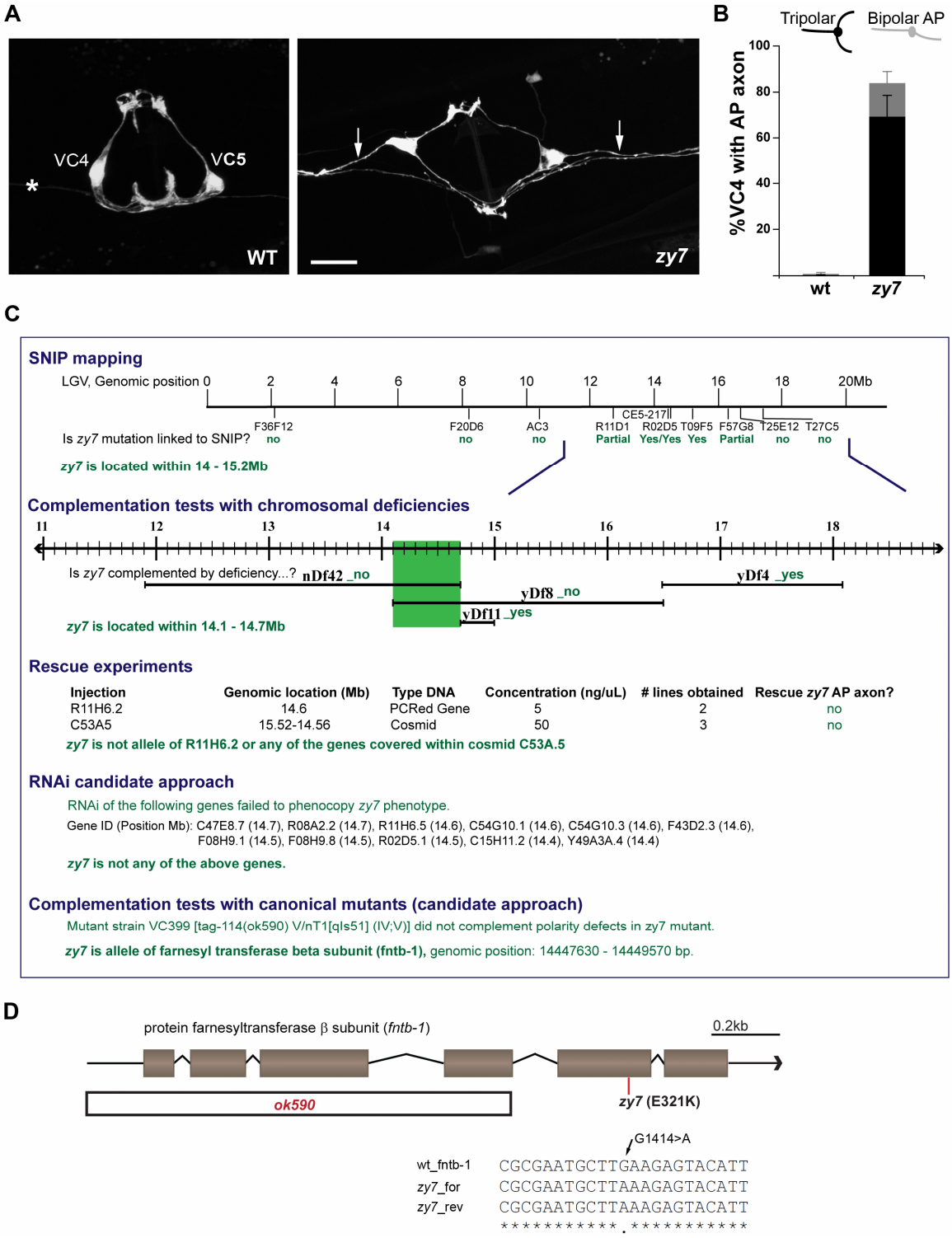
A
VC4
VC5
*
WT
zy7
B
Tripolar
Bipolar AP
%VC4 with AP axon
100
80
60
40
20
wt
zy7
C
SNIP mapping
LGV, Genomic position 0 2 4 6 8 10 12 14 16 18 20Mb
CE5-217II
F36F12 F20D6 AC3 R11D1 R02D5 T09F5 F57G8 T25E12 T27C5
Is zy7 mutation linked to SNIP? no no no Partial Yes/Yes Yes Partial no no
zy7 is located within 14 - 15.2Mb
Complementation tests with chromosomal deficiencies
11 12 13 14 15 16 17 18
Is zy7 complemented by deficiency...? nDf42 _no
yDf4 _yes
yDf8 _no
yDf11 _yes
zy7 is located within 14.1 - 14.7Mb
Rescue experiments
Injection | Genomic location (Mb) | Type DNA | Concentration (ng/uL) | # lines obtained | Rescue zy7 AP axon?
R11H6.2 | 14.6 | PCRed Gene | 5 | 2 | no
C53A5 | 15.52-14.56 | Cosmid | 50 | 3 | no
zy7 is not allele of R11H6.2 or any of the genes covered within cosmid C53A.5
RNAi candidate approach
RNAi of the following genes failed to phenocopy zy7 phenotype.
Gene ID (Position Mb): C47E8.7 (14.7), R08A2.2 (14.7), R11H6.5 (14.6), C54G10.1 (14.6), C54G10.3 (14.6), F43D2.3 (14.6), F08H9.1 (14.5), F08H9.8 (14.5), R02D5.1 (14.5), C15H11.2 (14.4), Y49A3A.4 (14.4)
zy7 is not any of the above genes.
Complementation tests with canonical mutants (candidate approach)
Mutant strain VC399 [tag-114(ok590) V/nT1[qIs51] (IV;V)] did not complement polarity defects in zy7 mutant.
zy7 is allele of farnesyl transferase beta subunit (fntb-1), genomic position: 14447630 - 14449570 bp.
D
protein farnesyltransferase β subunit (fntb-1)
0.2kb
ok590
zy7 (E321K)
G1414>A
wt_fntb-1 CGCGAATGCTTGAAGAGTACATT
zy7_for CGCGAATGCTTAAAGAGTACATT
zy7_rev CGCGAATGCTTAAAGAGTACATT

A mutation in the *C. elegans prkl-1* locus results in tripolar VC4/5 motorneurons, displaying ectopic anterior-posterior directed neurites.

The PRICKLE protein is phylogenetically conserved (Figure II-2). Modular PRKL proteins are generally composed of a single PET domain and three LIM domains (Gubb et al., 1999b). Protein alignment of PRKL proteins reveal that the PET domain of *C. elegans* is 59% identical to the human sequence, which may suggest that PRKL-1 function in the *C. elegans* nervous system is likely conserved in humans. Previous data, showing that RNAi-induced *prkl-1* downregulation resulted in a mild polarity phenotype (Visanuvimol, J and Su, A, unpublished), with VC4/5 extending neurites along the AP axis and away from the vulva, similar to those displayed by *vang-1* mutants, suggested a new role for PRKL-1 in neuronal polarity. Furthermore, uncovering mutations in the *fntb-1* locus which resulted in a similar polarity phenotype (see previous result), and its potential role in modifying *prkl-1* post-translationally for membrane localization, further hinted at the importance of *prkl-1* in a PCP-like neuronal polarity pathway with *vang-1*.

At the beginning of my degree there was no *prkl-1* mutant available in the *C. elegans* community, which prompted me to initiate my studies by obtaining *prkl-1* alleles, via genetic screens, which could be used for phenotypic characterization, rescue experiments and genetic analysis. Accordingly, my first objective became to isolate *prkl-1* mutants by performing non-complementation and forward genetic screens in parallel.

The strategy for the non-complementation screen is described in the Methods section. The rationale was that F1 animals with a lesioned *prkl-1* gene placed hemizygous over deficiency *nDf41* which lacks p*rkl-1* locus, will display VC4/5 polarity defects (Figure II-

3A). From this screen, I was able to recover a single allele of *prkl-1* named *zy11*, which resulted in tripolar VC4 and VC5 motorneurons (Figure II-3B). DNA sequencing of the *prkl-1(zy11)* allele revealed a transition T **C**AA to T **T**AA, which created a nonsense mutation Q101Stop and truncated the protein short within the PET domain (Figure II-3C). Conveniently, this mutation introduced a single nucleotide polymorphism (SNP) that can be easily identified by PCR amplification, followed by restriction digest, which greatly facilitates the genotyping of the *zy11* allele. Briefly, a 757bp fragment is PCR-amplified using primers 5'..cgtataatttgccattctcttatg..3' and 5'..gtcataataaggccgggtgacg..3', and genomic DNA as template. The product is then digested with the *MseI* restriction endonuclease, which gives 3 bands for each mutant and wt DNA. The presence of a 229bp band identifies wt, whereas a 186bp band identifies *prkl-1(zy11)* homozygous worms (Figure II-3C).

Importantly, the *prkl-1(zy11)* allele was obtained in a *him-8(e1489)* mutant background. DNA lesions in the *him-8* gene cause hermaphrodites to produce a high incidence of male progeny due to meiotic nondisjunction of the X chromosome (reference). Therefore, it was desirable to clean up the genetic background and to segregate *zy11* from the double *prkl-1*, *him-8(e1489); cyIs4.* The *him-8* gene like *prkl-1* is located in LGIV, just ~ 3.6 Mb to the right of *prkl-1* locus. The two genes are separated by about 1.36 % recombination frequency, based on their genomic position. The *zy11* allele was therefore linked to the *him-8* mutation and several attempts at outcrossing *zy11* at 20 ^{o}C failed. To increase the chances of obtaining *prkl-1* single mutants as segregants, several mating plates with *prkl-1*, *him-8(e1489); cyIs4* hermaphrodites and N2 males, were set at 25 ^{o}C and a large number of F1s recombinants were cloned. F2 worms were then singled into new plates. A quick visual exam of the F3 progeny sufficed to discern plates where no segregation around the *him-8* locus had

occurred. As such, to isolate *prkl-1; cyIs4* as a single mutant, only plates containing no males were inspected for polarity defects in VC4 and VC5. Single *prkl-1; cyIs4* was eventually achieved, and subjected to four more back crosses to N2 strain, in order to clean up the background genome.

Figure II-2. PRICKLE is highly conserved across species. *C. elegans* PRKL-1 (NP-741435) sequence is aligned with *Drosophila melanogaster* PK isoform A (NP_724534), *Danio rerio* PK2 (NP_899186), *Mus musculus* PK2 isoform A (NO_001074615), and *Homo sapiens* PK2 (NP_942559). Alignment of proteins was performed using ClustalW2 and visualized with Boxshade 3.31. Black shading indicates identical amino acids and grey shading, similar amino acids. Conserved PET, LIM and CAAX domains are bracketed by red, lime and grey coloured boxes, respectively.

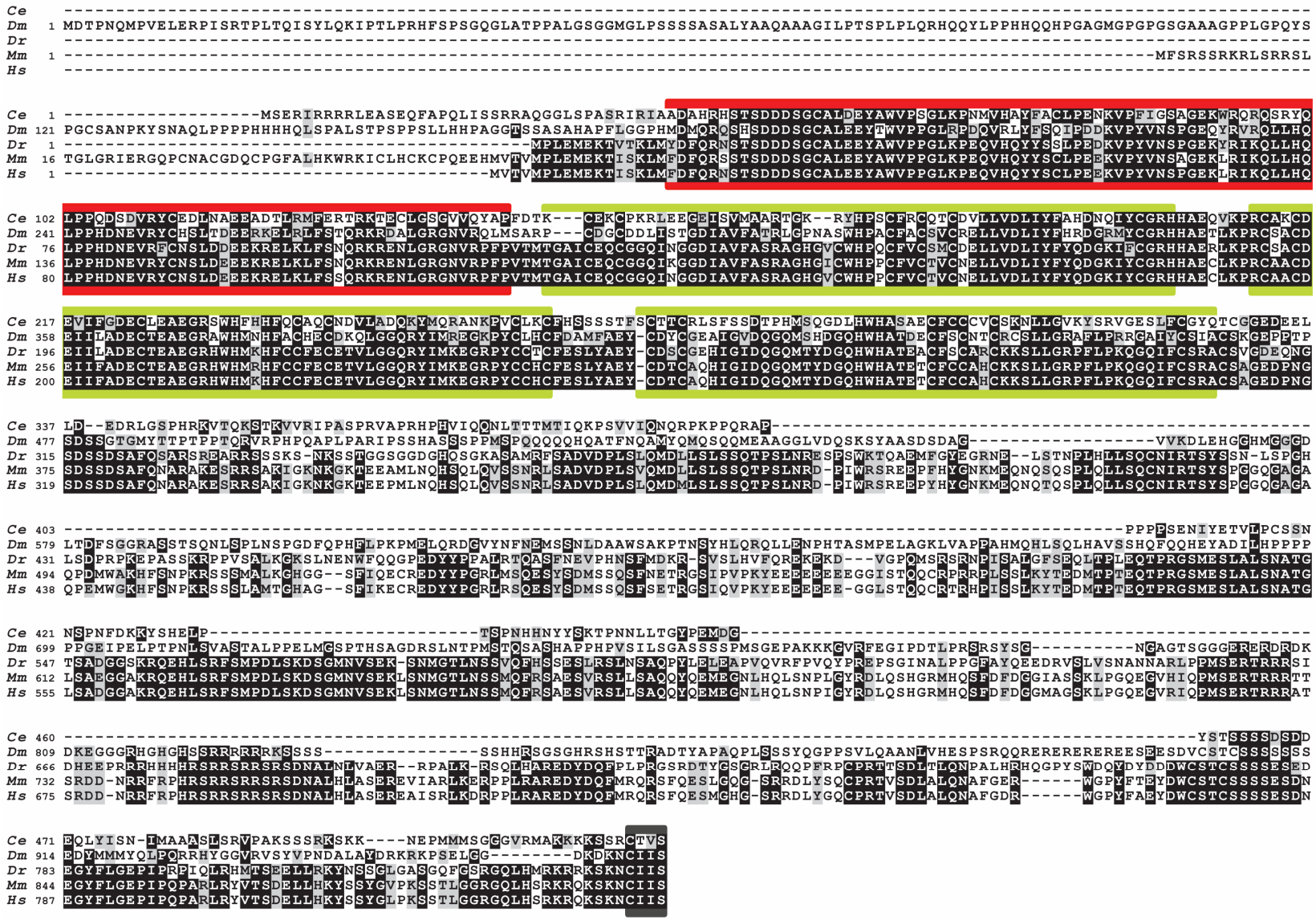

Figure II-3. Loss-of-function of PCP gene *prkl-1* results in ectopic axon outgrowth along the AP axis. A) Strategy for the non complementation screen used to isolate *prkl-1* alleles. Briefly, polarity defective F1 progeny, resulting from the cross of mutagenized *him-8(e1489);cyIs4* males and heterozygous hermaphrodites from deficiency *nDf41*, were isolated based on the genetic inability to compensate for the polarity defective phenotype caused by *prkl-1* deletion. **B)** *prkl-1* allele *zy11* was isolated from the above screen. A genetic lesion in *prkl-1* gene results in ectopic AP axon outgrowth in VC4/5 motorneurons. Confocal images of wild type VC4/5 (Left) and *prkl-1(zy11)* (Right) visualized with *cyIs4* reporter. **C)** DNA sequencing reveals a nucleotide transition C>T which creates an early stop codon, and an MseII endonuclease restriction site (TTAA) that have proven useful to genotype the allele. **D)** Schematics of PRKL-1 modular composition consisting of a PET domain and three LIM domains. *zy11* DNA lesion results in an early protein truncation (Top). Representative *zy11* genotyping (bottom).

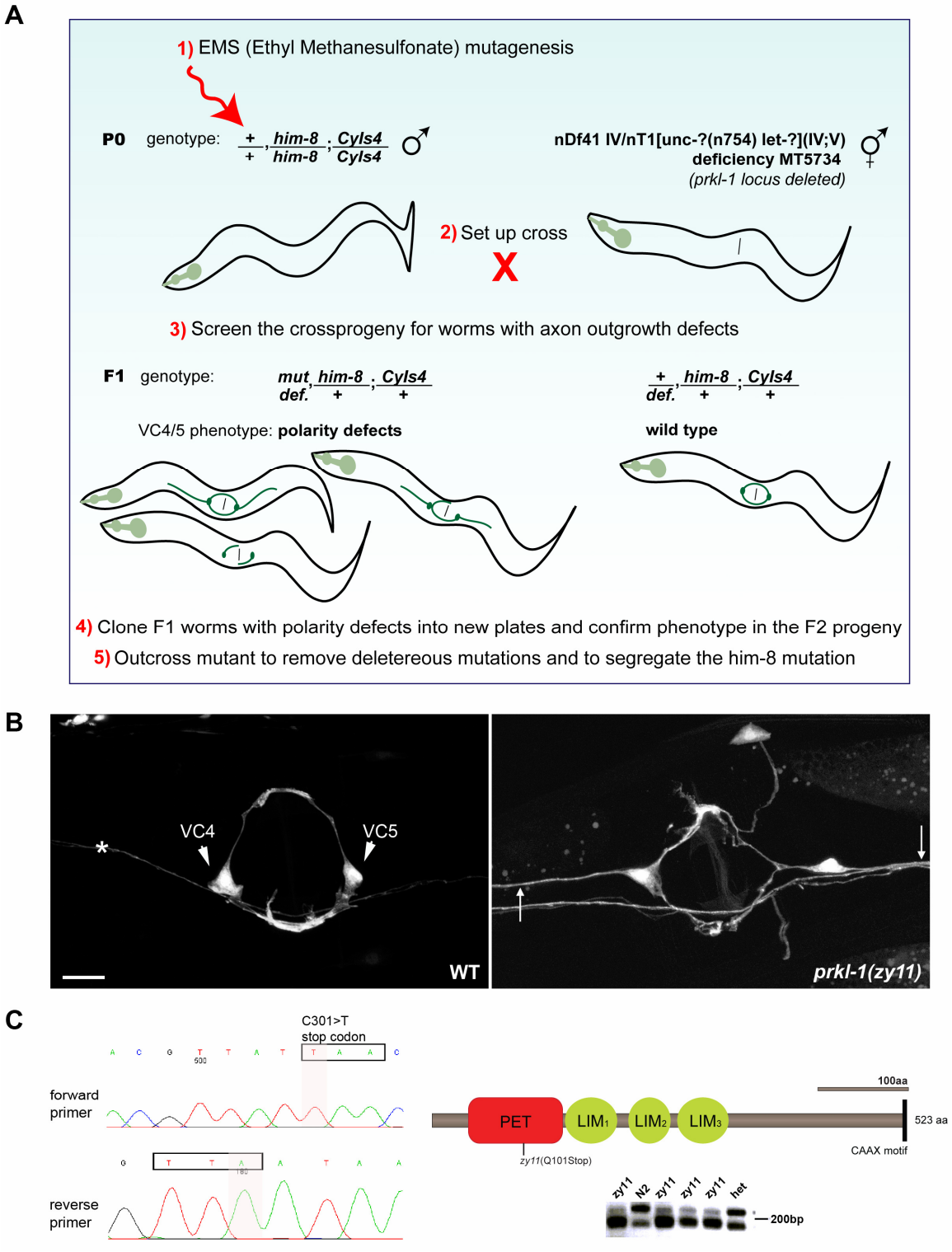
A
1) EMS (Ethyl Methanesulfonate) mutagenesis
P0 genotype: + / + , him-8 / him-8 ; Cyls4 / Cyls4
nDf41 IV/nT1[unc-?(n754) let-?](IV;V)
deficiency MT5734
(prkl-1 locus deleted)
2) Set up cross
X
3) Screen the crossprogeny for worms with axon outgrowth defects
F1 genotype: mut / def. , him-8 / + ; Cyls4 / +
+ / def. , him-8 / + ; Cyls4 / +
VC4/5 phenotype: polarity defects
wild type
4) Clone F1 worms with polarity defects into new plates and confirm phenotype in the F2 progeny
5) Outcross mutant to remove deletereous mutations and to segregate the him-8 mutation
B
VC4
VC5
WT
prkl-1(zy11)
C
C301>T
stop codon
forward primer
reverse primer
100aa
PET
LIM1
LIM2
LIM3
523 aa
CAAX motif
zy11(Q101Stop)
zy11
N2
zy11
zy11
zy11
het
200bp

Recovery of mutant strains *zy19* and *zy22* from a forward genetic screen.

To obtain new alleles of *prkl-1* and also new mutants with defective VC4/5 polarity, I performed a forward genetic screen using standard procedures (Brenner, 1974) (see strategy in Figure II-4A). In essence, The F3 generation of EMS-treated *cyIs4* worms were screened for VC4 and VC5 with polarity defects such as tripolar neurons, or bipolar neurons with axons oriented in the AP direction instead of right-left, and unipolar neurons. As a result, two new mutants with tripolar neurons were isolated, named *zy19* and *zy22* (see Figure II-4B for images and Table II-4 for gene assignments and sequence change).

Figure II-4. *zy19* and *zy22* polarity mutants with ectopic AP axons, were isolated from a forward genetic screen. A) Strategy of a forward genetic screen to isolate VC4/5 polarity mutants. Briefly, progeny of EMS-mutagenized *cyIs4* worms were screened for VC4/5 polarity defective neurons, including unipolar, tripolar or AP bipolar morphologies. Polarity defective worms were singled out, and confirmed or discarded by the F3 generation. Of ~5000 haploid genomes screened, two mutant lines (*zy18* and *zy22*) displaying predominantly tripolar VC4/5 morphology were established. **B)** Representative confocal images of a wild type worm (top) and of mutants *zy19* (middle) and *zy22* (bottom) displaying a third neurite along the AP axis.

A

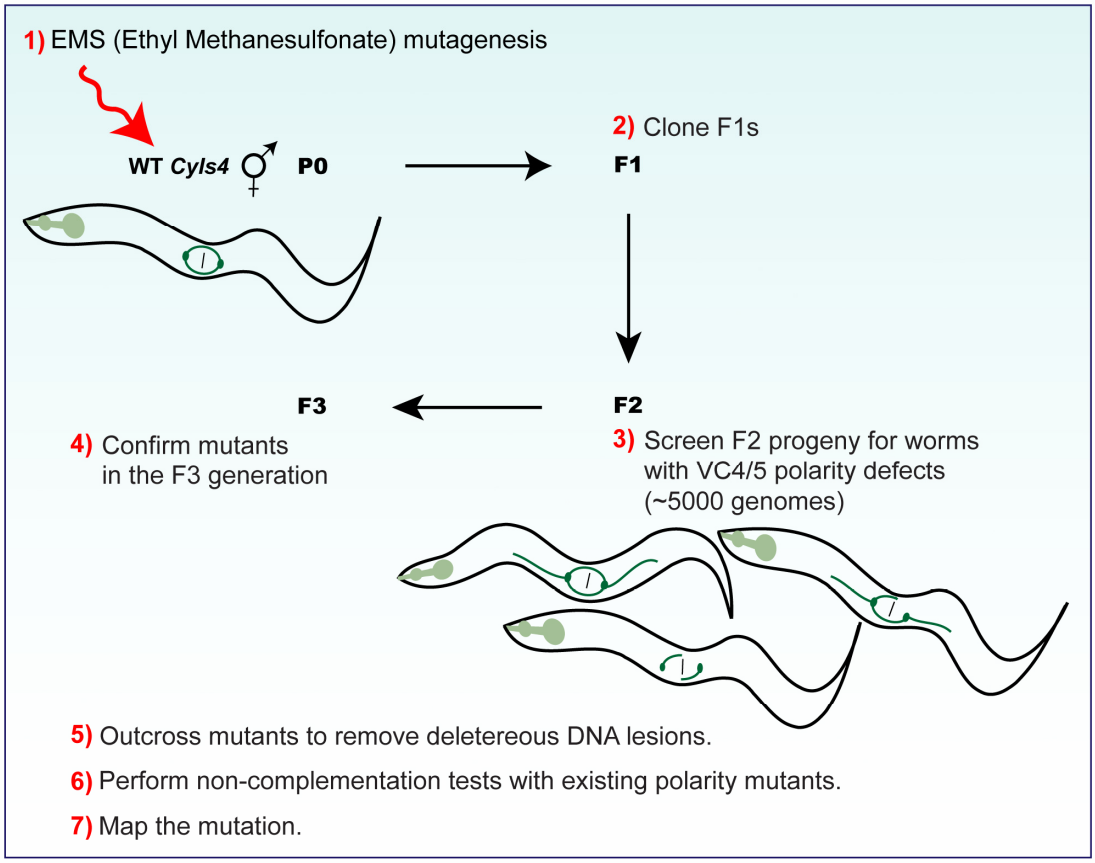
1) EMS (Ethyl Methanesulfonate) mutagenesis
WT Cyls4
P0
2) Clone F1s
F1
F2
3) Screen F2 progeny for worms with VC4/5 polarity defects (~5000 genomes)
F3
4) Confirm mutants in the F3 generation
5) Outcross mutants to remove deletereous DNA lesions.
6) Perform non-complementation tests with existing polarity mutants.
7) Map the mutation.

B

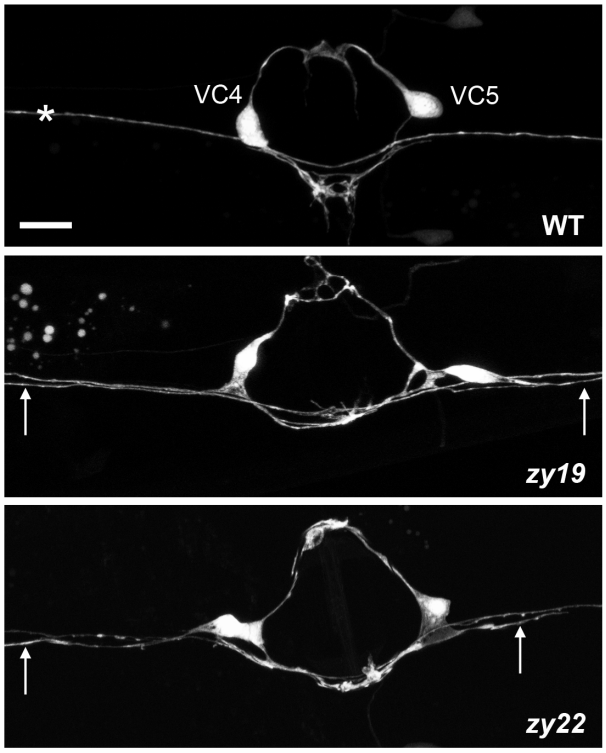
VC4
VC5
*
WT
zy19
zy22

Eleven new mutants, with similar neuronal polarity defects, were mapped to four complementation groups: LGII ***dsh-1*****,** LGIV ***prkl-1*****,** LGV ***fntb-1*** **and** LGX ***vang-1*****.**

To learn the identity of the affected genes, and the phenotype-causing DNA lesions in *zy19* and *zy22* mutants, isolated from a forward genetic screen (previous section), and also in nine other mutants with similar polarity defects, isolated from independent large scale forward screens (Janice Imai, unpublished data), we performed linkage analysis and complementation tests. Thus, we investigated the allelic relationships between mutants by crossing homozygous hermaphrodites from one strain to heterozygous males from the other (see Methods section). The F1 progeny was then scored for the presence of worms with polarity defective neurons (non complementation) or complete wild type morphology (complementation).

To facilitate gene assignments, we made use of a group of known and available polarity mutants, most of them with easy genotyping, including *prkl-1(zy11); cyIs4* and *fntb-1(zy7), cyIs4* from previous screenings; and also predicted strong LOF PCP mutants, *dsh-1(ok1445)* and *vang-1(tm1422)*, deletion alleles obtained from the CGC lacking 0.6 kb and ~ 1 kb genomic sequence, respectively. Using the above mutants, the following testers strains were generated: *zy7; dpy-20(e1282), cyIs4* also used *dsh-1(ok1445); dpy-20(e1282); cyIs4* and *vang-1(zy1); dpy-20(e1282); cyIs4,* to allow for the cross progeny to be distinguished from the self-progeny (*i.e.* dumpy worms) in complementation tests.

Importantly, by crossing *dsh-1(ok1445)* to the *cyIs4* reporter strain we found that lesions in *dsh-1* also resulted in AP axon outgrowth in VC4 and VC5, similar to *vang-1(tm1422), cyIs4* mutants; thus confirming previous results using *dsh-1* RNAi expression

knockdown. This result positioned *dsh-1* as another PCP core gene regulating VC4 and VC5 morphology/orientation, which together with *prkl-1* and *vang-1* may function in a polarity pathway to suppress AP axon growth in VC4/5 motorneurons.

As result of this mapping project we identified one allele of *dsh-1(zy12)*, three additional alleles of *prkl-1(zy17, zy18 and zy19)*, five more alleles of *fntb-1(zy20, zy21, zy22, zy23 and zy24)* and one additional allele of *vang-1(zy10)* (Table II-4). Moreover, DNA sequencing revealed that, with the exception of two mutants, which contained no change within the gene's open reading frame (ORF); all DNA lesions were transitions C > T or G > A, resulting in four nonsense, four missense and two splicing errors.

Table II-4. Mutants displaying VC4/5 polarity defects map to four complementation groups. Of these, loci: *dsh-1, prkl-1* and *vang-1* are core components of the PCP signalling pathway.

LG	Locus	Allele	Nt. change	Mutant DNA sequence	Protein change
II	***dsh-1***	*zy12*	C > T	GTC AAA **T**AG CAA CCA	Q64Stop
IV	***prkl-1***	*zy11*	C > T	CGT TAT **T**AA CTA CCA	Q101Stop
		zy17		No mutation in coding region	
		zy18	C > T	GCA CCG **T**AG CTC ATC	Q19Stop
		zy19	G > A	tcttaca**a**GTT CAT GCC	splice acceptor
V	***fntb-1***	*zy7*	G > A	ATG CTT **A**AA GAG TAC	E321K
		zy20	G > A	TGC TAC A**A**C TTC TGG	S289N
		zy21	C > T	ATG GAA **T**GA GAA GGC	R305Stop
		zy22		No mutation in coding region	
		zy23	G > A	CAC GGA G**A**A TAC ACT	G238E
		zy24	G > A	TGG ATG T**A**C TAC TGG	C92Y
X	***vang-1***	*zy10*	G > A	GGA AGA CG**a**taaatgtt	splice donor

Obvious pleiotropies observed:

prkl-1(zy11) homozygous males are sterile.

prkl-1(zy17), unlike the remaining *prkl-1* alleles, displays a highly penetrant and severe HSN axon guidance defects (not quantified).

fntb-1 alleles display a visible *egl* phenotype.

Note: coding sequence is represented in uppercase and introns, in lowercase.

Overall examination of polarity mutants reveals clear pleiotropies.

Interestingly, the first *prkl-1* allele *zy11* was obtained in a fertile *him-8(e1489)* background; so in order to backcross the mutant into wild type background and to eliminate deleterious mutations and polymorphisms introduced by EMS, the obvious/fastest way would be mating homozygous males *prkl-1(zy11),him-8(e1489);cyIs4* with N2 hermaphrodites; however, despite numerous attempts this cross was not successful and no cross progeny was obtained. The inability to produce crossprogeny with fertile hermaphrodites suggested that ***prkl-1(zy11)*** **homozygous males are sterile.** This phenotype may hint at a role for *prkl-1* in male fertility and could be related to *prkl-1* expression in the male tail (Supplemental Figure III-3). A different allele, ***prkl-1(zy17)***, with no mutations within the *prkl-1* ORF or promoter and 3'UTR regions, displayed severe **HSN guidance defects** (not quantified). In chapter III, I will discuss a potential explanation as to why only the *zy17* allele but not the remaining *prkl-1* mutants displays this phenotype. Interestingly both *prkl-1* and *fntb-1* mutants display **uncoordinated swimming behaviour** (personal observation), which may suggest that, in both mutants strains, neurons that are crucial to a smooth sinusoidal movement could be affected. Similarly both strains display **uncoordinated locomotion** on agar plates, which is more noticeable in *fntb-1* mutants (personal observation). In addition, *fntb-1* mutants display obvious **egg-laying *(egl)* defective phenotype** (personal observation), but not as severe as the well characterized reference *egl-1(n986)* mutants (Waggoner et al., 1998) (*i.e.* "bags of worms" is not as frequent occurrence). Finally, *dsh-1(ok1445)*, a *dsh-1* deletion allele from the CGC, displayed **lack of and shortening of PDE posterior axons**, suggesting that *dsh-1* is required for PDE posterior axons wild type extension to their final destination near the anus.

Evolutionary conserved PCP genes *dsh-1* and *prkl-1*, and *fntb-1,* suppress AP axon outgrowth in VC4 and VC5 neurons.

The core PCP gene ***Dishevelled*** encodes a multidomain protein composed of an N-terminal DIX domain, mostly involved in the canonical pathway (Pan et al., 2004), a central PDZ domain, and a C-terminal DEP domain, crucial for PCP signalling (Wang et al., 2006a). C. elegans *dsh-1* is located in LGII. Figure II-5B-C displays the domain organization of *C. elegans* DSH-1 and its similarity to DSH proteins from five other species including fly, fish, frog, mouse and human. The multifunctional DSH is a signal transducer for both the canonical β-catenin signalling pathway and in the Fz/PCP pathway (Wang and Wynshaw-Boris, 2004; Wallingford and Habas, 2005; Wang et al., 2006a)

Significantly, the two highest conserved domains in *C. elegans* DSH-1 are the PDZ domain with ~ 70 % identity and the DEP domain with ~ 54 % identity to all analyzed species. Precisely, these two domains are critical to the PCP pathway. The DIX domain, which has been mostly associated with the canonical pathway, only displays ~ 33 % identity across phyla. This observation may suggest that the DSH-1 PCP functions in the *C. elegans* nervous system, dependent on PDZ and DEP domains, might be conserved in humans.

Importantly, sequencing of the candidate locus in the *zy12* polarity mutant revealed an early stop codon (Q64Stop) in the *dsh-1* gene, just before the DIX domain, a premature termination compared to 702 residues in wild type, which likely results in a null phenotype (Table II-4 and Figure II-5). Qualitative and quantitative phenotypic analysis of *dsh-1(zy12)* and deletion allele *dsh-1(ok1445)* showed that both mutants result in similar polarity defects (Figure II-5A and Figure II-8). VC4 and VC5 in both *dsh-1* mutants display the following

morphologies, in order of occurrence 1) tripolar [left and right primary axons and ectopic AP axons], 2) bipolar AP [default morphology, similar to VC1-3, 6] and 3) unipolar neurons [*i.e.* only lacking the left axon]. The above polarity defects incorporate *dsh-1* as another essential player in a neuronal polarity pathway that regulates the morphology/orientation of VC4 and VC5.

In addition, promoter activity from the *cyIs4[Pcat-1::GFP]* reporter appears to be mildly affected in *dsh-1* mutants, for instance in *dsh-1(ok1445)*, ~ 30 % of VC4 and ~ 10 % of VC5 are GFP negative (Table II-5). This effect is relatively minor when compared to the dramatic effect of *Fz/lin-17* and *Wnt/lin-44* mutations in VC4 and VC5 *Pcat-1* transcriptional activity. In *Fz/lin-17* and *Wnt/lin*-44 mutants 100 % of VC4/5 neurons fail to express GFP (Table II-5). Other VC4/5 features appeared normal in *dsh-1(zy12*) and *dsh-1(ok1445)* mutants including pathfinding of primary axons, branching, and vulval morphology.

In addition, because there are two other *dsh-like* genes in the *C. elegans* genome*, dsh-2* and *mig-5,* we considered evaluating the specificity of *dsh-1's* function in the polarity of VC4/5 neurons. We aimed at analyzing the neuronal phenotype in *dsh-2(or302*) and *mig-5(tm2639)* mutants, by crossing them into *cyIs4* background. However, a mutation in *mig-5* resulted in a striking canonical defect similar to *lin-17* mutants, as VC4 and VC5 failed to express GFP, which prevented the analysis of polarity defects (Table II-5, p105). In contrast, mutations in *dsh-2* did not affect *Pcat-1* expression. A quick analysis of VC4/5 phenotype did not reveal any orientation or morphological defects; however no conclusion could be drawn from this, as DNA genotyping was not successful and *dsh-2* homozygotes were only identified by the embryonic lethal phenotype. In order to further assess the specificity *dsh-1*

in VC4/5 polarity, genotyping of *dsh-2* mutants should be optimized and *mig-5* mutants should be crossed into a different reporter that allows for VC4/5 phenotypic analysis.

Figure II-5. Loss-of-function of PCP gene *dsh-1* results in ectopic AP axon growth. A) Representative pictures of VC4 and VC5 motorneurons in wild type (left) and *dsh-1* mutants (middle and right) **B)** Schematic representation of *C. elegans dsh-1* gene and localization of mutations (*zy12* and deletion *ok1445*) at genomic level. **C)** Schematic representation of DSH-1 conserved domain organization. DISHEVELLED is a modular protein with highly conserved DIX, dsh, PDZ and DEP domains. The percentage of identity between DSH-1 domains to the following orthologues is indicated: *Drosophila melanogaster* DVL (AAF438033.1), *Danio rerio* DVL-3 (NP_571832.1), *Xenopus laevis* DVL-3 (NP_001086098), *Mus musculus* DVL-1 (NP_034221.3) and *Homo sapiens* DVL-3 (AAB65244).

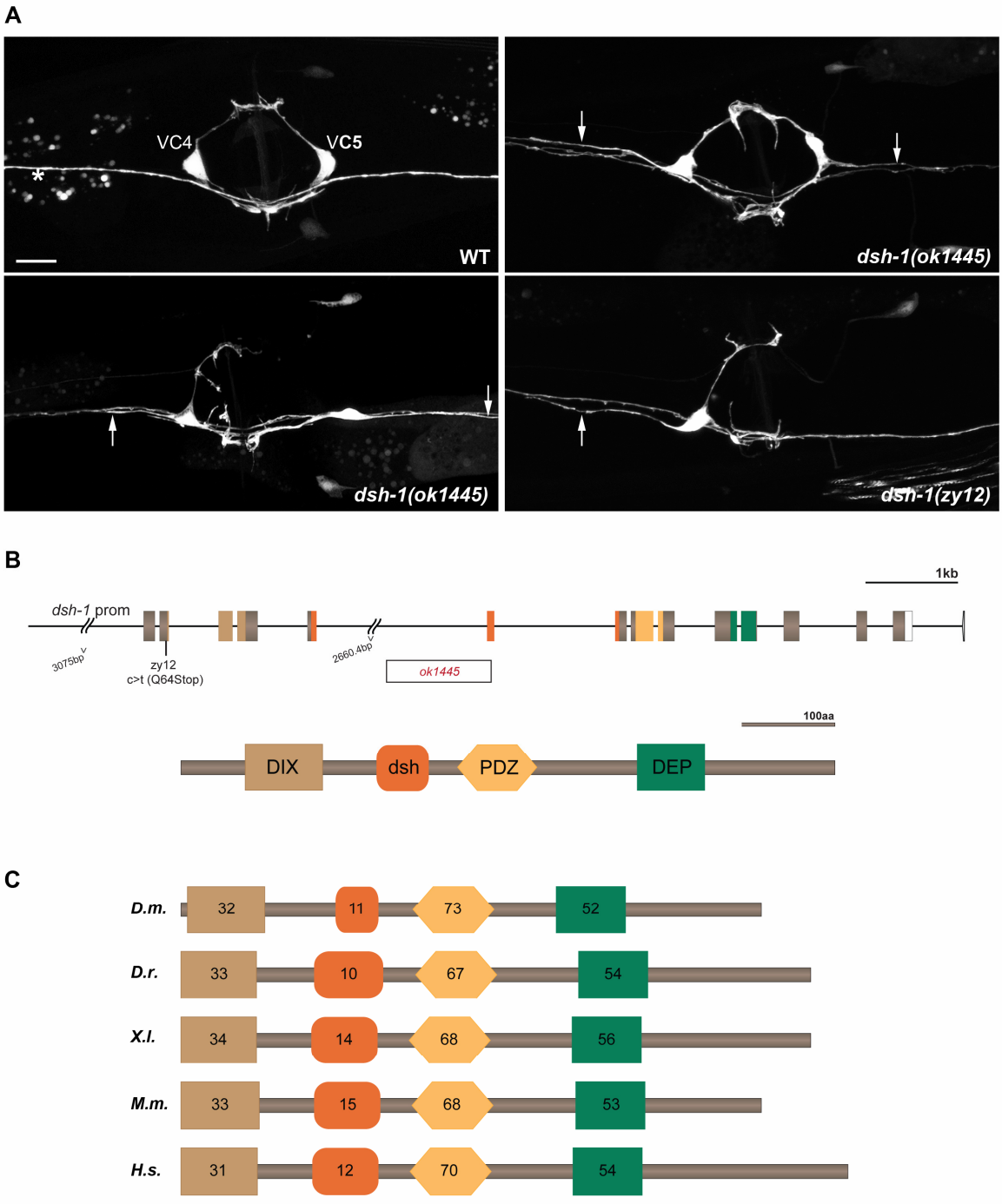
A
VC4
VC5
*
WT
dsh-1(ok1445)
dsh-1(ok1445)
dsh-1(zy12)
B
1kb
dsh-1 prom
3075bp
zy12
c>t (Q64Stop)
2660.4bp
ok1445
100aa
DIX
dsh
PDZ
DEP
C
D.m.
32
11
73
52
D.r.
33
10
67
54
X.l.
34
14
68
56
M.m.
33
15
68
53
H.s.
31
12
70
54

The core PCP gene ***prickle*** encodes a modular protein containing one PET domain and three LIM domains. *C. elegans prkl-1* is located on LGIV. Protein sequence alignment of PRKL-1 reveals a high degree of similarity among homologs across species (Figure II-2). Mutations in *prkl-1* result predominantly in tripolar VC4/5 neurons (Figure II-6). The penetrance of polarity defects in *prkl-1* mutants was higher than in *dsh-1* or *vang-1* mutants (Figure II-8). In addition, contrary to *dsh-1*, in *prkl-1* and *vang-1* mutants, VC4/5 neurons with AP bipolar phenotype are a rare occurrence (Figure II-8).

prkl-1 alleles *zy18* and *zy11* are nucleotide transitions within the coding sequence for the PET domain; resulting in early stop codons located at the first and second exons, respectively (Table II-4 and Figure II-6). Allele *zy18* encodes an 18-residues-long polypeptide, whereas *zy11* encodes a 101-residues-long polypeptide, two prematurely terminated proteins compared to the wild type length of 523 amino acids. Moreover, allele *zy19* is a putative splicing acceptor error that would splice the second exon out and could continue in frame by using the 3rd exon's splice acceptor or out of frame by using any alternative sequence as acceptor. The molecular lesion in *prkl-1(zy17)* has not yet been found, despite having sequenced most of the gene (grey boxed gene area in Figure II-6).

Next, we wanted to explore whether the role of *prkl-1* in VC4/5 morphology was specific or whether other *prkl-like* genes would also be important for the polarity of these motorneurons. Thus, we characterized VC4/5 polarity phenotype in mutants of two other genes encoding PET/LIM-containing proteins. The *C. elegans* genome contains two other *prkl-like* genes, *tag-15* (a.k.a *lim-9*, with 1 PET & 6 LIM domains) and *tag-224* (a.k.a *tes-1*, with 1 PET & 3 LIM domains). By mating these two mutants with a *cyIs4* reporter strain, to

visualize VC4/5, I found that the morphology of VC4/5 neurons was unaltered (Table II-5). This result indicates that there is no redundancy in *prkl* gene activity and that *prkl-1* is a specific and essential regulator of VC4/5 polarity.

We also considered the possibility that *prkl-1* and its PCP-like polarity pathway would be required to polarize other neurons. Thus, since the wild type orientation of PLM mechanosensory neurons, with long process to the anterior and short process to the posterior, is reversed in PCP mutants *Wnt(lin-44)* and *Fz(lin-17)* (Hilliard and Bargmann, 2006), we asked whether *prkl-1* was also involved in regulating the PLM polarity. However, we found that PLM orientation was unaffected in *prkl-1* mutants (not shown), which suggests that different Fz/PCP signalling pathways regulate polarity in different neuron types.

Additionally, except for the extension of ectopic AP axons in *prkl-1* mutants, VC4 and VC5 did not display any other significant morphological abnormalities. Importantly, none of the four *prkl-1* mutants had additional VC4/5 neuronal defects, including axon pathfinding, axon outgrowth and extension, and/or branching of primary left and right axons. Thus, the circular circuitry around the vulva develops properly in *prkl-1* mutants. This finding suggests *prkl-1* function specifically in preventing axon growth in the AP direction and do not disrupt VC4/5 neurons ability to specify, extend, guide and branch their primary axons. In addition, the spatial-temporal activity of the *cat-1* reporter in *prkl-1* mutants was similar to wild type nematodes, suggesting that the identity of VC4/5 was not affected in *prkl-1* mutants, and that the tripolar phenotype does not result from a cell fate change.

Figure II-6. ***C. elegans prkl-1*** **suppresses ectopic axon outgrowth along the AP axis. A)** Confocal images of VC4/5 morphologies in a wild type nematode (top) and *prkl-1* alleles *zy18* and *zy17* (bottom). **B)** Top) Schematic representation of the *prkl-1* locus, with annotations for *prkl-1* alleles from EMS genetic screens: *zy11*(Q101Stop), *zy18*(Q19Stop), *zy19*(splice error), and *prkl-1* deletion alleles from CGC: *ok3182* and *tm3440*. Allele *zy17* does not carry a mutation within *prkl-1* coding region or within non-coding region highlighted in grey hue. Bottom) Schematics of PRKL-1 primary structure and molecular lesions in *prkl-1* mutants. Exons are represented as grey blocks, except for the PET and LIM domains which are highlighted in red and lime, respectively.

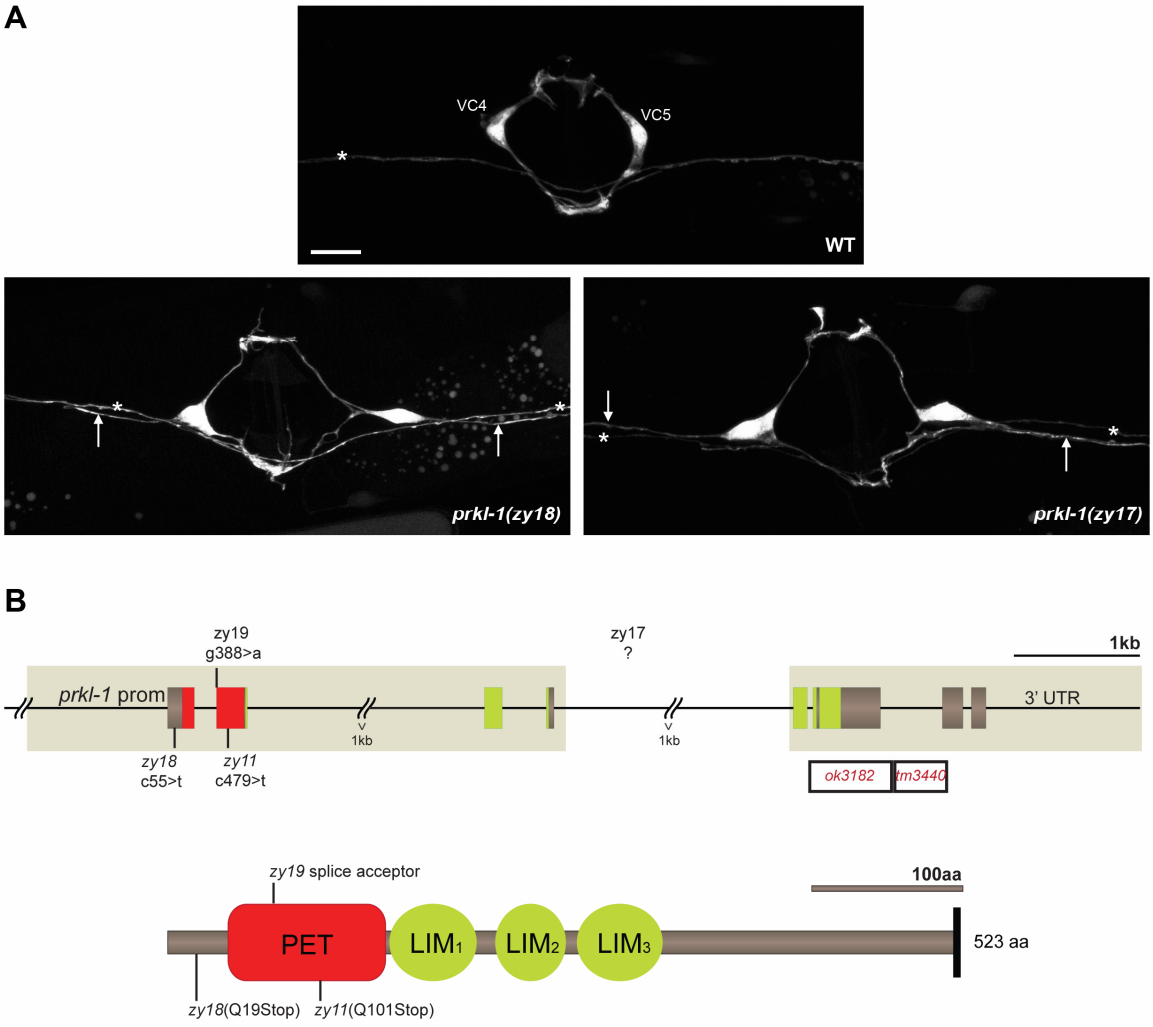

We have isolated and identified a total of six alleles of *C. elegans* ***fntb-1***. All of which display VC4/5 neurons with ectopic AP axon growth (Table II-4). To date we have defined the molecular lesions in five of the alleles (Figure II-7). Three of the lesions involve missense changes in 100% conserved amino acids (C92Y, G238E and S289N) (Figure II-7). These mutants are invaluable findings, since the identity of the mutated amino acids in all species linked to penetrant VC4/5 polarity defects, suggests that these residues are likely crucial for *fntb-1* enzymatic activity.

Figure II-7. Highly conserved *C. elegans* FNTB-1 is 44% identical to human FNTB. Amino-acids changed in FNTB-1 alleles are invariant across evolution. A) Schematic representation of the *fntb-1* gene and DNA lesions in four alleles. **B)** *C. elegans* FNTB (F23B12.6) was aligned with *Rattus norvegicus* FNTB (NP_742031.1) and *Homo sapiens* FNTB (NP_002019). Alignment of proteins was performed using ClustalW2 and visualized with Boxshade 3.31. Black shading indicates identical amino acids and grey shading, similar amino acids. Percentage of identity of *C. elegans* FNTB to rat's and human's FNTB are specified at the amino-terminus. Lesions in *fntb-1* alleles are denoted. Red residues indicate missense mutations in *fntb-1* alleles: *zy24*(C92Y), *zy23*(G238E), *zy20*(S289N), and *zy7*(E321K). Vertical red line represents nonsense mutation in *fntb-1* allele *zy21*(R305Stop). Underneath sequence alignment, schematic representation of rat FTase/FNTB secondary structure (based on C), open boxes represent α helices (β stands for β subunit), diagonally-stripped boxes represent 3_{10} short helices, and black arrows represent β strands. **C)** Topology diagram of rat FTase secondary structure. Adapted from (Park et al., 1997) with permission from corresponding author, Dr. Lorena S. Beese, and copyright permission from The American Association for the Advancement of Science.

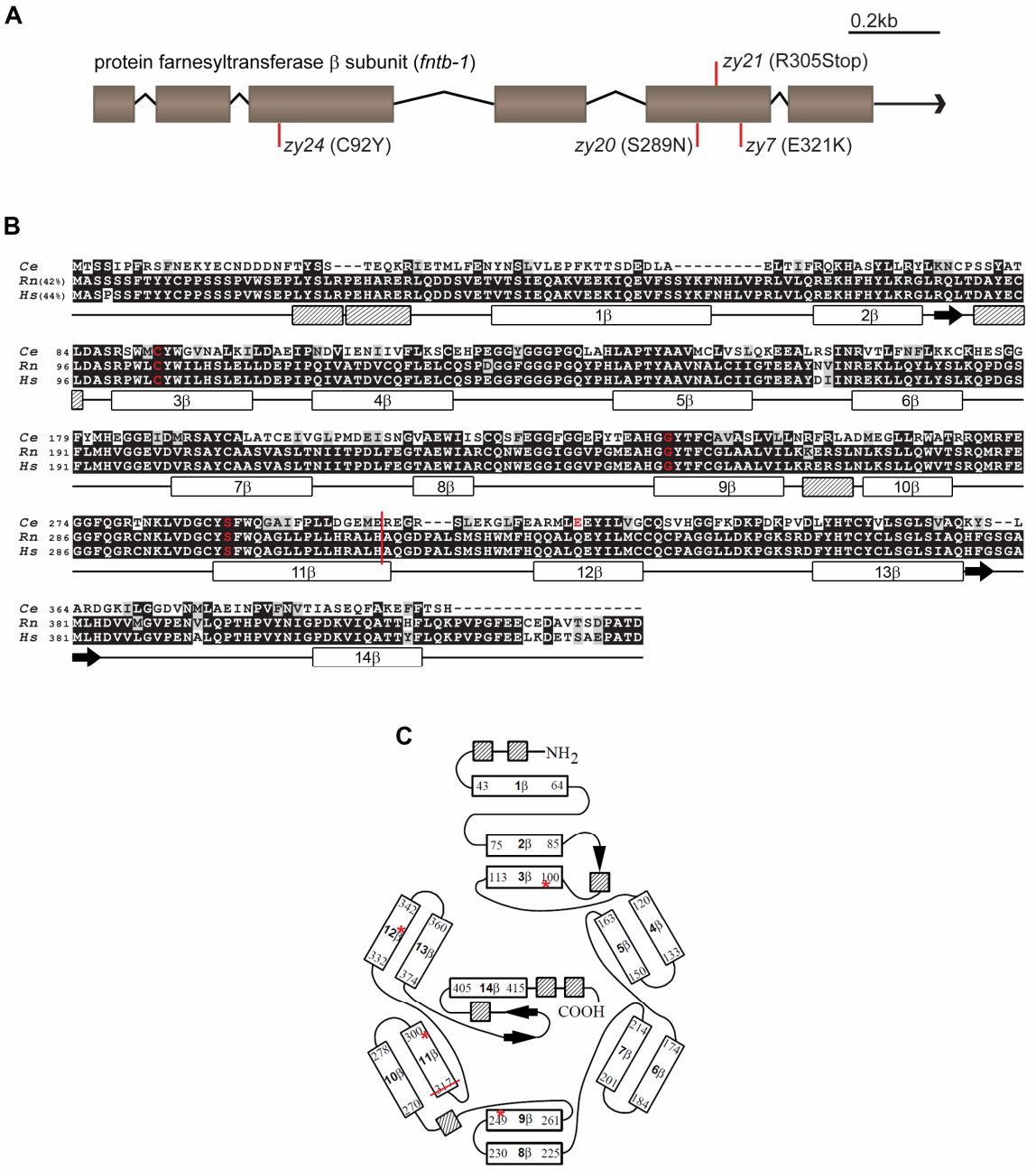
A
0.2kb
protein farnesyltransferase β subunit (fntb-1)
zy21 (R305Stop)
zy24 (C92Y)
zy20 (S289N)
zy7 (E321K)
B
Ce
Rn(42%)
Hs(44%)
1β
2β
3β
4β
5β
6β
7β
8β
9β
10β
11β
12β
13β
14β
C
NH2
COOH

Mutations in core PCP genes *flamingo* and individual *frizzled* do not result in VC4/5 polarity defects.

We tested whether other PCP gene orthologues have a role in specifying axon orientation in VC4/5. Core components in the PCP pathway also include atypical cadherin Flamingo (*fmi*), Wingless (*wnts)* and *wnt* receptors Frizzled (*fz*). Interestingly, a putative null allele of *flamingo*, *fmi-1(tm306)* did not show VC4/5 polarity defects (Table II-5). The *C. elegans* genome contains four Frizzled (*lin-17*, *cfz-2, mig-1* and *mom-5*) and four Wnt (*egl-20*, *lin-44*, *cwn-1* and *cwn-2*) genes. Since loss of function of some *Wnts* and *Fz* genes result in embryonic lethality (*Wnt/mom-2(lf)*), and vulva abnormalities (*Wnt/mom-2*, *Wnt/lin-44*, *Fz/lin-17* and *ryk/lin-18*) caused by defective VPC cell fate specification and/or polarity (Eisenmann, 2005; Gleason et al., 2006; Green et al., 2008), we limited the genetic analysis of VC4/5 polarity to viable homozygous mutants with normal vulval morphology (Table II-5). In addition, the GFP signal from vulval-proximal VCs reporter *cyIs4* was entirely lost in VC4/5 neurons in *lin-44*/Wnt, *lin-17*/Fz, *mig-5*/Dsh, and *bar-1*/β-catenin mutants (Table II-5), while GFP expression was largely unaffected in other dopaminergic neurons with endogenous *cat-1* activity, including PDEs, HSNs and nerve ring neurons. The latter suggests that a non canonical *lin-44*/Wnt-*lin-17*/Fz β-catenin-dependent pathway regulates *cat-1* expression specifically in VC4/5. Importantly, mutations in core PCP genes *prkl-1* and *vang-1* displayed normal *Pcat-1* driven GFP expression, while in *dsh-1* mutants it was mildly affected (Table II-5), which suggest that 1) PCP genes regulate VC4/5 polarity independently of a canonical β-catenin dependent pathway that regulates cell fate decisions in VC4/5, and 2) VC4/5 AP axon growth does not result from abnormal VC cell fate specification.

Other Fz however, are not involved in VC4/5 cell fate decisions, including *cfz-2* and *mig-1* (Table II-5). Notably, we did not observe significant ectopic AP axon outgrowth in *cfz-2* and *mig-1* single or double mutants (Table II-5), suggesting that, at least the combination of *cfz-2* and *mig-1* is not redundantly regulating VC4/5 polarity. However, we cannot exclude a redundant role for other Frizzleds in this neuronal polarity pathway, since loss of VC4/5-specific GFP expression from the *cyIs4 [Pcat-1::gfp]* reporter (Table II-5), together with vulva abnormalities in *lin-17* mutants, including bivulva and protruding vulva, precluded the analysis of all mutant combinations.

Additionally, a *vang-1* pathway including *egl-20* and *cam-1/Ror* regulates the polarity of VPCs (Green et al., 2008). However, *cam-1/Ror* and *egl-20/Wnt* null mutants displayed normal VC4/5 polarity (Table II-5). In addition, we considered whether *lin-18* (*Ryk /Derailed* ortholog) was involved. *Lin-18* is a tyrosine kinase-related receptor which functions as a Wnt receptor and acts independently and parallel to *lin-17* to regulate cell fate patterning in the P7.p vulval lineage (Inoue et al., 2004). Hence, we examined VC4/5 morphology in a *lin-18* null allele. Although, *lin-18(e620)* nematodes display a significant P7.p VPC reverse polarity defect (Green et al., 2008), VC4/5 neurons exhibit normal bipolar ML polarity (Table II-5). Collectively, these data, together with the finding that *prkl-1*, *dsh-1* and *vang-1* mutants display normal vulva morphology, suggest that the VC4/5 polarity defects in PCP mutants are likely not secondary to abnormal vulval morphogenesis.

Table II-5. **VC4 and VC5 polarity defects and *cat-1* promoter activity in various genetic backgrounds.**

	VC4			VC5			
Genotype*	**% AP-oriented neurites**	**% Pcat-1::GFP positive**	**n**	**% AP-oriented neurites**	**% Pcat-1::GFP positive**	**n**	**# worms**
Wild type	1	100	548	0.6	99.8	547	548
Prkl-like							
prkl-1(zy11)	95.9	97.8	217	96.3	97.3	216	222
tag-224(ok1036)	0	100	62	1	100	62	62
tag-15(gk106)	0	98	151	0	95.4	147	154
Dishevelled							
dsh-1(ok1445)	76.8	68.9	155	64	90.2	203	225
dsh-2(or302) †	nd	nd	-	nd	nd	-	-
mig-5(tm2639)	nd	0	-	nd	0	-	>100
Van Gogh							
vang-1(tm1422)	66.6	97.7	543	68.7	97.3	216	222
Flamingo							
fmi-1(tm306)	0	100	128	0	100	128	128
Frizzled							
cfz-2(ok1220)	1.9	99	103	1.9	99	103	104
mig-1(n687)	3	99	147	2	99	145	148
mig-1(n687);cfz-2(ok1220)	1	96	146	1	97	149	157
lin-17(n677)	nd	0	-	nd	0	-	>100
mom-5(or57) **	0	95.8	23	0	100	24	24
Ryk							
lin-18(e620)	0.5	97	196	1.4	99	199	201
Wnt							
lin-44(n1792)	nd	0	-	nd	0	-	>100
egl-20(n585)	2.2	97.9	46	0	100	47	47
Ror							
cam-1(gm122) ‡	0	88.7	63	3	92.9	66	71
β-catenin							
bar-1(ga80)	nd	0	-	nd	0	-	>100

* All lines contain *cyIs4[Pcat-1::GFP]* reporter except *fmi-1(tm306)* which contains *cyIs1[Pcat-1::GFP]* .

** Maternally rescued *mom-5(or57)* worms from *dpy-5(e61), mom-5(or57)/hT2; +/hT2[bli-4(e937) let-?(h661)]* were scored.

† *or302* is embryonic lethal.

‡ Some *cam-1* mutants display mispositioned VC neurons or additional *Pcat-1::GFP* positive neurons flanking the vulva.

The search for components of the polarity pathways regulating VC4 and VC5 morphology/orientation has been narrowed, through forward and reverse genetics, to a handful of genes (Table II-5). Thus, a group of twelve mutants with VC4/5 polarity defects have been mapped, including four prkl-1, one dsh-1 and six fntb-1 alleles; their DNA lesions have been defined and their overall phenotype has been characterized. However, from this moment on, I aimed my thesis work at understanding how prkl-1 and dsh-1, the two core PCP genes, polarize C. elegans motorneurons. Thus, the next focus of Chapter II was to perform genomic rescue of polarity defects in prkl-1 and dsh-1 mutants and to study their genetic interactions, between them and with vang-1 in a PCP-like pathway that shapes the neural circuitry formed by VC4/5 around the vulva.

prkl-1 and _dsh-1_ VC4/5 polarity defects are rescued using genomic constructs.

To establish the link between the polarity phenotype observed in *prkl-1* and *dsh-1* mutants to the DNA lesions found in *Prkl-1* and *Dsh-1* loci, respectively; we performed rescue experiments using GFP-tagged genomic constructs. Thus, GFP-tagged *prkl-1* was injected into *prkl-1(zy11)* mutants at a concentration of 1 ng/µl, which rendered three transgenic lines that exhibited full rescue of the tripolar phenotype. Data from a representative transgenic strain are shown in Figure II-8. Similarly, *dsh-1(ok1445)* deletion mutants were injected with 10 ng/µL GFP-tagged *dsh-1* genomic construct which generated three lines that significantly rescued the mutants' polarity defects (see representative result in Figure II-8). The ability of both, *prkl-1* and *dsh-1* genomic constructs to rescue the polarity defects displayed by *prkl-1* and *dsh-1* mutants, respectively, revealed that 1) both GFP-tagged genomic constructs and transgenes were functional and therefore useful for further

studies including localization and gain-of-function experiments; 2) that the polarity phenotype observed in *prkl-1* and *dsh-1* mutants were caused by lesions in *prkl-1* and *dsh-1* loci, respectively, and not due to additional deleterious changes in the genome. Finally, it confirmed that both *prkl-1* and *dsh-1* are essential components of a polarity pathway that establishes and/or maintains the wild type bipolar morphology of VC4 and VC5 neurons by suppressing AP axon outgrowth.

prkl-1 and _vang-1_ function in a common pathway to suppress axon outgrowth along the AP axis.

The similar VC4/5 polarity phenotype displayed by *dsh-1*, *prkl-1* and *vang-1* mutants suggested that these genes function in a PCP-like pathway to suppress axon growth along the AP axis. To address this notion, I made double mutant combinations *prkl-1(zy11);vang-1(tm1422)* and *prkl-1(zy11);vang-1(tm1422)* and quantitatively analyzed the phenotypes at adult and mid L4 stages (Figure II-8A & B). Based on the premature termination in gene products, *prkl-1(zy11)* and *vang-1(tm1422)* single mutants are likely phenotypic nulls and/or strong loss of function, making the interpretation of double mutant results straightforward. Interestingly, *prkl-1;vang-1* double mutants exhibited a polarity phenotype that was quantitatively similar to either *prkl-1* or *vang-1* single mutants, hinting at a role for *prkl-1* and *vang-1* in a common pathway to regulate neuron polarity. However, because of the highly penetrant defective phenotype (~ 92 % tripolar neurons) of the null *prkl-1(zy11)* strain at adult stage, we considered it more meaningful to quantify the polarity defects at mid L4 stage, when polarity phenotypes had not reached peak values (Figure II-8). Again, consistent with the disruption of a single pathway, polarity defects in *prkl-1;vang-1* double mutant were

not more severe than the *prkl-1* single mutant (Figure II-8). Thus, the combined percentage of VC4/5 neurons with AP directed neurites in *prkl-1(zy11)* nematodes is ~ 82 % at mid L4 stage, while in *prkl-1(zy11);vang-1(ok1445)* double mutants is ~ 69 % (Figure II-8). Taken together, the finding that simultaneous loss of *prkl-1* and *vang-1* does not have any additive effect on the penetrance of the polarity phenotype of the single mutants, suggests that *prkl-1* and *vang-1* function in a common PCP-like pathway to prevent AP axon growth.

The *dsh-1;prkl-1* and *dsh-1;vang-1* double mutants display a higher incidence of AP bipolar morphology, recapitulating the phenotype of VC4/5 in vulva-ablated nematodes.

Double mutant combinations: *dsh-1(ok1445)*; *prkl-1(zy11)* and *dsh-1(ok1445)*; *vang-1(tm1422)* resulted in 100 % of VC4 and VC5 displaying ectopic AP axons directed away from the vulva (Figure II-8). Because *dsh-1; vang-1* and *dsh-1; prkl-1* double mutants, unlike single mutants, display about 20-30 % vulval morphological defects at mid L4 stage (Sanchez-Alvarez et al., 2011), caution was taken so that only adult mutants with grossly normal vulva morphology were scored. Although, we can not exclude the possibility that some of the VC4/5 polarity phenotype might be a consequence of underlying vulval defects, it is unlikely that the polarity phenotype in double mutants is due entirely to abnormal vulva cell fate specification, because single mutants *prkl-1* and *dsh-1* mutants exhibit a normal vulva morphology (not shown), while their VC4/5 neurons display a highly penentrant AP axon phenotype, mostly tripolar neurons (Figure II-8). In addition, although *dsh-1* mutants display normal vulva morphology, their VC4/5 neurons display a mild bipolar AP phenotype (*e.g.* ~ 18 % VC4 and ~ 30 % VC5 display bipolar AP phenotype in *dsh-1(zy12)* nematodes)

Remarkably, the percentage of bipolar AP phenotype in *dsh-1(ok1445); vang-1(tm1422)* and *dsh-1(ok1445); prkl-1(zy11)* double mutants was dramatically increased compared to the respective single mutants (Figure II-8 and Figure II-9). For example, while ~ 15 %, ~ 5 % and ~ 6 % of VC4 neurons in *dsh-1(ok1445), prkl-1(zy11) and vang-1(tm1422)* single mutants, respectively, displayed bipolar AP morphology; ~ 69 % and ~ 60 % did in *dsh-1;prkl-1* and *dsh-1;vang-1* double mutants, respectively. In addition, half of VC4+VC5 neurons with AP axons in *dsh-1(ok1445);vang-1(tm1422)* double mutants had a bipolar AP morphology while the other half displayed a tripolar phenotype. In *dsh-1(ok1445);prkl-1(zy11)* mutants, 60 % displayed bipolar AP polarity and the remaining 40 % showed tripolar phenotype (Figure II-9). Interestingly, this AP bipolar morphology is reminiscent of the VC4/5 phenotype in vulvaless animals, and resembles the phenotype of vulval distal VCs, suggesting that in the absence of at least two core PCP components, VC4/5 fail to sense or to respond to ML polarizing cues from the vulva. It is possible that VC4/5 neurons fail to grow left and right axons because vulval ML polarizing cues are not produced in the absence of PCP. A link between vulva and PCP will be further explored in Chapter III. Altogether, the significant increase in AP bipolar morphology may suggest that *prkl-1;vang-1* function in a parallel pathway with *dsh-1* to prevent AP axon growth and/or to promote axon growth along the ML axis created by the vulva. At this point, with the current experimental evidence, it is not possible to conclude that *dsh-1* is also acting in a common pathway with *prkl-1* and *vang-1*.

Figure II-8. ***prkl-1*** **and** ***vang-1*** **function in a common pathway to suppress ectopic axon outgrowth along the AP axis. A)** Quantification of polarity defects in VC4 (left) and VC5 (right) in single and double PCP mutant combinations, at adult stage. Polarity defects in *prkl-1* and *dsh-1* mutants are rescued by *prkl-1* and *dsh-1* genomic constructs, respectively. Double mutants of *dsh-1(ok1445)* with *vang-1(tm1422)* and *prkl-1(zy11)* result in a significant increase of the AP bipolar morphology. **B)** Quantification of VC4/5 ectopic axons at L4 stage further confirms *prkl-1* and *vang-1* act in the same pathway as the phenotype of the double mutant is not quantitatively superior to any of the single mutants. Statistic significance was assessed by one way ANOVA followed by Bonferroni test. Error bars represent SEM, ***P<0.001. Data published in (Sanchez-Alvarez et al., 2011).

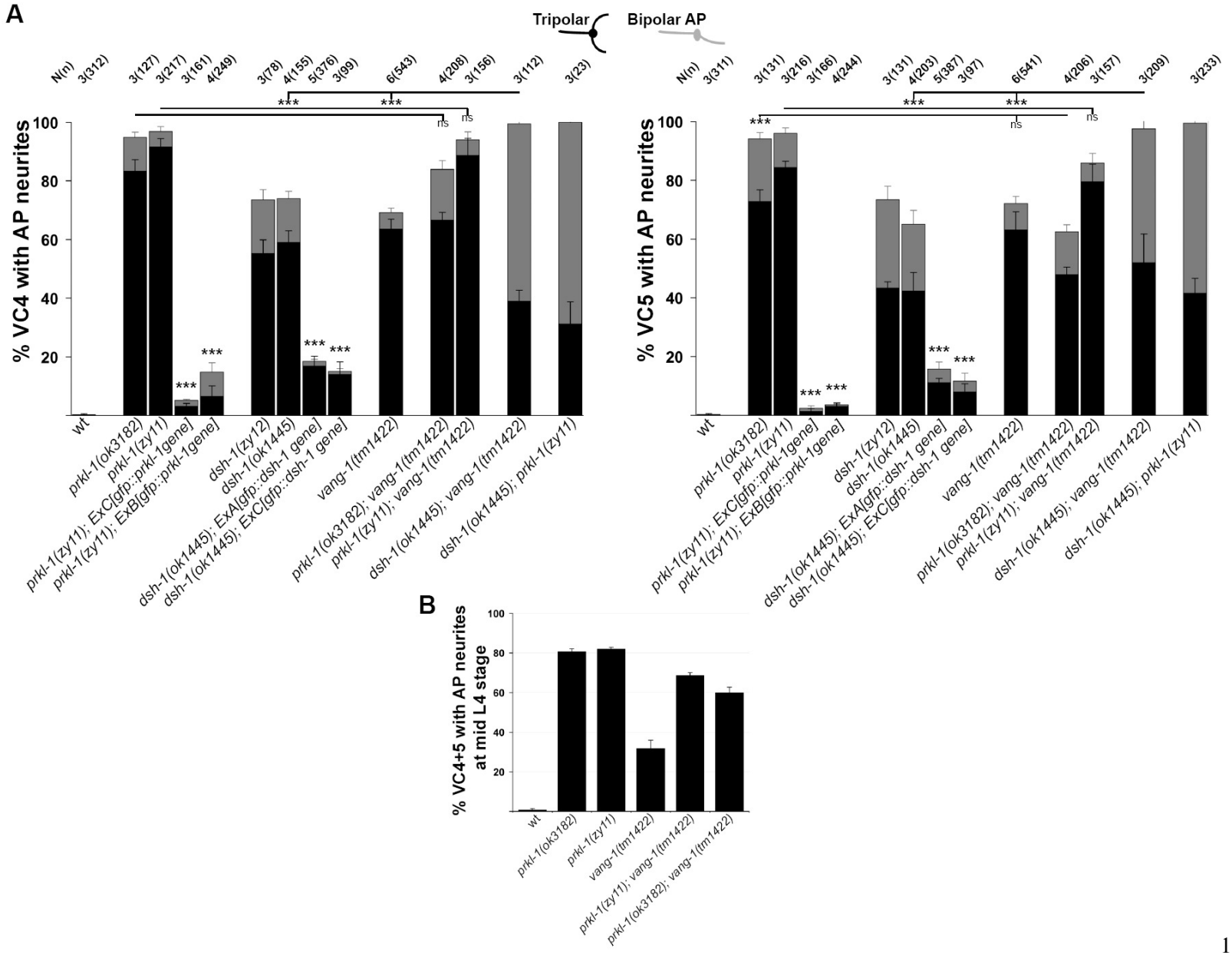
A
Tripolar
Bipolar AP
N(n)
3(312)
3(127)
3(217)
3(161)
4(249)
3(78)
4(155)
5(376)
3(99)
6(543)
4(208)
3(156)
3(112)
3(23)
% VC4 with AP neurites
100
80
60
40
20
***
ns
wt
prkl-1(ok3182)
prkl-1(zy11)
prkl-1(zy11); ExC[gfp::prkl-1gene]
prkl-1(zy11); ExB[gfp::prkl-1gene]
dsh-1(zy12)
dsh-1(ok1445)
dsh-1(ok1445); ExA[gfp::dsh-1 gene]
dsh-1(ok1445); ExC[gfp::dsh-1 gene]
vang-1(tm1422)
prkl-1(ok3182); vang-1(tm1422)
prkl-1(zy11); vang-1(tm1422)
dsh-1(ok1445); vang-1(tm1422)
dsh-1(ok1445); prkl-1(zy11)
N(n)
3(311)
3(131)
3(216)
3(166)
4(244)
3(131)
4(203)
5(387)
3(97)
6(541)
4(206)
3(157)
3(209)
3(233)
% VC5 with AP neurites
B
% VC4+5 with AP neurites at mid L4 stage
wt
prkl-1(ok3182)
prkl-1(zy11)
vang-1(tm1422)
prkl-1(zy11); vang-1(tm1422)
prkl-1(ok3182); vang-1(tm1422)

Figure II-9. Double mutant combinations *dsh-1; prkl-1* and *dsh-1; vang-1* recapitulate the VC4/5 phenotype in vulva ablated animals. A) Top) confocal images of VC4/5 morphologies in *cyIs4* (left) and *dsh-1(ok1445)* (right), displaying typical wild type and tripolar morphologies. Bottom) confocal images of VC4/5 in *dsh-1(ok1445);vang-1(tm1422)* (left) and *dsh-1(ok1445);prkl-1(zy11)* (right) displaying an AP bipolar orientation, consequence of the lack of primary Left axons. White star denotes the ventral nerve cord and white arrows, ectopic AP axons. This morphology is reminiscent of default VC1-3 and VC6 morphologies. Scale bar, 10 µm. **B)** Ratio AP bipolar/Tripolar morphologies in single versus double PCP mutants. Statistic significance was assessed by one way ANOVA followed by Bonferroni test. Error bars represent SEM, ***P<0.001, **p<0.01 and *p<0.05.

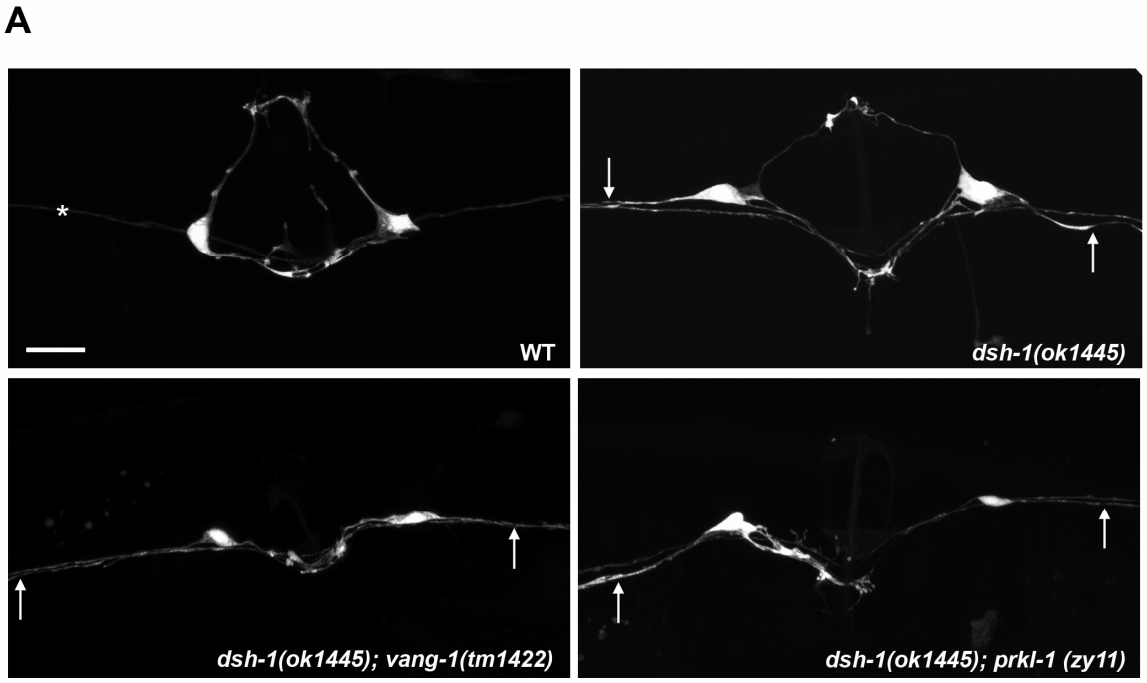
A
*
WT
dsh-1(ok1445)
dsh-1(ok1445); vang-1(tm1422)
dsh-1(ok1445); prkl-1 (zy11)

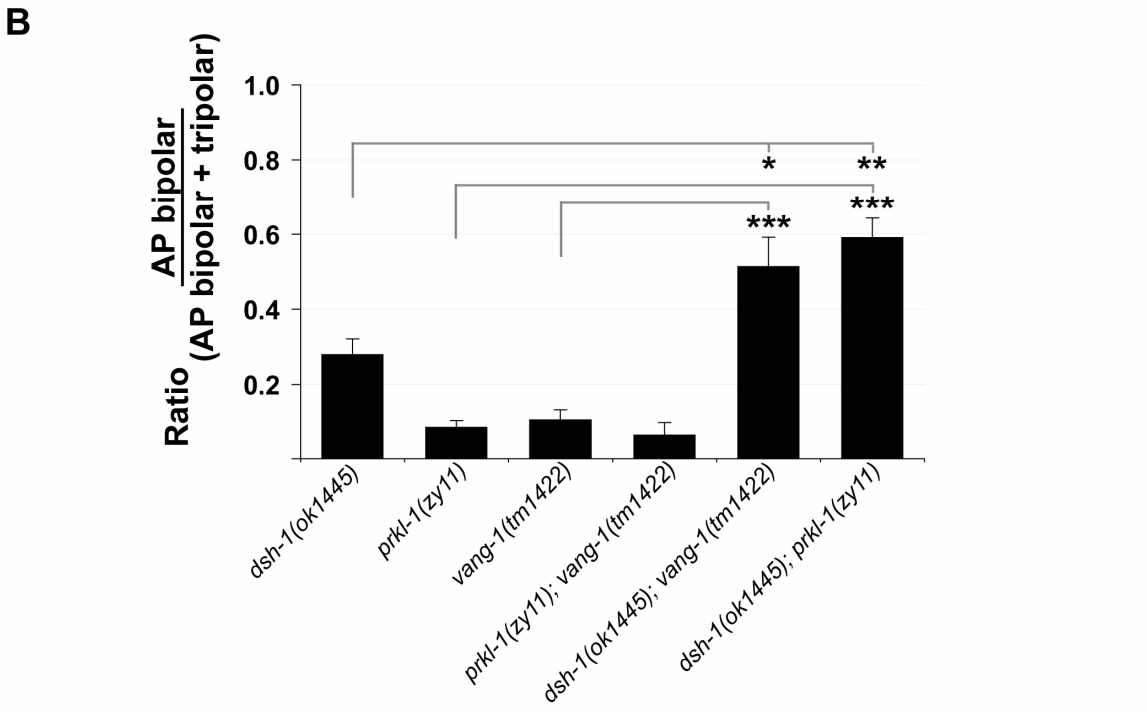
B
Ratio AP bipolar / (AP bipolar + tripolar)
1.0
0.8
0.6
0.4
0.2
*
**
***
***
dsh-1(ok1445)
prkl-1(zy11)
vang-1(tm1422)
prkl-1(zy11); vang-1(tm1422)
dsh-1(ok1445); vang-1(tm1422)
dsh-1(ok1445); prkl-1(zy11)

DISCUSSION

PCP genes *prkl-1* and *dsh-1* suppress axon formation along the AP axis.

In this manuscript we described the isolation of four *prkl-1* alleles (*zy11*, *zy17*, *zy18* and *zy19*) and one *dsh-1* allele (*zy12*), all of which displayed tripolar VC4/5 neurons with anterior-posteriorly directed ectopic axons. Phenotypic characterization of *prkl-1* and *dsh-1* mutants suggests a new role for the PCP genes *prkl-1* and *dsh-1* in neuron morphology/polarity by preventing axon growth along the AP axis, unlike *dsh-2*, *mig-5*, and *prkl*-like genes *tag-15* and *tag-224*. This result contrasts with *in vitro* studies showing that murine *prkl-1* and *prkl-2* instead promote axon outgrowth via *dvl* (Okuda et al., 2007;Fujimura et al., 2009). Collectively, these results indicate that the roles of *prkl* and *dsh* in neuron development depend on the cell/tissue context.

prkl-1 and *vang-1* interact in a common PCP pathway, whereas *dsh-1* acts in a parallel pathway.

Genetic analysis of double mutants showed that *prkl-1* and *vang-1* are in a common pathway to prevent AP axon growth. In addition, we showed that *dsh-1* genetically interacts with both *prkl-1* and *vang-1* to prevent AP axon growth. The significantly enhanced phenotype of *dsh-1* double mutants may suggest that *dsh-1* functions in a parallel pathway. Notably, although *dsh-1; prkl-1* and *dsh-1; vang-1* double mutants develop a functional vulva, most VC4 and VC5 neurons display an AP bipolar morphology similar to vulval-distal VCs. This phenotype resembles the morphology of VC4/5 neurons in vulva-less nematodes (Li and Chalfie, 1990); which suggests that in the absence of PCP signalling VC4/5 neurons are not able to read the mediolateral polarizing

cues and not able to suppress the response to anterior-posterior polarizing cues. In a wild type background, these polarizing signals induce a 90^{o}C rotation of VC4/5 orientation with respect to vulva distal VCs. In other words with the loss of PCP signalling the presence of the vulva is irrelevant to VC4/5 orientation, so that the neurons assume the default AP orientation of VCs, failing to polarize in the ML direction to innervate the egg laying muscles. Altogether, these observations may suggest that the vulva triggers some signalling in VC4 and VC5 which silence the default responsiveness to AP cues, to which the VC family of neurons are responsive to, resulting in a perpendicular rotation of the site of permissive axon outgrowth in VC4/5, to innervate the organ medial-laterally.

Are Fzs and Wnts involved?

In the PCP signalling paradigm, Wnts function upstream of Fzs, and Dvl functions downstream of Fz (Seifert and Mlodzik, 2007; Gros et al., 2009). Previously, Wnts and Fzs were mainly known for their role in β-catenin dependent canonical pathways. Although the role of Fz in the PCP pathway was discovered more than 20 years ago (Vinson et al., 1989), the role of Wnts in the PCP pathway has also been reported. For instance, zebrafish Wnt11 mutant (*silberblick*) displays gastrulation defects which can be rescued with a mutant *dsh* allele that activates PCP and not β-catenin pathway (Heisenberg et al., 2000). Also, Wnt11 regulates the oriented elongation of myocytes during early chick myogenesis, in a PCP signalling pathway which requires Wnt11 as an instructive cue (Gros et al., 2009).

What genes act upstream of *dsh-1* to regulate VC4/5 polarity? To answer this question, we checked whether other core PCP genes were also involved in regulating

VC4/5 morphologies. We found that mutations in individual *Fzs* (*cfz-2*, *mig-1*, *mom-5*), *Wnt/egl-20* and *Fmi* mutants; and double mutant *mig-1*; *cfz-2* did not result in VC4/5 polarity defects. However, these findings are insufficient to rule out *Fz*, *Wnt* and *Fmi* involvement. For instance, double mutants *prkl-1*; *fmi* and *vang-1*; *fmi* resulted in significant suppression of *prkl-1* and *vang-1* polarity phenotypes, suggesting a role for *Fmi* in promoting neurite growth (Sanchez-Alvarez et al., 2011).

The *C. elegans* genome encodes four Frizzled (*lin-17*, *cfz-2, mig-1* and *mom-5*) and four Wnt (*egl-20*, *lin-44*, *cwn-1* and *cwn-2*) genes. It is not known whether *wnts* and *fz* redundantly regulate the polarity of VC4/5 neurons. Because *lin-44/Wnt* and *lin-17/Fz* are involved in a β-catenin dependent pathway affecting expression of *Pcat-1* in VC4/5, and Wnts and Fzs genes play a critical role in vulva morphogenesis (Green et al., 2008), the assessment of the upstream components of this pathway was limited. Mutations in Wnts and Fzs genes alter the vulval cell fate by inhibiting the canonical Wnt pathway, which results in vulval abnormalities. Thus, the involvement of several Wnts and Fzs in vulval morphogenesis precludes the use of forward genetic analysis to study their role in VC4/5 polarity. To overcome this difficulty, a suitable approach could be to specifically downregulate Wnt and Fz function (individually and in combinations) using tissue-specific RNAi experiments, as has been previously described for other genes (Qadota et al., 2007), designed in a way that it would not interfere with vulva organogenesis.

FNTB-1 prevents ectopic AP axon growth in VC4/5.

Positional mapping of the phenotype-causing mutation in neuronal polarity-defective *zy7* mutant, identified the *fntb-1* locus; which encodes the sole worm

orthologue of Farnesyl Transferase β subunit. Protein farnesyl transferases (FTases) are enzymes of high importance in cancer research (McTaggart, 2006). They catalyze the addition of a hydrophobic farnesyl isoprenoid to the cysteine thiol of a carboxy-terminal CaaX motif, in acceptor proteins such as Ras (McTaggart, 2006). Addition of a 15-carbons farnesyl moiety to the C-terminal, anchors the modified proteins to cell membranes (Bos, 1989). The "a", in CaaX motif, represents an aliphatic amino acid, while X is generally a methionine or less frequently serine and glutamine (McTaggart, 2006). Farnesyl transferases exist as heterodimers, consisting of α and β subunits (McTaggart, 2006). While the α subunit is shared with geranyltransferases, the β is exclusive of FTases and binds the prenyl donor for the catalytic reaction (McTaggart, 2006). Significantly, it has been shown that attachment of a farnesyl group to oncogenic variants of Ras is critical to their malignant transformation of cells in a variety of human cancers (Bos, 1989). This finding has made FTases a main target for anticancer therapies, in particular the quest for specific inhibitors to the β subunit (Long et al., 1998).

In addition, we performed genetic screens to enrich the repertoire of *fntb-1* mutants with the aim of gaining insight into how FNTB-1 regulates the polarized morphology of VC4/5 neurons. This project resulted in a collection of six *fntb-1* alleles (*zy7* and *zy20-24)*, all displaying tripolar VC4/5 neurons. These findings suggest a novel function for farnesyl transferases enzymes in neuronal polarity, by preventing axon growth along the AP axis. Furthermore, we found that three of the lesions involved missense changes in 100% conserved amino acids (C92Y, G238E and S289N). Would these be disease-causing missense mutations in humans? I anticipate that these mutations may have a

deleterious effect in other tissues and species, as well. These findings may give researchers additional clues as to which residues are essential to FTase enzymatic activity, which might be linked to disease predisposition.

Notably, all known PRICKLE proteins contain a CaaS carboxy-terminal motif, which could be potential substrates for FTases (See PRKL alignment in Figure II-2). Recently, a research group showed that FTases are critical for the polarized tangential migration of facial branchiomotor neurons in the zebrafish hindbrain, which is dependent on PRKL nuclear localization (Mapp et al., 2011). Thus, using a combination of genetic (translation-blocking morpholino to FTase) and pharmacological (use of potent FTase inhibitors) approaches, the authors demonstrated that FTases are required cell autonomously for PRKL nuclear localization in the neurons, and consequently, for their tangential migration (Mapp et al., 2011). Importantly, zebrafish FNTB does not play a role in the plasma membrane targeting of PRKL in FBMN neurons; instead it regulates PRKL's nuclear localization, which is linked to their polarized tangential migration in the vertebrate hindbrain (Mapp et al., 2011). Altogether, the role of FTases in a vertebrate nervous system development suggests that FNTB-1, may regulate VC4 and VC5 neurons polarity, similarly through PRKL.

Here, I will briefly discuss how FNTB-1 may be linked to neuron polarity. Hypothetically, FNTB's function could be mediated by 1) its ability to attach a membrane-anchor moiety to PRKL proteins, thus regulating their membrane targeting and consequently their function, or by 2) its ability to post-translationally modify other likely substrates such as the family of cytoskeleton-remodelling small GTPases which

also contain C-terminal CaaX motifs (Glomset and Farnsworth, 1994;Zhang and Casey, 1996). Small GTPases have been shown to regulate neuronal polarity *in vitro* (Schwamborn and Puschel, 2004;Watabe-Uchida et al., 2006;Iden and Collard, 2008) and *in vivo* (Yang et al., 2006).

Finally, the missense changes in FNTB-1 allelic variants may 1) directly affect substrate binding and/or the catalytic activity; or 2) exert a dominant negative effect, hence abolishing the function of the wild type protein in heterozygous combinations; or alternatively, 3) disrupt FNTB-1's 3D structure affecting stability, and in extreme case abrogate enzyme activity altogether. To better understand how this enzyme regulates neuron polarity it would be important to 1) assess whether it is acting cell autonomously or cell non-autonomously, 2) identify substrate(s) by performing genetic screenings, 3) perform genetic analysis with other mutants which display a similar phenotype, including *prkl-1*, *vang-1* and *dsh-1*, 4) study how enzyme activity is affected in the allelic variants isolated from the screen, and 5) perform structure-function experiments.

CHAPTER III

prkl-1 regulates the orientation and number of axons in *C. elegans* motorneurons during organogenesis.

Preface

In Chapter II, we isolated four alleles of *prkl-1* and identified their genetic lesions. We demonstrated a link between mutations in the *prkl-1* gene and polarity defects in VC4 and VC5. We uncovered *prkl-1*'s specific requirement to polarize VC4/5 along the left-right axis by suppressing ectopic anterior-posterior axon outgrowth. In addition, we provided evidence for *prkl-1* interaction with *vang-1* and *dsh-1* in a PCP-like pathway which suppresses AP axon growth. In Chapter III, I aimed at understanding when and how *prkl-1* regulates neuron morphology, and to explore the molecular mechanisms that underlie its ability to halt AP axon emergence.

ABSTRACT

The *prkl-1* gene is required for the ML orientation of *C. elegans* VC4/5 motorneurons in a PCP-like signalling pathway which prevents AP axon growth. Where and how is *prkl-1* acting? In this manuscript we show that *prkl-1* is dynamically expressed in both VC4/5 neurons and vulva epithelium. Interestingly, we found that *prkl-1* expression in VC4/5 is induced by vulva epithelium. In addition, our studies reveal that *prkl-1* functions autonomously in VC4/5 neurons to establish and maintain neuronal polarity. Moreover, we show that contrary to the *prkl-1 lof* phenotype (tripolar neurons), *prkl-1* overexpression results in a *gof* phenotype, too few neurites (unipolar neurons). Interestingly, while further exploring the interaction of *prkl-1* with *vang-1* and *dsh-1,* we have found that *prkl-1* overexpression restores VC4/5 wild type morphology in *vang-1* and *dsh-1* mutants, which is suggestive of a downstream role. Furthermore, we provide evidence supporting that *prkl-1* acts instructively to regulate neuron morphology. Also, we provide structure-function evidence showing that of the two putative PRKL-1 isoforms, only the PET-domain-containing one (PRKL-1.A) is necessary and sufficient to regulate neuronal polarity. In addition, structure-function results suggest that while PRKL-1 LIM domains are dispensable to suppress ectopic axon outgrowth they may play a role in the formation of VC4/5 primary axons. Altogether, our studies reveal a novel role for *prkl-1* in regulating the orientation and number of axons during organ innervation.

INTRODUCTION

PRKL is a phylogenetically conserved core element of the PCP signalling pathway. Prkl interacts with other PCP genes including Fz, Vang, Dsh, Dgo, Fmi to regulate a vast array of developmental functions, including the planar polarity of the compound eye and epithelial/cuticular structures in *Drosophila* (Maung and Jenny, 2011) and polarization of vestibular sensory epithelia in the mouse (Deans et al., 2007). Previously, we showed that *prkl-1* interacts with *vang-1* and *dsh-1* to prevent AP axon growth in developping *C. elegans* VC4/5 motor neurons, a newly found role for PRKL in neuronal polarity, which we have further investigated in this manuscript.

PRICKLE is a modular protein containing a row of three LIM domains, which are cysteine-histidine-rich double zinc-binding fingers (Dawid et al., 1998). PRKL LIM domains match the consensus sequence CX2CX16–23HX2CX2CX2CX16–21CX2(CH/D), which is characteristic of zinc-fingers involved in protein-protein interactions; and unlike the GATA type, do not appear to bind DNA (Freyd et al., 1990;Dawid et al., 1998). LIM domains were originally discovered in homeodomain proteins (Dawid et al., 1998), but have since been described in association with kinase (*i.e.* LIM kinases) and GAP domains (Dawid et al., 1998), and in proteins with no other conserved domains, such as LIM only proteins (LMO) (Bach, 2000). The fact that all known PRKL proteins contain at least a triplet of LIM domains may suggest that LIM domains are required as a group rather than as individual subunits (Beckerle, 1997). The fact that the three LIM domains are different may suggest that they interact with different proteins. LMO proteins consist mainly of two LIM domains and are localized in the

nucleus (Bach, 2000). However, other LIM-containing proteins are cytosolic; for instance, many non-homeodomain proteins with multiple LIM domains are associated with the cytoskeleton (Sadler et al., 1992;Dawid et al., 1998); whereas PRKL proteins are localized in the nucleus and plasma membrane (Mapp et al., 2011).

Although several proteins contain multiple LIM domains with similar characteristics, only PRKL proteins contain a single PET (**P**rickle, **E**spinas, **T**estin) domain located upstream of the LIM triplet. PET domains are highly conserved across species and were first identified in the fly PRKL (Gubb et al., 1999b). To date, the 3D structure and function of the PET domain is unknown. Yet, it has been shown that the PET and LIM domains together bind DVL *in vitro*, consistent with a feedback loop mechanism to generate and maintain asymmetric Fz/PCP signalling across wing cells (Tree et al., 2002). A recent report provides structural evidence for a model in which the PET domain penetrates the lipid membrane where it attains a more stable helical conformation (Sweede et al., 2008). This study suggested that the PET domain is involved in targeting the protein to the membrane and the LIM domains modulate this function through protein folding . PRKL-1 also contains a C-terminal CAAX consensus motif which suggests that it may be post-translationally modified by farnesylation and that this domain may be important for membrane localization (Zhang and Casey, 1996).

In this manuscript, we describe the molecular and functional features of the *C. elegans* PCP gene PRKL-1 in the context of developing VC4 and VC5 motor neurons. We show that *C. elegans Prkl-1* encodes two isoforms, one with and one without the conserved PET domain. The PET domain-containing isoform is necessary and sufficient

to establish and maintain the polarity of VC4/5 neurons, whereas a short PET-less isoform is dispensable for this role. Interestingly, PRKL-1 expression in VC4/5 is induced by the vulva epithelia, suggesting a functional link between organogenesis and neuron polarization. In addition, we show that PRKL-1 functions cell autonomously in VC4/5 neurons and that it is localized in symmetric puncta by the plasma membrane and also uniformly in the nuclei. Moreover, PRKL-1 not only regulates neurite orientation in VC4/5 neurons, but also neurite number in a dose-dependent manner. That is, at low levels of PRKL-1 or lack of, VC4/5 acquire a tripolar morphology, whereas at high levels, VC4/5 exhibit a unipolar morphology. Interestingly, *prkl-1* overexpression rescues *dsh-1* and *vang-1* defects, which may be suggestive of a downstream role. Lastly, we undertook a structure-function analysis of PRKL-1 which revealed that the PET domain and the carboxy terminal region are required to suppress AP ectopic axon growth, whereas the triplet of LIM domains are dispensable for this role. Thus, we have dissected PRKL-1 protein and found that the minimal structure required to prevent AP axon growth contains the N-terminal, PET domain and C-terminal regions.

MATERIALS AND METHODS

Materials.

Vectors: pPD95.77 and pPD49.78 were kindly provided by A. Fire from the *C. elegans* Vector Kit. Datasheets and maps are available at:

http://www.addgene.org/docs/fire/andrew/datasheets.pdf

Plasmids used as coinjection reporters: pRF4 [*rol-6(su1006)*] which encodes a mutant collagen that induces a dominant roller phenotype (Kramer et al., 1990;Mello et al.,

1991) and *Podr-1:rfp* containing the promoter of transmembrane guanylyl cyclase ODR-1 which labels AWC sensory neurons in the head (L'Etoile and Bargmann, 2000).

Cosmid: ZK381 containing *prkl-1* gene was obtained from Caenorhabditis Genetics Center (CGC).

cDNA EST clones: *y1233d09* (pME18s-FL3 vector containing *prkl-1.a*) and *yk184d8.5* (phage vector containing *prkl-1.b*) were gifts from Dr. Yuji Kohara (National Institute of Genetics, Mishima, Japan). *y1233d09* was sequenced with primers pME18s-forward and reverse.

***C. elegans* strains.** Worms were cultured by standard methods (Brenner, 1974). All strains were maintained with OP50 *E. coli* on nematode growth medium (NMG) at 20°C, unless otherwise specified. Some nematode strains used in this work were provided by CGC, which is funded by the NIH National Center for Research Resources (NCRR).

Wild type: N2/Bristol and *cyIs4* reporter (see Chapter II).

See Table III-1 for description of mutants used in this study.

Table III-1. Mutant strains used in this study.

Chrom.	Gene	Mutant alleles	Strain
LGIII	*Mpk-1*	*mpk-1(ga117)/dpy-17(e164) unc-79(e1068)*	SD378
LGIV	*Prickle-1*	*prkl-1(ok3182)*	RB2346
		prkl-1(tm3440), prkl-1(zy11), prkl-1(zy17), prkl-1(zy18) and prkl-1(zy19)	-

More details on strains SD378 and RB2346, and allele *prkl-1(tm3440)* can be found at www.wormbase.org.

Microscopy and Phenotypic Quantification from early L4 to adult stage. Worms were visualized using an LSM510 confocal microscope (Zeiss) and an AxioplanII/Apotome microscope (Zeiss) with the Axiovision software. Nematodes were staged with respect to vulval developmental milestones (http://www.wormatlas.org), visualized using differential interference contrast (DIC) microscopy. See Figure I-2D (General Introduction) for images of developmental stages used in this study. All fluorescence photographs were taken with the confocal microscope, with the exception of fluorescence pictures in Figure III-7B, which were taken with the AxioplanII microscope. In order to take images, worms were immobilized with 2 % Levamisole (Sigma) on 2 % agar pads, unless otherwise specified. An AxioplanII microscope was used to quantify polarity defects. Morphology of VC4 and VC5 motorneurons was examined with the *cyIs3* reporter at early and mid L4 stages and with the *cyIs4* reporter at mid L4 and adult stages. A tripolar neuron was scored if the length of the ectopic AP neurite was equal to 1X VC cell diameter (~ 5 µm) in early and mid L4 animals and equal to 3X VC cell diameters or the length of a primary VC4/5 neurite (~ 15 µm) in adults.

Scoring lamellipodial protrusions during L3 stage. We used the *cyIs3* reporter to visualize the morphology of VC4/5 during L3 stage, prior to axonogenesis. The orientation of lamellipodial protrusions was determined from ApotomeII/Axiocam paired fluorescence-DIC images at 1-cell, 2-cell and 4-cell stages of P6.p VPC. Protrusions were defined as any lamellipodial extension from the cell soma. If the VC soma displayed one

anterior- and one posterior-directed protrusion, an AP bipolar morphology was scored, if VC extended only one in either direction, the neuron was scored as unipolar.

Generation of transgenic *C. elegans* strains. Transgenic worms were generated by standard germ line transformation methods (Mello and Fire, 1995). Briefly, expression vectors were co-injected with a reporter plasmid [pRF4 (*rol-6(su1006*)) or *Podr-1::rfp* or *Plin-11::rfp*] into the gonads of young *C. elegans* adults. The DNA injection mixture was prepared to a total concentration of 100 ng/µL by adding pBluescript SK+ or KS+ empty vectors, as needed. When the procedure is successful, injected DNA forms an extrachromosomal array that is heritably transmitted to subsequent generations (Mello and Fire, 1995). Accordingly, transgenic animals were confirmed in the F2 generation by transmission of the roller phenotype (*rol-6*) or a robust red fluorescence in the two AWC head neurons (*Podr-1::rfp*). For each experiment, 2-4 transgenic lines were maintained. Transgenic strains were analyzed by scoring the polarity/orientation of specific neurons or in the case of transcriptional and translational reporters by quantifying the expression profile. The extrachromosomal arrays were placed into different genetic backgrounds by mating with established lines.

Total RNA extraction and RT-PCR for cloning and/or sequencing. Worms from 4 confluent plates were washed with M9 solution and briefly centrifuged at 3000 rpm in 15 mL tubes. Pelleted worms were treated with 4 mL Trizol (Invitrogen). The suspension was vortexed and snap-frozen in $N_{(l)}$, then immediately used or kept at - 80 ^{o}C for further use. To purify total RNA, tubes were allowed to thaw on ice for 1 h and vortexed every 10 min. The content was split into 4 Eppendorf tubes and cleared by centrifugation at

12,000 rpm for 10 min at 4 ^{o}C. The supernatants were combined with 200 µL of chloroform, vortexed for 15 sec and placed on ice for 3 min. After centrifuging at 15,000 rpm for 10 min at 4 ^{o}C the aqueous phase was transferred to a new tube and RNA precipitated with 500 µL of isopropanol during 10 min incubation. RNA was pelleted at 15,000 rpm for 10 min at 4 ^{o}C and washed with 70 % Ethanol. Air dried RNA was then dissolved in 25 uL DEPC water and incubated at 70 ^{o}C for 10 min. Contaminated DNA was removed with a DNAse treatment using DNAse Amplification grade (Invitrogen) following manufacturers instructions. After digestion, DNAse was heat inactivated and the volume of reaction was increased to 200 µL to remove the enzyme with equal volume of Phenol::Chloroform::Isoamyl alcohol. RNA was precipitated, washed and resuspended as described above. 2.6 µg and 1.3 µg of total RNA was used to amplify *prkl-1* and control *myo-3* cDNAs respectively, in single step RT-PCR reaction using Superscript III (Invitrogen) and following manufacturer's procedure. The program to synthesize *prkl-1* cDNA was optimized: 55 ^{o}C 30 min, 94 ^{o}C 2 min, 40 cycles of (94 ^{o}C 15 sec, 59 ^{o}C 30 sec, 68 ^{o}C 1 min & 15 sec) and 68 ^{o}C 2 min. To synthesize internal control *myo-3* cDNA, 30 sec extension time was used instead. Primers combinations employed are listed below. Product DNA was used for sequencing and/or cloning. Before sequencing PCR product was treated with RNAse to remove any interference from template RNA. The following sets of primers were used to RT-PCR-amplify partial fragments of the two *prkl-1* isoforms a and b (*prkl-1.a* and *prkl-1.b*, respectively) from the six current *prkl-1* mutant strains, to diagnose/confirm their occurrence, size and sequence. *myo-3* was amplified as total RNA loading control.

prkl-1.a fragments

forward (f1): 5'cgaattgcagctgatgctcacag 3'

reverse up (r1): 5'gatgtaggaagctcatgagagtac3' (product size 1199bp)

reverse down (r2): 5'gcaggaactctactcaacgag3' (product size 1358bp)

prkl-1.b fragments

forward (f2): 5'caggattattcaattattcaaca3'

reverse up (r1): See isoform a (product size 914bp)

reverse down (r2): See isoform a (product size 1073bp)

myo-3 control fragment

forward: atgtctggaaatccagacgcattc

reverse: cgtggctccaacaatagcgaagtag (product size 600bp)

Transcriptional reporters. Two transcriptional reporters were generated by subcloning specific regions of *prkl-1* promoter into the pPD95.77 backbone vector, which contains the *gfp* coding sequence and the 3' untranslated region (UTR) of the *unc-54* gene.

The constructs, which overlap from positions -1.28 kb to + 0.17 kb, were named *upPprkl-1::gfp* (5.8 kb, containing the entire upstream intergenic region) and *Pprkl-1::gfp* (4.86 kb, containing 1.28 kb upstream of the *prkl-1.a* ATG codon and 3.58kb downstream, until the third exon). See Figures III-3 and Supplemental Figure III-1 for schematic representations of the constructs. Genomic regions were PCR amplified using

cosmid ZK381 as template and the following primers (restriction sites are in capital letters):

upPprkl-1::gfp (5.8 kb)

forward, *Sph1*: 5'ctGCATGCaccagaatttcccacttttcttcac3'

reverse, *Xba1* 5'gcTCTAGAcaaagcacatccactgtcatcatc 3'

Pprkl-1::gfp (4.86 kb)

forward, *Sph1*: 5'ctGCATGCgctatacacattctggtgttctgg3'

reverse, *Xba1*: 5'gcTCTAGAaagtagaacatcacacgtttgacacc3'

The constructs were individually injected at 30 ng/µL with 40 ng/µL *rol-6(su1006)* containing-plasmid (pRF4) as coinjection marker into wild-type worms; and where specified, also coinjected with 10 ng/µL *Plin-11::rfp* to label VC1-6. Transgenic lines were then isolated and maintained to study *prkl-1* promoter activity.

Cell-specific expression: Full length *prkl-1.a* cDNA was generated by RT-PCR from N2 RNA extracts (see methods, "Total RNA extraction..."), using primers 5'caTCTAGAatgagcgaacgaattcgccgtc3' and 5'caGGATCCtcaagatactgtacatctggaac3' and inserted into *XbaI*/*BamHI* sites of a *gfp*-less pPD95.77 vector. A *gfp* cassette was then PCR-amplified from pPD95.77 using primers 5'caaGTCGACatgagtaaaggagaagaac3' and 5'ccTCTAGAatcgattttgtatagttcatccatgcc3' and then inserted in-frame into *SalI*/*XbaI* sites upstream the atg codon of *prkl-1.a* to generate *gfp::prkl-1.a*. Cell-specific promoters *Punc-4*, *Pcat-1*, *Pcol-10* were PCR-amplified (primer sequences below) from *C. elegans*

genomic DNA and inserted upstream of *gfp::prkl-1* to generate *Punc-4::gfp::prkl-1.a*, *Pcat-1::gfp::prkl-1.a*, and *Pcol-10::gfp::prkl-1.a* respectively. Correctness of the constructs was verified by restriction digest and sequencing. All constructs were injected at 10 ng/µL with 40 ng/µL of *Podr-1::dsRed* into *prkl-1(zy11), cyIs4* mutant background to generate the following transgenes: *[Punc-4::gfp::prkl-1.a]*, *[Pcat-1::gfp::prkl-1.a]*, *[Pcol-10::gfp::prkl-1.a]*. All experiments were performed using at least two independent transgenic lines per construct. Primers to amplify promoters are as follows:

Punc-4*::gfp::prkl-1.a*

forward, Pst1: 5'ctatCTGCAGccacctctgtcttcaaggcgacctacac3'

reverse, Pst1: 5'ttacCTGCAGgatatctttcacttttggaagaagaagatcctc3'

Pcat-1*::gfp::prkl-1.a*

forward, Pst1: 5'tatCTGCAGcaaggctctgcagggtacctatg3'

reverse, Pst1: 5'ccgCTGCAGctgatccaatcaagaatgtacgac3'

Pcol-10*::gfp::prkl-1.a*

forward, HindIII: 5'gtacAAGCTTgtcgactctagaactagtggatc3'

reverse, Pst1: 5'ctaaCTGCAGaccttattcagtgttacccttcc3'

Overexpression experiments. *prkl-1* overexpression was carried out by injecting *gfp*::*prkl-1* transgene and *Punc-4::gfp::prkl-1.a* at increasing concentrations in *prkl-1(zy11)* and wild type nematodes. Transgenic lines were generated and the

overexpression phenotype was scored. A control construct *Punc-4::gfp* was generated by *XbaI*/*BamHI* excision of *prkl-1.a* cDNA from *Punc-4::gfp::prkl-1.a* followed by re-ligating the vector. A negative control *gfpstop*::*prkl-1* gene was made as described below.

Fusion PCR to introduce a STOP codon/frame shift into *gfp*::*prkl-1* gene. To generate a negative control for the overexpression experiments performed with *gfp*::*prkl-1* gene, we engineered a stop codon after the *gfp* sequence using the Fusion PCR method as previously described (Hobert, 2002). Briefly, we generated the altered gene by fusing two PCR fragments containing a 22bp overlapping sequence and a sequence change (introduced in the fragments by the primers). Thus, a single nucleotide "A" (see primers below) was added in the 5' inside primer C to generate a stop codon after the *gfp* sequence and a consequent frame shift in the *prkl-1* coding region. This construct would fail at expressing PRKL-1 protein while preserving all the regulatory sequences within *prkl-1*. The *gfp*::*prkl-1* construct was used as template to amplify the individual upstream (I) and downstream (II) amplicons. Amplicon I contains *prkl-1* promoter and *gfp* sequence and amplicon II, the stop codon and the remaining of *prkl-1* gene including 3'UTR. The following primers were used:

Amplicon I (7.74 kb)

forward A, 5' outside: 5'ttacaggcaagcgatccgtcc3'

reverse B, 3' inside: 5'catccactgtcatcatcagatg3'

Amplicon II (8.53 kb)

forward C, 5' inside: 5'aacatctgatgatgacagtggat**gA**ctttggacgagtatgcatggg3'

reverse D, 3' outside: 5'tgcattaccaatggcttctg3'

Fusion of amplicons I and II, 16.2 kb

forward A*, nested to A: 5'tgcattcttcggcaacacagc3'

reverse D*, nested to D: 5'aaaagcgtggtgcactctcag3'

The underlined sequence corresponds to the overlap region between both amplicons. The grey highlighted triplet represents the stop codon and frame shift created by inserting a single adenine "A".

PCR conditions were optimized. Polymerase and buffers from Expand Long Template PCR System (Roche) were used. The amplification program for the individual amplicons was as follows: 94 ^{o}C 2 min, 6 cycles of (94 ^{o}C 10 sec, 63 ^{o}C 30 sec minus 1 sec/cycle, 68 ^{o}C 7 min), 4 cycles of (94 ^{o}C 15 sec, 57 ^{o}C 30 sec, 68 ^{o}C 7 min), 20 cycles of (94 ^{o}C 15 sec, 57 ^{o}C 30 sec, 68 ^{o}C 7 min:20 sec + 20sec/cycle), 68 ^{o}C 7 min and 4 ^{o}C forever. A longer extension time was required to amplify the fusion (16.197 kb). Thus, underlined steps in the program above were modified: …68^{o}C_13 min:10 sec, ...68^{o}C_13min:10sec ,…68^{o}C_13 min:30 sec, respectively.

***Phsp16-2::prkl-1* sense and *Phsp16-2::prkl-1* antisense.** A 1.1 kb fragment from *prkl-1* cDNA was PCR-amplified (not including start codon) using primers: forward, *BamH1*: 5' attGGATCCtgtgctttggacgagtatgc3' and reverse, *BamH1*: 5'tatGGATCCgctctttgtggtggttttgg3'. The PCR fragment was digested and inserted in sense and antisense orientations in the *BamH1* site of pPD49.78 backbone vector, downstream the *hsp16-2* promoter, to generate *Phsp16-2::prkl-1* sense and *Phsp16-*

2::prkl-1 antisense. These plasmids were then co-injected at 30 ng/µl each with 40 ng/µl of *Podr-1::dsRed* into *cyIs4* worms.

Inducible RNAi. Worms expressing *Phsp16-2::prkl-1*sense; *Phsp16-2::prkl-1*antisense; *Podr-1::DsRed* were grown to the specified developmental stage at 20 °C, shifted to 35 °C for 2 h and recovered at 20 °C. VC4 and VC5 morphology was scored after 32-34 h of recovery at 20 °C. Synchronized populations were obtained by allowing gravid worms (50 worms per plate) to lay eggs for 1 h at 20 ^{o}C. Worms were further staged following developmental hallmarks (i.e. L3 stage, by distal tip cell migration (Normaski) and L4 stage, by the vulva invagination (Normaski) and half moon appearance of the vulva under the dissecting microscope. In order to obtain "before" and "after" pictures of the same animal, individual worms at mid L4 stage were gently immobilized in a bed of 2 % agar on a microscope slide using 0.0025 % of Levamizol, followed by placing the slide at 4 ^{o}C for a few minutes. The worms were then photographed, washed in M9 and placed in individual OP50 seeded plates. They were immediately heat shocked as described before and then incubated at 20 ^{o}C where they grew to the adult stage for the "after" picture.

Semi-quantitative single worm RT-PCR. Total RNA from individual synchronized nematodes (chosen blindly from heat shocked and control) was isolated using Trizol reagent (Invitrogen) following manufacturer's instructions, with modifications. Briefly, worms were washed off bacteria in M9 solution and individually picked into eppendorf tubes. Following the addition of 200 µL of Trizol, the tubes were snap-frozen in $N2_{(l)}$, then allowed to thaw on ice for 1 h while being vortexed every 10 min. After spinning at 14,000 rpm for 10 min at 4 ^{o}C, the supernatant was mixed with 40 µL of Chloroform in a

new tube and vortexed for 15 sec, then placed on ice for 3 min and centrifuged as before. RNA, in the supernatant, was precipitated with 100 µL Isopropanol. Because of the small amounts, to facilitate RNA recovery, a final 20 ng/ml glycogen was added with the alcohol. Then RNA was pelleted, washed with 70 % Ethanol, air-dried and solubilized in 25 µL DEPC-treated water at 60 ^{o}C. A single step of reverse transcription (RT) using oligodT primers (Invitrogen) combined with PCR was performed according to manufacturer's instructions (Superscript III One-Step RT-PCR System, Invitrogen). Gene-specific primers were used to amplify the transcript of interest *prkl-1* (forward 5'cgaattgcagctgatgctcacag3' and reverse 5'gatgtaggaagctcatgagagtac3'), and the internal control myo-3 (forward 5' atgtctggaaatccagacgcattc 3' and reverse 5' cgtggctccaacaatagcgaagtag 3'). 15 uL RNA was used as template for *pkl-1* reaction and 5uL, for *myo-3*. For each primer pair, cycle times and primer concentrations were optimized to ensure linear amplification. RTPCR program for *prkl-1*: 53 ^{o}C 30 min, 94 ^{o}C 15 sec, 35 cycles of (94 ^{o}C 2 min, 53 ^{o}C 30 sec and 68 ^{o}C 1 min:15 sec) and 68 ^{o}C 2 min. The program for *myo-3* 55 ^{o}C 30 min, 94 ^{o}C 2 min, 40 cycles of (94 ^{o}C 15 sec, 59 ^{o}C 30 sec and 68 ^{o}C 30 sec) and 68 ^{o}C 2 min. Data were analyzed by measuring the area and density of the electrophoresis bands using Scion software. Changes in *prkl-1* mRNA levels before and after RNAi induction were quantified using Scion software, normalized to the *myo-3* transcripts and expressed as arbitrary densitometry units.

Construction of PRKL-1 deletions. To dissect the functional modules of PRKL-1 protein, we deleted entire motifs from the cDNA sequence and scored for the ability of the truncated protein to rescue polarity defects in *prkl-1(zy11)* mutant. To delete internal domains we made use of the redundancy in the genetic code and engineered

translationally silent endonuclease restriction sites at convenient locations within *prkl-1* cDNA, while not disrupting the amino acid sequence. Upstream and downstream DNA fragments were assembled together in between the *XbaI* and *BamH1* sites of pD95.77, in frame and downstream from *Punc-4::gfp*. PCR primers included silent changes in the nucleotide sequence aimed at generating restriction sites that were used to join both PCR fragments. PCR-amplified up and down DNA fragments were digested with restriction enzymes and ligated in a three pieces reaction (vector, upstream insert and downstream insert). All constructs were sequenced to insure fidelity of the seams. The following primers were used to amplify full length *prkl-1* isoforms a and b and to generate deletion constructs of *prkl-1.a*. Synthetic restriction sites are capitalized.

*Punc-4::gfp::**prkl-1.a*** (1572 bp, 523 aa)

forward, *XbaI*: 5'caTCTAGAatgagcgaacgaattcgccgtc3'

reverse, *BamH1*: 5'caGGATCCtcaagatactgtacatctggaac3'

*Punc-4::gfp::**prkl-1.b*** (lacks 38 N-terminal residues and the PET domain of PRKL-1A, 1326 bp, 442 aa)

forward, *XbaI*: 5'cgcTCTAGAatgaaaatgaaattgagacac3'

reverse, *BamH1*: See isoform a

*Punc-4::gfp::**prkl-1.a* ΔC terminus** (984 bp, 327 aa, missing aa 328-523)

forward, *XbaI*: See isoform a

reverse, *BamH1*: 5'caGGATCCtcattgatatccacaaaataggg3'

*Punc-4::gfp::**prkl-1.a*** **ΔCTVS** (1560 bp, 519 aa, missing aa 520-523)

forward, *XbaI*: See isoform a

reverse, *BamH1*: cgGGATCCtcatctggaacttttcttttttctttgccattcg

*Punc-4::gfp::**prkl-1.a*** **ΔLIM1** (1401 bp, 466 aa, missing aa 147-203)

upstream fragment

forward, *XbaI*: See isoform a

reverse, *Bpu1102I*: 5'ctgGCTCAGCatgatcaaatggagcatattgaacaacacc3'

downstream fragment

forward, *Bpu1102I*: 5'catGCTGAGCaggtcaagccgagatgtgccaagtgtg3'

reverse, *BamH1*: See isoform a

*Punc-4::gfp::**prkl-1.a*** **ΔLIM2** (1416 bp, 471 aa, missing aa 271-329)

upstream fragment

forward, *XbaI*: See isoform a

reverse, *SacII*: 5'gtaCCGCGGcttgacctgttcagcatggtgtcttcc3'

downstream fragment

forward, *SacII*: 5'gtaCCGCGGtttcactcatcttcatcaacattttc3'

reverse, *BamH1*: See isoform a

***Punc-4::gfp::prkl-1.a* ΔLIM3** (1398 bp, 465 aa, missing aa 271-328)

upstream fragment

forward, *XbaI*: See isoform a

reverse, *SalI*: 5'cgattcaGTCGACgaagatgagtgaaaacatttcaagcacac3'

downstream fragment

forward, *SalI*: 5'catcgttcGTCGACatgtggtggagaagacgaagagttgcttg3'

reverse, *BamH1*: See isoform a

***Punc-4::gfp::prkl-1.a* ΔLIM1-3** (1029 bp, 342 aa, missing aa 147-327)

upstream fragment

forward, XbaI: See isoform a

reverse, *Eco72I*: 5'ggaCACGTGtcaaatggagcatattgaacaacacc3'

downstream fragment

forward, *Eco72I*: 5'ctaagtaCACGTGtggtggagaagacgaagagttgcttg3'

reverse, *BamH1*: See isoform a

Each construct was injected at 10 ng/µL with 40 ng/µL *Podr-1::rfp* as coinjection marker in the gonads of *prkl-1(zy11)* mutant strain. At least 2-4 transgenic lines were isolated for each construct and scored for polarity defects and the rescue thereof. Transgene *[Punc-4::gfp::prkl-1.a]* was outcrossed into knock out strain *prkl-1(zy17)* to

study the role of *prkl-1* isoform A in neuronal polarity. Since the only actual way to genotype allele *zy17* is by the absence of *prkl-1* transcripts via RT-PCR, an approach was taken to make sure that *[Punc-4::gfp::prkl-1.a]* transgene was effectively placed in the *zy17* background. Hence, a cross was set between *prkl-1(zy11)*; *cyIs4*; Ex*[Punc-4::gfp::prkl-1.a]* and N2 males. Heterozygous *prkl-1(zy11)*; *cyIs4* males carrying the transgene were then mated with homozygous hermaphrodites *prkl-1(zy17).* The F1 crossprogeny was singled out into individual plates and allowed to self-fertilize. F2 transgenic plates with non transgenic siblings displaying ~ 95 % tripolar VC4/5 were considered for genotyping. Non transgenic siblings from these plates were then carefully isolated using the fluorescence microscope and genotyped for *prkl-1(zy11)* using single worm PCR. A plate with a wild type DNA pattern (*i.e.* with no *zy11* genotyping bands) was maintained and the ones with the parental *zy11* pattern were discarded. Finally, the putative *prkl-1(zy17); cyIs4; Ex[Punc-4::gfp::prkl-1.a]* strain was confirmed by the absence of *prkl-1* transcripts in the non transgenic segregated siblings via RT-PCR, as described above in "semi-quantitative single worm RT-PCR"

Statistical analysis. All experiments were performed at least 3 times (N). The actual number of neurons scored (n) in each experiment is included in the Figures. Quantitative data were analyzed using Prism V software (Graphpad). Data are reported as mean ± SEM. Differences between groups were investigated with ANOVA followed by the post Hoc test Bonferroni. P values of < 0.05 were considered significant.

RESULTS

C. elegans prkl-1 encodes two isoforms.

The core PCP gene *prkl-1* is encoded on the negative strand of chromosome IV in the *C. elegans* genome; specifically at genetic position 3.28 +/- 0.001 cM, spanning from genomic position 6986924 bp to 6978764 bp (from atg to 3'UTR) [www.wormbase.org]. The protein predictor software featured at Wormbase estimates the transcription of two isoforms from the *prkl-1* locus. Sequence analysis of EST *C. elegans* clones *yk1233d09.3* and *yk184d8.5* validated the existence of two *prkl-1* mRNAs, a long transcript *prkl-1.a* (1572 bp, encodes a 523 aa PRKL-1 protein) and a short transcript *prkl-1.b* (1230 bp, encodes a 409 aa protein), respectively. To confirm the occurrence of both transcripts, total RNA isolated from wild type N2 strain was used as template for cDNA synthesis using Oligo(dT) primers followed by a PCR with isoform specific primers. RT-PCR-amplified cDNAs were then sequenced. Indeed, sequencing results confirmed a second open reading frame (ORF) corresponding to isoform b that could be generated by alternative 5' splicing or the use of different promoters (See Figure III-1). Consequently, *prkl-1.b* lacks the PET domain and possesses a distinctive 37aa N terminus which is encoded by an intron sequence of *prkl-1.a*. Both proteins share three LIM domains. However, only PRKL-1.a conforms to the domain composition of a *Drosophila* PRKL homologue, since *prkl-1.a* unlike *prkl-1.b* contains a PET domain preceding the LIM domains. To date, the function of the conserved PET motif remains unknown.

Altogether, with the identification of two *prkl-1* transcripts another question arises: are they both relevant to neuron polarity? Only immunochemistry data using isoform specific antibodies can help determine whether one or both isoforms are actually expressed and where. However, cell-specific rescue experiments can help determine where *prkl-1* is required; and structure-function analysis can assess the relative significance of PRKL-1 isoforms to VC4/5 morphology (see later in Chapter III).

Figure III-1. Long (a) and short (b) *prkl-1* transcripts. Schematic representation of *Prkl-1* gene, *prkl-1.a* and *prkl-1.b* transcripts, and putative (by conceptual translation) PRKL-1.A and PRKL-1.B isoforms. PET and LIM domains are colour coded as indicated. PRKL-1.B contains a unique N-terminus encoded by an alternative exon within the second intron of the long isoform.

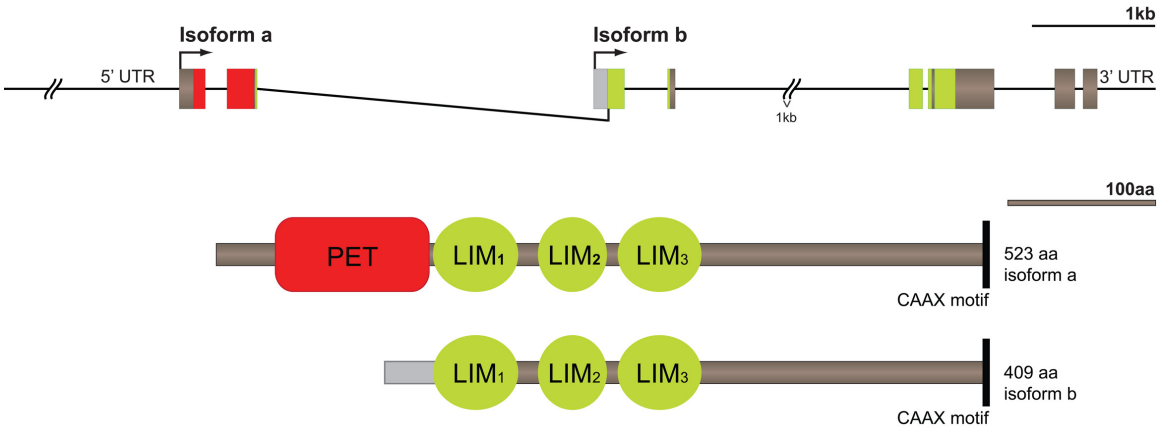

Molecular and phenotypic characterization of *prkl-1* mutants.

To gain insight into the role of *prkl-1* in regulating neuron orientation/polarity, I carried out a molecular and phenotypic characterization all the *prkl-1* mutant strains available to us, including four alleles from our genetic screens and two deletion alleles, *ok3182* and *tm3414,* obtained from the *C elegans* Knock out consortium. Figure III-2A indicates the genomic lesions in all *prkl-1* strains excluding *zy17*. As of today, we have not found the phenotype-causing mutation in the *zy17* allele. We know however, the DNA lesion is not located within the open reading frame, or the promoter region, or the 3'UTR; a segment within the fourth intron remains to be sequenced.

None of the *prkl-1* alleles have been characterized at the transcriptional level. Therefore, to obtain more information regarding how the DNA molecular lesion in each allele translates at the protein level and to correlate the results to the phenotype, I synthesized and sequenced *prkl-1* transcripts from each mutant strain. Accordingly, I performed RT-PCR for both *prkl-1* isoforms and for *myo-3* cDNA as loading control (see methods section for primers and PCR conditions). I used two pairs of primers to amplify each *prkl-1* isoform via RT-PCR (Figure III-2A); however, for sequencing I used several primers to cover the entire length of each transcript. A representative RT-PCR gel, of three independent experiments, is shown in Figure III-2B. Strikingly, I consistently found that no *prkl-1* transcripts either short or long are produced in the *zy17* strain, suggesting that the *zy17* mutation abolishes both transcripts. This result signifies that *zy17* is a knock out allele. In other words, the *zy17* is RNA null, therefore protein null, therefore phenotypic null. What sort of a DNA lesion could result in the lack of *prkl* mRNA

production? A number of possibilities may account for this result, including a) a mutation in a *cis* regulatory element within *prkl-1* locus that is necessary for its transcription (*e.g.* enhancer or intronic region), which have escaped sequencing, b) a *trans* mutation in a *prkl-1* specific transcription factor, or c) a mutation which affects stability of *prkl-1* transcripts (*i.e.* too short half life to be detected using semiquantitative RT-PCR). Since *myo-3* RT-PCR from *zy17* strain displays normal levels, it is unlikely that lack of *prkl-1* transcripts in *zy17* underlies a general transcription deficiency (Figure III-2B). In addition, I examined whether the phenotype-causing mutation in the *zy17* allele was linked to F38a5, a SNIP located at 3.21 cM. *prkl-1* locus is located at 3.28 cM. I found that 6/6 N2-hawaiian recombinants, with homozygous mutant phenotype, displayed the N2 F38a5 pattern. This linkage may suggest that *zy17* lesion is likely within, or near the proximity of the *prkl-1* locus.

In addition, three of four *prkl-1* alleles isolated from our genetic screens contain mutations in the PET domain, all of which affect exclusively the long and not the short isoform (Figure III-2A). Two of them (*zy11* and *zy18*) are stop codons that truncate the protein very early and result in a highly penetrant tripolar VC4 and VC5 phenotype (~ 90 %) (Figure III-2C). This data suggests that the long isoform is important to suppress AP axon formation in VC4/5. In addition, because the difference between the long and short isoforms reside in the 38 N-terminal residues and the conserved PET domain only present in all PRKL-like proteins, it is reasonable to hypothezise that the PET domain is important for VC4/5 polarity. However, the specific role of PET domains has not been yet characterized in any of the PCP model systems. Hence it will be important to test the

notion that the PET domain is indeed critical and to learn how, by performing structure-function and directed mutagenesis studies. The third mutation (*zy19*) is a splice acceptor error (ag to aa), which might result in 1) a protein with middle portion of the PET domain spliced out, if a different splice acceptor is used, or alternatively in 2) a protein that terminates prematurely. The evidence seems to fit the first possibility. In three independent experiments, using the same experimental conditions, mRNA from *zy19* was purified in parallel with mRNA of the other alleles followed by RTPCR and sequencing. Interestingly, sequencing results invariably read as clean profiles up to the mutated nucleotide, and from then on it will show as several superimposed transcripts. Upon careful examination of the profile some short sequences could be distinguished belonging to the PET domain within the second exon, located posterior to the ag>aa splice acceptor transition, which suggests that alternative splice acceptors are used. The weak phenotype (~ 20 - 25 %) of *zy19* (Figure III-2C), is consistent with the notion that out-splicing of the first intron takes place while using other potential in-frame acceptors in the vicinity, therefore rendering functional PRKL-1 proteins with in frame deletions. The finding that 80 - 75 % of VC4/5 neurons in *zy19* allele display wild type morphology may suggest that hat the whole PET domain is not absolutely critical to prevent AP axon growth.

Interestingly, analysis of the RT-PCR gel in Figure II-2B uncovers that the size of long *prkl-1* transcripts in deletion allele *ok3182* are significantly shifted to a faster migrating band. The smaller size of these transcripts is accounted for by the removal of the entire sixth exon from *Prkl-1* gene (see predicted protein sequence in Figure II-2D). Because the r1 reverse primer is located within *ok3182* deletion, no bands showed in the

ok3182 lanes on the top gels. Based on RT-PCR/sequencing, the *Prkl-1* coding region in *ok3182* mutant is thrown out of frame, which results in a PRKL-1 protein that is cut short at the second LIM domain and attaches an unrelated polypeptide carboxy-terminal tail of 52 amino acids (depicted in blue in Figure III-2D). Although the combined penetrance of VC4/5 polarity defects in *ok3182* nematodes appear similar to KO *zy17*, or phenotypic nulls *zy11* and *zy18* (Figure III-2C), when VC5 neurons are individually assessed the phenotype appears less severe than in *zy17* nematodes, with a significantly higher contribution of bipolar AP species, suggesting that it is not a phenotypic null allele, but rather a strong *lof*. The strong phenotype in *ok3182* mutants may suggest that the 3rd LIM domain and/or C-terminal region are critical to PRKL-1's PCP function in VC4/5 neurons; or alternatively, that the resulting truncated protein is unstable, with a short half life.

Moreover, from examining the RT-PCR agarose gels, it is evident that contrasting to the *ok3182* allele, the *tm3440* deletion did not appear to significantly affect the size of the long transcripts (Figure III-2B). *tm3440* deletion removes 411 bp within the 5th intron-6th exon boundary, 378 bp to the intron and 33 bp to the exon. If the sixth exon was not transcribed at all, then a downshift of 162 bp would be apparent from the gel. In addition, RT-PCR sequencing of *tm3440 prkl-1.a* cDNA resulted in a clear sequence profile until the end of exon 5th and then it reads as several coexistent transcripts, a situation similar to the splice acceptor mutant *zy19* allele. Together, both observations (*i.e.* no shift in migration and the sequencing chromatogram) suggests the use of alternative splice acceptors in the vicinity of the wild type acceptor, resulting in

transcripts of similar size to wild type. In addition, the finding that *tm3440* mutants display a weak ectopic AP axon phenotype, ~ 20 % of VC4/5 is consistent with the notion that alternative nearby in-frame splice acceptors are used.

Conveniently, the *ok3182* and *tm3440* deletions are located one next to the other, and do not overlap. Briefly, the *ok3182* allele, which lacks the 3rd LIM domain and the 1st half of the C-terminal domain, and has the 2nd half of the C-terminal tail changed into irrelevant sequence, results in strong loss of function; while *tm3440* allele, which contains 3rd LIM domain and the 1st half of the C-terminal domain, results in a weak loss of function. Regardless of what the *tm3440* deletion does to the other half of the C-terminal region, the above complementary results may hint at a role for the 3rd LIM domain and/or the 1st half of the C-terminus in suppressing ectopic axon growth along the AP axis. Structure-function studies would help discern the individual contributions of each PRKL-1 domains to its polarity function in VC4/5.

Altogether, molecular and phenotypic characterization of *prkl-1* alleles reveal that ***zy17* is a knock-out allele, *zy11* and *zy18* are phenotypic nulls, *ok3182* is a strong hypomorph and *zy19* and *tm3414* are weak hypomorphs**. In addition, the results presented in this section, hint at critical roles for the PET domain-containing isoform and the 3rd LIM domains and/or the C-terminal region, in preventing axon formation along the AP axis.

Figure III-2. Molecular and phenotypic characterization of six *prkl-1* alleles. Correlating DNA/protein lesion to polarity defects. A) Schematic representation of *Prkl-1* locus with all available alleles (top), and *prkl-1.a* and *prkl-1.b* transcripts (bottom). Forward (f1, f2) and reverse (r1, r2) primers used for RTPCR, are indicated. **B)** Isoform specific RTPCR amplifies *prkl-1.a* and *prkl-1.b*, using RNA extracts from *prkl-1* alleles: *zy11*, *zy18*, *zy19*, *ok3182* and *tm3440* as templates, and four primer combinations, as indicated. Myosin-3 (*myo-3*) cDNA was amplified from each extract as a loading control. **C)** Quantification of VC4 and VC5 polarity defects in *prkl-1* alleles, in the adult stage. **D)** Predicted PRKL-1.A protein sequence for *prkl-1* mutant strains.

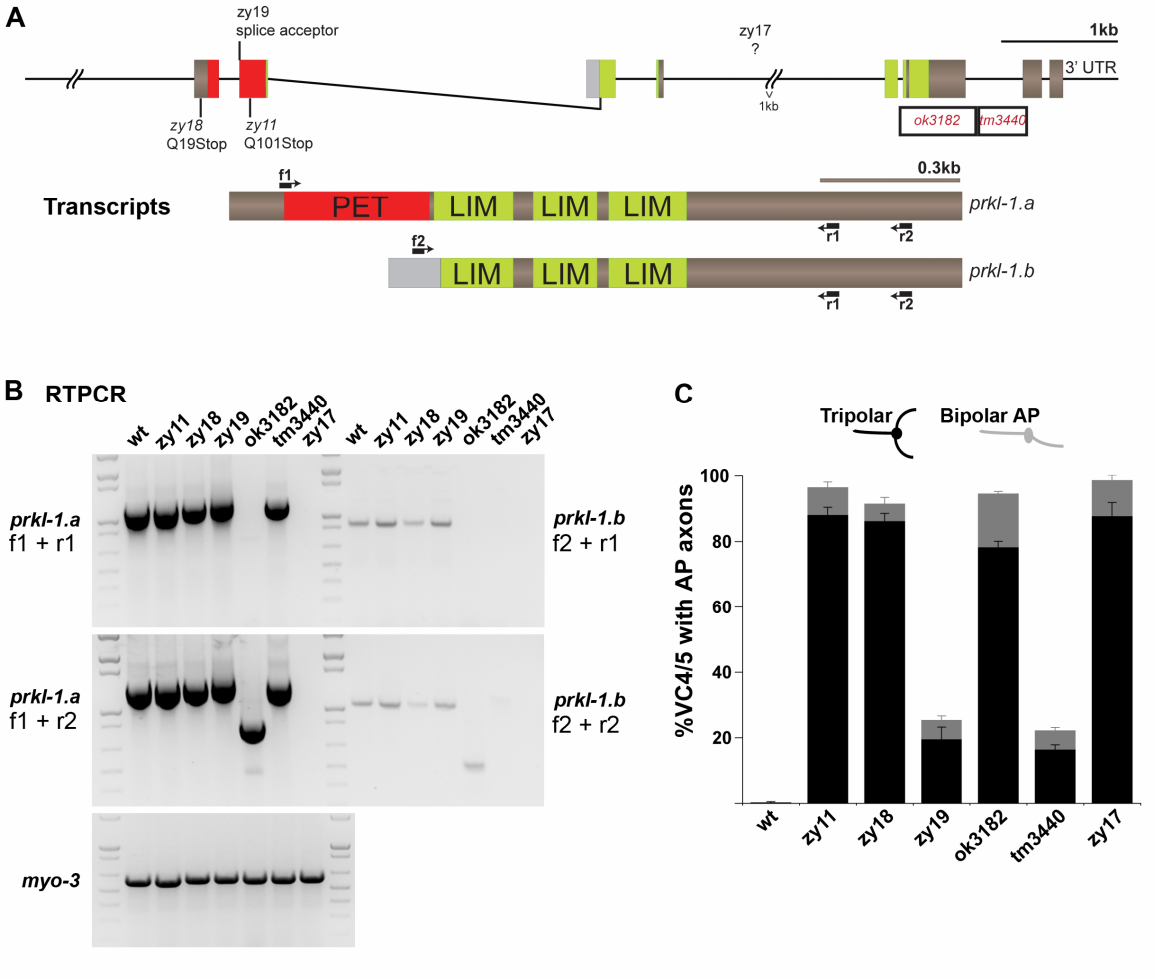

D

cDNA sequence/Predicted protein

wt

```
MSERIRRRRLEASEQFAPQLISSRRAQGGLSPASR
IRIAADAHRHSTSDDDSGCALDEYAWVPSGLKPNM
VHAYFACLPENKVPFIGSAGEKWRQRQSRYQLPPQ
DSDVRYCEDLNAEEADTLRMFERTRKTECLGSGVV
QYAPFDTKCEKCPKRLEEGEISVMAARTGKRYHPS
CFRCQTCDVLLVDLIYFAHDNQIYCGRHHAEQVKP
RCAKCDEVIFGDECLEAEGRSWHFHHFQCAQCNDV
LADQKYMQRANKPVCLKCFHSSSSTFSCTTCRLSF
SSDTPHMSQGDLHWHASAECFCCCVCSKNLLGVKY
SRVGESLFCGYQTCGGEDEELLDEDRLGSPHRKVT
QKSTKVVRIPASPRVAPRHPHVIQQNLTTTMTIQK
PSVVIQNQRPKPPQRAPPPPPSENIYETVLPCSSN
NSPNFDKKYSHELPTSPNHHNYYSKTPNNLLTGYP
EMDGYSTSSSSSDSDDEQLYISNIMAAASLSRVPAK
SSSRKSKKNEPMMMSGGGVRMAKKKKSSRCTVS
```

zy18

```
MSERIRRRRLEASEQFAP
```

zy11

```
MSERIRRRRLEASEQFAPQLISSRRAQGGLSPASR
IRIAADAHRHSTSDDDSGCALDEYAWVPSGLKPNM
VHAYFACLPENKVPFIGSAGEKWRQRQSRY
```

ok3182

```
MSERIRRRRLEASEQFAPQLISSRRAQGGLSPASR
IRIAADAHRHSTSDDDSGCALDEYAWVPSGLKPNM
VHAYFACLPENKVPFIGSAGEKWRQRQSRYQLPPQ
DSDVRYCEDLNAEEADTLRMFERTRKTECLGSGVV
QYAPFDTKCEKCPKRLEEGEISVMAARTGKRYHPS
CFRCQTCDVLLVDLIYFAHDNQIYCGRHHAEQVKP
RCAKCDEVIFGDECLEAEGRSWHFHHFQCAQCNDV
LADQKYMQSFLHLLTTIITTQKHQIICLLGIPKWM
DIVHHLRRIQMMNSFTFQILWQPPR
```

tm3440

```
MSERIRRRRLEASEQFAPQLISSRRAQGGLSPASR
IRIAADAHRHSTSDDDSGCALDEYAWVPSGLKPNM
VHAYFACLPENKVPFIGSAGEKWRQRQSRYQLPPQ
DSDVRYCEDLNAEEADTLRMFERTRKTECLGSGVV
QYAPFDTKCEKCPKRLEEGEISVMAARTGKRYHPS
CFRCQTCDVLLVDLIYFAHDNQIYCGRHHAEQVKP
RCAKCDEVIFGDECLEAEGRSWHFHHFQCAQCNDV
LADQKYMQRANKPVCLKCFHSSSSTFSCTTCRLSF
SSDTPHMSQGDLHWHASAECFCCCVCSKNLLGVKY
SRVGESLFCGYQTCGGEDEELLDEDRLGSPHRKVT
QKSTKVVRIPASPRVAPRHPHVIQQNLTT...?
```

prkl-1 reporter transgenes are dynamically expressed in the VC motorneurons and in the vulva epithelium.

To obtain clues as to when and where *prkl-1* is required to regulate neuronal polarity, I constructed two *prkl-1* transcriptional reporters and studied their spatial-temporal transcriptional regulation, *Pprkl-1up::GFP* comprising 5.8 kb of 5' flanking region and fused in frame with GFP at exon 1, and *Pprkl-1::GFP* comprising 4.86 kb genomic region (including 1.28 kb of 5' flanking region) fused in frame with GFP at exon 3 (Figure III-3 and Supplemental Figure III-1). See Methods for details on construction. Although I qualitatively characterized reporter lines harboring each of the two constructs, the *Pprkl-1::GFP* transgene was characterized and quantified more thoroughly (Figure III-3). The expression pattern of *Pprkl-1up::GFP* is presented in Supplemental Figure III-1. Briefly, *Pprkl-1up* is expressed consistently in the vulval-proximal VC4/5 neurons from L4 to adulthood, and in the head and tail, and variably in the vulva epithelium. Because *Pprkl-1up* was expressed in several VNC neurons including commissures, it was not possible to discern expression in vulval-distal VCs.

We obtained two transgenic lines with *Pprkl-1::GFP* at 30 ng/µL with partially overlapping, spatial-temporal expression patterns, Ex2 and Ex26 (Figure III-3A,B). Notably, Ex2 GFP expression was restricted to the head (including some unidentified neurons), tail, VC4 and VC5 and the vulva epithelium (Figure III-3A). In addition to these locations, Ex26 was also expressed in vulval-distal VCs (Figure III-3B). We further confirmed that *Pprkl-1::GFP* was expressed in vulval distal VCs and not in other VNC neurons with similar positioning by coinjecting 50 ng/µL *Pprkl-1::GFP* with 10 ng/µL *Plin-11::RFP* (a VC-specific reporter, used to label all VCs with RFP) and 40 ng/µL pRF4 [*rol-6(su1006)*] and

assessing colocalization of both reporters in the resulting transgenic line (Supplemental Figure III-2).

Significantly, both Ex2 and Ex26 extrachromosomal arrays, display a dynamic but consistent expression pattern. For instance in Ex2, the percentage of worms expressing GFP in VC4 and VC5 neurons was high and unaffected from early L4 to adulthood, in the range of ~ 81-98 % for VC4, and ~ 77-95 % for VC5; whereas the percentage of worms expressing GFP at the vulva was ~ 48 % at early L4 and then increased with developmental age, peaking at late L4 with 100 % GFP+ vulvas. This maximum was followed by a dramatic decline to 9 % of GFP+ adult vulvas. The finding that *Pprkl-1* activity in VC4 and 5 persists through adulthood, while expression in the vulva extinguishes, suggests the notion of *prkl-1* playing a continuous role in maintaining neuronal morphology. Importantly, the other transgenic line Ex26 with similar expression patterns confirmed this finding. In addition to VC4/5, Ex26 also displayed a variable expression in some vulval-distal VCs at 20^{o}C. However the intensity of GFP in these neurons, when animals are raised at 20 ^{o}C, is too dim to allow for accurate scoring. At the same time, we found that culturing the worms at 25 ^{o}C made green fluorescence significantly brighter without affecting the overall patterns of expression. Consequently, aiming for a brighter GFP we grew both transgenic lines at 25 ^{o}C and quantified the neurons with green fluorescence. We found that both strains expressed GFP dynamically in VC1-3 & 6. The percentage of worms with GFP+ vulval distal VCs peaked at early L4 and fades away by late L4 stage (*e.g.* 38.9 % VC3 at early L4 drops to 0 % in the young adult), contrasting with the temporal pattern of GFP expression at the vulva, which peaks at late L4. Interestingly, the nearer the VC is to the vulva the higher the percentage of GFP+ worms for that particular VC; for instance while 51 % of animals were GFP+ for VC6, only 18 % were GFP+ for VC1

(Figure III-3D). This result is suggestive of a correlation between vulva proximity and *Prkl-1* expression. Would this suggest that the vulva epithelia induce *Prkl-1* gene expression in the VCs? This idea will be explored in the next result section.

In summary, expression of both transcriptional reporters specifically in VC4/5 persists throughout adulthood; this finding may suggest that *prkl-1* is required early to initiate/establish neuronal polarity and also later in development (after neurons have matured/branched) to maintain AP axon growth blocked. We later tested this notion through controlled knock down of *prkl-1* gene expression while VC4/5 ML primary axons were still forming. Finally, it appears as if once VC4/5 neurons have innervated the egg laying system and have extended branches, *prkl-1* expression in the vulva is no longer required and is turned OFF. Would *prkl-1* expression in the vulva be relevant to or independent (*i.e.* vulva cell fate/ morphogenesis) of *prkl-1* function in preventing AP axon growth in VC4/5? Cell specific rescue experiments would help discern if *Prkl-1* expression at the vulva plays a role in VC4/5 polarity.

Figure III-3. ***prkl-1*** **promoter is dynamically expressed in VC neurons and vulva epithelium. A)** Schematic representation of the *Pprkl-1::gfp* transcriptional reporter used in this study. **B)** Top, representative whole worm confocal picture of transgenic strain Ex2[*Pprkl-1::gfp; rol-6(su1006)*] at young adult stage. Bottom left; representative pictures showing progression of *Pprkl-1* transcriptional activity at the vulva area with developmental age (late L4 and adult). Bottom right; quantification of GFP expression in transgenic strain Ex2. **C)** Representative whole worm confocal picture of transgenic strain Ex26[*Pprkl-1::gfp; rol-6(su1006)*] at mid L4 stage. **D)** Quantification of *Pprkl-1::gfp* dynamic transgene expression in VC neurons at various stages, in Ex2 and Ex26 independent transgenic lines. Error bars, SEM. Number of worms counted per stage is indicated. Scale bar, 20 μm.

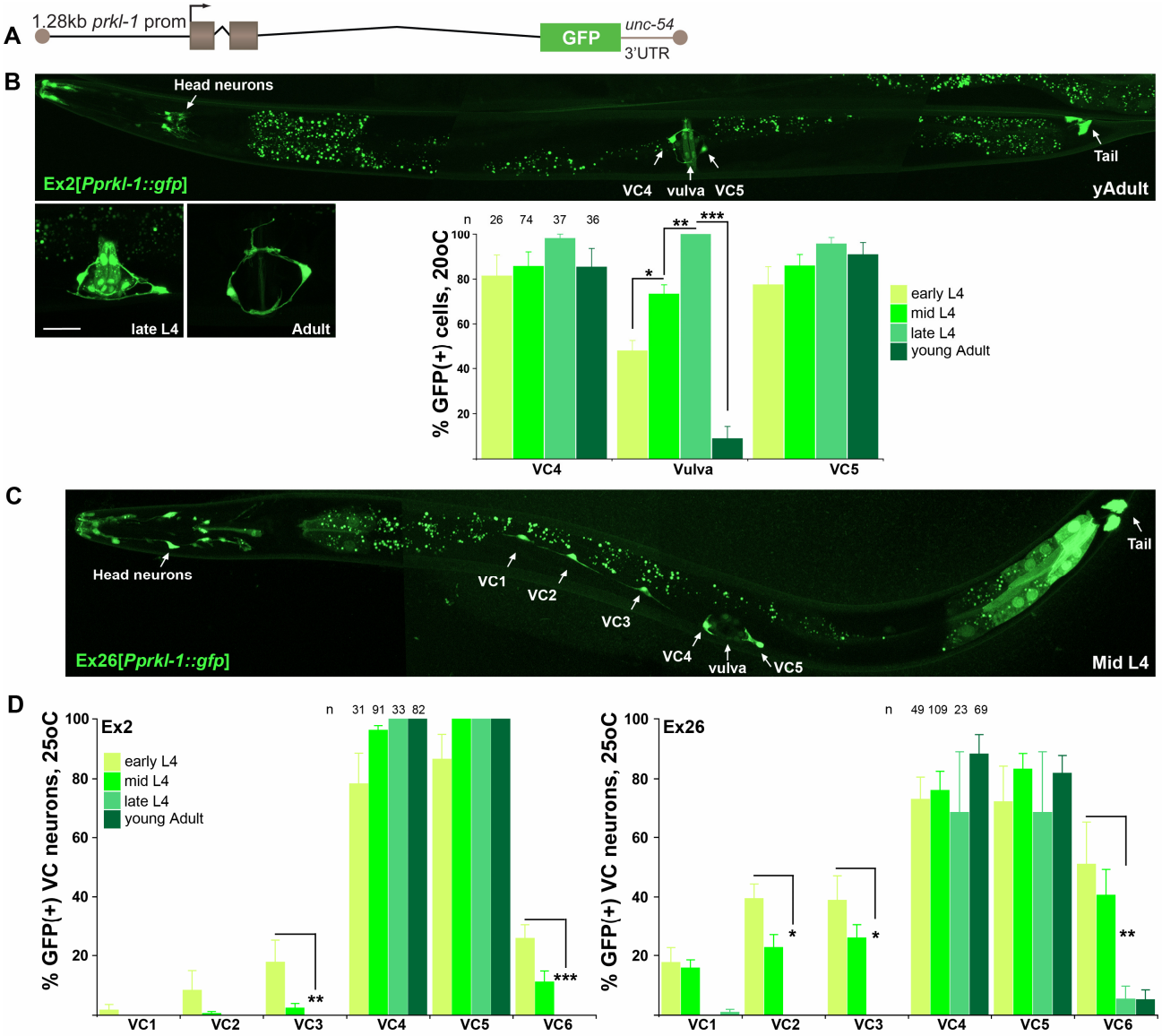
A
1.28kb prkl-1 prom
GFP
unc-54
3'UTR
B
Head neurons
Tail
Ex2[Pprkl-1::gfp]
VC4
vulva
VC5
yAdult
late L4
Adult
n 26 74 37 36
% GFP(+) cells, 20oC
early L4
mid L4
late L4
young Adult
VC4
Vulva
VC5
C
Head neurons
VC1
VC2
VC3
VC4
vulva
VC5
Tail
Ex26[Pprkl-1::gfp]
Mid L4
D
% GFP(+) VC neurons, 25oC
Ex2
n 31 91 33 82
early L4
mid L4
late L4
young Adult
VC1
VC2
VC3
VC4
VC5
VC6
Ex26
n 49 109 23 69

prkl-1 reporter expression in VC4 and VC5 motorneurons is induced by the vulva epithelium.

A relationship between the vulva epithelium and VC4/5 polarity was first demonstrated 22 years ago in a seminal experiment by Li and Chalfie 1990. They demonstrated that VC4 and VC5 motorneurons adopt an AP bipolar morphology in vulva-ablated animals, signifying that the vulva is a source of polarizing cues necessary for the medial-lateral (ML) orientation (Li and Chalfie, 1990). The observed AP phenotype is reminiscent of the wild type VC1-3 & 6 morphologies, whose cell bodies are relatively distant from the vulva and could be out of reach or irresponsive to vulva polarizing cues. Based on 1) Li and Chalfie's publication, 2) on the previous result suggesting that VCs nearer to the vulva display higher *prkl-1* reporter gene expression, and 3) on the newly found role of PCP gene *Prkl-1* in polarizing VC4/5 along the ML axis by preventing AP axon growth; we hypothesized that there is a link between the vulva epithelia and the triggering of PCP signalling in VC4/5 to orient processes in the ML axis instead of the AP axis, and that this link is a graded signal emanating from the vulva.

How could the vulva trigger PCP in VC4/5? To investigate this notion, we assessed the expression of Ex26[*Pprkl-1::gfp*] transcriptional reporter in nematodes with genetically ablated vulva epithelia. We made use of a balanced strain containing a loss-of-function *mpk-1* allele [*mpk-1(ga117)/dpy-17(e164) unc-79(e1068)*III] with a highly penentrant vulvaless phenotype (Figure III-4A). The *mpk-1* gene encodes a mitogen-activated protein kinase involved in Ras-mediated induction of vulval cell fates (Lackner

and Kim, 1998). We mated Ex[*Pprkl-1::gfp, rol-6(su1006)*] males to heterozygotes hermaphrodites (wt segregants) from the vulvaless strain and quantified *Pprkl-1* activity in the vulvaless crossprogeny. The restricted expression pattern of *Pprkl-1* allowed us to objectively monitor and score *Pprkl-1*-driven GFP expression in the VCs and vulva epithelium, relative to the invariable GFP expression in head and tail, at mid L4 and young adult stage. The developmental stages in wild type nematodes were assessed based on vulval developmental hallmarks. For instance, mid L4 was recognized by the Christmas tree vulva morphology (*i.e*. the shape of the vulva invagination resembles a Christmas tree, on a side view) and the young adult by the fully formed vulva combined with absence of eggs. In the case of vulvaless *mpk-1* background the stages were matched according to uterus/gonad development [www.wormatlas.org].

Interestingly, we found that *prkl-1* transcriptional reporter in VC4/5 is specifically turned off in vulvaless *mpk-1* mutants at mid L4 and young adult stages while the transient expression in the other VCs appeared unaffected (Figure III-4B). We considered whether the lack of *Pprkl-1::GFP* signal in VC4/5 in vulvaless *mpk-1* mutants was due to neuronal death, however we found that the neurons were alive and displaying a similar polarity to vulval distal VCs. Altogether, these data suggest that *prkl-1* expression in VC4/5 neurons is induced by the vulva epithelia. In addition, this result suggests that during vulva morphogenesis the vulva epithelium continuously stimulates *prkl-1* transcription in VC4/5. Taken together, this result is in agreement with the finding that in vulvaless mutants, VC4/5 neurons adopt a bipolar AP morphology similar to the other VCs; whereas in multivulva mutants, VC neurons that normally send AP axons, may adopt a VC4/5-like bipolar ML morphology, depending on their proximity to a

pseudovulva (Li and Chalfie, 1990). Thus, in vulvaless mutants, *Prkl-1* expression is not induced, therefore VC4/5 extend AP axons as there is no PRKL-1 to prevent AP axon growth. In order to confirm whether the lack of GFP fluorescence in VC4/5 neurons in vulvaless worms is a consequence of the lack of vulva, and not due to disrupted *mpk-1* signalling in the neurons, a control experiment consisting of restoring the *mpk-1* gene specifically in VC4/5 using *Pcat-1* may provide valuable information.

Figure III-4. ***prkl-1*** **reporter activity in VC4 and VC5 motor neurons is induced by the vulva epithelia. A)** Left, Outline of the *lin-13* mediated vulva patterning pathway (Wormbook). MPK is a protein tyrosine kinase that phosphorylates and inactivates transcriptional regulators LIN-1 and LIN-31, which leads eventually to the specification of the vulval fate. Right, Representative image of VC4/5 morphology (visualized with *cyIs3*) in vulvaless mutant nematodes: *mpk-1(ga117)/dpy-17(e164) unc-79(e1068)*III. **B)** A *prkl-1* reporter in VC4 and VC5 is specifically turned off in *mpk-1* mutants. Quantification of GFP positive VC neurons in wild type and *mpk-1* mutants at midL4 and Young adult stages. **C)** Fluorescence images of *Pprkl-1::gfp* expression in *mpk-1* genetic background, paired with DIC; displays GFP+ tail and GFP- VC4 and VC5.

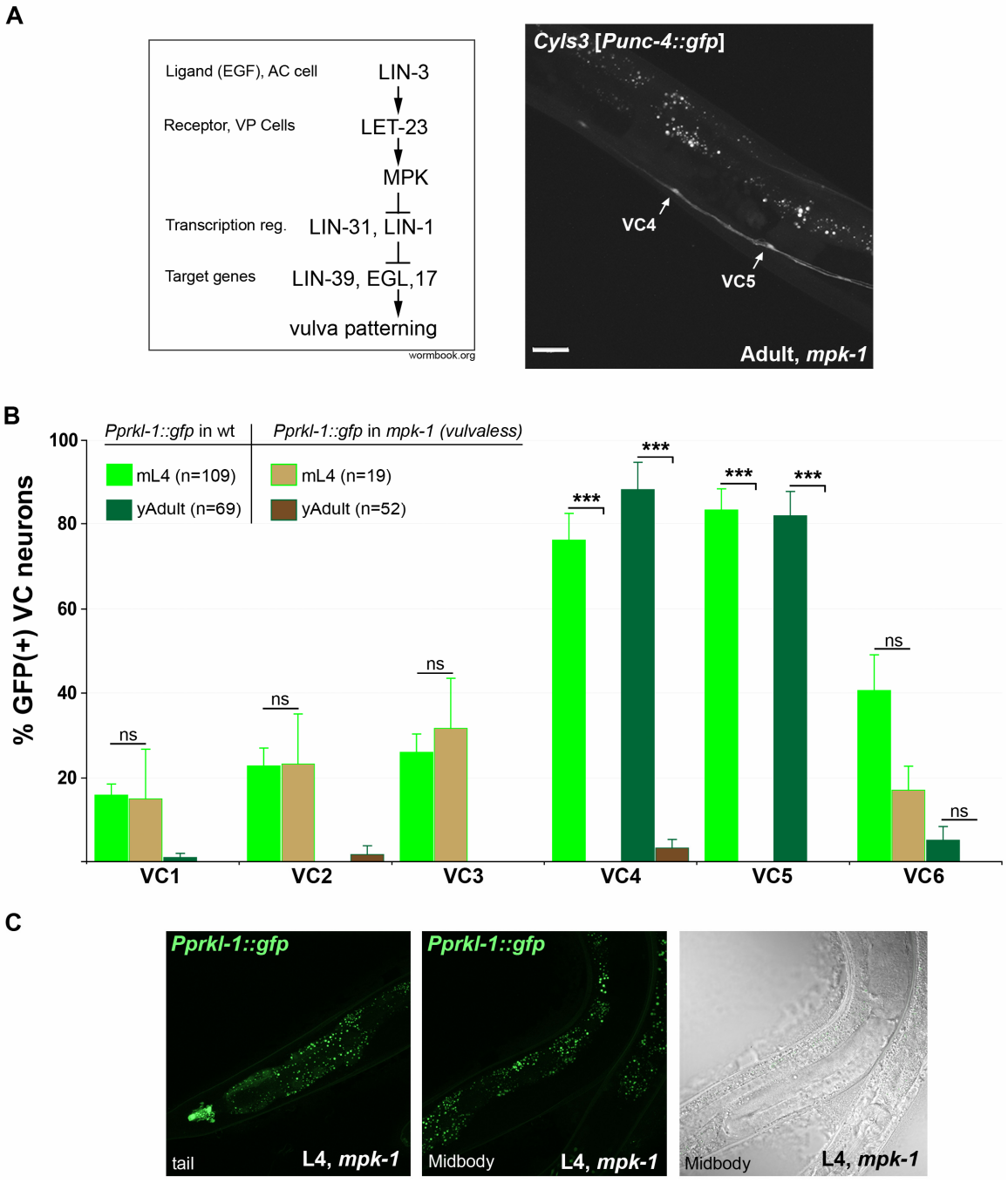
A
Ligand (EGF), AC cell
LIN-3
Receptor, VP Cells
LET-23
MPK
Transcription reg.
LIN-31, LIN-1
Target genes
LIN-39, EGL,17
vulva patterning
wormbook.org
Cyls3 [Punc-4::gfp]
VC4
VC5
Adult, mpk-1
B
Pprkl-1::gfp in wt
Pprkl-1::gfp in mpk-1 (vulvaless)
mL4 (n=109)
yAdult (n=69)
mL4 (n=19)
yAdult (n=52)
% GFP(+) VC neurons
100
80
60
40
20
ns
***
VC1
VC2
VC3
VC4
VC5
VC6
C
Pprkl-1::gfp
tail
L4, mpk-1
Pprkl-1::gfp
Midbody
L4, mpk-1
Midbody
L4, mpk-1

PRKL-1 is dynamically expressed in the VCs and in the vulva epithelia. Within VC4/5, PRKL-1 is expressed in puncta at the cell membrane, and smoothly in the nucleus.

The *Prkl-1* reporter gene expression suggested that PRKL-1 is dynamically expressed in the VCs and in the vulva epithelia. Would this promoter activity coincide with the protein expression pattern? Is PRKL-1 located to specific cellular compartments? To assess PRKL-1 cellular and sub cellular localization and consequently, to better understand *prkl-1* function in neuronal polarity; we generated transgenic lines with two independent constructs 1) a *gfp*-tagged genomic *prkl-1* and 2) a *gfp*-tagged *prkl-1.a cDNA* expressed from the *unc-4* promoter; and examined their expression patterns. Previously, I showed that a *gfp*-tagged *prkl-1* genomic construct was capable of rescuing VC4/5 polarity defects in *prkl-1* mutants, suggesting that it is functional and that the expression pattern likely reflects endogenous PRKL-1 expression (Chapter II). At rescuing concentration (1 ng/µL), no gfp signal was detected from *gfp*-tagged *prkl-1* genomic transgene, whereas at overexpressing concentration (10 ng/µL), it was visible and allowed for an overall qualitative assessment of PRKL-1 expression pattern. Consistent with the *prkl-1* promoter, the spatial-temporal expression of GFP::PRKL-1, expressed from the genomic array, also displayed a restricted and dynamic expression pattern. GFP::PRKL-1 was similarly expressed in VCs at earlier stages including late L3-early L4 but most noticeably at mid L4; and in the vulva epithelia (Figure III-5). In addition, similar to the *prkl-1* reporter, GFP::PRKL-1 levels in VC4/5 are maintained in adults, whereas in the vulva epithelia GFP::PRKL-1 expression fades away (see representative images in Figure III-5). This result further hinted at a role

for PRKL-1 in VC4/5 at later developmental stages, after neurons have began extending primary ML axons.

Importantly, GFP::PRKL-1 expressed from the genomic transgene at earlier developmental stages (late L3, early L4 and mid L4), was too faint to unequivocally assess PRKL-1 subcellular localization in the VCs; in addition to the limitation imposed by the small size of the VC cell bodies < 5 µm diameter. At the adult stage however, GFP::PRKL-1 was a bit brighter and appeared localized at the cell membrane of the VCs in a punctate pattern, and also uniformly in the nucleus (Figure III-5A).

Additionally, the significantly bigger size of epithelial cells and vulva syncytium allowed for some qualitative analyzes of PRKL-1 subcellular localization at the vulva, using the gfp-tagged *prkl-1* genomic transgene. For instance, at mid L4, consistently in every single nematode analyzed (n>100), GFP::PRKL-1 was asymmetrically localized towards the lumen of the vulva (Figure III-5A middle picture). Also, at late L3, GFP::PRKL-1 appeared smoothly localized in the nucleus of individual VPCs and at the cell membrane towards the intercellular contacts (n = 5) (Figure III-5 top picture). As mentioned, GFP::PRKL-1 was not expressed in the vulva epithelia of adult worms (Figure III-5 bottom picture). The significance of PRKL-1 spatial-temporal expression pattern and asymmetric localization in the vulva epithelia is not known; it could be related to vulva morphogenesis and/or to VCs polarization.

Importantly, to further study PRKL-1 subcellular localization in VC4/5 neurons we used an alternative source of GFP-fused PRKL-1. Reasoning that it would render higher expression levels, GFP-PRKL-1 was expressed transgenically from the *unc-4* promoter driving expression of a *prkl-1.a* cDNA. This construct is not subjected to *Prkl-1*

endogenous genomic control; PRKL-1.A expression is instead subjected to regulation by *Punc-4*. Thus, we obtained and examined a much brighter, although less physiological, PRKL-1 expression at earlier stages. Importantly, this transgene confirmed observations made with the genomic GFP-PRKL-1 array. Not only was GFP::PRKL-1 expressed in a punctate pattern at the cell membrane of VC4/5 and uniformly in VC4/5 nuclei of adult nematodes; but also, a similar subcellular distribution was observed at earlier stages including late L3, early L4 and mid L4 stages. Importantly, this expression pattern did not appear to change in *vang-1(tm1422)*, contrasting with findings in *Drosophila* epithelial cells, showing that PRKL localization at the membrane depends on its interaction with VANG (Bastock et al., 2003).

Additionally, since RFP (expressed from *Plin-11*) can shuttle between the cytosol and the nucleus and thus serves as intracellular marker, coexpression of GFP-PRKL-1 with RFP, further confirmed 1) the puncta at the plasma membrane, and 2) the nuclear expression (Figure III-5). The punctate expression pattern may suggest that PRKL-1 is forming polarizing multiprotein complexes at the cell membrane, similar to *Drosophila* cells undergoing PCP, including wing hair cells (Strutt and Strutt, 2009). Moreover, the carboxy-terminal tail of PRKL-1 contains two predicted NLS (by NLStradamus), and a CaaS farnesylation motif; which may underlie the nuclear and plasma membrane subcellular distribution. For instance, in the zebrafish hindbrain, PRKL-1 also localizes to the nuclei and plasma membrane of branchiomotor neurons during their polarized tangential migration (Mapp et al., 2011).

Figure III-5. GFP::PRKL-1 fusions localize to the plasma membrane and nucleus in VC4 and VC5 neurons. A) Representative images of GFP-tagged PRKL-1 expressing genomic construct at stages indicated. Yellow arrows denote nuclei, whereas green arrows denote membrane expression. **B)** GFP::PRKL-1 expressed transgenically from *Punc-4* ([*Punc-4::gfp::prkl-1*.a]) at the developmental stages indicated. **C)** Representative paired images of *Punc-4::gfp::prkl-1*.a and *Plin-11::RFP* co-expression in VC4 neuron at L3 stage. Scale, 10 µm. Modified version of data published in (Sanchez-Alvarez et al., 2011).

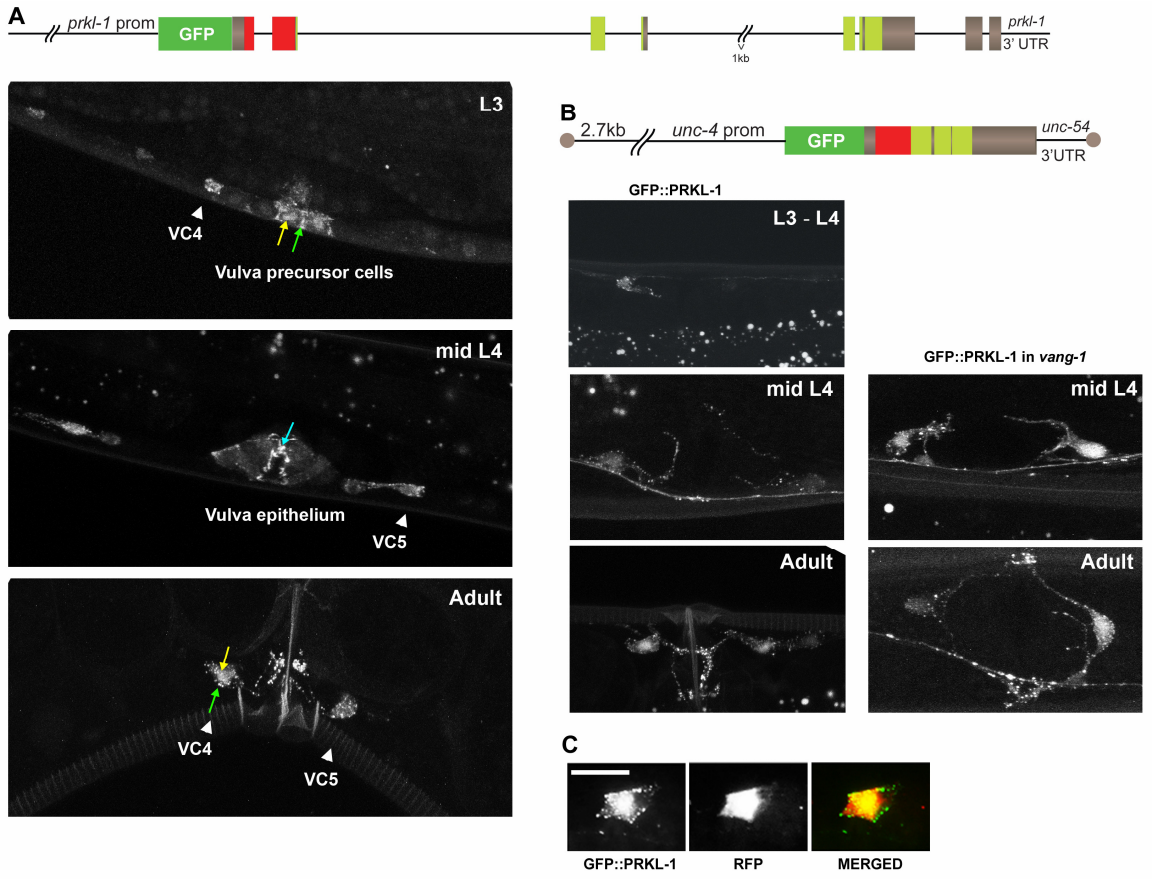

***prkl-1* acts cell autonomously to suppress ectopic axon outgrowth along the AP axis.**

Results obtained from *prkl-1* transcriptional activity and the expression patterns of a GFP-tagged *prkl-1* genomic transgene implicated *prkl-1* activity in VC4/5 neurons and/or the vulva. Consequently, we investigated whether *prkl-1* was required cell autonomously in the neurons or cell non-autonomously in the surrounding epithelium to regulate VC4/5 polarity, or both. To this end, a full length *prkl-1.a* cDNA was cloned downstream of the cell-specific promoters *Pcat-1*, *Punc-4* and *Pcol-10* in the pPD95.75 vector. The overall expression pattern of the chosen promoters encompasses the suspected sites of *prkl-1* action. Briefly, the *cat-1* gene, which encodes a synaptic vesicular monoamine transporter, is expressed in VC4 and VC5 neurons, HSN motorneurons, PDE and head neurons (Duerr et al., 1999). *Pcat-1* activity in VC4/5 begins in early L4. The *unc-4* gene, which encodes a homeodomain protein is expressed in the A-type motor neurons, DA and VA, the six VC motor neurons that innervate the vulval muscles, and the three SAB motor neurons (Lickteig et al., 2001). *Punc-4* activity in VCs begins in L3. *col-10* which encodes a collagen protein, is expressed in all hypodermal cells, including vulval cells (Liu et al., 1995). *Pcol-10* is an early promoter, active from the L1 stage. Thus, *prkl-1(zy11)* transgenic lines carrying extrachromosomal arrays [*Punc-4::gfp::prkl-1.a; Podr-1::rfp*], [*Pcat-1p::gfp::prkl-1.a; Podr-1::rfp*] and [*Pcol-10::gfp::prkl-1.a; Podr-1::rfp*] were generated (See Materials and Methods). Two and three independent transgenic lines harbouring *Pcat-1* and *Punc-4* driven *prkl-1.a* cDNA constructs, respectively, were obtained and quantified. All five lines fully rescued the tripolar VC4/5 defects in *prkl-1(zy11)* mutants (Figure III-6). Given that *Pcat-1* and *Punc-4* expression patterns overlap exclusively in VC4 and VC5 motorneurons; this result suggests that *prkl-1* acts cell

autonomously in VC4 and VC5 to suppress ectopic neurite outgrowth along the AP axis. Conversely, 3 out of 3 lines carrying extrachromosomal array *Pcol-10::gfp::prkl-1.a* failed to rescue polarity defects in *prkl-1(zy11)* mutant, suggesting that *prkl-1* does not regulate neuron polarity cell non-autonomously in epidermal cells (Figure III-6). In summary, *prkl-1* functions cell autonomously in VC4 and VC5 to inhibit ectopic AP axon outgrowth.

Figure III-6. ***prkl-1*** **gene functions cell autonomously in VC4 and VC5 motor neurons to suppress ectopic axon outgrowth along the AP axis.** Quantification of polarity defects of transgenic lines carrying cell-specific rescuing constructs *vs* control. N= 3-5 independent experiments for each construct and n>100 neurons counted per transgenic line. All error bars represent s.e.m. ***P<0.001. Data published in (Sanchez-Alvarez et al., 2011).

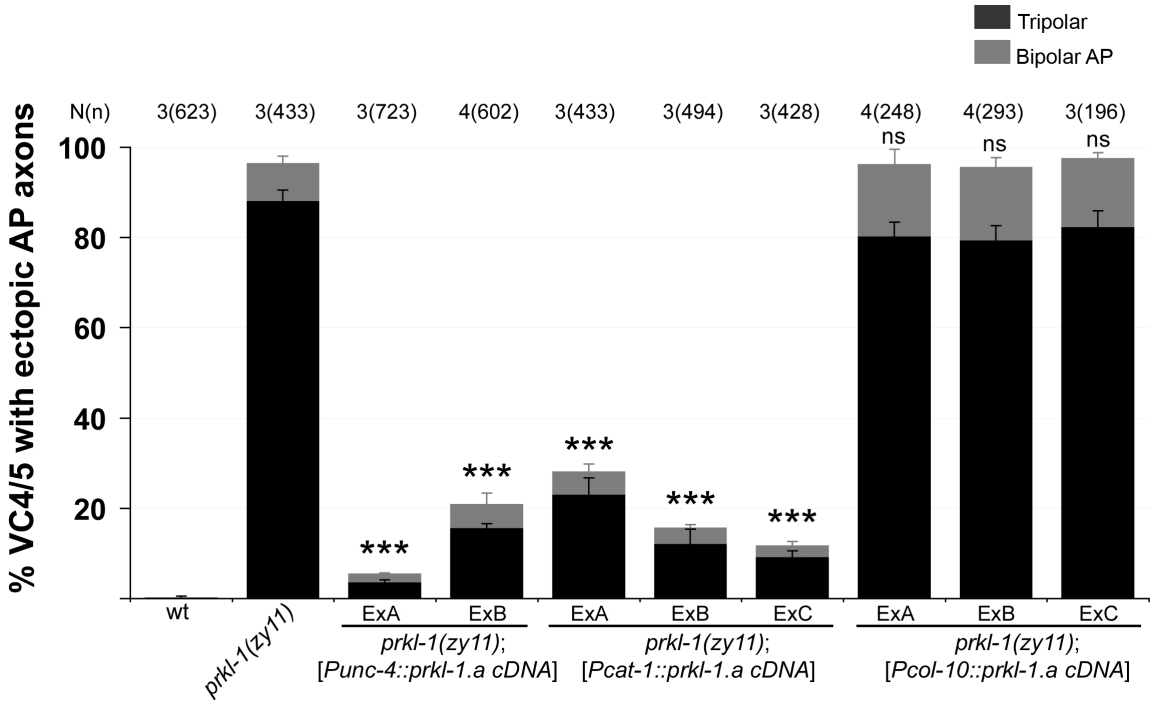

***prkl-1* is required early to establish neuronal polarity during organ innervation.**

To further understand when *prkl-1* is required to polarize neurons, we scored and compared the polarity phenotype of VC4 and VC5 in wild type and *prkl-1(zy11)* nematodes at different developmental stages. Specifically, we studied the progression of neuron morphology, from the first signs of polarization (lamellipodial protrusions) to the bipolar ML or tripolar axons in adults (Figure III-7). We used two complementary transgenic GFP reporters independently, to label VC4 and VC5 at distinct developmental stages *cyIs3 [Punc-4::gfp]* and *cyIs4 [Pcat-1::gfp]*. *cyIs3* is an excellent marker to study VCs morphology from L3 to mid L4 stage, thus revealing the evolution of wild type or mutant phenotypes from protrusions to ML and or AP oriented axons, respectively. Yet, the later onset of the *cat-1* promoter compared to *Punc-4* precludes its use at or before early L4 stage, since the GFP signal in VC4/5 is either off, or too dim for an objective scoring. *Pcat-1* however, was superb from mid L4 to adult stage, offering a cleaner picture of VC4/5 circuitry.

Although VC motorneurons are born during the L1 stage, the first axon-like processes are not seen until L3-L4 molt to early L4 transition, developing in synchrony with vulva primordial development. Interestingly, we found that prior to neurite outgrowth, during the L3 stage, VC4 and VC5 undergo significant morphogenetic remodelling along the AP axis, whereby anterior and/or posterior protrusions become reoriented to form a unique lamellipodial leading edge towards the vulva center of symmetry. These morphological transitions correlate with vulva developmental milestones (Figure III-7A). Notably, anterior protrusions in wild type VC4 neurons

virtually disappear by the 4-cell stage; while posterior protrusions consolidate, and by early L4 they are largely resolved into left and right axons which encircle the developing vulva (Figure III-7B, C & top D). With VC5 being a mirror image of VC4, the opposite takes place; while the posterior protrusion is largely dissolved by the 4-cell stage, the anterior protrusion bifurcates to give rise to left and right neurites extending around the vulva by early L4 (Figure III-7B, C & bottom D). However, in *prkl-1(zy11)* mutants, VC4 anterior protrusions and VC5 posterior protrusions fail to retract (Figure III-7B, C & top, bottom D). Instead the bipolar AP morphology in these neurons consolidates, rendering them receptive to AP-distributed axon growth signals; which results in the extension of axons away from the vulva, and consequently tripolar neurons. Quantitatively, the proportion of VC4 with A-P protrusions in wt nematodes decreases significantly from the 1-cell (48 %) to the 4-cell (3 %) stage; whereas in *prkl-1* animals VC4 morphology the proportions do not change significantly (45 % to 52 %), and tend to increase. Thus, the proportion of VC4 neurons with A-P protrusions in *prkl-1* mutants was significantly higher than that of wild type neurons by the 4-cell stage (Figure III-7D). These data suggest that *prkl-1* is playing an early role, prior to axon growth, in polarizing leading edge protrusions and therefore specifying the site of axon outgrowth.

Additionally, we noticed that primary and ectopic axons in *prkl-1* mutants are formed simultaneously during L3-L4 molt to early L4 stage, suggestive of an early role for *prkl-1* in the establishment of neuron polarity (see images Figure III-7C left). Scoring the percentage of neurons with polarity defects at early L4 showed a highly penetrant ectopic AP axon phenotype. In addition, while ~ 76 % VC4 and ~ 55 % VC5 displayed AP axons away from the vulva, a significantly higher percentage did at the adult stage

with ~97 % VC4 and 96 % VC5 (Figure III-7D right). These data suggests that *prkl-1* also plays a role in maintaining VC4/5 ML polarized morphologies by actively blocking AP axon formation.

Figure III-7. *prkl-1* acts early to establish neuron morphology in VC4 and VC5 neurons. A) Ventral view schematics depicting VC4, VC5 and vulva development from stage L3 to Adulthood. **B)** Representative fluorescence images displaying the morphology of VC3, VC4 and VC5 in wild type nematodes, and the morphology of VC4 in *prkl-1(zy11)* worms at the 4-cell VPC stage. While wild type VC4 and VC5 extend unidirectional protrusions towards the vulva axis of symmetry (unipolar arrows), *prkl-1* VC4 and VC5 extend anterior and posterior protrusions (bipolar arrows), resembling the bipolar AP orientation of VC3. **C)** Representative confocal images of VC4 and VC5 in *prkl-1* nematodes at developmental stages L3-L4 molt, and early and mid L4, and, of wild type VC4/5 at mid L4 stage. Axon-like processes identified at the L3/L4 are normally polarized unidirectionally toward the vulval axis of symmetry (unipolar arrows). Images of VC4 and VC5 neurons at the 4-cell stage resemble the A/P bipolar morphology of VC3 in *vang-1*, *prkl-1* and *dsh-1* mutants (bipolar arrows). **D)** Left) Quantification VC4 (top) and VC5 (bottom) neurons displaying protrusions away from the vulva. Error bars represent SEP, *$p<0.05$, Fisher's Exact test. Right) Quantification of VC4 anterior axons (top) and VC5 posterior axons (bottom), in *prkl-1(zy11)* from early L4 to adult. Error bars represent SEM, ***$p<0.001$, *$p<0.05$. Data published in (Sanchez-Alvarez et al., 2011).

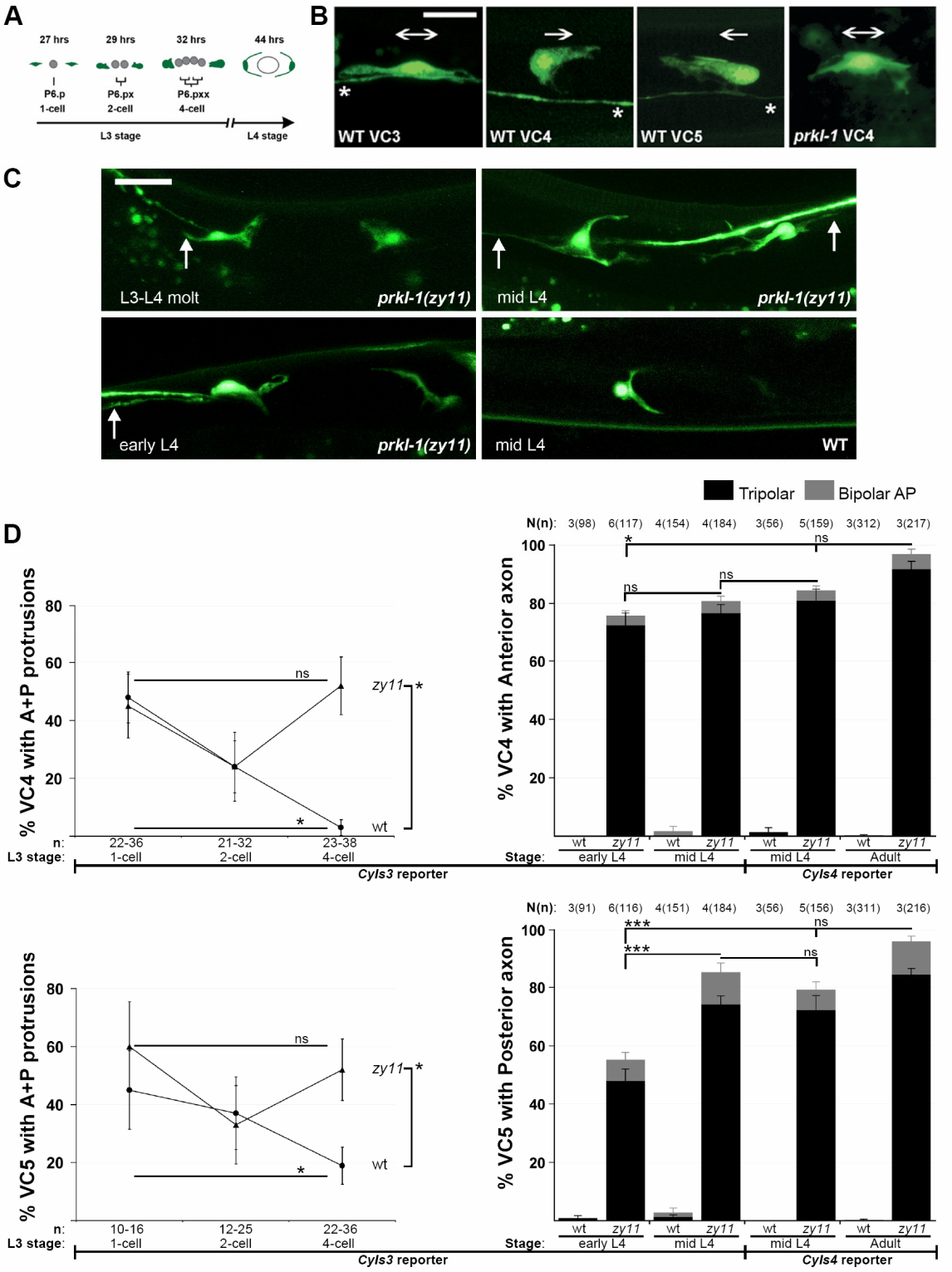
A
27 hrs
29 hrs
32 hrs
44 hrs
P6.p 1-cell
P6.px 2-cell
P6.pxx 4-cell
L3 stage
L4 stage
B
WT VC3
WT VC4
WT VC5
prkl-1 VC4
C
L3-L4 molt
prkl-1(zy11)
mid L4
prkl-1(zy11)
early L4
prkl-1(zy11)
mid L4
WT
D
Tripolar
Bipolar AP
% VC4 with A+P protrusions
ns
zy11
*
wt
n:
22-36
21-32
23-38
L3 stage:
1-cell
2-cell
4-cell
Cyls3 reporter
N(n): 3(98) 6(117) 4(154) 4(184) 3(56) 5(159) 3(312) 3(217)
% VC4 with Anterior axon
Stage:
wt zy11 wt zy11 wt zy11 wt zy11
early L4
mid L4
mid L4
Adult
Cyls4 reporter
% VC5 with A+P protrusions
10-16
12-25
22-36
N(n): 3(91) 6(116) 4(151) 4(184) 3(56) 5(156) 3(311) 3(216)
***
% VC5 with Posterior axon

***prkl-1* operates continuously through development to maintain neuronal polarity.**

The percentage of VC4/5 AP-directed axons in *prkl-1(zy11)* nematodes increases with developmental age, which may suggest that *prkl-1* activity is required continuously to maintain VC4/5 polarized ML morphology, by preventing AP axon growth. Consistently, we found that the *Pprkl-1* transcriptional reporter is active in VC4/5 from late L3/early L4 and persists throughout adulthood, contrasting with the loss of GFP expression in the vulva epithelium. The sustained expression of *Pprkl-1* in VC4 and VC5 into adulthood suggests that *prkl-1* is required later in development to maintain neuron morphology. To further explore this notion, we used a heat inducible dsRNAi cassette bearing sense and anti-sense *prkl-1* sequences under the control of the *hsp16-2* heat shock-inducible promoter (Figure III-8A). This transgene was used to downregulate *prkl-1* in wild type animals at mid-L4 stage, after VC4/5 after neurons have initiated normal polarization by extending axons along the ML axis (Figure III-8B). This extrachromosomal array is effective at decreasing *prkl-1* mRNA levels, as evidenced by a semiquantitative single worm *prkl-1* RT-PCR (Figure III-8D). We found that, even 20 hours after heat induction, levels of *prkl-1* mRNA normalized to *myo-3*, were significantly reduced (Figure III-8D). Notably, we found that *prkl-1* downregulation by inducible dsRNAi at L4 stage, after the bipolar medial-lateral orientation has been established, resulted in ~ 40 % of VC4/5 displaying new ectopic AP-directed axons in adults, compared to non-transgenic heat shocked (~ 1 %) or transgenic non-heat shocked (~ 1 %) controls (Figure III-8C & E). This result suggests an active role for *prkl-1* in maintaining neuron morphology, by continuously suppressing AP axon outgrowth throughout the life of VC4/5 neurons.

Figure III-8. ***prkl-1*** **is required continuously through VC4/5 development to inhibit ectopic neurite growth along the AP axis. A**) Schematic representation of *prkl-1.a* transcript. Arrowheads denote the position of primers used to diagnose the effectiveness of *prkl-1* dsRNAi by RT-PCR (shown in D). Horizontal arrows symbolize sense and antisense *prkl-1* sequences driven by *Phsp16-2* in the RNAi transgenic array. **B**) Timeline depicting the heat shock (HS) inducible RNAi approach to downregulate *prkl-1* in VC4/5, following normal polarity establishment. **C**) Quantification of VC4/5 neurons with tripolar morphology upon *prkl-1* dsRNAi mediated downregulation. *prkl-1* RNAi at mid-L4 stage (when VC4/5 exhibit normal medial-lateral morphology) resulted in a significant increase in AP-directed ectopic neurites (tripolar VC4/5) in the adult compared to non-HS or non-transgene (Tg) bearing animals. Error bars represent SEM. ***p<0.001, t-test. **D**) RNAi-induced depletion of *prkl-1* transcripts was validated by single worm RT-PCR in control and HS animals. Relative densitometry of *prkl-1* mRNA was normalized to control *myo-3* levels. **E**) Top, Tg+ worm was imaged prior to HS at mid-L4 displaying normal polarization and bottom, the same worm after HS induced-*prkl-1* RNAi showing ectopic VC4/5 neurites (arrows). VC neurons visualized using *cyIs4*. Scale bar, 10 μm. Data published in (Sanchez-Alvarez et al., 2011).

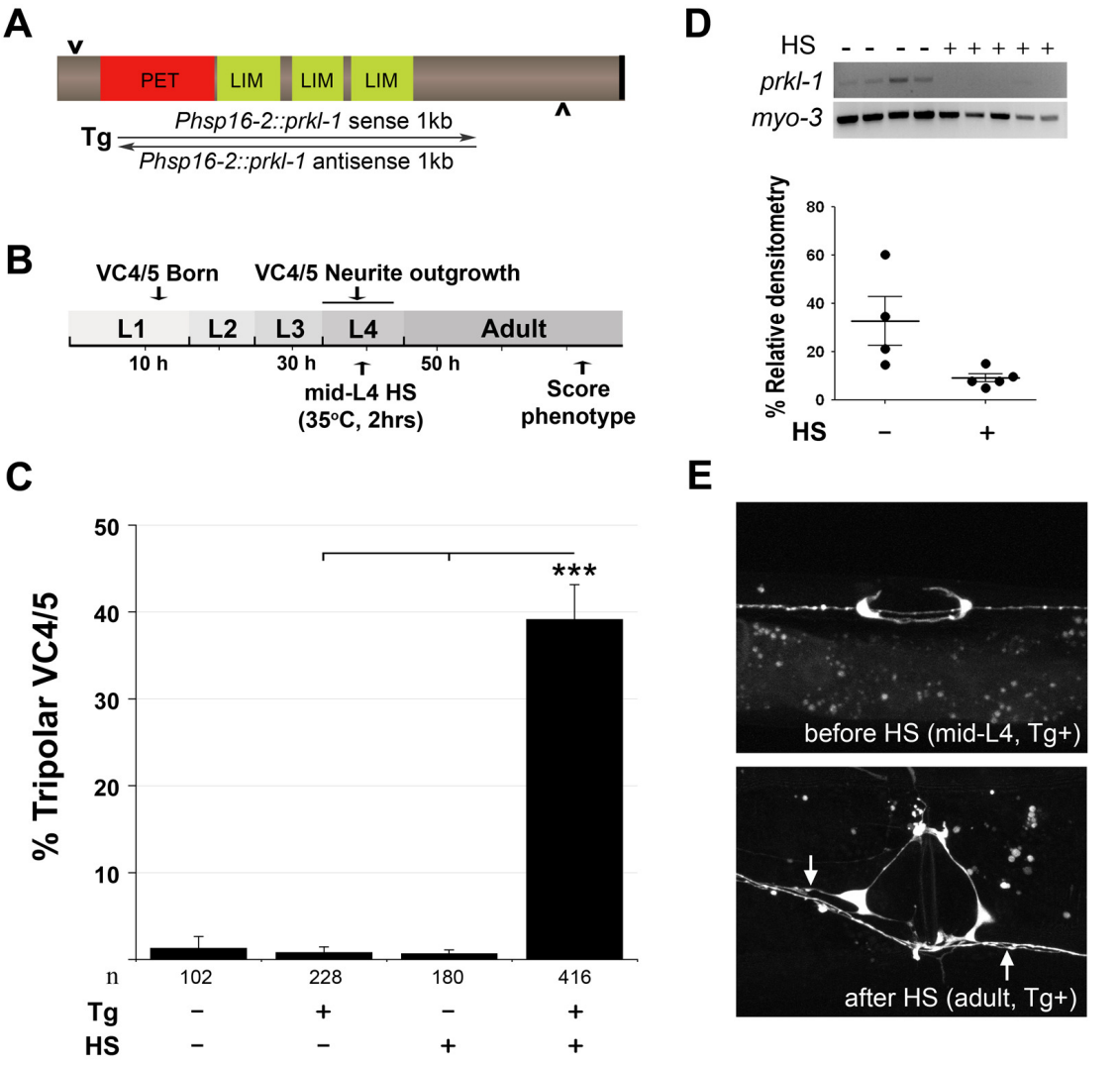
A
PET
LIM
LIM
LIM
Tg
Phsp16-2::prkl-1 sense 1kb
Phsp16-2::prkl-1 antisense 1kb
B
VC4/5 Born
VC4/5 Neurite outgrowth
L1
L2
L3
L4
Adult
10 h
30 h
50 h
mid-L4 HS
(35°C, 2hrs)
Score
phenotype
C
% Tripolar VC4/5
50
40
30
20
10
***
n
102
228
180
416
Tg
−
+
−
+
HS
−
−
+
+
D
HS - - - - + + + + +
prkl-1
myo-3
% Relative densitometry
80
60
40
20
0
HS
−
+
E
before HS (mid-L4, Tg+)
after HS (adult, Tg+)

***prkl-1* overexpression results in unipolar VC4 and VC5 neurons.**

Prkl-1 lof disrupts the establishment and maintenance of VC4 and VC5 polarity, as evidenced by a bipolar to tripolar change in neuron morphology. VC4/5 polarity defects in *prkl-1(zy11)* are completely rescued with a *gfp*-tagged *prkl-1* genomic construct injected at 1 ng/µL. This *prkl-1* genomic array contains the complete open reading frame and all of the regulatory regions including introns, 5' flanking region and 3' UTR. Interestingly, this same array injected at 10 ng/µL not only resulted in full rescue of VC4/5 tripolar phenotype, but also introduced a new phenotype, unipolar neurons, with only one primary axon (Figure III-9B & C). This result suggested that *prkl-1* overexpression instructed a reversal in polarized morphology, by transforming a strain with approximately 92 % tripolar, 3 % wild type and 0 % unipolar VC4 neurons, into a line with approximately 2 %, 64 % and 32 %, respectively (Figure III-9C). The transgenic array was in a *prkl-1(zy11)* background and could not be outcrossed into wild type background; likely because at 10 ng/µL this construct caused significant embryonic lethality and larval defects (Supplemental Figure III-3). This suggested that introducing the overexpressing *prkl-1* genomic construct in addition to the two wild type copies of *prkl-1* locus contained in N2 strain was not viable. However, a similar penetrance of unipolar neurons to the 10 ng/µL array was recapitulated using a 10 fold lower concentration (1 ng/µL) array in a wild type background (Figure III-9C).

To further test if the unipolar phenotype was a direct effect of overexpressing PRKL-1 and not a secondary consequence of 1) overexpressing any genomic regulatory regions that would for instance, deplete a transcription factor required for axon extension;

or 2) overexpressing GFP; I made additional constructs to use as controls (see Methods and Figure III-9A for details). One of them, a genomic construct with a stop codon engineered immediately after the GFP sequence did not result in significant polarity defects, suggesting that the unipolar phenotype is not an artefact of overexpressing *prkl-1* regulatory elements and/or GFP (Figure III-9A & C).

Similarly, a *prkl-1 cDNA* driven by *Punc-4*, an exogenous promoter with activity in VC4/5, resulted in unipolar neurons; whereas a control *Punc-4::gfp* did not affect neuron morphology (Figure III-9B top images, & C). This data further confirms that PRKL-1 overexpression results in unipolar neurons. As *prkl-1* genomic construct and *Punc-4::gfp::prkl-1.a* expression overlaps in the VCs and not in the vulva epithelia, where *prkl-1* gene but not *Punc-4* is expressed, and both constructs generate similar overexpression phenotypes, these results suggest that the unipolar phenotype is a cell autonomous, gain-of-function effect of *prkl-1* overexpression in VC motorneurons. In addition, three more aspects are worth highlighting 1) both VC4 and VC5 neurons can become unipolar upon *Prkl-1* overexpression, 2) both left or right axons can be affected and 3) unipolar neurons are noticed earlier than mid L4 suggesting that the axons don't grow to full length and then retract (Figure II-9B).

Number of axons in VC4 and VC5 neurons depends on *prkl-1* dosage.

How do neurons regulate the number of processes *in vivo*? In the current section, I explore this question and provide evidence for *prkl-1* as a dosage-dependent PCP signalling component, which regulates the number of axons in the context of developing VC4 and VC5 motorneurons.

Remarkably, a functional *prkl-1* genomic construct which achieves full rescue of VC4/5 polarity defects in *prkl-1(zy11)* mutants, also induced the formation of a new phenotype, neurons with a single axon (*i.e.* unipolar morphology). In addition, when the same genomic construct was injected at a 10 fold higher concentration than that required to rescue (1 ng/µL), the percentage of unipolar neurons significantly increased (Figure III-9C). Three independent lines harbouring 1 ng/µL *prkl-1* genomic transgene resulted in 8.8 %, 13.7 % and 15.9 % of unipolar VC4 neurons in *prkl-1(zy11)* background, whereas two independent lines with the construct at 10 ng/µL resulted in 21.1 % and 31.7 % of unipolar neurons, a significant 2 to 3.6 fold increase in the gain of function phenotype. To study whether the addition of a wild type *prkl-1* gene load also have a multiplying effect in the phenotype, a representative line of each concentration was crossed into N2 background. Outcrossing the 10 ng/µL array met with failure, likely due to embryonic lethality and larval arrest; whereas the 1 ng/µL transgene was successfully outcrossed after several attempts. Importantly, addition of the transgenic array to the two wt copies of *prkl-1* resulted in a higher percentage of unipolar neurons (23.9 % *vs* 15.9 %) (Figure III-9). This result suggests that there is a *prkl-1* dosage/response effect and that the number of axons in VC4 and VC5 neurons is very sensitive to *prkl-1* dosage.

Consistent with the above results, a similar dose-dependent gain of function phenotype was observed with arrays expressing *prkl-1.a* cDNA form *Punc-4* in wild type nematodes. Raising the concentration of the *Punc-4::prkl.a* array from 10 to 50 ng/µL in wt background caused an increment in the unipolar phenotype from 7 to 17 %.

***Prkl-1* overepression abolishes right and left axons indistinctively.**

To further explore *prkl-1* function in the polarity VC4 and VC5 motorneurons, we asked whether *prkl-1* overexpression was abrogating one of the primary axons preferentially. To assess this notion, I quantified the number of cell bodies with no left or right axons, independently. Interestingly, statistic analysis revealed no significant difference in the percentage of neurons lacking left *vs* right primary axons; a ratio of one was obtained using either *Punc-4::gfp::prkl-1*.a or genomic *gfp::prkl-1* extrachromosomal arrays (Figure III-10). This result indicates that *prkl-1* overexpression abrogates primary axons indistinctively. This result signifies that *prkl-1* does not discriminate between left or right primary axons, which grow in response to radially emanated polarizing signals from the developing vulva. Thus, it is plausible that *prkl-1* overexpression prevents the medial-lateral bifurcation of the lamellipodial protrusions directed towards the VPCs, resulting in the formation of only one axon around the vulva instead of two. Notably, the unique axon of unipolar neurons is never directed away from the vulva, suggesting that *prkl-1*'s primary function in VC4/5 neurons is to suppress axonal growth in response to AP polarizing cues.

Figure III-9. ***prkl-1*** **overexpression results in unipolar VC4 and VC5 neurons. A**) Schematic representation of the constructs used in this study: *prkl-1* gene, *Punc-4* driven *prkl-1* cDNA, and their respective controls. **B)** *prkl-1* overexpression results in a gain of function phenotype, manifested as too few neurites. Representative confocal images of unipolar VC4 and/or VC5 at mid L4 stage, from transgenic worms overexpressing *Punc-4::GFP::prkl-1* (top); and adult stage, from transgenic worms overexpressing *GFP::prkl-1 gene* (bottom). **C)** Quantification of unipolar VC4 neurons. Statistic significance was assessed by one way ANOVA followed by Bonferroni test, ***P<0.001. Different version of data published in (Sanchez-Alvarez et al., 2011).

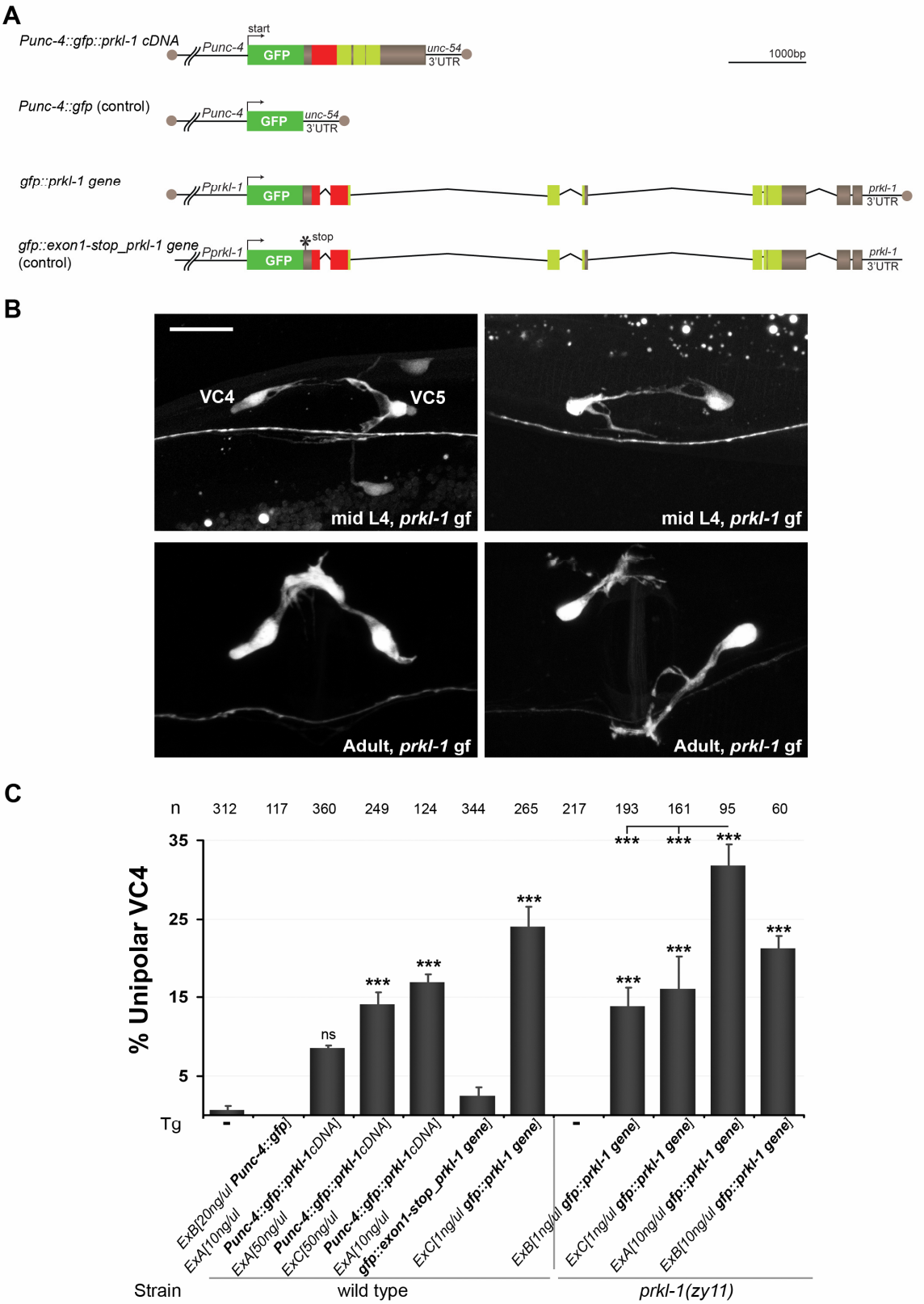
A
Punc-4::gfp::prkl-1 cDNA
Punc-4
start
GFP
unc-54 3'UTR
1000bp
Punc-4::gfp (control)
gfp::prkl-1 gene
Pprkl-1
prkl-1 3'UTR
gfp::exon1-stop_prkl-1 gene (control)
stop
B
VC4
VC5
mid L4, prkl-1 gf
Adult, prkl-1 gf
C
n
312 117 360 249 124 344 265 217 193 161 95 60
% Unipolar VC4
35
25
15
5
Tg
ns
***
Strain
wild type
prkl-1(zy11)
ExB[20ng/ul Punc-4::gfp]
ExA[10ng/ul Punc-4::gfp::prkl-1cDNA]
ExA[50ng/ul Punc-4::gfp::prkl-1cDNA]
ExC[50ng/ul Punc-4::gfp::prkl-1cDNA]
ExA[10ng/ul gfp::exon1-stop_prkl-1 gene]
ExC[1ng/ul gfp::prkl-1 gene]
ExB[1ng/ul gfp::prkl-1 gene]
ExC[1ng/ul gfp::prkl-1 gene]
ExA[10ng/ul gfp::prkl-1 gene]
ExB[10ng/ul gfp::prkl-1 gene]

Figure III-10. ***prkl-1*** **overexpression removes left and right primary axons indistinctively.** Quantification of *prkl-1* gain-of-function phenotype. Percentage of VC4 neurons lacking right or left primary axons.

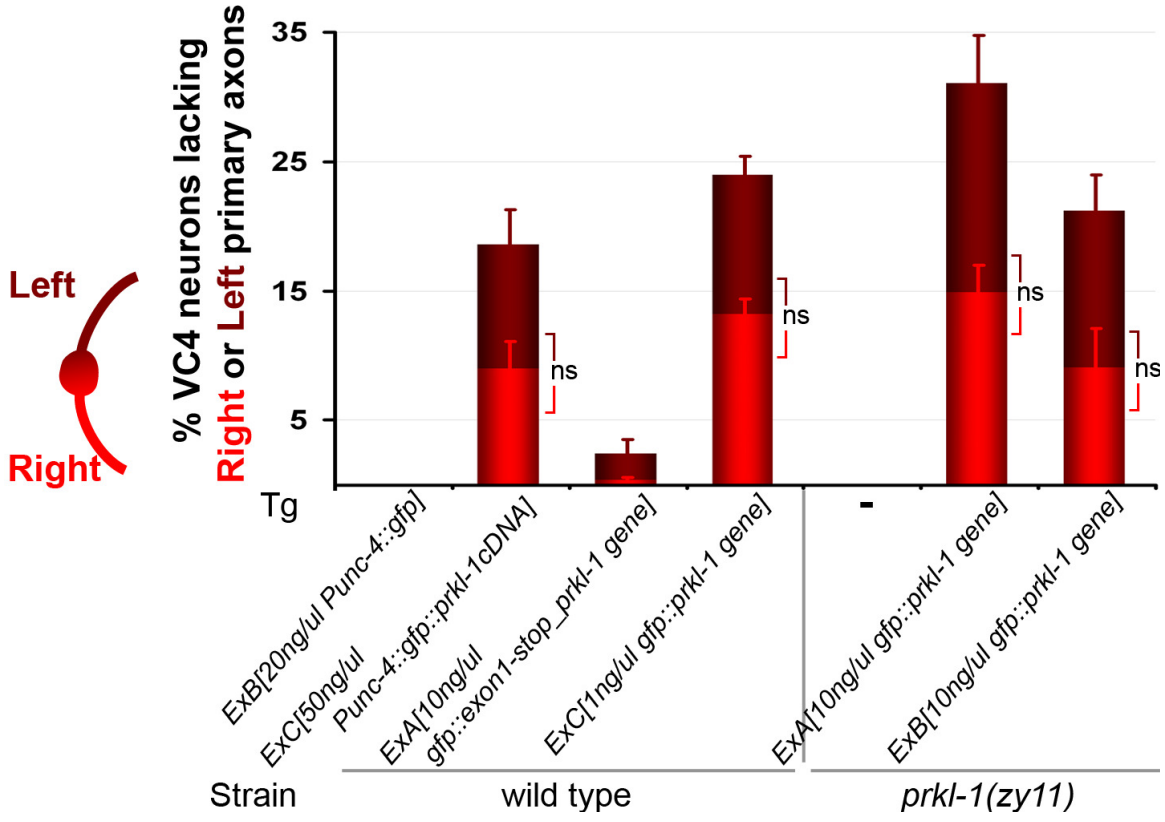

***prkl-1* is sufficient to prevent AP neurite formation in *vang-1* and *dsh-1* mutants.**

Since *prkl-1* overexpression resulted in unipolar neurons, which is opposite to the tripolar phenotype caused by the loss-of-function, we then asked whether a *prkl-1 gof* transgenic array would be sufficient to restore the wild type morphology of VC4 and VC5 neurons in *vang-1* and *dsh-1* mutants. Accordingly, to better understand their genetic interactions in PCP signalling, a *gfp*-tagged *prkl-1* genomic construct injected at 1 ng/µL, named *prkl-1(+)* transgene, capable of fully rescuing *prkl-1(zy11)* polarity defects was placed into *vang-1(tm1422)* and *dsh-1(ok1445)* mutant backgrounds. Remarkably, the *prkl-1(+)* transgene rescued the polarity defects in *vang-1* and *dsh-1* mutants at the same level as their respective rescuing *vang-1(+)* and *dsh-1(+)* genomic transgenes (Figure III-11). Similarly, rescue of *vang-1* and *dsh-1* ectopic AP axon phenotype was also achieved with a *Punc-4::gfp::prkl-1.a* transgene. Taken together, these data suggests that *prkl-1* is sufficient to prevent axon outgrowth along the AP axis in VC4 and VC5 neurons.

Interestingly, not only did the *prkl-1(+)* transgene revert the effects of *vang-1* and *dsh-1 lof* (*i.e.* tripolar to wt morphology), but it also induced a *prkl-1* gain of function phenotype (*i.e.* unipolar morphology). For instance, in *dsh-1* background the percentage of VC4/5 unipolar neurons significantly increased from 7 % to 24 % (~ 3 fold) and in *vang-1* background, from 5 % to 11 % (~ 2 fold) unipolar neurons.

Figure III-11. ***prkl-1*** **overexpression restores normal polarity in** ***vang-1*** **and** ***dsh-1*** **mutants.** Quantification of VC4/5 with AP ectopic axons. Extrachromosomal arrays expressing *prkl-1* gene and *prkl-1* cDNA rescue AP axon outgrowth in *vang-1* and *dsh-1* mutants. Error bars represent SEM. Significance was assessed by one-way ANOVA followed by Bonferroni post-hoc test, ***p<0.001. Data published in (Sanchez-Alvarez et al., 2011).

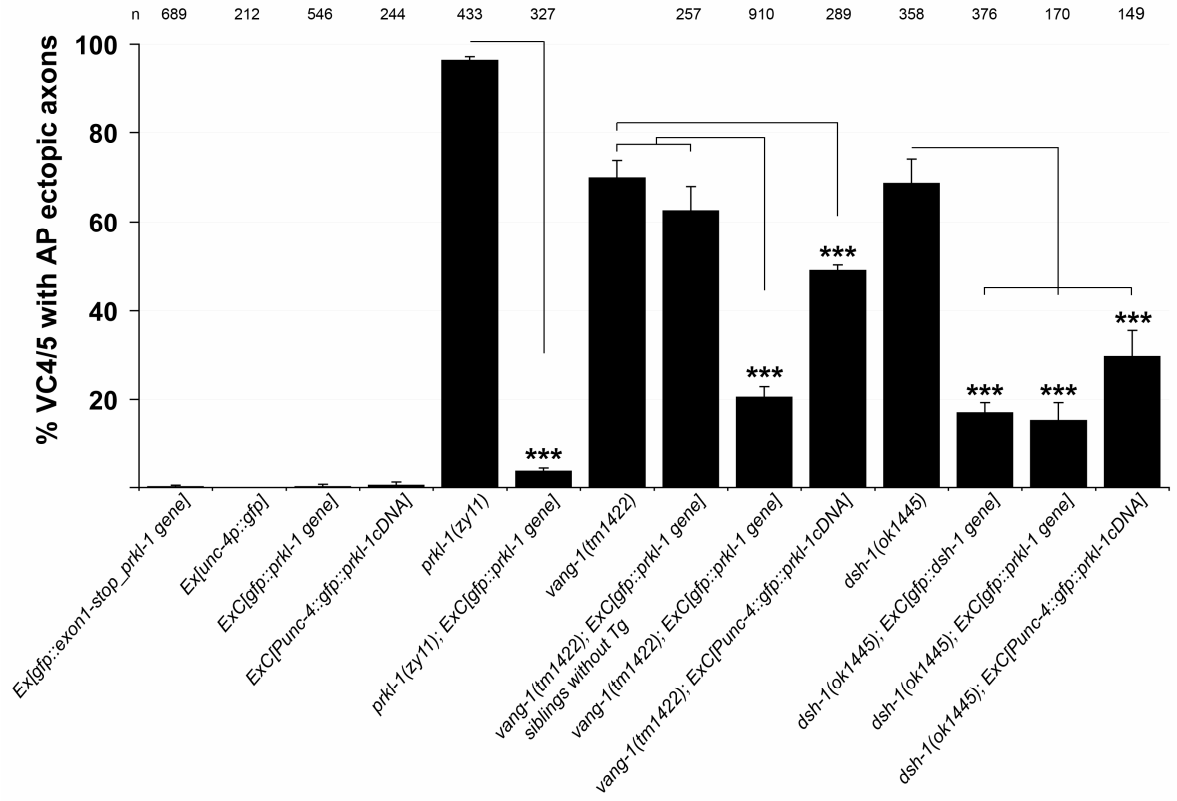

***prkl-1* overexpression in vulval distal VC3 and VC6 motorneurons results in lack of posterior and anterior axons, respectively.**

Prkl-1 overexpression results in unipolar VC4 and VC5 motorneurons in wild type nematodes and also in *prkl-1*, *dsh-1* and *vang-1* mutant backgrounds, which suggests that *prkl-1* is sufficient to suppress AP axon outgrowth. The overlapping expression patterns of both the *prkl-1* promoter and *gfp-tagged prkl-1* genomic constructs in VC1-6 motorneurons, suggests that *prkl-1* may also function in the AP oriented VCs (*i.e.* VC1-3, 6). We then asked whether *prkl-1* overexpression would prevent the outgrowth of primary AP axons in vulval distal VC3 and VC6 neurons, similar to ML oriented VCs (*i.e.* VC4, 5). To study the effect of *prkl-1* overexpression in VC3 and VC6, a *prkl-1(+)* transgene was crossed into *cyIs3* [*Punc-4::gfp*] reporter strain to visualize the VC family of neurons. Notably, *prkl-1* overexpression using the *prkl-1(+)* transgene resulted in VC3 and VC6 neurons lacking anterior and posterior axons, respectively (Figure III-12B). Since processes of VCs are juxtaposed along their lengths, most of them can not be individually visualized and consequently quantified in *cyIs3* background. To unequivocally assess VC6 morphology, we crossed two independent overexpressing 50 ng/µL *Punc-4::gfp::prkl-1.a* transgenes into a wild type strain carrying *cyIs4[Pcat-1::GFP]* and *zyIs1[Plin11::RFP]* to visualize VC4 and VC5 (GFP) and VC1-6 (RFP) respectively (Figure III-12A & C). Although the *Punc-4::gfp::prkl-1* transgene is not as effective at inducing *gof* phenotype in VC4/5 as *prkl-1(+)* transgene (FigureIII-9C), it was chosen to quantify *prkl-1* overexpression in VC6 because 1) it can be easily transferred from one strain to the other via crosses and 2) it expresses *prkl-1* continuously starting in L3, prior to neuritogenesis, and is not subject to a decline in *prkl-1* expression

in VC1-3, 6 that we have observed with the *prkl-1(+)* genomic construct. We found that the *Punc-4::gfp::prkl-1* extrachromosomal array resulted in loss of anterior axons in 14 – 17% VC6 neurons, compared to 0% VC6 neurons from nematodes without the array. This finding signifies that *prkl-1* overexpression has the ability to prevent AP axon growth in vulval distal AP oriented VC neurons.

Figure III-12. Bipolar VC3 and VC6 motor neurons become unipolar upon *prkl-1* overexpression. A) Wild type VC3 and VC6 extend one axon anteriorly and one posteriorly (top). Their morphologies are unaffected in *prkl-1* mutant background (middle and bottom). VC morphologies are visualized with *zyIs1* [*Plin-11::rfp*] (top) and *cyIs3* [*Punc-4::gfp*] (bottom). **B)** *prkl-1* gene overexpresion results in the lost of VC3 anterior axon (top) and VC6 posterior axon (bottom). Right panel, a zoom in at unipolar VC3 and VC6 neurons. **C)** Similar results are achieved overexpressing *prkl-1* cDNA driven by *Punc-4*. Graph shows percentage of VC6 neurons lacking the anterior axon upon *prkl-1* overexpression. Neurons were visualized with *zyIs1*[Plin-11::rfp] and *cyIs4* [*Pcat-1::gfp*] reporters. Modified version of data published in (Sanchez-Alvarez et al., 2011).

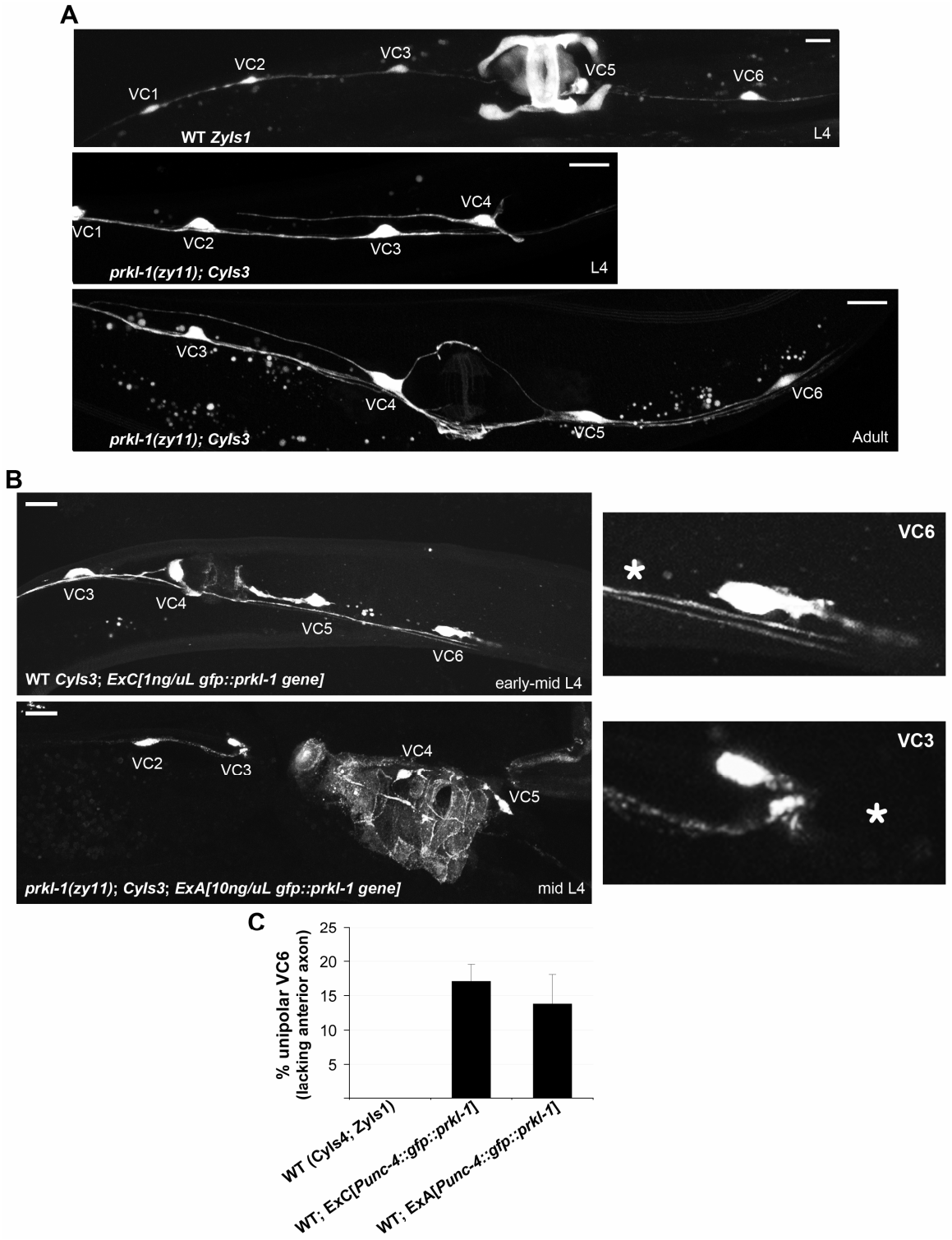
A
VC1
VC2
VC3
VC5
VC6
WT Zyls1
L4
VC1
VC2
VC3
VC4
prkl-1(zy11); Cyls3
L4
VC3
VC4
VC5
VC6
prkl-1(zy11); Cyls3
Adult
B
VC3
VC4
VC5
VC6
WT Cyls3; ExC[1ng/uL gfp::prkl-1 gene]
early-mid L4
VC6
VC2
VC3
VC4
VC5
prkl-1(zy11); Cyls3; ExA[10ng/uL gfp::prkl-1 gene]
mid L4
VC3
C
% unipolar VC6
(lacking anterior axon)
25
20
15
10
5
WT (Cyls4; Zyls1)
WT; ExC[Punc-4::gfp::prkl-1]
WT; ExA[Punc-4::gfp::prkl-1]

Ectopic expression of *prkl-1* in PDE neurons results in premature termination of anterior axons.

prkl-1 overexpression results in unipolar VC neurons. Would *prkl-1* overexpression affect the polarity of non VC neurons? While performing *prkl-1* rescue experiments in VC4/5 using *Pcat-1*, the presence of the PDE anterior axon in worms carrying [*Pcat-1::gfp::prkl-1.a*] transgene at the vulva area was lost, hinting at aborted extension of PDE's anteriorly directed axons. Mechanosensory PDE neurons are generated postembryonically (White et al., 1986). They are a pair of dopaminergic neurons located in the posterior body, with bilateral symmetry. PDE axons extend ventrally and then enter the right bundle of the ventral nerve cord where they bifurcate to form a pseudo-bipolar neuron (White et al., 1986) (Figure III-13A). Each PDE extends an axon anteriorly to a position near the pharynx and an axon posteriorly to a position near the anus, in a bundle with the ventral nerve cord (Sulston et al., 1975)(Figure III-13). A quick examination of PDE neurons in nematodes harbouring the [*Pcat-1::gfp::prkl-1.a*] transgene revealed that the anterior axons were prematurely terminated (Figure III-13A, B & C). We scored PDE defects in *prkl-1(zy11); cyIs4* nematodes carrying the *Pcat-1::gfp::prkl-1.a* transgene, and siblings without the array were quantified as control. Three transgenic strains displayed similar results. Data from a representative line is presented in Figure III-13D. It became clear that driving *prkl-1* expression ectopically in PDE neurons disrupts the normal extension of the anterior axon, whereas the posterior axon was unaffected (Figure III-13A, B & C). Approximately, 48 % of anterior PDE axons terminated prematurely before the vulva in *prkl-1(zy11)* nematodes carrying *Pcat-1::gfp::prkl-1.a* array, compared to 0 % in nematodes without the transgene (Figure III-13D). Of all neurons

with anterior axons terminated before the vulva, 20 % were stalled at the base of the ventral process, lacking anterior axons altogether.

It is unlikely that the premature termination is caused by overexpressing GFP in PDEs, because PDEs display normal morphology in wild type *cyIs4* nematodes, carrying a *Pcat-1::gfp* overexpressing transgene. Although, *cyIs4* is not a PDE specific reporter, since it lights up several other dopaminergic neurons including VC4/5, HSNs and head neurons, it reveals the morphology of PDEs with no ambiguity. PDEs are two of the many neurons extending axons along the VNC, but the only ones labelled with the *cyIs4* array, thus serving as VNC passageway indicators. Thus, the GFP signal in PDEs axons, expressed from *cyIs4* reporter identifies the trajectory of the right bundle of the VNC.

Importantly, multiple transgenic lines carrying *prkl-1* transcriptional reporters and *gfp*-tagged *prkl-1(+)* genomic constructs failed to express any GFP in PDE neurons, suggesting that PRKL-1 is not endogenously produced in PDE neurons. Also, *prkl-1* mutants do not display PDE axon extension defects. These observations, together with the finding that *prkl-1* ectopic expression in PDE neurons causes premature termination of anterior axons imply that *prkl-1* plays an instructive role on neuronal polarity.

It would have been preferable to quantify defects caused by *Pcat-1::gfp::prkl-1.a* transgene in wild type nematodes. These arrays were originally obtained in a *zy(11)* background, and five attempts at outcrossing it into wild type nematodes failed. Besides, three transgenic lines with similar PDE defects (qualitatively and quantitatively) were obtained with no difficulty, by injecting 10 ng/µL *Pcat-1::gfp::prkl-1.a* construct in the gonads *prkl-1(zy11)* nematodes; whereas, the same construct was injected on multiple

occasions in a wt background, at decreasing concentrations starting from 10 ng/µL to as low as 0.5 ng/µL, with no success. It is possible that additional *Pcat-1*-driven *prkl-1* expression in a wild type background results in inviability? This is a technical drawback that might be solved by using an alternative promoter.

Plausibly, exogenous expression of *prkl-1* in the PDEs, overrides the endogenous PDEs polarization program that instructs anterior axon extension to its final target, the head. It is reasonable to hypothesize that the defects caused by *prkl-1* ectopic overexpression in PDE neurons involve *prkl-1* interacting genes, potentially in a PCP-like pathway. A notion that generates more questions, such as which other PCP players are regularly expressed in the PDEs that could potentially interact with *prkl-1* in preventing anterior axon extension? If *prkl-1* is not endogenously expressed in PDE neurons, as suggested by *prkl-1* transcriptional and translational reporters; are there other *prkl-like* genes playing a role in the wt morphology of PDE neurons, whose normal function could be overridden by *prkl-1* ectopic expression? A blast search of the *C. elegans* proteome identifies two other PRKL-like proteins containing PET and LIM domains, *tag-15* (1 PET, 6 LIM domains) and *tag-224* (1 PET, 3 LIM domains). To assess whether PDE neurons in *tag-15* and *tag-224* mutant backgrounds display premature termination of anteriorly-directed axons or any other defective phenotype, I crossed *tag-15(gk106)* and *tag-224(ok1036)* alleles into *cyIs4* reporter and examined PDEs morphology. We found that PDEs had a normal morphology (not shown), which may suggest that *tag-15* and *tag-224* are not involved. Taken together, these data suggest that *prkl-1* plays an **instructive role** in regulating neuron orientation along the AP axis with the potential to prevent AP axon growth in various neuron types.

Figure III-13. ***prkl-1*** **acts instructively to terminate anterior axon growth in PDE neurons. A**) Representative photograph of wild type trajectory of PDE axons visualized with *cyIs4* array. PDE anterior axons terminate at the head ring and posterior terminates close to the anus (represented by white stars). **B**) Representative image of truncated anterior PDE axons in a *prkl-1(zy11)* worm carrying transgene [*Pcat-1::prkl-1.a*]. Shorten right axon indicated by a blue star and shorten left axon, by a yellow star. Note wild type morphology of VC4/5 results from rescuing transgene. **C**) Schematics of wt and prematurely terminated PDE anterior axon. **D**) Quantification of PDE's anterior axon extension defects in worms carrying *Pcat-1::prkl-1.a* transgene. Scale bar, 20um.

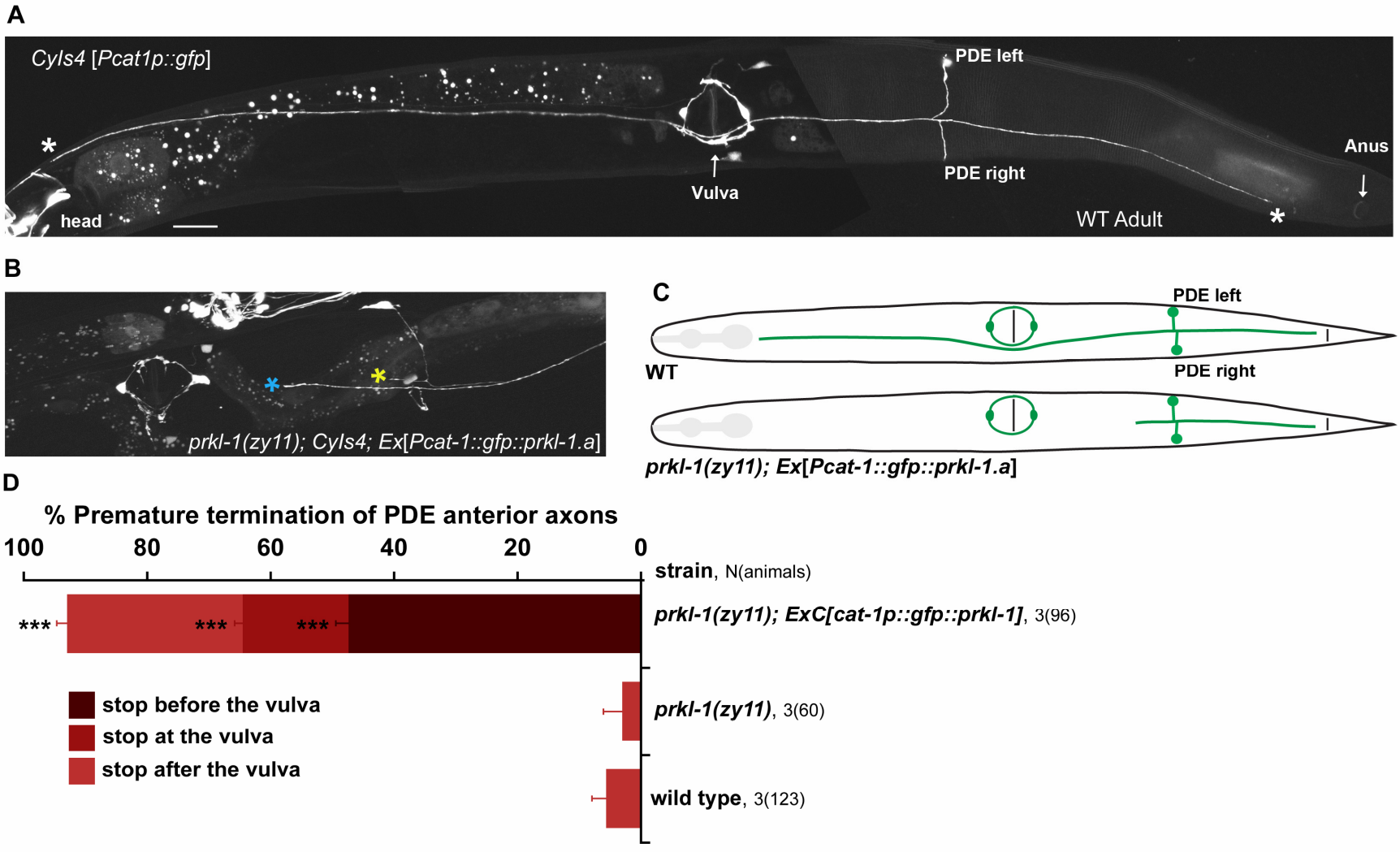
A
Cyls4 [Pcat1p::gfp]
PDE left
PDE right
Vulva
Anus
head
WT Adult
B
prkl-1(zy11); Cyls4; Ex[Pcat-1::gfp::prkl-1.a]
C
PDE left
WT
PDE right
prkl-1(zy11); Ex[Pcat-1::gfp::prkl-1.a]
D
% Premature termination of PDE anterior axons
100
80
60
40
20
0
strain, N(animals)
***
***
***
prkl-1(zy11); ExC[cat-1p::gfp::prkl-1], 3(96)
prkl-1(zy11), 3(60)
wild type, 3(123)
stop before the vulva
stop at the vulva
stop after the vulva

How does prkl-1 regulate neuron polarity? To further explore the mechanism by which prkl-1 prevents AP axon outgrowth, I performed structure-function studies by injecting prkl-1 deletion constructs into prkl-1 mutants, and scoring for rescue of VC polarity defects in the resulting transgenic lines. Thus, deleting one domain at a time helped uncover the minimal functional PRKL-1 protein. All experiments were performed using at least two independent lines per construct. For molecular biology details see Methods section and Supplemental Figure III-4. Importantly, to assess the validity of this experiment, every single transgenic construct was designed as a GFP-tagged PRKL-1 full length or deletion, expressed from the unc-4 promoter, with the purpose of examining if the fusion protein is indeed expressed and where. All transgenic lines quantified in Figure III-14 express GFP::PRKL-1 fusions, as indicated, in the VCs. Hence, structure can be correlated to function using these extrachromosomal arrays.

PRKL-1 long isoform is <u>necessary and sufficient</u> to polarize VC4 and VC5 motorneurons.

Three of four *prkl-1* mutants obtained from our genetic screens contain lesions within the PET domain coding exons (*i.e.* first and second exons); two of them contain premature stops codons at precisely the PET domain, which would only affect expression of PRKL-1.A (long isoform), while the short isoform is spared, resulting in phenotypic null alleles *zy11* and *zy18*. In addition, I previously showed that VC4 and VC5 defects in *prkl-1(zy11)* mutants were rescued almost entirely with GFP-tagged PRKL-1.A expressed from the *unc-4* promoter, using a *Punc-4::gfp::prkl-1.a* transgene (Figure III-5 and Figure III-14). Collectively, these findings may be suggestive of the importance of the

PET-domain-containing isoform (PRKL-1.A) on suppressing AP axon growth in VC4/5. Conversely, a *Punc-4::gfp::prkl-1.b* transgene coding for the short isoform expressed in a *prkl-1(11)* mutant strain is not capable of significantly restoring normal polarity in VC4/5 neurons, contrasting with the almost full rescue achieved with long isoform transgene (Figure III-14). These data suggests that the PET-domain-containing isoform (*prkl-1.a*) is **critical** to *prkl-1* polarity function in preventing axon growth along the AP axis.

However, *prkl-1(zy11)* could theoretically still express the *prkl-1.b*, which could limit the interpretation of results, as we can not exclude the potential contribution of the short isoform in the long isoform's ability to rescue defects (*e.g.* by forming dimers). Thus, I outcrossed the best rescuing *Punc-4::gfp::prkl-1.a* transgene (line A) away from *prkl-1(zy11)* and into the *prkl-1 knock out* strain, allele *zy17*, which does not synthesize neither short nor long *prkl-1* transcripts. Remarkably, the *prkl-1.a* transgene was capable of fully rescuing VC polarity defects (see mauve-outlined data bars in Figure III-14). Thus, restitution of exclusively the *prkl-1* long isoform is sufficient to fully restore normal VC bipolar medial-lateral polarity in *prkl-1* KO nematodes. Altogether, these data indicate that 1) PRKL-1 **long isoform is necessary and sufficient to prevent axon growth along the AP axis**, 2) PRKL-1 **PET domain is critical to rescue neuronal polarity defects in *prkl-1* mutants**, and 3) **PRKL-1 short isoform is dispensable for the polarity of VCs**.

The PRKL-1 C-terminus is critical to rescue neuronal polarity defects in *prkl-1* nematodes.

From the molecular and functional characterization of *ok3182* and *tm3440 prkl-1* deletion alleles, we previously learned that the third PRKL-1 LIM domain and/or the C-terminal tail might be important to suppress AP axon growth. Accordingly, to further explore the contribution of the *prkl-1* C-terminal, a *Punc-4::gfp::prkl-1*ΔC-terminal, deleted for the C-terminal 196 residues of PRKL-1, was scored for its ability to rescue VC polarity defects. Consistent with previous observations, a C-terminal-deleted PRKL-1.A failed to rescue the VC tripolar phenotype in *prkl-1(zy11)* nematodes (Figure III-14), suggesting that the C-terminal tail is critical to prevent AP axon growth in VC motorneurons.

In addition, the last four C-terminal residues (CTVS) form a consensus motif for farnesylation, a posttranslational modification involved in membrane targeting (McTaggart, 2006). Thus, we explored whether the lack of CaaX motif accounts for the C-terminal-deleted construct failure to rescue, for instance by interfering with PRKL-1 subcellular localization and therefore function. However, we found that a CTVS deleted PRKL-1 transgene was at least partially effective in rescuing *prkl-1* polarity defects contrasting with the null activity of the C-terminal deletion. These data may suggest that 1) CTVS is not critical for PRKL-1 function, and that 2) ΔCTVS PRKL-1 has other means to reach functionally important subcellular locations, including the plasma membrane and nucleus, without the need for the fine localization tuning imposed by the posttranslational addition of the isoprenoid moiety. For instance, the PET domain could

be a candidate for such a role, as it has been recently shown to be sufficient to target PRKL-1 to the membrane (Sweede et al., 2008). Besides, it is important to mention that all deletion plasmid were used at 10 ng/µL. At this concentration, the C-terminal deletion did not cause a *prkl-1 gof* phenotype (*i.e.* unipolar neurons). Therefore, it is unlikely that CTVS-deleted PRKL-1 is reaching functionally important subcellular compartments as a consequence of an overexpressing transgene, which further supports the notion that PRKL-1 has alternative means to become localized to functionally important compartments. Importantly, to further understand the significance of the CTVS motif to PRKL-1 polarity function it would be important to compare the effects of deleting the C-terminal region and the CTVS motif on PRKL-1 subcellular localization.

PRKL-1 LIM domains are dispensable to suppress ectopic AP axon outgrowth but required for primary ML axon formation and to limit VC4/5 axon branching.

VC4/5 neurons in *prkl-1(ok3182)* nematodes, a deletion allele that lacks the third LIM domain and the C-terminal tail, display a highly penetrant ectopic AP axon phenotype. Semiquantitative RT-PCR revealed that levels of *prkl-1* mRNA in *ok3182* strain were comparable to those of wt strain (see Figure III-15), suggesting that fast decay of *ok3182 prkl-1* mRNA and subsequent lower rate of PRKL-1.A protein synthesis is unlikely to account for the strong *lof* phenotype. It seems plausible that the protein is being produced but the lack of the third LIM domain and the C-terminal tail render the protein inactive, for instance 1) these domains might be required for PRKL-1.A to reach an active 3D conformation, or 2) the truncated protein may still fold properly but the activity of the deleted regions is critical to prevent AP axon growth, or alternative 3) the

truncated protein may function in a dominant negative manner. Since we have already shown that the C-terminal domain is important for PRKL-1.A function in VC4/5 morphology; we next considered based on the molecular properties of the strong hypomorph *prkl-1(ok3182)*, whether the 3rd LIM domain was also relevant to this pathway.

C. elegans LIM domains are highly conserved across evolution, displaying 40-55 % identity to the human PRKL-2 LIM domains, suggesting they likely play a conserved role in PRKL-1 polarity function. Thus, deletion constructs of individual LIM domains, or all three LIM domains simultaneously were injected in *prkl-1(zy11)* nematodes and scored for their ability rescue VC polarity defects. Surprisingly, transgenes with individual or group deletions of LIM domains were able to rescue the tripolar defects in *prkl-1* nematodes, with quantitatively similar results to the full length PRKL-1 expressing transgene (Figure III-14). These data strongly suggest that LIM domains are not required to prevent AP axon outgrowth.

However, expression of LIM-deleted transgenes, more specifically ΔLIM-3 and ΔLIM1-3, resulted in significant percentage of unipolar VC4/5 neurons. Thus, LIM-deleted transgenic lines that best rescued the tripolar VC morphology were quantitatively compared for their ability to cause VC4 unipolar neurons (Figure III-15A). Simultaneous deletion of the three LIM domains resulted in 32 % of unipolar VC4 neurons, representing a 7 fold increase in the efficacy to prevent ML axons, relative to PRKL full length with 4.7 % of unipolar VC4s. Remarkably, expression of these constructs in a *prkl-1* null background also resulted in an excess branching phenotype. *prkl-1(zy11)*

worms carrying ΔLIM-3 and ΔLIM1-3 expressing transgenes displayed a mild but penetrant VC4/5 excess branching phenotype, which includes midline crossing and long terminal branches (Figure III-15A & C-D, respectively).

Collectively, these data suggest that 1) PRKL-1 ΔLIM1-3 is a minimal functional protein required to prevent AP axon growth in VC4/5, in other words, LIM domains do not appear to be required to prevent AP axon growth in VC4/5; and that 2) the LIM domains are required to promote ML axon growth and to control axon branching, a terminal feature of polarity maintenance in VC4/5. Importantly, these results were obtained by injecting LIM-deletion constructs at 10 ng/μL, a dose at which full length *prkl-1* construct rescues VC4/5 polarity defects and does not cause any branching defects and does not generate significant unipolar phenotype (Figure III-15A).

Figure III-14. Structure-function analysis of PRKL-1. ***prkl-1*** **long isoform is necessary and sufficient to suppress ectopic axon outgrowth along the AP axis. PET and C-terminal domains are critical to this function. Left)** Schematic representation of deletion constructs used in this study. **Right)** Quantification of polarity defects in transgenic lines carrying the arrays depicted on the left. The ability of each transgenic line to rescue the polarity defects in the parental strain *prkl-1(zy11)* was evaluated, with the exception of the mauve-outlined bars which represent data in *prkl-1(zy17)* background. Arrow bars represent S.E.M. Statistic significance was assessed by ANOVA followed by Bonferroni test. $^{\&\&\&}p<0.001$ compared to transgene-less *prkl-1(zy17)*, ***p<0.001, *p<0.05 compared to transgene-less *prkl-1(zy11)*.

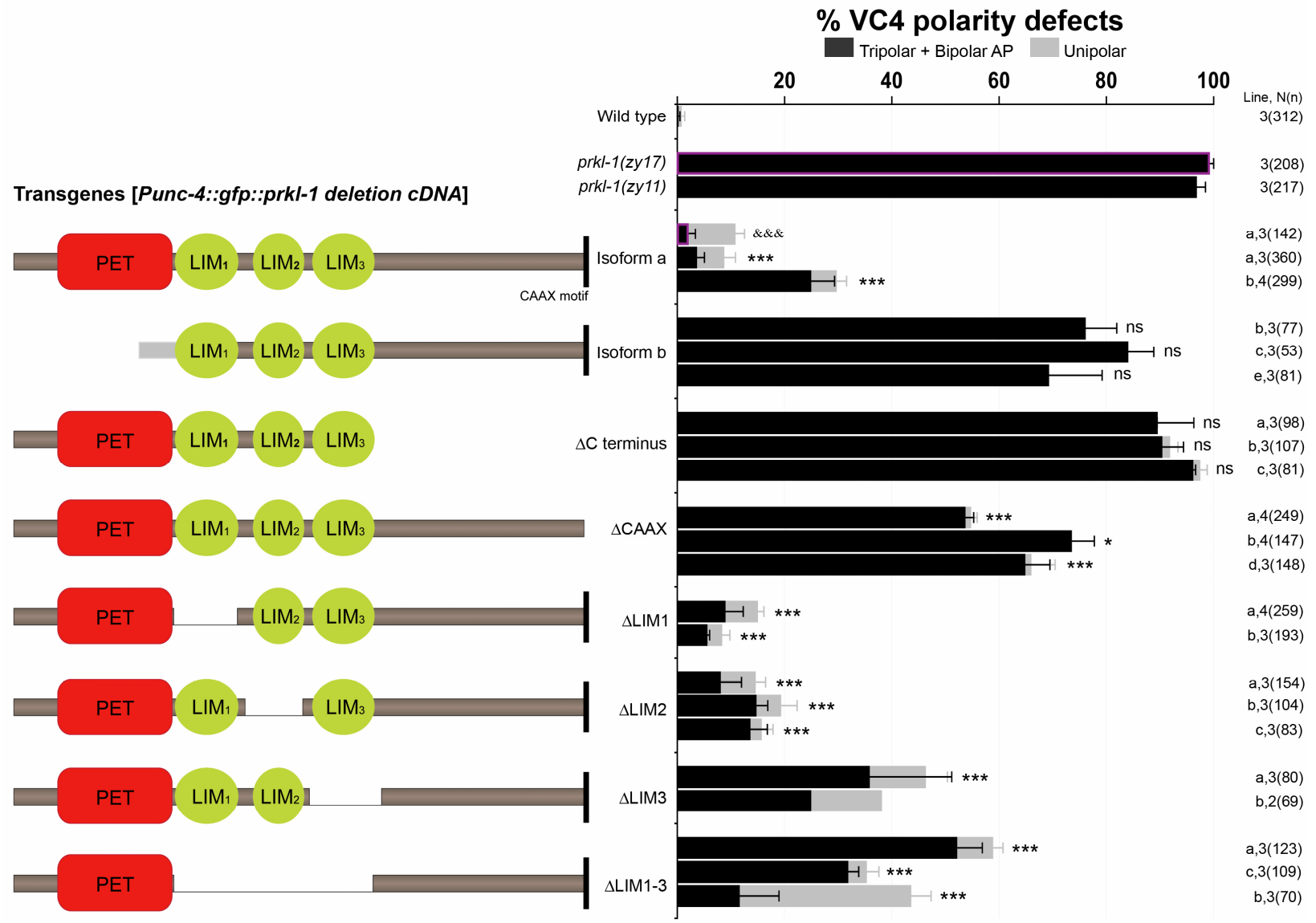
% VC4 polarity defects
Tripolar + Bipolar AP
Unipolar
20
40
60
80
100
Line, N(n)
Transgenes [Punc-4::gfp::prkl-1 deletion cDNA]
PET
LIM1
LIM2
LIM3
CAAX motif
Wild type
3(312)
prkl-1(zy17)
prkl-1(zy11)
3(208)
3(217)
Isoform a
&&&
***
***
a,3(142)
a,3(360)
b,4(299)
Isoform b
ns
ns
ns
b,3(77)
c,3(53)
e,3(81)
ΔC terminus
ns
ns
ns
a,3(98)
b,3(107)
c,3(81)
ΔCAAX
***
*
***
a,4(249)
b,4(147)
d,3(148)
ΔLIM1
***
***
a,4(259)
b,3(193)
ΔLIM2
***
***
***
a,3(154)
b,3(104)
c,3(83)
ΔLIM3
***
a,3(80)
b,2(69)
ΔLIM1-3
***
***
***
a,3(123)
c,3(109)
b,3(70)

Figure III-15. PRKL-1 is required to promote ML axons growth and to regulate VC4/5 axon branching. A) Quantification of unipolar VC4 neurons in *prkl-1(zy11)* carrying the indicated *prkl-1* deletion transgenes. **B)** Confocal photograph of wild type VC4/5 neurons. **C-G)** Images of VC4/5 neurons in *prkl-1(zy11)* mutants carrying a transgene that expresses PRKL-1.a ΔLIM1-3 from the *Punc-4* promoter. Notice VC4/5 bipolar morphologies due to rescue of *prkl-1* polarity defects by the LIM-deleted array, and excess branching indicated by green stars. Arrow bars represent S.E.M. Statistical significance was assessed by one-way ANOVA followed by Bonferroni test. ***$p<0.001$, compared to PRKL-1.a ΔLIM1-3 expressing *prkl-1(zy11)* worms; $^{\&}p<0.05$ and $^{\&\&\&}p<0.001$, compared to a transgene-less *prkl-1(zy11)* mutant background. Scale bar, 10 μm.

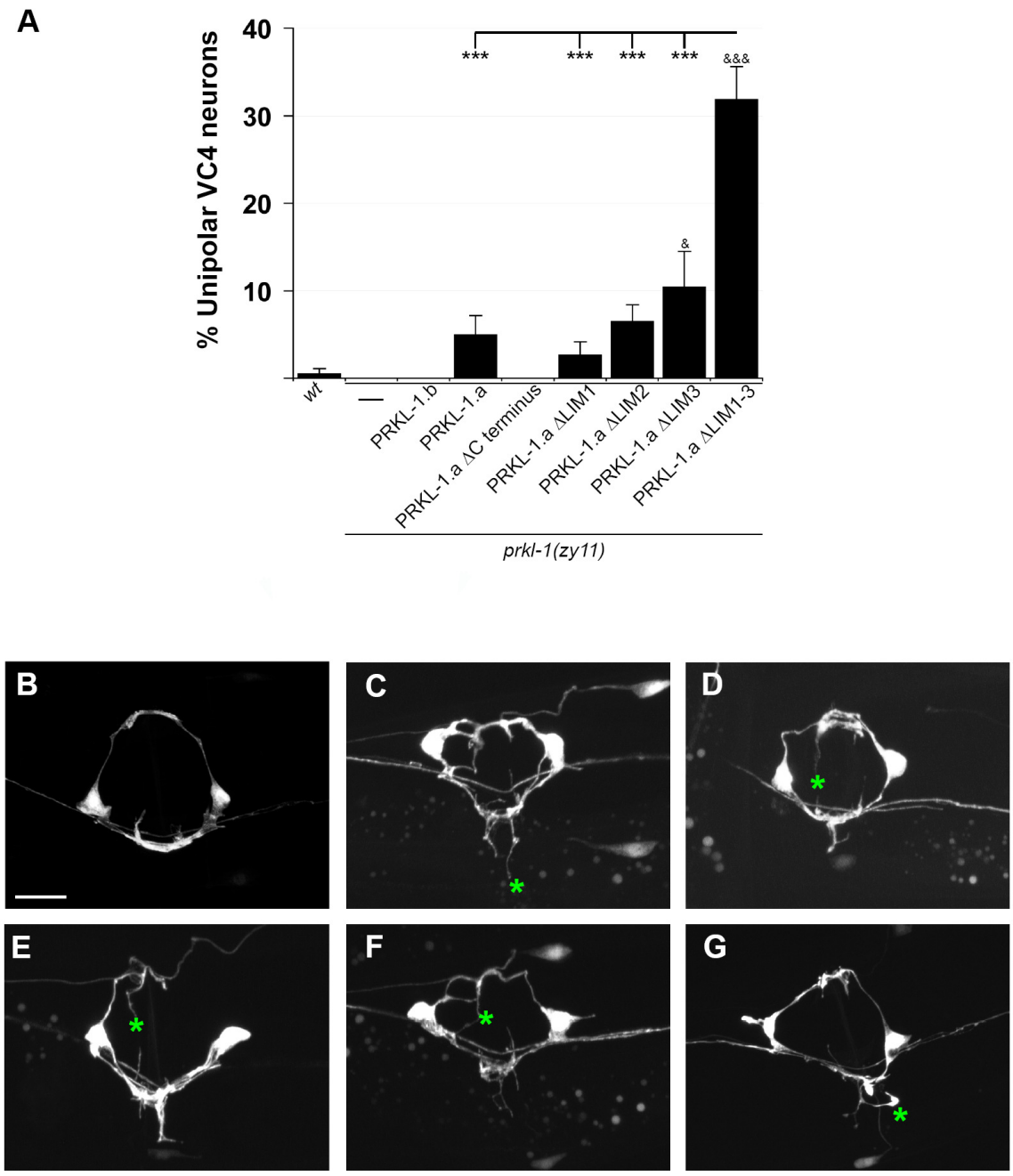
A
% Unipolar VC4 neurons
40
30
20
10
***
***
***
***
&&&
&
wt
—
PRKL-1.b
PRKL-1.a
PRKL-1.a ΔC terminus
PRKL-1.a ΔLIM1
PRKL-1.a ΔLIM2
PRKL-1.a ΔLIM3
PRKL-1.a ΔLIM1-3
prkl-1(zy11)
B
C
D
E
F
G

DISCUSSION

PRKL-1 is a core element of the PCP pathway, well known for polarizing cells within the planar dimension of the tissue they inhabit, including epithelial hair cells in the fly wings (Gubb et al., 1999b) and the vestibular sensory epithelia of the mouse inner ear (Deans et al., 2007), and for the proper ML migration of masses of cells along the body axis, during vertebrate gastrulation (Veeman et al., 2003). In *C. elegans prkl-1* genetically interacts with *vang-1* and *dsh-1* to regulate the ML morphology of vulval proximal VC neurons. In *prkl-1* mutants, VC4/5 neurons extend an ectopic axon along the AP axis. Here, I have provided evidence for when, where and how *prkl-1* is required to prevent AP axon growth.

PRKL-1 is required to establish and maintain VC4/5 neuron morphology.

Prior to our work, the role of *prkl-1* in neuronal polarity *in vivo* was unknown. Here we showed that *prkl-1* controls the orientation of VC4/5 motorneurons by suppressing axon growth along the AP axis, and/or promoting axon growth along the ML axis, around the developing vulva. Interestingly, *prkl-1* appears to reorient lamellipodial protrusions towards the VPCs, suggesting that *prkl-1* functions prior to axonogenesis. This result, together with the finding that VC4/5 primary ML and ectopic AP axons emerge simultaneously in *prkl-1* mutants, suggests that *prkl-1* acts early to establish neuron polarity. These data resemble the function of *prkl-1* in prehair cells in the fly wing during PCP establishment, in which *prkl* orients and controls the number of hairs prior to any signs of polarized cytoskeletal growth (Gubb and Garcia-Bellido, 1982). Importantly, dsRNA-induced *prkl-1* downregulation after the ML bipolar morphology of VC4/5

neurons was established with the extension of left and right primary axons, also resulted in tripolar neurons; suggesting that *prkl-1* plays an active role in maintaining VC4/5 ML morphology, by continuously preventing AP axon growth.

PRKL-1 functions cell autonomously in VC4 and VC5 motorneurons, following vulva induction, to prevent AP axon growth.

Although, *prkl-1* gene is transcriptionally and translationally active in both VC4/5 and the vulva epithelium, only PRKL-1 expressed in the neurons appears to be essential for VC4/5 polarity. Similarly, *Drosophila prickle* functions cell autonomously in epithelial cells to regulate hair orientation (Adler et al., 2000). In addition, PCP genes are known to act cell non-autonomously as well (McNeill, 2010). For instance, somatic mosaic analysis of Fz mutant cells revealed a form of non-autonomous alteration of the polarity of wild type adjacent cells, termed domineering non-autonomy (Adler et al., 2000). In this new form of regulation, wild type neighbouring cells to a PCP mutant patch display a disrupted PCP phenotype (Adler et al., 2000). Notably, *Prkl* homologs operate differently depending on the context. For instance, zebrafish pk1b is required cell non-autonomously for proper gastrulation CE movements of both the mesendoderm and neuroectoderm (Veeman et al., 2003), whereas the same gene is required cell autonomously in tangentially migrating Facial Branchiomotor Neurons (Rohrschneider et al., 2007). These are two examples of contexts which despite of sharing a functional feature, the polarized migration of masses of cells, *prkl* is needed differently; suggesting different governing PCP mechanisms for each cell type.

Notably, we found that although epithelial *prkl-1* is not required for VC4/5 polarity; the epithelia appear to be a timely regulated environmental trigger which induces *prkl-1* expression in VC4/5 neurons. The latter may hint at a canonical pathway, triggered by the epithelia, which regulates PCP manifestation in VC4/5 neurons.

The number of axons in VC4/5 neurons is sensitive to *prkl-1* levels.

Notably, the levels of *prkl-1* expression in VC4/5 must be precisely controlled by the vulva. In this chapter I have shown that while *prkl-1 lof* results in supernumerary neurites (tripolar neurons), *prkl-1* overexpression results in too few neurites (unipolar neurons). A dose-dependent signalling role for *prkl-1* or any other core PCP gene has not been reported in any model organism. This result contrasts with the role of murine *prickle-1 and prickle-2* in retinoblastoma cell lines in culture, where *prickle*1-2 downregulation results in too few neurites, suggesting that in this context *prickle* promotes neurite formation (Okuda et al., 2007;Fujimura et al., 2009). Although, neurons in culture may not exactly recapitulate the timing and natural environmental conditions that neurons possess in vivo, these contrasting data are suggestive of *prkl* playing a context-dependent role neuronal polarity.

PCP signalling in *Drosophila* wing cells not only controls the subcellular position of the hair but also hair orientation and hair number. Typically, overexpression of PCP genes leads to a *lof* phenotype. For instance, in flies too much and too little *prkl* leads to multiple hairs per wing cell, causing a similarly disorganized hair patterning (Fanto and McNeill, 2004). Similarly, the PCP pathway in VC4/5 regulates axon orientation and axon number. The common link between these two systems is that PCP signalling

modulates the tight control over the number and orientation of cytoskeleton filled protruding structures.

GFP::PRKL is localized at the plasma membrane of VC4/5 neurons in a uniform punctate pattern and uniformly in the nuclei.

GFP::PRKL-1 is consistently expressed in a punctate pattern at the plasma membrane and smoothly in the nucleus of VC4/5 neurons. The significance of the PRKL-1 puncta and of the nuclear localization is unknown. Uncovering the composition of the puncta would provide important insight into the mechanism by which PRKL-1 prevents AP axon growth. Importantly, PRKL has been shown to be expressed in a similar pattern in other cell types undergoing PCP, including zebrafish facial branchiomotor neurons during their tangential migration in the hindbrain (Mapp et al., 2011).

Notably, PCP proteins are asymmetrically expressed in many cell types undergoing polarization, including *Drosophila* wing hair cells and ommatidia (Tree et al., 2002;Strutt, 2003;Das et al., 2004); while in others they are symmetrically localized (Gros et al., 2009). Based on previous reports showing that the asymmetric localization PRKL is dependent upon and required for PCP signalling in some PCP tissues, we looked for evidence of PRKL-1 asymmetric localization in VC4/5 neurons but did not find significant enrichment in any side of the plasma membrane, suggesting that the location of axon growth or suppression do not correlates with asymmetric distribution of PRKL-1. Instead, PRKL-1 puncta in VC4/5 appeared distributed around the plasma membrane without apparent asymmetry. However, we can not rule out PRKL-1 asymmetric activity, because 1) asymmetries could be masked by higher, non-physiological expression levels

from transgenic arrays, and 2) asymmetric activity may be expressed at the posttranslational level, such as upon phosphorylation. For instance, although GSK-3β is symmetrically localized to all immature processes of hippocampal neurons, phosphorylated and thus inactive GSK-3β is localized to the axon-to-be-neurite and excluded from dendrites, whereas non-phosphorylated and thus active GSK-3β is recruited to dendrites and excluded from axons (Jiang et al., 2005).

Another possible explanation is that the use of overexpressing arrays may have masked transiently expressed asymmetries at lower, more physiological levels; particularly in VC4/5, which have a significantly smaller size (~ 5 µm diameter) than the vulval syncythia (with many epithelial cells fused together). Additionally, we found that the puncta at the plasma membrane and the nuclear expression were not significantly affected in a *vang-1* mutant background. This result contrasts with findings in the fly wing epithelia, where interdependent asymmetric distribution of PCP proteins is necessary and sufficient for PCP activation (Jenny and Mlodzik, 2006;Seifert and Mlodzik, 2007). For instance, VANG and PRKL form a complex that is enriched at the proximal end of the plasma membrane, and *vang-1* is required for PRKL asymmetric localization (Jenny et al., 2003). These discrepancies between tissues, could be interpreted as different PCP mechanisms that function in different contexts.

Importantly, GFP::PRKL-1 expressed in the syncythial vulva epithelium was asymmetrically localized towards the vulva lumen, in a non-punctate, rather uniformly distributed expression pattern, in every single examined worm ($n > 50$). The significance

of PRKL-1 expression at the vulva is unknown; it is possible that *prkl-1* is involved in some polarized activity during vulva morphogenesis.

Finally, in order to better understand the role of PRKL-1 in VC4/5 polarity, its subcellular localization before and during axon outgrowth (*i.e.* from late L3 to mid L4) localization needs to be further explored using alternative strategies. Immunostaining using PRKL-1 specific antibodies would be a more reliable method to assess asymmetries.

The PET-domain-containing long PRKL-1 isoform is necessary and sufficient to prevent AP axon growth.

In this chapter, I showed that *C. elegans prkl-1* locus generates two transcripts. A longer mRNA (*prkl-1.a*), encoding a protein with a PET domain and three LIM domains, which conforms to the domain composition of PRKL-like proteins; and a shorter PET-less transcript which encodes an isoform with triple LIM domains (*prkl-1.b*). The short transcript, arising from alternative 5' splicing or possibly from use of alternative promoters, harbours a distinctive N-terminal resulting from retention of an intronic sequence, which encodes a unique 37 aa polypeptide.

Alternative RNA splicing is a way to regulate gene function and expand the proteome of an organism (Zahler, 2005). For instance, the generation of multiple isoforms from a single gene may serve 1) to turn off gene expression post-translationally (Zahler, 2005), 2) to diversify gene function in space, by producing tissue specific isoforms with potentially distinct roles, or 3) to diversify gene function in time, by

producing distinct isoforms within the same cells/tissues, under a tightly regulated developmental timer. Diverse protein variants from a single locus contribute to specifying the precise connections of nerve cells, in certain cases by displaying opposing functions. One example of this is illustrated by the two isoforms of axon guidance Slit-receptor Robo3.1 and Robo3.2. While 3.1 is expressed in the progressing segment of commissural axons and facilitates midline crossing, 3.2 is expressed in the post crossing segment, and blocks midline crossing (Chen et al., 2008). Hence, the two Robo3 isoforms cooperate so that fidelity of axon guidance can be achieved.

Interestingly, the sole *prkl* gene in *Drosophila* also undergoes 5' alternative splicing rendering three isoforms with different N-terminals lengths (Gubb et al., 1999b). Unlike *C. elegans* PRKL-1 variants, the three fly isoforms share the PET domain and the three LIM domains (Gubb et al., 1999b). Different N-terminal polypeptides are critical to the isoforms tissue-specificity and their qualitatively distinct functions; however the balance between isoforms is essential for PCP specification in *Drosophila* (Gubb et al., 1999b). Our structure-function results suggest that the two *C. elegans* PRKL-1 isoforms do not act redundantly in VC4/5, instead they appear to have divergent functions. While the longer isoform prevents ectopic AP axon growth in VC4/5, the shorter PET-less variant is not required. Interestingly, functional analyzes of allele *prkl-1(zy17)*, a null for both transcripts, hinted at a new role for *prkl-1* in axon guidance. Altogether, the inability of the PET-less isoform to rescue VC4/5 polarity defects in *prkl-1(zy11)* mutants suggests that the PET domain is crucial to prevent AP axon growth.

PRKL-1 C-terminal domain is critical to prevent AP growth.

The inability of a C-terminal-deleted PRKL-1 expressing transgene to rescue VC4/5 polarity defects in *prkl-1(zy11)*, suggested that the C-terminal region is essential for PRKL-1 to regulate VC4/5 neurons polarity. Because the deleted region is too large (196 residues), this result doesn't allow to assign any specific role to the C-terminal. It is known however, that both the PET domain and C-terminal of *Drosophila* PK interact with VANG-1 and that this interaction is essential for the asymmetric distribution of the VANG/PK complex to the proximal edge of the apical membrane in hair cells (Seifert and Mlodzik, 2007). It would be interesting to follow up this result by deleting smaller sections in the C-terminal, and performing mutagenesis of highly conserved residues, potentially important to rescue VC4/5 tripolar neurons, and examine how these affect protein localization and the ability to rescue polarity defects.

PRKL-1 LIM domains promote ML axon formation and control terminal branching in VC4/5, but appear dispensable to prevent AP axon growth.

Structure-function analysis revealed that PRKL-1ΔLIM1-3 is the minimal protein required to rescue polarity defects in *prkl-1(zy11)* mutants. Interestingly, deletion of all three domains caused ~ 32 % of unipolar neurons, a six fold increase with respect to the full length construct, at a similar concentration. This result implicated the trio of LIM domains in promoting ML axon formation; contrasting with the role of *prkl-1* in preventing axon formation in the AP direction. Altogether, PRKL-1 is implicated in the fine tuning of VC4/5 responses to ML *vs* AP polarizing cues, resulting in the left-right orientation of primary axons and the lack of AP axons.

In addition, the LIM-deleted construct caused excess branching, hinting at a role for LIM domains in controlling branch formation. It is plausible that the PET-C terminal regions play a role in promoting branch formation and that the LIM domains regulate the extent of this function, acting as a physiological brake so that the number and size of branches are kept controlled. Ideally we would confirm this hypothesis by examining a mutant which only lacks the LIM domains while the rest of the protein is in frame. Alternatively, an equivalent approach to assess the role of PRKL-1 LIM domains in promoting ML axon growth and controlling branching could be 1) by transferring the LIM deleted transgene into *prkl-1(zy17)* KO nematodes, so that the only copy of the gene comes from the LIM-deleted expression array, and scoring for the unipolar and excess branching phenotypes relative to a full length PRKL-1 transgene; and 2) by overexpressing ΔLIM1-3 in a wild type background. Would ΔLIM1-3 behave as a dominant negative array? Answering these and other questions will help clarify the molecular mechanism by which PRKL-1.A polarizes neurons.

Interestingly, the Wnt/PCP pathway, specifically *prkl*, *dsh*, *vang* and *Fz,* has been shown to regulate the stereotyped branching pattern of *Drosophila* mushroom body (MB) neurons (Ng, 2012). PCP mutants failed to extend the dorsal and/or medial branches of MB axons, in a context dependent manner (Ng, 2012). Similarly another PCP gene, atypical cadherin Flamingo has been implicated in the development of dendritic arborisation in flies (Gao et al., 2000) and mouse (Shima et al., 2004), which involves cytoskeleton decisions on branch formation and maintenance.

Prkl-1 overepression in VC4/5 circumvents the need for functional _vang-1_ and _dsh-1_ alleles in regulating neuron polarity.

Prkl-1 overexpression restores wild type VC4/5 morphology in *vang-1(tm1422)* and *dsh-1(ok1445)* nematodes. Based on this result, it is tantalizing to predict some epistatic relationships between the three PCP genes in VC4/5 polarity pathway. For example, such genetic interactions in a linear pathway would suggest that *prkl-1* functions downstream of both *vang-1* and *dsh-1*. However, caution should be used when interpreting these data, as there are some caveats to it, for instance 1) PCP signalling in other models is not a linear cascade of events, which might also be the case in VC4/5 neurons, and also 2) contrasting with *prkl-1* which only acts cell autonomously, *vang-1* and *dsh-1* function in both the neurons and the epithelia; which adds to the complexity to this pathway.

Prkl-1 plays an instructive role in neuron polarity.

Expression analysis of *prkl-1* promoter and *gfp*-tagged PRKL-1 from a genomic array, indicate that *prkl-1* expression is highly restricted, especially within the nervous system. Thus, while *prkl-1* is expressed in the VCs it is not expressed in many ventral cord neurons with AP axons, including the pair of PDE mechanosensory neurons. In addition, *prk-1* mutants do not display PDEs morphological defects, suggesting that PDEs do not require *prkl-1* for their normal polarization and or axon extension. However, ectopic *prkl-1* expression in the PDEs using a *cat-1* promoter resulted in premature termination of anterior axons, with ~ 48 % of axons terminated before the vulva including ~ 12 % of PDEs lacking anterior axons. This result indicates that *prkl-1*

is able to revoke the polarity program of neurons in which it is not normally expressed and is suggestive of *prkl-1* playing an instructive role in neuron polarity.

Importantly, using PDE-specific promoters would allow for a better understanding of what is happening in the neurons upon *prkl-1* overexpression. What would be the effect of *prkl-1* expression in the PDEs under an earlier promoter, before neuritogenesis? Would the extension of the ventrally directed process be arrested? Or, Is this a specific effect on the anterior axons, independent of the timing of *prkl-1* expression? Is ectopic PRKL-1 expressed asymmetrically in the anterior axon or is it evenly localized on both the anterior and posterior processes. Would *prkl-1* then depend on the specificity of downstream effectors to halt the anterior axon exclusively? This is an extremely exciting result and a great model in which to obtain further answers on how *prkl-1* regulates neuron morphology.

Altogether, *prkl-1* expression appears to be excluded from PDE neurons, and *prkl-1 lof* does not cause PDE defective phenotype while *prkl-1* overexpression abrogates formation or extension of the anterior axon, these results not only indicate that *prkl-1* plays an instructive role in neuron polarity but also this result is consistent with *prkl-1* involvement in VC4/5 polarity (*i.e. Prkl-1* overexpression → block AP outgrowth/extension).

SUPPLEMENTARY DATA

<u>Supplemental Figure III-1.</u> Expression pattern of *prkl-1* upstream promoter. *Pprkl-1up* is expressed in the head and tail, vulva epithelia, VC4 and VC5 and other VNC motorneurons including commissures. Scale bar, 20 µm. Molecular biology details can be found in the Methods section.

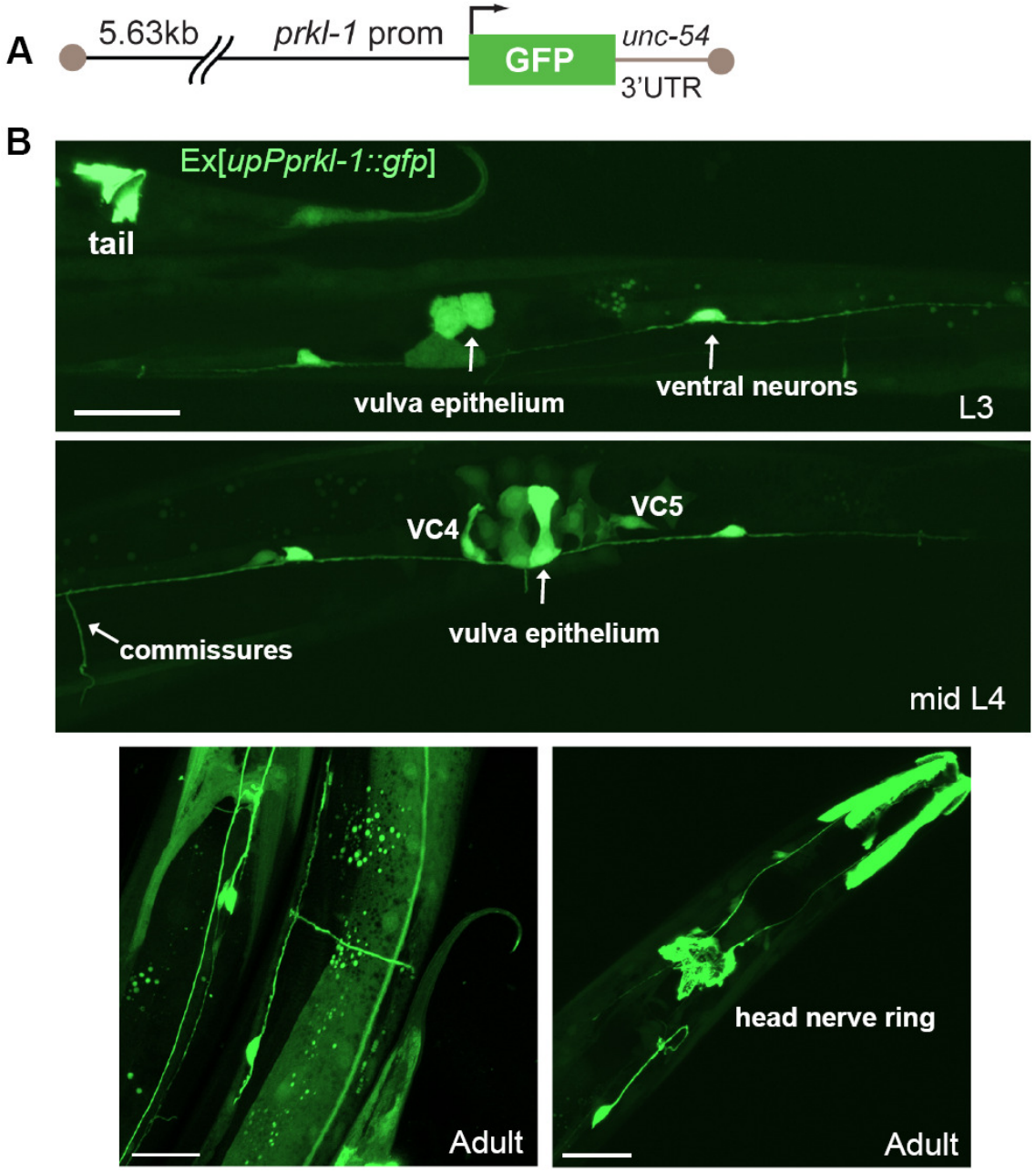

Supplemental Figure III-2. Colocalization of *Pprkl-1::GFP* and *Plin-11::RFP* transcriptional reporters, reveals *Pprkl-1* activity in VC1-6 motorneurons. Images of a representative transgenic worm at early L4 stage.

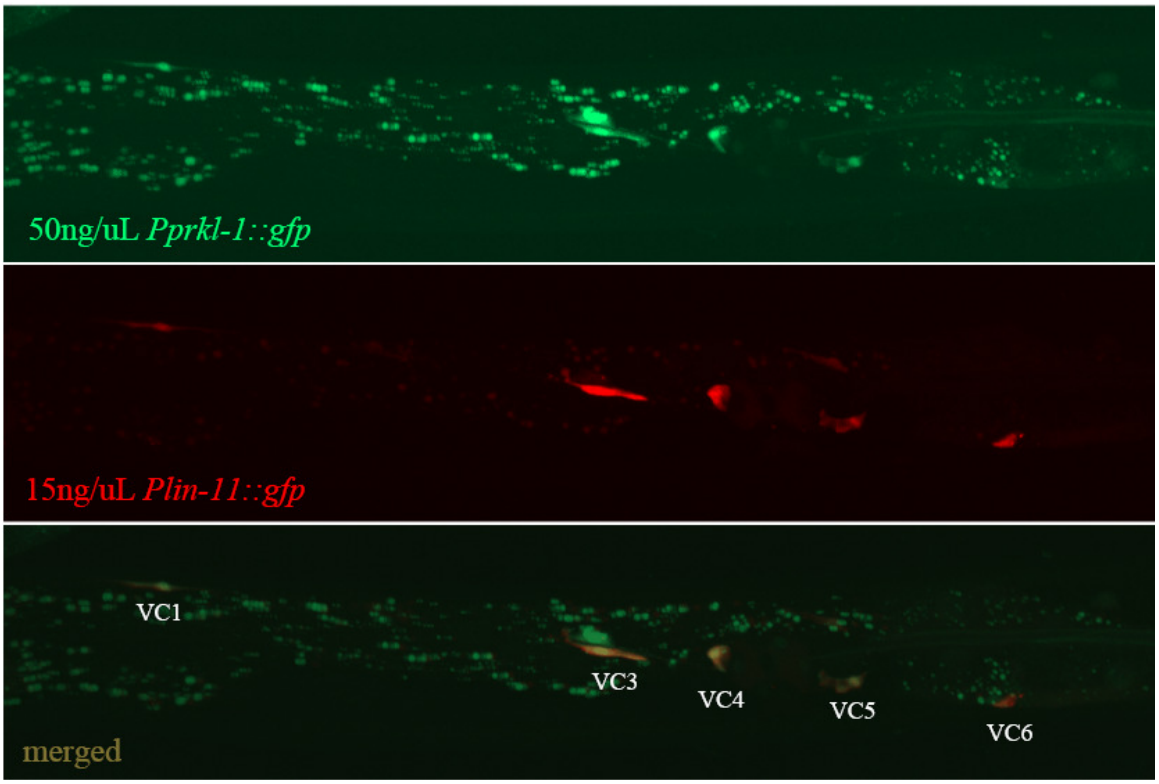

Additional phenotypes resulting from *prkl-1* overexpression

prkl-1 overexpression, using a functional GFP-tagged genomic transgene injected at 10 ng/µL, 10 times the concentration required to fully rescue *prkl-1(zy11)* defects, resulted in **dead eggs, larval arrest** and **morphologically abnormal larvae** (Supplemental Figure III-3). This interesting phenotype may be related to *prkl-1* hypodermal expression during embryogenesis and larval development. Contrastingly, overexpression of *prkl-1 cDNA* driven by *Punc-4* did not have any effect on the larvae morphology; however it caused **uncoordinated locomotion** and **swimming**. This result may suggest that *prkl-1* overexpression is detrimental to motorneurons which normally express *unc-4* and which are important for locomotion, resulting in uncoordinated movement.

Supplemental Figure III-3. Non-neuronal PRKL-1 overexpression phenotypes. A) Representative DIC image of a larvae carrying genomic PRKL-1 overexpressing transgene, with abnormal body morphology. B) PRKL-1::GFP is expressed in the *C. elegans* male sexual organ; which might be linked to the inability of homozygous *prkl-1* mutant males to generate crossprogeny.

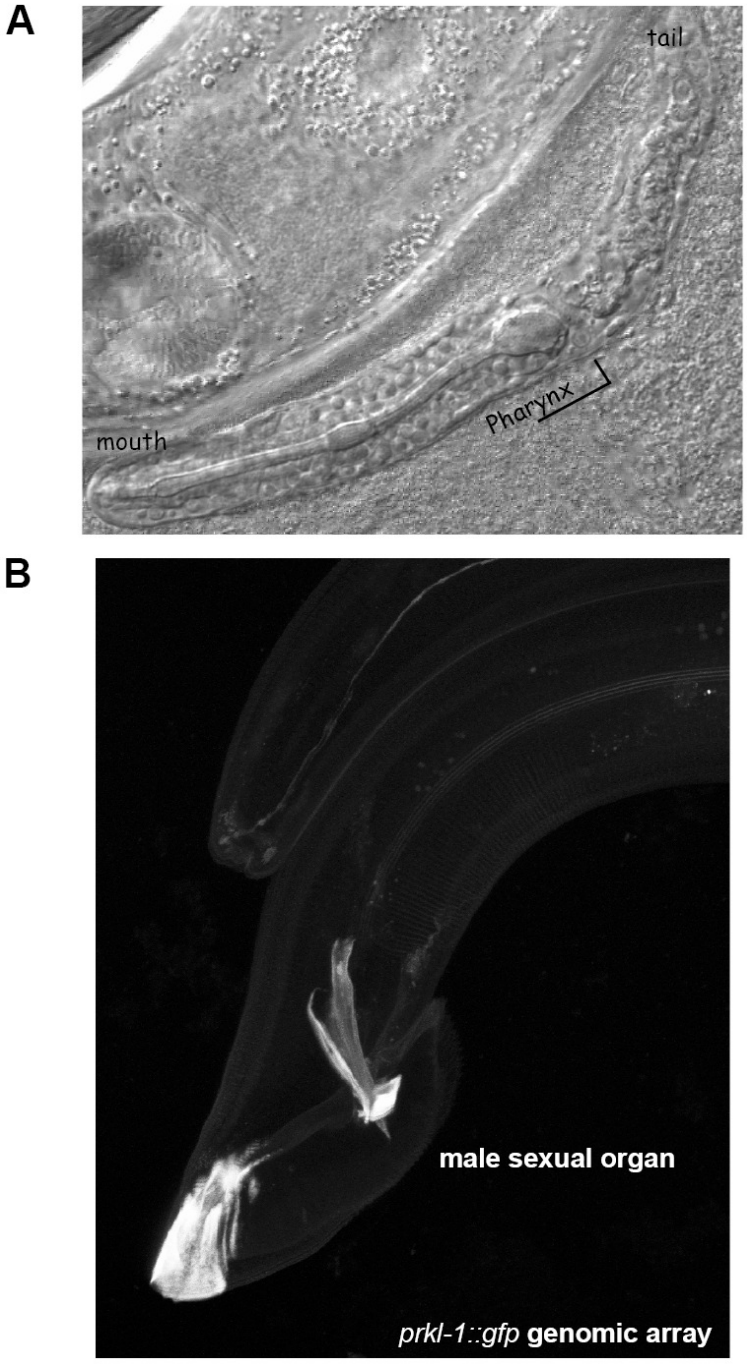
A
tail
Pharynx
mouth
B
male sexual organ
prkl-1::gfp genomic array

Supplemental Figure III-4. Strategy and sequence of PRKL-1 deletion constructs used for structure-function studies. Approach used to delete the three internal LIM domains individually and in group. Translationally silent endonuclease restriction sites (boxed sequences) were engineered in order to fuse 3' and 5' DNA fragments, while deleting internal cDNA regions, in order to keep the open reading frame in the truncated protein. Synthetic restriction sites were created by changing individual nucleotides (circled), within the primer sequences. The horizontal brown arrow denotes reverse primer of the upstream fragment, while the green arrow denotes forward primer of the downstream fragment. The numbers of the last amino acid of the upstream fragment and the first amino acid of the downstream fragment, which were attached in the fused sequence, are indicated.

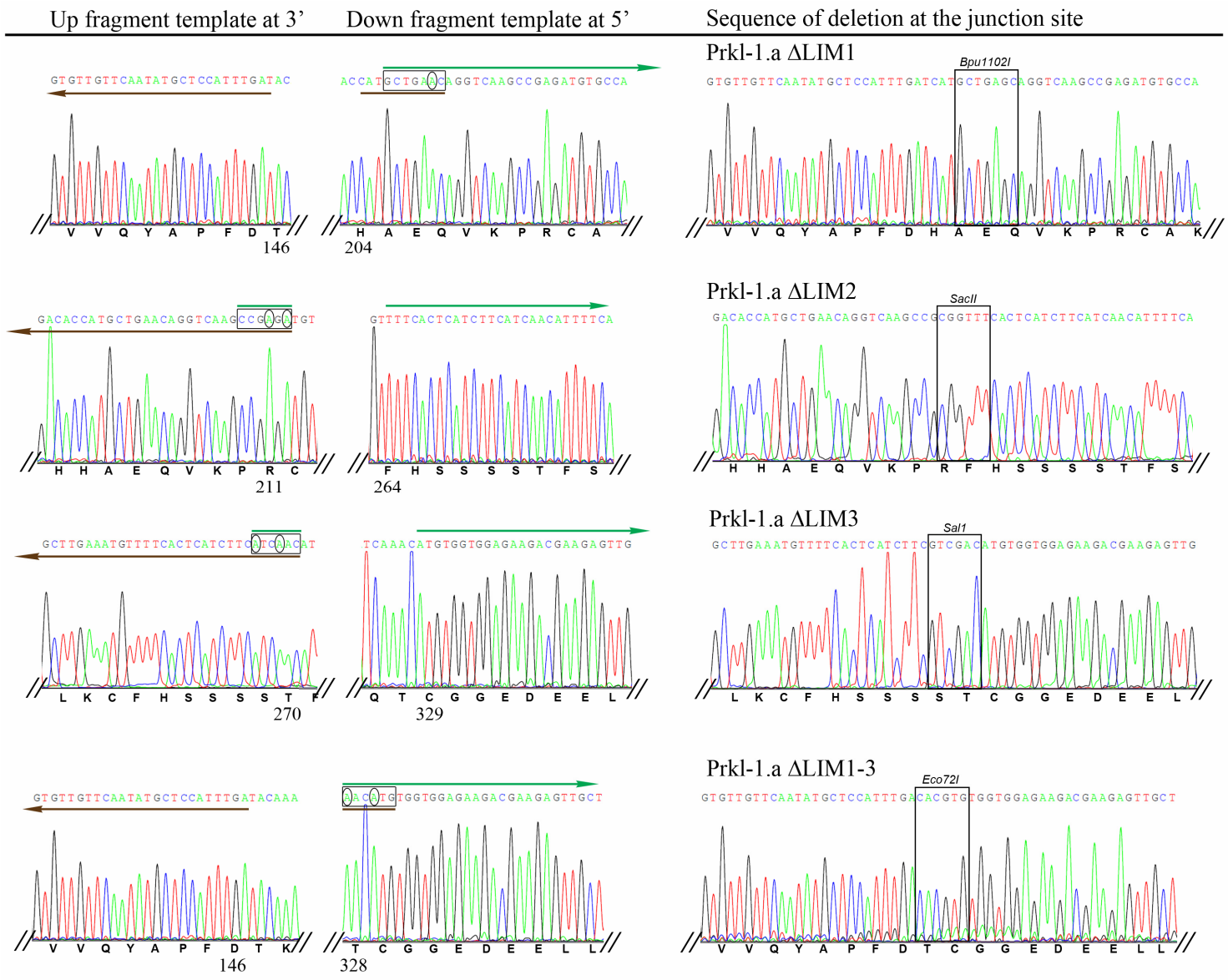
Up fragment template at 3'
Down fragment template at 5'
Sequence of deletion at the junction site
Prkl-1.a ΔLIM1
Bpu1102I
Prkl-1.a ΔLIM2
SacII
Prkl-1.a ΔLIM3
Sal1
Prkl-1.a ΔLIM1-3
Eco72I
146
204
211
264
270
329
146
328

Polyclonal antibodies to PRKL-1.

Although *gfp*-tagged gene expression has a good predictive value on protein localization; it may not exactly equal endogenous protein expression. Thus, immuno-histochemical staining with antibodies specific to PRKL-1, would reveal endogenous expression more accurately. To address this question we generated three peptide antibodies to PRKL-1 and one to full-length protein in rabbits (Supp. Figure III-5). Although the N-terminal and PET antibodies are capable of detecting full length PRKL-1 in ELISA format, they were not able to successfully immunostain endogenous *C. elegans* PRKL-1. In addition to the challenges of obtaining good immuno-histochemistry data in *C elegans* neurons, the finding that PRKL appears to be required and expressed at very low levels in VC4/5 neurons may have contributed to the lack of signal. Hence, immuno-purifying PRKL-1 antibodies might increase the chances of future success. These antibodies will then need to be optimized for staining and other uses.

Supplemental Figure III-5. Polyclonal antibodies to PRKL-1. A) Schematic representation of PRKL-1 protein and position of peptides used to raise rabbit polyclonal antibodies. Antibodies to the following peptide sequences were generated by Sigma, N-terminal: MSERIRRRRLEASEQFAPQLISSC, PET: RQRQSRYQLPPQDSDVC and C-terminal: IQNQRPKPPQRAPPC. B) ELISA results of bleed #3. Plates were coated with either 10 µg/mL of each peptide or full length recombinant PRKL-1. Goat antirabbit-HRP (BIORAD) was used as secondary antibody and soluble TMB, as substrate. To assess the specificity of the antibody and whether the antibody is capable of recognizing immobilized full length PRKL-1, a competitive assay was performed using 10 µg/ml peptide in solution with the serum dilution.

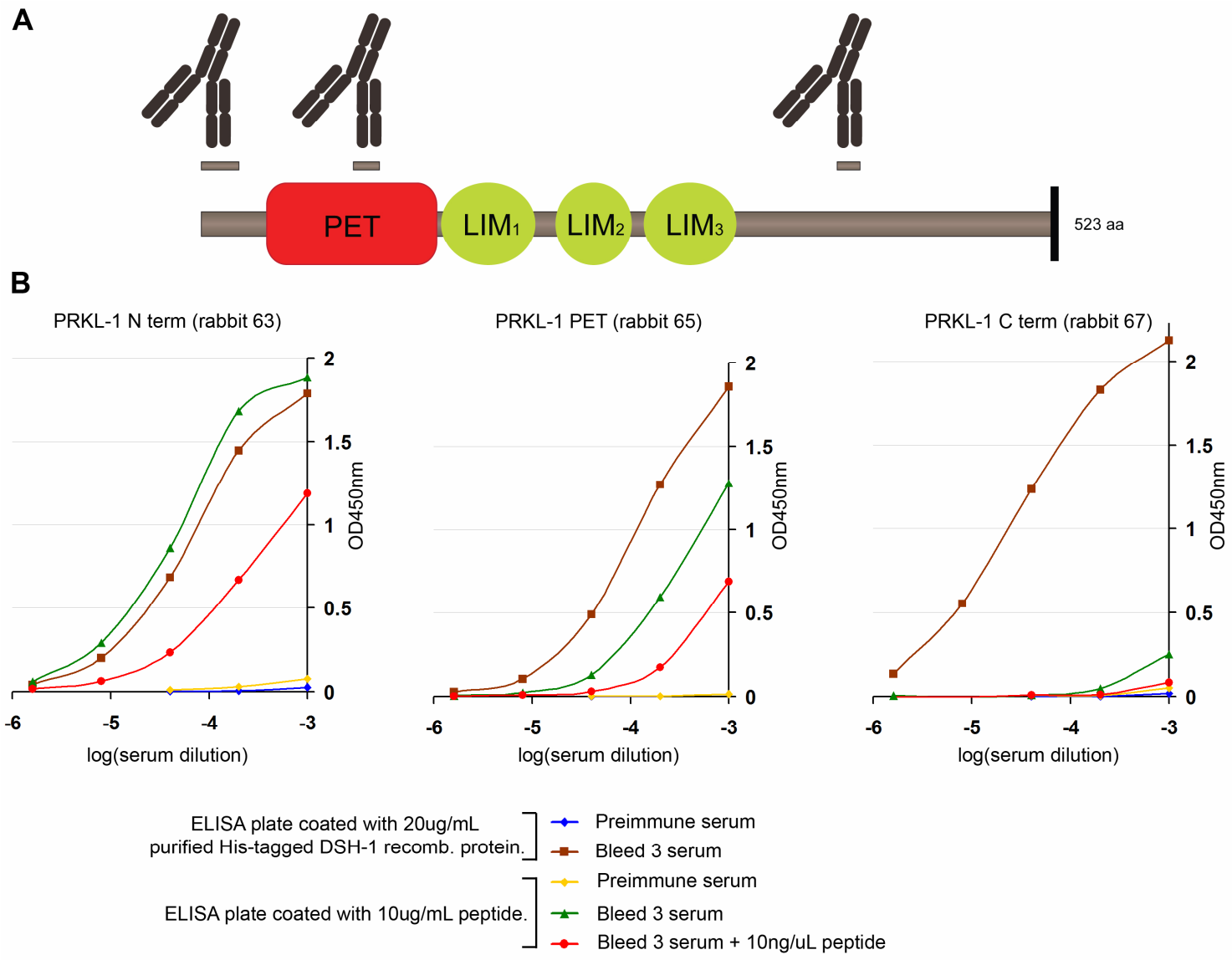
A
PET
LIM1
LIM2
LIM3
523 aa
B
PRKL-1 N term (rabbit 63)
PRKL-1 PET (rabbit 65)
PRKL-1 C term (rabbit 67)
OD450nm
log(serum dilution)
ELISA plate coated with 20ug/mL purified His-tagged DSH-1 recomb. protein.
Preimmune serum
Bleed 3 serum
ELISA plate coated with 10ug/mL peptide.
Preimmune serum
Bleed 3 serum
Bleed 3 serum + 10ng/uL peptide

CHAPTER IV

C. elegans dsh-1 is required cell autonomously in the neurons and cell non-autonomously in the epithelium to regulate neuronal polarity.

Preface

In Chapter II, we showed that *dsh-1* mutations resulted in VC4/5 ectopic AP axon growth, displayed as tripolar and bipolar AP morphologies. Specifically, *dsh-1* regulates the morphology of *C. elegans* VC4/5 motorneurons by suppressing ectopic AP axon growth and may also be involved in the formation of primary axons along the left/right axis created by the developing vulva. In addition, we showed that *dsh-1*, together with *prkl-1* and *vang-1,* is an essential component of a PCP-like pathway which polarizes VC4/5 motorneurons *in vivo*. To further learn how *dsh-1* regulates neuron polarity, in Chapter IV I focused on 1) studying the *dsh-1* gene expression profile, by examining transcriptional and translational GFP reporters; 2) assessing when and where *dsh-1* is required to suppress ectopic AP axon growth in VC4/5, by quantifying the phenotype at different developmental stages and performing cell specific rescue experiments; 3) studying the effects of *dsh-1* overexpression on VC4/5 morphology; and finally 4) assessing *dsh-1* function in PDEs, a pair of *C. elegans* dopaminergic neurons with a pseudo bipolar AP morphology.

ABSTRACT

dsh-1 genetically interacts with *prkl-1* and *vang-1* to prevent ectopic AP axons and promote ML axons in VC4/5 motorneurons. Here we show that the *dsh-1* promoter is transcriptionally active in VC motorneurons, vulva epithelium and vulva muscles at various developmental stages. In addition, *dsh-1* functions both cell autonomously in VC4/5 neurons and cell non-autonomously in the vulva epithelium, to establish and to maintain VC4/5 ML polarity. Also, we show that within VC4/5, DSH-1::GFP is expressed as puncta at the plasma membrane and smoothly in the cytosol. Notably, *dsh-1* overexpression in VC4/5 resulted in tripolar neurons similar to *dsh-1*, *prkl-1* and *vang-1* loss of function phenotypes (Chapter II), which contrasts with the unipolar phenotype resulting from *prkl-1* overexpression (Chapter III). Finally, I show that *dsh-1* does have the ability to regulate neuron polarity in other neurons besides VC4/5. For instance, both *dsh-1 lof* and *dsh-1* overexpression in PDE dopaminergic neurons result in lack of and/or premature termination of posterior axons, while extension of the ventral axon prior to bifurcation is unaffected, which suggests that *dsh-1* normally functions to regulate PDE posterior axons formation and/or extension to their wild type position near the anus. Altogether, these data indicate that *dsh-1* promotes axon outgrowth and extension along the AP axis in the PDE neurons which is opposed to its role in the VC4/5 neurons, where it functions to prevent axon growth along the AP axis; indicating that *dsh-1* role in neuron polarity is context-dependent.

INTRODUCTION

Dishevelled (DSH in *C. elegans*, XDSH in *Xenopus* and DVL in mammals) is a multifunctional protein required to transduce all branches of Wnt/Fz signalling, including the canonical Wnt/β-catenin pathway, and non canonical Wnt/Ca^{2+} and PCP pathways (Wallingford and Habas, 2005). In the canonical pathway, upon Wnt stimulation, DVL becomes activated and recruits/inhibits the axin scaffolding complex; thus blocking β catenin phosphorylation (Wallingford and Habas, 2005). This is followed by accumulation of unphosphorylated β catenin in the cytoplasm, which then migrates to the nucleus and regulates transcription via LEF/TCF transcription factors (Wallingford and Habas, 2005). In the absence of Wnt stimulation, phosphorylated β catenin is targeted for degradation through the proteasomal pathway (Aberle et al., 1997). β catenin signalling results in the expression of Wnt target genes which regulate cell fate decisions (Ciani and Salinas, 2005). In the Wnt/Ca^{2+} pathway, Wnt signalling through Fz, leads to DVL and G protein activation causing the release of intracellular Ca^{2+} and subsequent signalling via phospholipase C, CamKII and PKC (Kuhl et al., 2000). This pathway regulates developmental functions such as convergent extension during gastrulation, cell movements during heart development (Sheldahl et al., 2003) and axon pathfinding (Li et al., 2009). In the PCP pathway, DVL participates with a different core group of proteins, including PRKL, VANG, FMI and DGO to regulate/orient the cytoskeleton (Klein and Mlodzik, 2005). PCP signalling controls a wide spectrum of developmental functions, including the orthogonal polarity of cellular structures within the plane of the epithelium (Maung and Jenny, 2011), patterning of the *Drosophila* compound eye (Maung and Jenny, 2011), convergent extension during gastrulation (Darken et al., 2002; Wang et al.,

2006a), orientation of cochlear cells in the inner ear (Dabdoub et al., 2003), neural tube closure (Wang et al., 2006a) and neuron polarization (Sanchez-Alvarez et al., 2011).

Dishevelled is a modular protein containing three conserved domains, DIX (for dishevelled and axin), PDZ (for postsynaptic density 95, discs large, and zonula occludens 1), and DEP (for dishevelled, egl-10 and plekstrin) (Wharton 2003). In addition, DVL/DSH proteins share a conserved dsh motif, located before the PDZ domain. Each domain has been associated with different pathways. For instance, the DIX domain is required for the canonical pathway, while the DEP domain is required for the PCP and the Wnt/Ca^{2+} pathways. The PDZ domain, however, is required for both canonical and non canonical pathways. The PDZ domain functions as a switch between signalling cascades, in dependence of its binding partners (Wallingford and Habas, 2005). For example, the PDZ domain binds to VANG, PRKL, DGO, PAR1 and DAAM1 in the PCP pathway; whereas it associates with Frodo, Dapper, IDAX (inhibitor of Dishevelled and Axin), and GSK-3β in the canonical pathway (Wallingford and Habas, 2005).

Although individual Wnt/Fz pathways specialize in distinct developmental processes, there is some functional overlapping (Sheldahl et al., 2003). Not only do Wnt/Fz pathways share common upstream genes but also they intersect at basic downstream elements. For instance, DVL has been reported to display supracanonical activity as it regulates MT stability through GSK-3β, a component of the axin scaffolding complex, which branches away from the β catenin pathway (Krylova et al., 2000; Ciani et al., 2004). GSK-3β is a multitasking ser/thr kinase that not only phosphorylates to and inhibits β catening from signalling in the canonical pathway, but also regulates MT

stability (Doble and Woodgett, 2003). The later function is associated to its role in the establishment and maintenance of neuronal polarity in neuronal cell cultures, by phosphorylating and inactivating collapsin response mediator protein-2 (CRMP-2) (Jiang et al., 2005; Yoshimura et al., 2005). A closer link for DVL to the cytoskeleton appears to be its ability to bind to and relieve autoinhibition of formin protein DAAM1, which nucleates and stabilizes cytoskeleton polymerization, and is implicated in convergent extension movements during *Xenopus* gastrulation (Liu et al., 2008).

C. elegans DSH-1 is required to prevent AP axon growth and to promote ML axon formation in VC4/5 neurons (Chapter II). Double mutant analysis suggested that DSH-1 functions in a parallel pathway to PRKL-1;VANG-1 to regulate VC4/5 morphology. However, how and where *dsh-1* controls neuronal polarity *in vivo* remains unknown. Here, we show that DSH-1 functions both cell autonomously in VC4/5 neurons and cell non-autonomously in the vulva epithelium, to establish and maintain VC4/5 ML polarity. In addition, we find that a DSH-1::GFP genomic transgene is expressed as puncta at the plasma membrane and smoothly in the cytosol of VC4/5 neurons. Moreover, *dsh-1* overexpression in VC4/5 resulted in tripolar neurons similar to *dsh-1*, *prkl-1* and *vang-1 lof* phenotypes, contrasting with the unipolar phenotype caused by *prkl-1* overexpression (Chapter III). Furthermore, both *dsh-1* overexpression and *dsh-1 lof* result in lack of and premature termination of posterior axons in the AP-oriented PDE dopaminergic neurons. Altogether, our data suggests that DSH-1 regulates morphology/polarity of AP-oriented neurons in a context-dependent manner.

MATERIALS AND METHODS

***C. elegans* strains.** Worms were cultured by standard methods (Brenner, 1974). All strains were maintained with OP50 *E. coli* on nematode growth medium (NMG) at 20°C, unless otherwise specified. Some nematode strains used in this work were provided by CGC, which is funded by the NIH National Center for Research Resources (NCRR).

Wild type strains: N2/Bristol and *cyIs3* and *cyIs4* reporter.

Mutant strains: RB1328 [*dsh-1(ok1445)*II, a 1132bp deletion] and [*dsh-1(zy12)*,Q64Stop]

cDNA EST clones. *yk291a11 (dsh-1.c,* isoform C*)* and *yk1082g05 (dsh-1.b,* isoform B*)* were gifts from Dr. Yuji Kohara (National Institute of Genetics, Mishima, Japan).

Transcriptional reporter. A 4.3kb genomic region, upstream of *Dsh-1*, was PCR-amplified using primers 5'cctGTCGACgatcaatcgtggagcacatc3' and 5'ctGGATCCgtttggagcatttaatgacg3' and then inserted into *Sal1*/*BamH1* sites pPD95.77 vector to generate *Pdsh-1::gfp*. Correctness of the constructs was verified by restriction digest and sequencing. The construct was injected at 10 ng/µL with 40 ng/µL of *pRF4(rol-6(su11006)* which cause a roller phenotype for visual identification and 15 ng/µL *Plin-11::rfp* to label VC1-6, as co-transformation markers into wild type worms to generate [*Pdsh-1::GFP; Plin-11::RFP]* transgenes.

Cell-specific expression. Full length *dsh-1.c* cDNA was PCR-amplified using *yk291a11* as template and primers 5'tatCTGCAGatggccgagtctccacctcc3' and 5'ctacatCCCGGGacatactcgtatctttgtcc3', and then inserted into *PstI*/*SmaI* sites of

pPD95.77 vector to generate *dsh-1.c::gfp*. Cell-specific promoters *Punc-4*, *Pcat-1*, *Pcol-10* were PCR-amplified (primer sequences below) from *C. elegans* genomic DNA and inserted upstream of *dsh-1.c::gfp* to generate *Punc-4::dsh-1.c::gfp*, *Pcat-1::dsh-1.c::gfp*, and *Pcol-10::dsh-1.c::gfp*, respectively. Correctness of the constructs was verified by restriction digest and sequencing. All constructs were injected at 10 ng/µL with 40 ng/µL of *Podr-1::dsRed* into *dsh-1(zy12); cyIs4* and/or deletion allele *dsh-1(ok1445); cyIs4* mutant background to generate the following transgenes: *[Punc-4:: dsh-1.c::gfp]*, *[Pcat-1::dsh-1.c::gfp]*, *[Pcol-10::dsh-1.c::gfp]*. All experiments were performed using at least two independent transgenic lines per construct. Primers to amplify cell-specific promoters are as follows:

Punc-4*:: dsh-1.c::gfp*

forward, *Pst1*: 5'ctatCTGCAGccacctctgtcttcaaggcgacctacac3'

reverse, *Pst1*: 5'ttacCTGCAGgatatctttcacttttggaagaagaagatcctc3'

Pcat-1*:: dsh-1.c::gfp*

forward, *Pst1*: 5'tatCTGCAGcaaggctctgcagggtacctatg3'

reverse, *Pst1*: 5'ccgCTGCAGctgatccaatcaagaatgtacgac3'

Pcol-10*:: dsh-1.c::gfp*

forward, *HindIII*: 5'gtacAAGCTTgtcgactctagaactagtggatc3'

reverse, *Pst1*: 5'ctaaCTGCAGaccttattcagtgttacccttcc3'

For overexpression experiments and to examine DSH-1 protein localization in VC4/5 and *Punc-4:: dsh-1.c::gfp* was injected at 50 ng/µL in N2 strain and at 10 ng/µL in *dsh-1(ok1445)* mutants, respectively.

Scoring lamellipodial protrusions during L3 stage. We used the *cyIs3* reporter to visualize the morphology of VC4/5 during L3 stage. The orientation of lamellipodial protrusions was determined from ApotomeII/Axiocam paired Fluorescence-DIC images at 1-cell, 2-cell and 4-cell stages of P6.p VPC. Anteriorly-directed VC4 protrusions and posteriorly-directed VC5 protrusions were scored as "away from VPC".

Scoring the posterior axon of PDE neurons. The PDE motorneurons were visualized with the *cyIs4* reporter. PDE posterior axon was examined and scored for length defects in transgenic lines overexpressing *[Pcat-1::dsh-1::gfp]*, using the anus as anatomic hallmark. The data was grouped into two categories: 1) no posterior axons and 2) axons with ½ the length of wt axons.

RESULTS

The deletion allele *dsh-1(ok1445)* encodes a truncated protein lacking the *dsh* conserved motif.

The core PCP gene homologue *dsh-1* is encoded on the minus strand of chromosome II in the *C. elegans* genome. The gene *dsh-1* is located at genetic position -1.93 +/- 0.028 cM spanning from genomic position 5225361 to 5214430 bp (from atg to 3'UTR) (Wormbase). The *dsh-1* locus is predicted to produce three isoforms, by the protein predictor software featured at Wormbase. Sequence analysis of EST *C. elegans* clones *yk291a11* and *yk1082g05* confirmed the existence of two of *dsh-1* mRNAs, corresponding to isoforms c and b, respectively. The transcript *dsh-1.c* encodes the longest isoform, 702 aa. These ESTs provide information on gene expression profile, but they can't predict whether the proteins are actually synthesized and in which cells, and if they are relevant to the phenotype.

To gain insight into how *dsh-1* regulates neuron orientation/polarity we first aimed at correlating molecular lesions in *dsh-1* alleles to their polarity phenotype. There are two available *dsh-1* deletion alleles, *or301* and *ok1445*. The allele *or301*, a predicted null reported to delete 1594 kb genomic region including exons 7 and 8 entirely, which would remove part of the dsh conserved domain and most of the PDZ. This allele exists in a balanced strain NG3190 [*dsh-1(or301)/mIn1[dpy-10(e128) mIs14*]II, as it generates an embryonic lethal phenotype, which is suggestive of how important *dsh-1* is for multiple functions during embryonic development. Unfortunately, we were not able to genotype it successfully and confirm *or301* deletion. Thus, we began by sequencing of the *dsh-*

1(ok1445) allele. We found that the *ok1445* mutation deletes 1132 kb of *dsh-1* genomic sequence including the first 19 nucleotides of exon 6, which encodes part of the *dsh* conserved motif that is found in all DSH proteins. This deletion affects all three isoforms (see Figure IV-1). RTPCR-sequencing of *dsh-1.c* cDNA from *dsh-1(ok1445)* mutant, predicts a truncated protein with 227 residues (Figure IV-1). Thus, in the lack of the 6th exon's splice acceptor an alternative downstream acceptor is used. Consequently, the transcript is out-of-frame, resulting in premature termination of translation, with the addition of an extraneous polypeptide C-terminal tail of 44 residues. Thus, conceptual translation revealed a truncated protein lacking about 4/6th of the wild type full length sequence, including the entire second half with the PDZ and DEP domains. This premature termination leaves intact the conserved DIX domain and a fragment of the *dsh* conserved motif. The DEP domain is known to confer DVL/DSH with membrane targeting properties, which is critical to PCP in various tissues (Wong et al., 2000;Wang et al., 2006a). The PDZ domain forms a hydrophobic cleft important for protein-protein interactions, which has been shown to bind Fz (Wong et al., 2003). In addition, both the PDZ and the DEP domains have been shown to be critical for the PCP pathway in various tissues (Axelrod et al., 1998;Wallingford et al., 2000). Accordingly, *dsh-1(ok1445)* is likely a strong loss of function or a phenotypic null for this neuronal PCP pathway.

Finally, sequencing of the allele *dsh-1(zy12),* obtained in our laboratory from a forward genetic screen (J. Imai, unpublished data), revealed a Q64Stop which would affect longer isoforms A and C, but not B. The *zy12* allele displays a strong polarity phenotype, quantitatively similar to *dsh-1(ok1445)*. The latter suggests that one or both of these two isoforms are critical to prevent AP axon growth in VC4/5 neurons. Because

DSH-1.C contains a longer non-consensus C-terminal than DSH-1.A, a segment of which is unique to isoform C, we characterized isoform C for the remaining of the Chapter so that we wouldn't miss any function associated with it, if any.

<u>Figure IV-1.</u> Primary structures of wild type DSH-1 and deletion allele *ok1445*. A) Schematic representation of the *Dsh-1* isoforms A, B and C. Deletion in *ok1445* affects all three isoforms, and premature stop codon in *zy12* affects isoforms A and C. **B)** DSH-1.C amino acid sequence in wt and *dsh-1(ok1445)* mutant. *ok1445* deletion terminates DSH-1 protein prematurely and adds an extraneous tail of 44 residues (blue font).

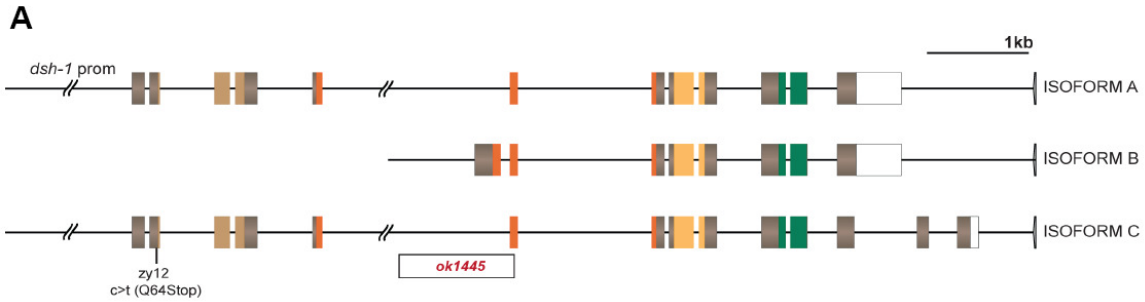

B

Wild type DSH-1.C, (D I X)-(D S H)-(P D Z)-(D E P)

M A E S P P P V D S S L N A P N V G S P T T M M E R L R L R D Q T E
E N G K E D D F D N K S V S S A Q Y S Q T S E A T T A V K Q Q P F L
H T M T K V Y C H I D D E T D P Y M L E V H V P P D L I T L G D L K
R V L M R T N F K Y Y R K A L D P D S G Y E V K A E I R D D S Q R L
T P S P N N L F E L F L L T I E G S T H S D G S S G K M R K Y P S V
P G P A P S N R N G P P M N Y Q H A A Y Q F D N S M M S T D S E S M
I S A A I P G Y L K S A A Y N R R F P Q H Y L G H R R H L E E S T I
G S E S D A R V F S D D D D R G S T T T D F T S V S R Q H E K M A K
K K K N K R N F R K P S R A S S F S S I T E S S M S L D V I T V N L
N M D T V N F L G I S I V G Q T S N C G D N G I Y V A N I M K G G A
V A L D G R I E A G D M I L Q V N E T S F E N F T N D Q A V D V L R
E A V S R R G P I K L T V A K S F E N G Q S C F T I P R N S R E E P
V R P I D T Q A W I Q H T N A M R G M P S I V E E S A P T P I P G E
W P H G R P P S S S T V T S N G S N G Q N T V V G G G A H I I L D I
H T D K K K V V E I M A M P G S G L D I K N R T W L K I P I P M S F
L G S D L V E W L L D H V E G L R E R K T A R N F A A D L L K L K Y
I A H V V N K V T F T E Q C Y Y V L G D E C S D Y A R F R N E D G G
P K Y Q W T I G M N G M S A G N G S S V M L P P P H L P G G M A G P
P G A F K G M A P S M V S G Y A S M P A S P F P P A Q L Q Q Q R S E
G S T T S G S S G G G I R K Q R V V V L P R K P S S S A N V P F D D
S S T I Y E E S N N S F L M A T G Q R Y E Y

DSH-1 OK1445

M A E S P P P V D S S L N A P N V G S P T T M M E R L R L R D Q T E
E N G K E D D F D N K S V S S A Q Y S Q T S E A T T A V K Q Q P F L
H T M T K V Y C H I D D E T D P Y M L E V H V P P D L I T L G D L K
R V L M R T N F K Y Y R K A L D P D S G Y E V K A E I R D D S Q R L
T P S P N N L F E L F L L T I E G S T H S D G S S G K M R K Y P S V
P G P A P S N R N G P P M N Y Q H A A Y Q F D N S M M S T D S E S M
I S A A I P G Y L K S A A Y N R R F P Q H Y L E A L Q Q P I S H Q Y
P D N M K K W Q R K R R I K E I S E N P L E H L R F Q V S Q S P L

DSH-1 establishes and maintains VC4/5 morphology by preventing ectopic AP axon growth.

To gain insight into when *dsh-1* is required to polarize VC4/5 neurons, we compared the progression of VC4/5 morphology in wild type and *dsh-1(ok1445)* nematodes, from the first signs of polarization (lamellipodial protrusions) to the bipolar ML or tripolar axons in adult stage (Figure IV-2). Interestingly, during early L3 stage, prior to axonogenesis, VC4/5 neurons display anterior and posterior protrusions in both *dsh-1* mutants and wt nematodes. However, by late L3 stage (4-cell) while the anteriorly-directed protrusion in wt VC4 and posteriorly-directed protrusion in wt VC5 have largely dissolved or reoriented towards the vulva, in *dsh-1* nematodes these away-from-vulva directed protrusions are consolidated in significant proportions, rendering VC4/5 neurons responsive to AP polarizing cues (Figure IV-2B & D left). This early defective polarity phenotype suggests that *dsh-1* plays a role in the establishment of VC4/5 polarity by dissolving, reorienting or retracting the away-from-vulva directed protrusions (Figure IV-2B & D left). The significant difference in the morphology of *dsh-1 vs* wt neurons is also clear with from the first signs of axon formation, as the persistent away-from-vulva protrusions develop into AP axons by L3-L4 molt to early L4. Thus, ectopic AP axons and primary ML axons develop simultaneously (Figure IV-2B), further signifying that *dsh-1* plays an early role in establishing VC4/5 polarity. Moreover, the percentage of neurons with AP directed axons significantly increases with developmental age (Figure IV-2D right). For instance, the percentage of VC4 with anterior axons increases from ~ 40 % in early L4 to ~ 74 % in adult *dsh-1(ok1445)* nematodes and the percentage of VC5 with posterior axons increases from ~ 40 % in early L4 to ~ 65 % in adult *dsh-1(ok1445)*

nematodes (Figure IV-2D right). These data suggests a later role for *dsh-1* in maintaining VC4/5 morphology, by continuously preventing AP axon growth.

Figure IV-2. VC4/5 polarity defective phenotype in *dsh-1* mutants starts early and increases with developmental age. A) Ventral view schematic representation depicting VC4, VC5 and vulva development from stage L3 to Adulthood. **B)** Representative fluorescent images of wild type VC4 (top) morphology displaying unidirectional posterior protrusions, and *dsh-1(ok1445)* VC4 (bottom) displaying bidirectional anterior-posterior protrusions at 4-cell stage. **C)** Confocal images of VC4/5 neurons displaying AP axons at different stages. Ectopic AP axons grow simultaneously with ML primary axons. **D)** VC4/5 polarity defects in *dsh-1* mutants begin early in development and get worse with developmental age. **Left)** Quantification of VC4 (top) and VC5 (bottom) neurons displaying lamellipodial protrusions away from the vulva at 1-cell, 2-cell and 4-cell L3 stages. Error bars represent SEP, *$p<0.05$, Fisher's Exact test. **Right)** Quantification of VC4 anterior axons (top) and VC5 posterior axons (bottom), in *prkl-1(zy11)* from early L4 to adult. Error bars represent SEM, **$p<0.01$.

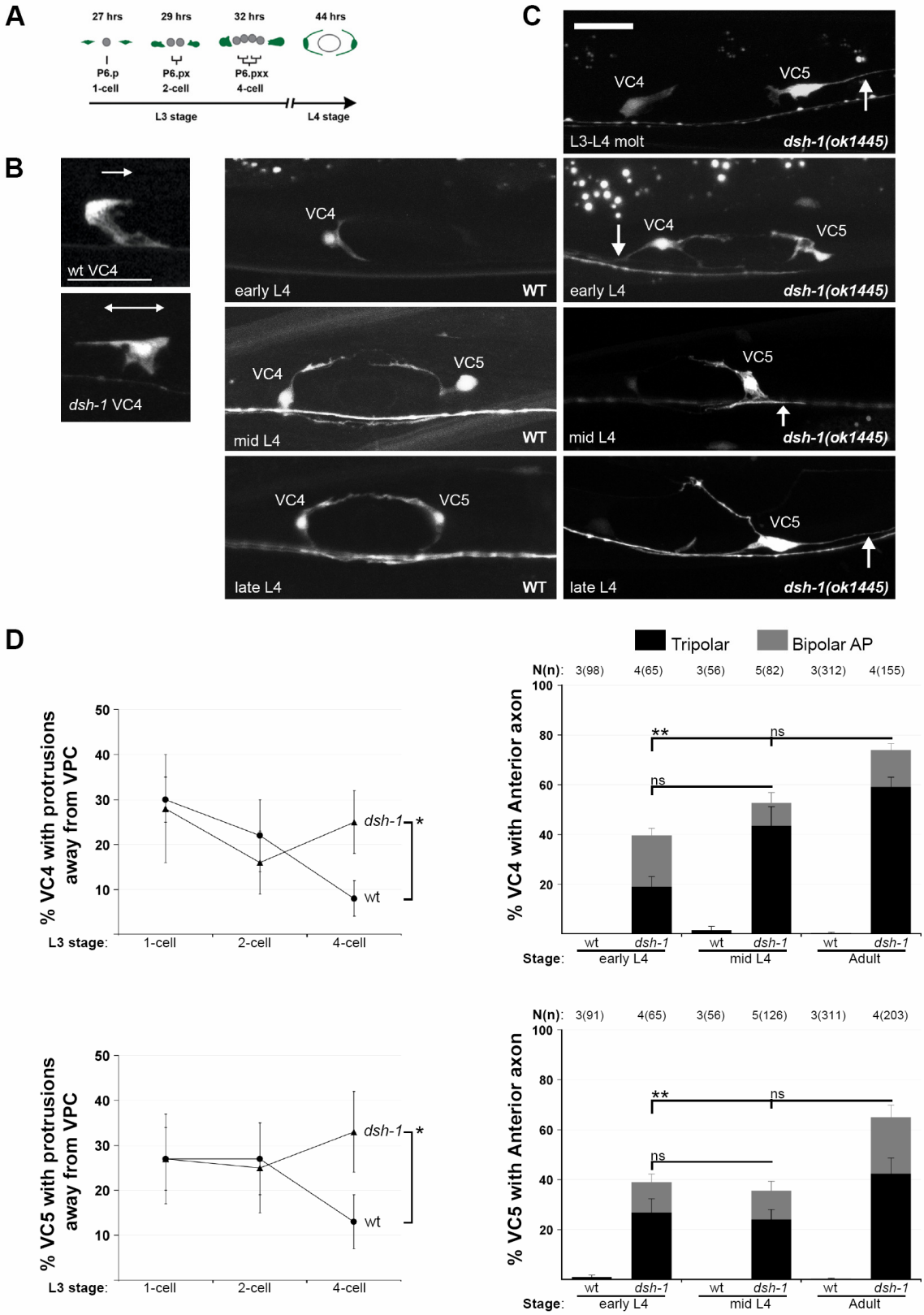
A
27 hrs
29 hrs
32 hrs
44 hrs
P6.p
1-cell
P6.px
2-cell
P6.pxx
4-cell
L3 stage
L4 stage
B
wt VC4
dsh-1 VC4
C
VC4
VC5
L3-L4 molt
dsh-1(ok1445)
early L4
WT
mid L4
late L4
D
% VC4 with protrusions away from VPC
% VC5 with protrusions away from VPC
L3 stage:
1-cell
2-cell
4-cell
dsh-1
wt
Tripolar
Bipolar AP
% VC4 with Anterior axon
% VC5 with Anterior axon
N(n):
3(98)
4(65)
3(56)
5(82)
3(312)
4(155)
3(91)
4(65)
3(56)
5(126)
3(311)
4(203)
**
ns
Stage:
early L4
mid L4
Adult

The *dsh-1* promoter is active in VC4 and VC5, vulva epithelia and muscles, ventral nerve cord and pharynx

To further understand when and where *dsh-1* is required to regulate VC4/5 bipolar ML orientation, we studied *dsh-1* transcriptional regulation by generating transgenic lines which express GFP from the *dsh-1* promoter. Thus, a genomic region comprising 4.3 kb upstream of *Dsh-1.c* ATG was fused in frame to gfp at exon 1, and the resulting construct was co-injected with pRF4 [*rol-6(su1006)*] as a transformation marker and/or [*Plin-11::rfp*] as a VC1-6 reporter (see Methods).

Interestingly, the *dsh-1* reporter construct is widely expressed in *C. elegans* nervous system (Figure IV-3A) including many neurons in the VNC such as VC4 and VC5, commissures, nerve ring neurons, and other neurons in the head and tail. It is also expressed in the egg-laying muscles, vulva epithelia and pharynx. *Pdsh-1,* similarly to *Pvang-1,* displays a broad expression pattern in the nervous system especially in the VNC (Sanchez-Alvarez et al., 2011), precluding the identification of individual VC neurons by morphology. Hence, transgenic lines co-expressing of *Pdsh-1::gfp* and *Plin-11::rfp* were obtained. These reporter strains clearly revealed *Pdsh-1* activity in vulval distal VC neurons, as well as in vulva epithelial cells.

Figure IV-3. ***dsh-1*** **promoter is widely expressed in neurons, epithelia and muscles at different developmental stages. A)** Schematic representation of *dsh-1* transcriptional reporter used in this study. **B)** Representative whole body fluorescent image (constructed from individual panels) of an adult worm carrying extrachromosomal array [*Pdsh-1::gfp; rol-6(su1006)*]. Arrows indicate expression in pharynx, VC4 motorneuron and ventral nerve cord. **C)** Representative images of the vulva region in transgenic worms at early, mid and late L4 stages. Arrows indicate expression in VC4, VC5, and vulva epithelium and muscle. **D)** VC1-6 and vulva cell reporter *Plin-11::rfp* was used to unmistakably identify VC neurons within the ventral cord. Representative photographs of a single worm's vulva area at mid L4 stage. Merged image (bottom) composed of green channel *Pdsh-1::gfp* reporter) and red channel (*Plin-11::rfp* reporter) identified expression in VC3-6 (yellow cells). Scale bars, 20 μm. Published in (Sanchez-Alvarez et al., 2011).

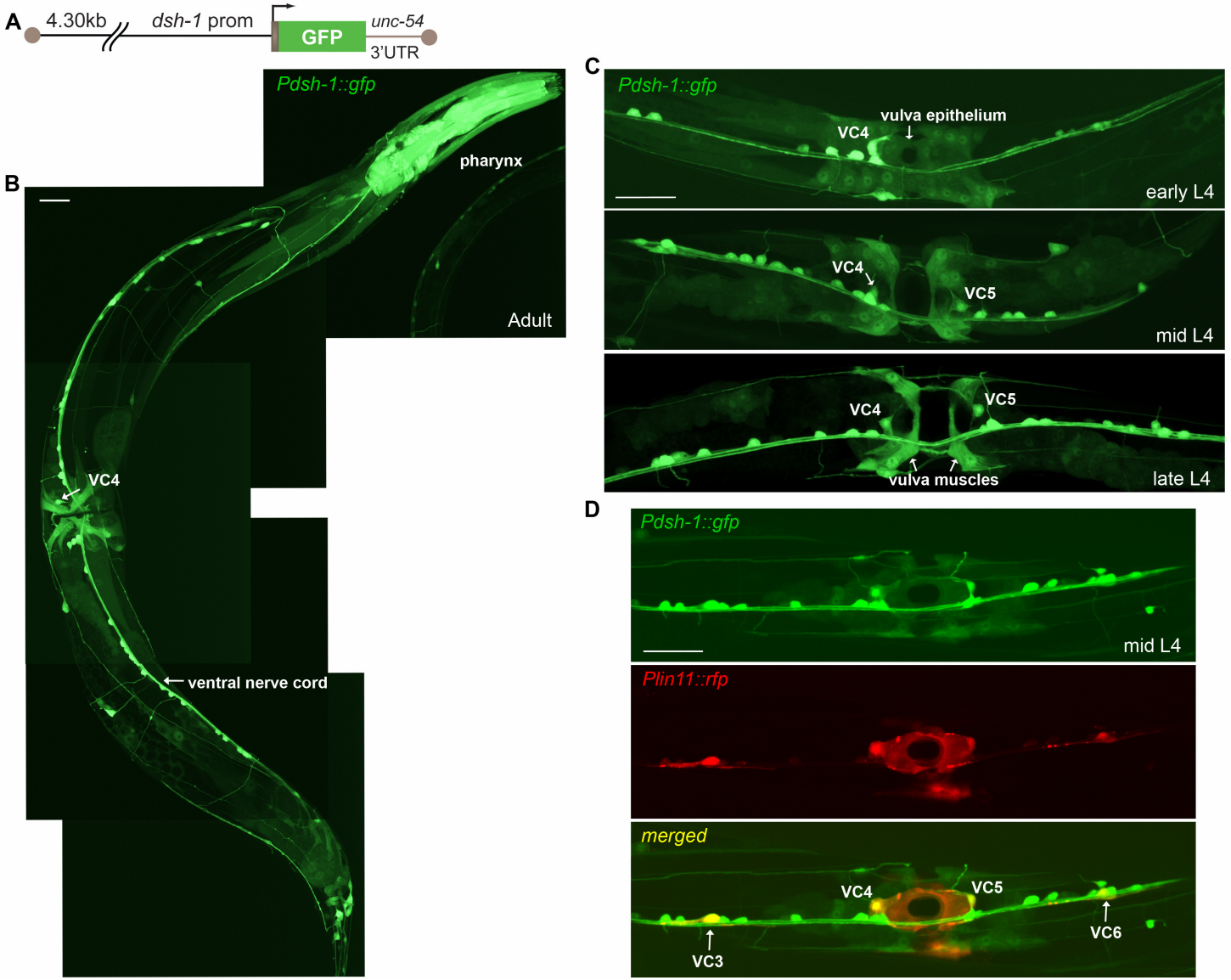
A
4.30kb
dsh-1 prom
GFP
unc-54
3'UTR
B
Pdsh-1::gfp
pharynx
Adult
VC4
ventral nerve cord
C
Pdsh-1::gfp
vulva epithelium
VC4
early L4
VC4
VC5
mid L4
VC4
VC5
vulva muscles
late L4
D
Pdsh-1::gfp
mid L4
Plin11::rfp
merged
VC4
VC5
VC6
VC3

DSH-1 functions cell autonomously and non-autonomously to halt AP neurite formation in VC4 and VC5.

Based on *dsh-1* transcriptional activity, we considered whether *dsh-1* was required cell autonomously in the neurons and/or cell non-autonomously in the surrounding epithelium to regulate VC4/5 polarity. To further understand where *dsh-1* is acting to prevent AP axon growth in VC4/5 we performed cell rescue experiments.

First, I injected a construct expressing DSH-1::GFP from the *Punc-4* [*Punc-4::dsh-1.c::gfp*] at 10 ng/µl and 30 ng/µl together with 30 ng/µl [*Podr-1::rfp*] into *dsh-2(zy12)* mutants and obtained four transgenic lines, three and one, respectively. The *unc-4* gene is expressed in the A-type motor neurons, DA and VA, the six VC motor neurons that innervate the vulval muscles, and the three SAB motor neurons (Lickteig et al., 2001). Notably, all the extrachromosomal arrays rescued the defects partially but significantly. While *dsh-1(zy12)* displays 73.7 % VC4/5 neurons with AP axons, transgenic strains injected with 10 ng/µl of *Punc-4* [*Punc-4::dsh-1.c::gfp*], display 36.2 to 42.9 % of defective neurons (Figure IV-4). Interestingly, the line harbouring a higher concentration of the construct (30 ng/µl) did not show an improved rescue, with 34.9 % VC4/5 neurons displaying AP axons; comparable to the numbers achieved at 10 ng/µl. The latter may imply that the rescuing ability of *Punc-4::dsh-1.c::gfp* has reached a plateau. Consistently, VC4/5 polarity defects in worms carrying the deletion allele *dsh-1(ok1445)* were rescued by 10 ng/µl *Pcat-1::dsh-1.c::gfp*, an array that is specifically expressed in dopaminergic neurons including VC4 and VC5. Three transgenic lines resulted in comparable rescue, with 31.3 to 35.7 % VC4/5 neurons displaying AP axons *vs* 68.7 % in

non transgenic *dsh-1(ok1445)*. These data suggest that *dsh-1* is acting cell autonomously in VC4/5 neurons to prevent AP axon growth. However, the partial rescue may be interpreted as 1) the gfp is somehow affecting the full activity of the protein, and/or 2) there is another component to *dsh-1* function (*i.e.* a cell non-autonomous role), and/or 3) the transgenic arrays are overexpressing *dsh-1* which could result in a *lof*-like phenotype. The first possibility is unlikely because the GFP-tagged *dsh-1* genomic array achieved close to full rescue of defects (Chapter II). Hence, to investigate a potential cell non-autonomous component we used *Pcol-10* to drive the expression of *dsh-1.c* cDNA in epithelial cells including the vulva and quantified VC4/5 phenotype. Notably, transgenic lines expressing *dsh-1.c* from the *col-10* promoter displayed the strongest rescue of polarity defects, with 18.7 – 20.9 % VC4/5 displaying AP axons *vs* 68.7 % in *dsh-1(ok1445)* (Figure IV-4), comparable to genomic *dsh-1* transgene (13.4 – 17.2 %) (Chapter II). These data suggest that *dsh-1* also functions cell non-autonomously in the epithelium to prevent AP axon growth. The finding that *Dsh-1* is also required from outside the neurons may explain why the rescue of VC4/5 polarity defects with *Punc-4* and *Pcat-1* driven *dsh-1.c* expression array was only partial.

Figure IV-4. ***dsh-1*** **functions cell autonomously in VC4/5 motorneurons and non-cell autonomously from epithelial cells to inhibit ectopic AP neurite growth.** A) Quantification of VC4/5 polarity defects in transgenic lines carrying cell-specific rescuing constructs *vs* control. B) Representative confocal image of a *dsh-1(ok1445)* VC4/5 polarity defective nematode rescued by [*Pcol-10::dsh-1.c::gfp*] transgene. White asterisks indicate DSH::GFP expression. All error bars represent s.e.m., ***P<0.001. Published in (Sanchez-Alvarez et al., 2011).

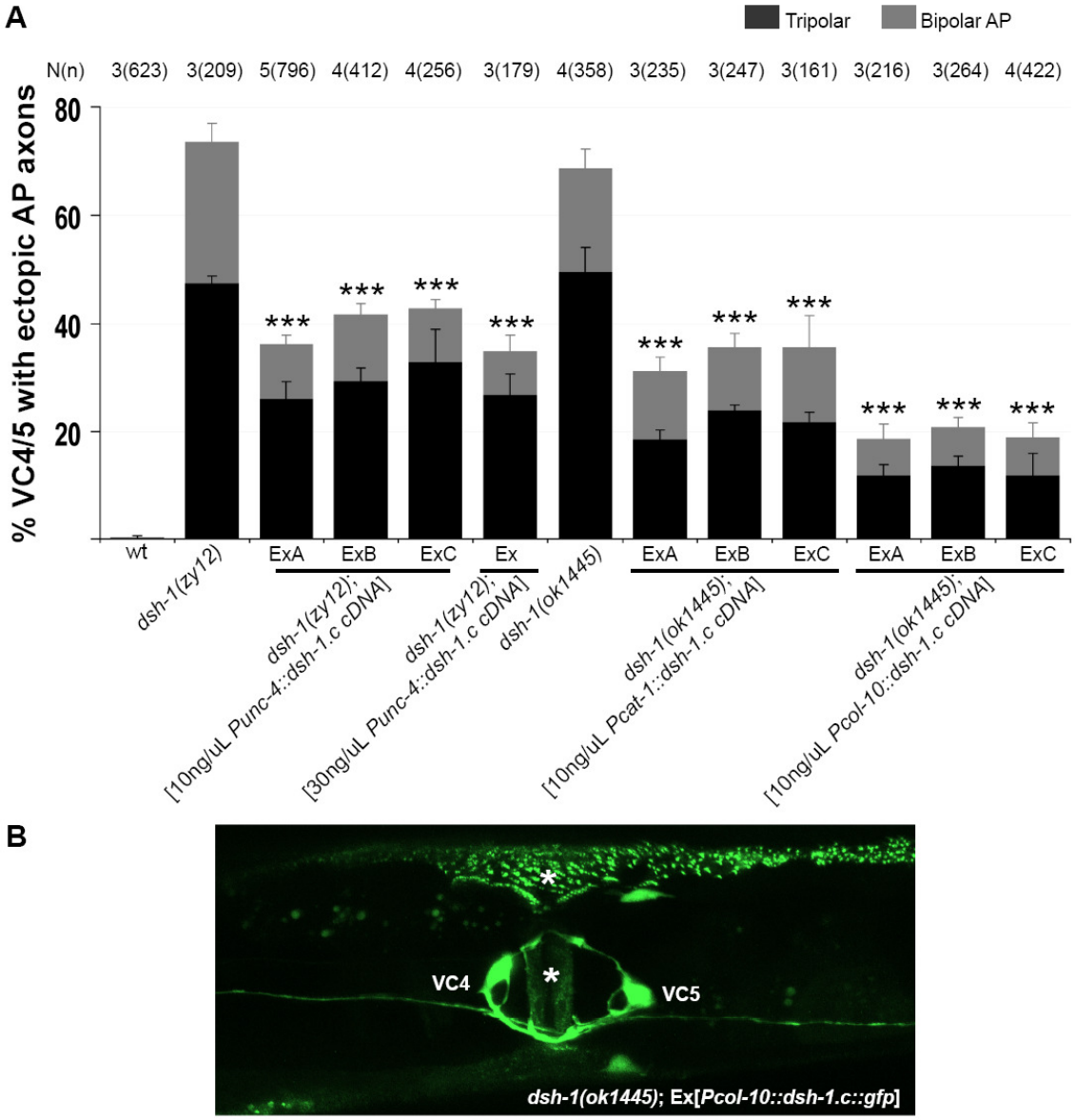

DSH-1 is expressed in VNC neurons and in the vulva area. DSH-1 is localized in puncta at the plasma membrane of VC4/5 neurons and uniformly in the cytosol.

The *dsh-1* promoter is transcriptionally active in VNC motorneurons, including the VCs and also in the vulva epithelia and muscles. We then asked whether a DSH-1::GFP expressing genomic construct, containing *dsh-1* regulatory regions, would reveal a similar expression pattern. In addition, since cell-rescue experiments indicated that *dsh-1* is acting in VC4/5 neurons and epithelia we were interested in using the DSH-1 genomic transgene, to obtain information on DSH-1 subcellular localization in VC4/5 and epithelia. Consistent with the *dsh-1* transcriptional reporter, DSH-1::GFP was expressed broadly in the nervous system including VNC neurons and tail neurons; it was also expressed in the vulva area including the vulva muscles (Figure IV-5A-E). Unfortunately, without the use of cell/tissue specific reporters it was not possible to individually identify neurons and vulva cells with GFP expression. Moreover, at 10 ng/µl, concentration that effectively rescues VC4/5 polarity defects, the intensity of GFP was not enough to obtain a detailed assessment of DSH-1 intracellular distribution. However, DSH-1 appeared consistently expressed in the cytoplasm while excluded from nuclei (Figure IV-5A-E). To further assess DSH-1 localization in VC4/5 we used a rescuing transgene, [*Punc-4::dsh-1.c::gfp*]. Interestingly, in the neuronal soma, DSH-1 appeared expressed at the plasma membrane in a punctate pattern, similar to GPP::PRKL-1 (Chapter III), which is suggestive of submembranous polarity complexes (Figure IV-5F-K). Consistent with the DSH-1 expressing genomic construct, DSH-1 was evenly expressed in the cytosol, while excluded from the nuclei (Figure IV-5F-K). We did not find evidence for asymmetric distribution. Moreover, DSH-1::GFP was also expressed copiously in the axons and

branches (n>100 L4 - adults) (Figure IV-5F-K). Although these data were obtained with DSH-1 expressing extrachromosomal arrays at rescuing concentrations, we considered whether the results might differ from endogenous DSH-1 localization; a concern to be addressed with good immunochemistry data.

Figure IV-5. Localization of DSH-1::GFP. A-E) Confocal images of DSH-1::GFP expressed from a genomic transgenic array. DSH-1 is expressed in VNC and tail neurons and also in the vulva area, including vulva muscles. On top, schematic representation of DSH-1::GFP genomic transgene. **F-K)** Confocal images of DSH-1::GFP expressed from a [*Punc-4::dsh-1.c::gfp*] transgenic construct. DSH-1::GFP is expressed in the cytoplasm of VC neurons and at the plasma membrane in a punctuate pattern. It is also heavily expressed in VC4/5 axons and branches. On top, schematic representation of [*Punc-4::dsh-1.c::gfp*] transgene. White stars indicate puncta in DSH-1::GFP expressing axons. Scale bar, 10 µm.

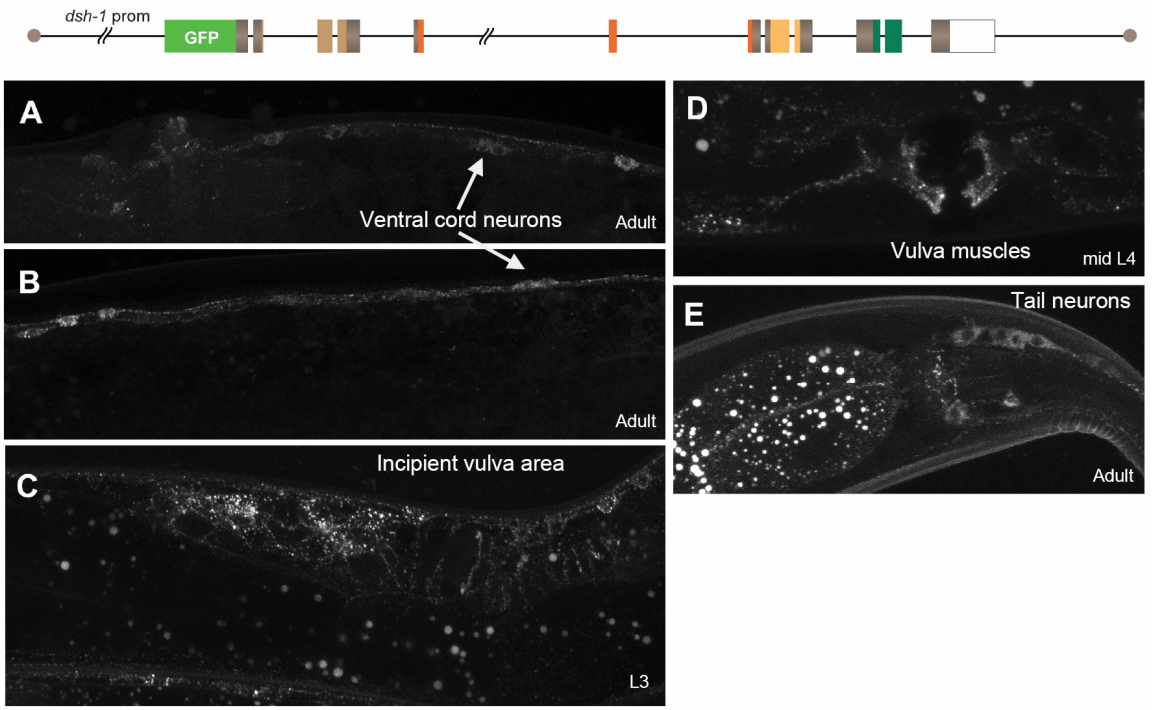
dsh-1 prom
GFP
A
Ventral cord neurons
Adult
B
Adult
C
Incipient vulva area
L3
D
Vulva muscles
mid L4
E
Tail neurons
Adult

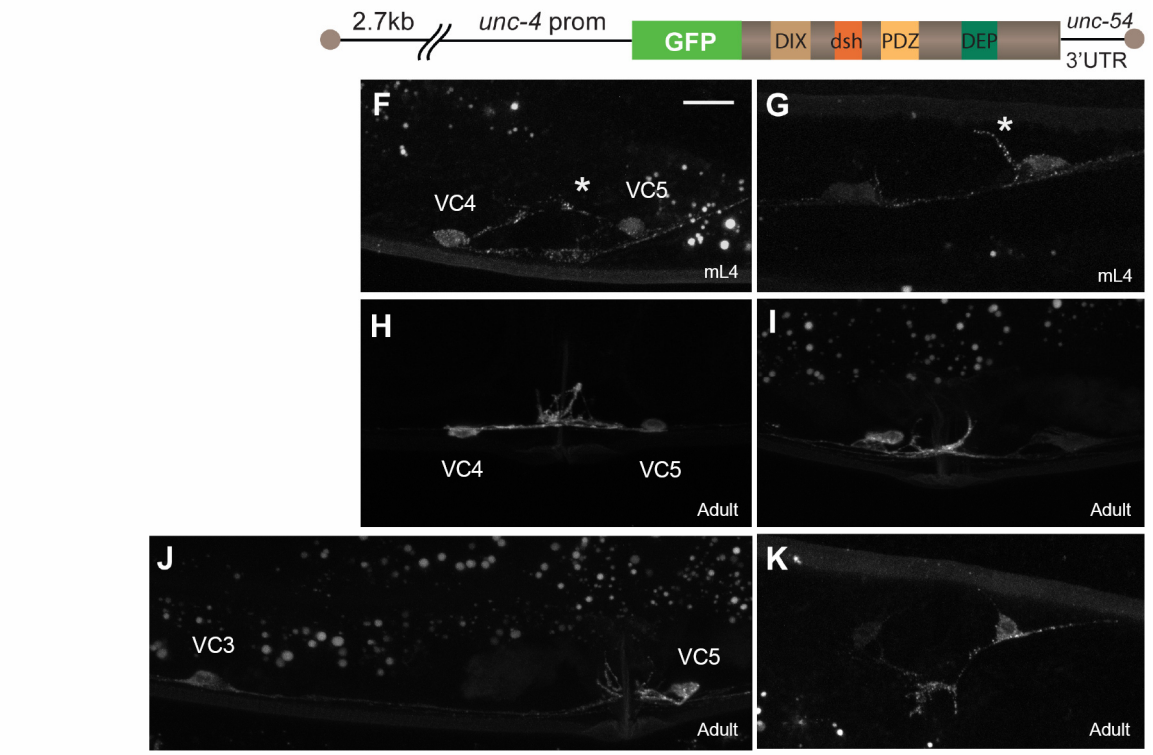
2.7kb
unc-4 prom
GFP
DIX
dsh
PDZ
DEP
unc-54
3'UTR
F
VC4
*
VC5
mL4
G
*
mL4
H
VC4
VC5
Adult
I
Adult
J
VC3
VC5
Adult
K
Adult

***Dsh-1* overexpression in VC4/5 neurons results in tripolar neurons, similar to the *lof* phenotype.**

Next, the effect of *dsh-1* overexpression in VC4/5 was examined. I generated N2 transgenic lines overexpressing *dsh-1.c* from the *unc-4* promoter, injected at two different concentrations 10 and 50 ng/µL. Remarkably, *dsh-1* overexpression resulted in a *lof* phenotype (Figure IV-6). Approximately 27 to 38 % of VC4/5 neurons in *Punc-4::dsh-1* overexpressing lines displayed AP axons. Notably, the penetrance of tripolar neurons in trangenic worms harbouring 10 ng/µL array was not significantly different from that of nematodes with 5-fold higher concentration of the construct, suggesting no dose-dependent overexpression phenotype (Figure IV-6). Moreover, contrary to *prkl-1* overexpression, *dsh-1* and *vang-1* overexpressing nematodes did not show unipolar neurons (Figure IV-6) (Sanchez-Alvarez et al., 2011). These data suggests that maintaining a suitable level of DHS-1 activity is important to prevent AP axon growth. Interestingly, *vang-1* overexpression, similar to *dsh-1* overexpression, results in tripolar neurons (Sanchez-Alvarez et al., 2011).

Figure IV-6. *dsh-1* overexpression results in tripolar VC4/5 neurons, similarly to *lof* phenotype. A) Representative confocal image of a worm carrying *dsh-1* overexpressing transgene displaying VC4/5 tripolar neurons. Scale bar, 20 µm. **B)** Quantification of *dsh-1* overexpression phenotype. Published in (Sanchez-Alvarez et al., 2011).

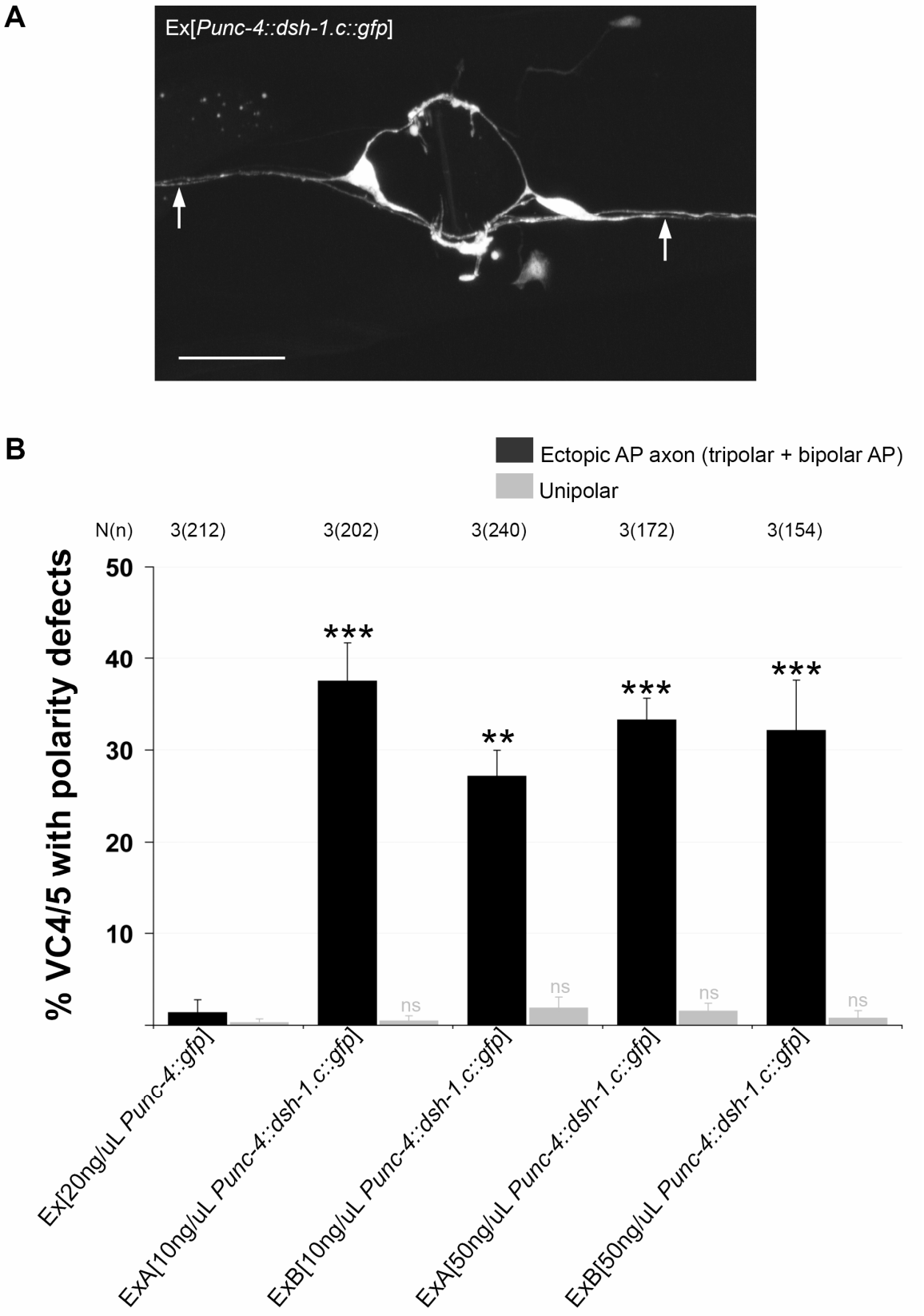
A
Ex[Punc-4::dsh-1.c::gfp]
B
Ectopic AP axon (tripolar + bipolar AP)
Unipolar
N(n)
3(212)
3(202)
3(240)
3(172)
3(154)
% VC4/5 with polarity defects
50
40
30
20
10
***
**
***
***
ns
ns
ns
ns
Ex[20ng/uL Punc-4::gfp]
ExA[10ng/uL Punc-4::dsh-1.c::gfp]
ExB[10ng/uL Punc-4::dsh-1.c::gfp]
ExA[50ng/uL Punc-4::dsh-1.c::gfp]
ExB[50ng/uL Punc-4::dsh-1.c::gfp]

Both *dsh-1* lof and *dsh-1* overexpression in PDE neurons result in lack of or premature termination of posterior axons.

Postembryonic mechanosensory PDE neurons are located bilaterally in the posterior half of the nematodes. PDEs grow axons ventrally to the right VNC which then bifurcate to extend an anterior axon to a position close to the pharynx and a posterior axon to a position close to the anus (White et al., 1986). Since ectopic expression of *prkl-1* in PDE neurons caused premature termination of anterior axons but *prkl-1* loss-of-function did not, we decided to investigate if *dsh-1* overexpression would result in a similar phenotype. I then examined PDE neurons in *dsh-1* overexpressing *Pcat-1::dsh-1.c::gfp* transgenic lines and found that the anterior PDE axon had a mild extension defect (not scored), whereby axons did not always reached the pharynx and terminated before their final destination. However, all anterior axons always extended past the vulva and past 3/4th of the wild type length. Instead, the most prominent phenotype, caused by *dsh-1* overexpression in PDE neurons, was the lack of or shortening of the PDE posterior axons (Figure IV-7). Remarkably, *dsh-1(ok1445)* mutants also display a PDE posterior axon phenotype, with ~ 91 % PDE exhibiting posterior axon extension defects; of which almost half lacked the posterior axon altogether, while the other half displayed prematurely terminated (before ½ wt length) posterior axons (Figure IV-7). This result suggested that *dsh-1* is required to promote the formation of PDE posterior axons, regulating their extension to their normal length near the anus and/or *dsh-1* is required to initiate posterior axon extension.

Moreover, these data hints at a role for *dsh-1* in PDE's posterior axons growth. A comparable percentage of worms displayed posterior axon defects in *dsh-1.c* overexpressing transgenic lines, injected with either 10 ng/µL or 50 ng/µL of *Pcat-1::dsh-1.c::gfp*, with ~ 88 % and ~90 %, respectively. Occasionally, in wild type animals PDE posterior axons failed to reach their normal destination, displaying a background of wt variability of ~12 % (Figure IV-7). However, no PDE in wt background lacks posterior axons; this phenotype appears to be specifically caused by disruptions in *dsh-1* function. In PDEs neurons without posterior axons, the ventral axonal segment however appeared to have grown normally to the VNC and then turned anteriorly with a 90^{o} angle, there is no signs of bifurcation. It is possible that upon disrupting *dsh-1* function the posterior axon fails to initiate or that any growth is followed by retraction. Using different promoters to induce *dsh-1* overexpression at different time points together with following and scoring the development of PDE phenotype in *dsh-1(ok1445)* mutants compared to wt nematodes, from early larval stages, will help elucidate how *dsh-1* is contributing to PDE AP pseudo bipolar morphology.

In addition, dissection of the defective phenotype in *dsh-1* overexpressing lines revealed a correlation between higher percentages of neurons without posterior axons at increasing concentrations of the *dsh-1* overexpressing array. Thus, while only 29 % of defective PDEs had no posterior axons in the 10 ng/µL transgenic line; 69 %, lacked posterior axons, in the 50 ng/µL *Pcat-1::dsh-1.c::gfp* transgenic strain (Figure IV-7). This dose-response relationship indicates the specificity of *dsh-1* overexpression on PDE axon extension defects.

Figure IV-7. ***dsh-1*** **loss-of-function and** ***dsh-1*** **overexpression in PDE neurons result in lack of, or premature termination of posterior axons. A**) Representative photograph of wild type PDE morphology visualized with *cyIs4* reporter. PDE anterior axons terminate at the head ring while posterior axons terminate close to the anus (represented by white stars). **B**) Representative image of truncated posterior PDE axon in a wild type worm carrying a *dsh-1* overexpressing transgene [*Pcat-1::dsh-1.c::gfp*]. Lack of posterior axon is indicated by yellow star. **D**) Quantification of PDE's posterior axon extension defects. Scale bar, 20 µm.

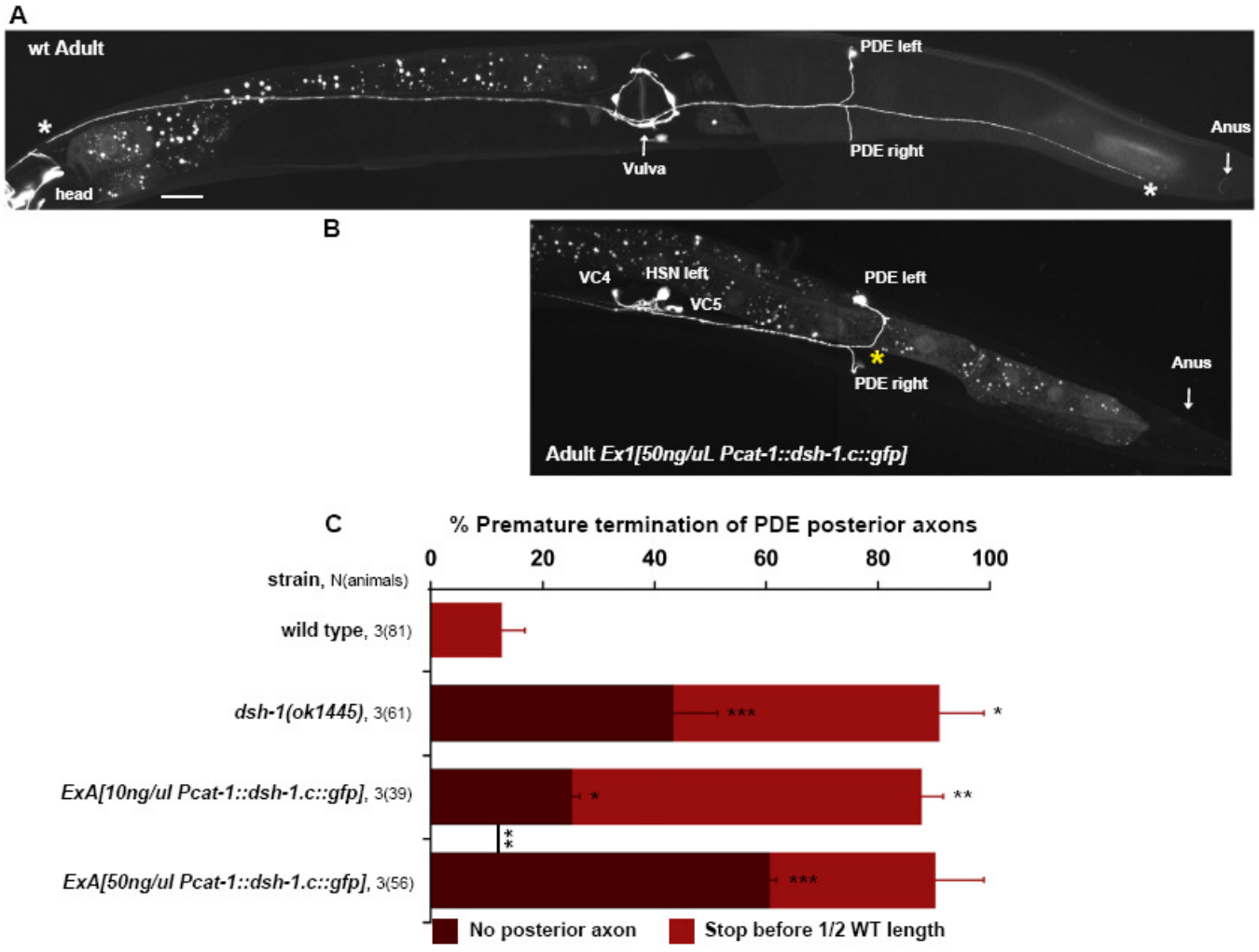
A
wt Adult
PDE left
PDE right
Vulva
Anus
head
B
VC4
HSN left
VC5
PDE left
PDE right
Anus
Adult Ex1[50ng/uL Pcat-1::dsh-1.c::gfp]
C
% Premature termination of PDE posterior axons
0
20
40
60
80
100
strain, N(animals)
wild type, 3(81)
dsh-1(ok1445), 3(61)
ExA[10ng/ul Pcat-1::dsh-1.c::gfp], 3(39)
ExA[50ng/ul Pcat-1::dsh-1.c::gfp], 3(56)
No posterior axon
Stop before 1/2 WT length

DISCUSSION

A steady-state level of DSH-1 is required to reach and maintain the ML orientation of VC4/5 neurons.

Quantitative analysis of defective VC4/5 morphologies in *dsh-1* mutant nematodes from early developmental stages to adult, revealed that *dsh-1* is required to prevent VC4/5 AP axon growth from late L3, before axon outgrowth, to adulthood. These data suggest that *dsh-1* functions to establish and maintain VC4/5 neuronal morphology. Notably, overexpressing *dsh-1* in VC4/5 neurons resulted in a similar *lof* phenotype, tripolar neurons. This finding is in agreement with most models of PCP signalling, where *lof* mutations and overexpression of PCP genes produce similar PCP phenotypes. For instance, both *lof* and overexpression of *Drosophila dsh* result in similar disruption of organized ommatidia patterning in the compound eye (Boutros et al., 1998). Furthermore, a five fold increase in the concentration of the *dsh-1* overexpressing construct in the transgenic array (from 10 to 50ng/uL) did not worsen the severity of the tripolar phenotype any further; which may suggest that the polarity phenotype results from causing homeostatic imbalance in the levels of *dsh-1,* rather than a dose-dependent effect. Altogether, our findings signify that steady-state levels of DSH-1 are precisely controlled to establish and maintain normal neuron morphology/orientation.

DSH-1::GFP is expressed in VC4/5 and vulva epithelia. In VC4/5 DSH-1::GFP is expressed in a punctate pattern at the plasma membrane and uniformly in the cytosol.

The *dsh-1* promoter is widely expressed in *C. elegans* nervous system and also in the vulva epithelia and egg-laying muscles. Within the nervous system, the *dsh-1* promoter is

active in many VNC motorneurons, including the VCs. A similar expression pattern is displayed by the GFP-tagged *dsh-1* genomic construct. Additionally, at the cellular level, we found that DSH::GFP is expressed in a punctate pattern at the plasma membrane of VC4/5 and uniformly in the cytosol. Notably, the puncta was symmetrically distributed, contrasting with the asymmetric enrichment of *Drosophila* DVL on the apical distal edge of wing cells (Axelrod, 2001). Symmetric membrane DSH puncta are also observed in other cell types undergoing PCP signalling. For instance, *Xenopus* DVL-2 localizes in a punctate pattern on the apical membrane of the mucociliary epithelium that is lining the epidermis; yet, it is asymmetrically enriched near the base of the cilia (Park et al., 2008). Altogether, these findings suggest that the function and subcellular distribution of DSH/DVL depends on the cellular context. How both distributions, the membrane puncta and cytosolic DSH-1, relate to the PCP pathway which prevents VC4/5 AP axon growth, remains unknown.

Even though DSH/DVL is a cytosolic hydrophilic protein, based on its primary and secondary structure, DSH is distributed in puncta by the plasma membrane, in many cell types undergoing polarization, such as mesodermal cells during *Xenopus* CE (Wallingford et al., 2000). DVL association with the plasma membrane in tissues undergoing PCP/CE has been linked to the membrane targeting properties of the DEP domain and to protein-protein interactions between DVL-PDZ domain and FZ PDZ-binding motifs (Wang et al., 2006a). In other contexts, PDZ domains are known to interact with the cytoplasmic tail of transmembrane receptors, and contribute to the clustering of signal transduction complexes. For example the clustering of AMPA receptors into macromolecular complexes at excitatory synapses, requires the involvement of PDZ-domain containing proteins (O'Brien et al., 1998). Thus, it is plausible that DSH/DVL recruitment to the neuronal plasma membrane may

involve protein-protein interactions with the cytosolic tail of other transmembrane PCP proteins and/or receptors, also through the PDZ domain. For example, *Drosophila* DVL is known to interact with the C-terminal tail of VANG/strabismus, which contains a PDZ binding motif (Park and Moon, 2002). Furthermore, *C. elegans* DSH-1 was recently reported to interact genetically and physically with Fz co receptor CAM-1/Ror to regulate the AP orientation of a pair of head motorneurons with long posterior processes, RMED/V (Song et al., 2010). Their physical interaction was mapped to the PDZ and DEP domains of DSH-1 and to the kinase domain and the region between kinase and transmembrane sequence of CAM-1 (Song et al., 2010). Interestingly, a *cam-1* null allele results in complete loss of RMED/V posterior axons, and a similarly strong phenotype is attained by double Frizzle mutants *cfz-2; mig-1*, whereas the single mutants display mild defects (Song et al., 2010). This report proposes that in the context of RMED/V neurons, CAM-1 acts as a main receptor for CWN-2 (Wnt), which functions as an attractive cue to regulate AP axon outgrowth, while frizzleds *cfz-2* and *mig-1* act as co-receptors (Song et al., 2010). Which transmembrane receptor/protein is upstream of DSH-1 to prevent AP axon growth in VC4/5?

Furthermore, *in vitro* experiments of *Xenopus* DVL-2 transfixed in COS-7 and 293T cell lines showed clear localization in puncta by the plasma membrane, contained in endocentric vesicles (Schwarz-Romond et al., 2005). Photo bleaching studies suggested that the puncta are protein assemblies, and there exist a dynamic equilibrium between the punctate and cytosolic pools (Schwarz-Romond et al., 2005). Moreover, the authors showed that a DVL-2 deletion construct lacking the DIX domain failed to localize in a punctate pattern and instead was diffusely distributed in the cytosol, suggesting that the puncta

forming ability of DVL-2 depends on the DIX domain, which mediates oligomerization (Schwarz-Romond et al., 2005).

DSH-1 acts both cell autonomously and non-autonomously in the epithelia to prevent AP axon growth in VC4/5 neurons.

Activity of *dsh-1* activity is required in both the vulva epithelium and in VC4/5 neurons. Cell-specific rescue experiments revealed that the AP axon phenotype in *dsh-1* mutants is rescued only partially with either a *Punc-4* driven or a *Pcol-10* driven *dsh-1.c* cDNA extrachromosomal array. This finding was an indication that simultaneous activity of *dsh-1* in the neurons and epithelial cells was critical to attain maximum VC4/5 wt morphology. This notion would be easily tested by co-transfecting *dsh-1* mutant nematodes with both constructs, which should render a significantly improved rescue rate compared to either construct separately. Similarly, *Drosophila* core PCP genes *fz* and *vang* have been shown to act both autonomously and cell non-autonomously in the wing hair cells, whereas *dgo*, *dsh* and *prkl* only function in a purely cell autonomous manner (Theisen et al., 1994; Klingensmith et al., 1994; Wu and Mlodzik, 2009).

DSH-1 promotes posterior axon extension in PDE neurons.

In addition to VC4/5, *dsh-1* also plays a role in the polarity of PDE motorneurons, which normally extend AP axons after a short ventral segment, rendering a pseudobipolar morphology. Both *lof* and *dsh-1* overexpression caused dramatic lack of or premature termination of posterior axons. Collectively, the finding that *dsh-1 lof* and *dsh-1* overexpression from the *cat-1* promoter causes lack of PDE posterior axons or their premature termination suggests that 1) dsh-*1* is required for PDE posterior axons extension to

wild type lengths and 2) *dsh-1* may function cell autonomously in the PDEs to initiate or extend posterior axon growth. Altogether, *dsh-1* function in the PDEs contrasts with *dsh-1* function in VC4/5, which signifies that *dsh-1* inhibits or promotes AP axon growth in a context dependent manner. In other words, *dsh-1* has different functions in different nerve cells. Notably, *vab-8* (for Variable Abnormal Morphology) *lof* disrupts the growth of most posteriorly directed axons in the worm (Wightman et al., 1996). For instance, the posteriorly directed PDE axons are shortened or missing in *vab-8* mutants (Wightman et al., 1996;Wolf et al., 1998), resembling PDE phenotype in *dsh-1* mutants. The *vab-8* gene encodes a protein which contains a domain similar to kinesin-like motors (Wolf et al., 1998). In addition, VAB-8 has also been shown to regulate the AP polarity of touch neurons, which extend long anterior axons (Levy-Strumpf and Culotti, 2007). For instance, *vab-8* overexpression, like *unc-40* overexpression, results in ALM axon reversal along the AP axis (Levy-Strumpf and Culotti, 2007). It was proposed that VAB-8 acts together with MIG-2 GTPase and UNC-73 (GEF) to regulate the subcellular localization of axon guidance receptor UNC-40 (Levy-Strumpf and Culotti, 2007). In summary, VAB-8, a kinesin protein, appears to play an important role in AP neuron polarity/orientation by interacting with small GTPases, which provides a link to the cytoskeleton. Based on the similar *dsh-1* and *vab-8 lof* phenotypes in PDE neurons, it would be interesting to explore a potential genetic link between these two genes in promoting PDE posterior axon formation. Analysis of genetic interactions between *vab-8* and *dsh-1* and other genes with similar PDE phenotype would help elucidate the genetic pathway by which *dsh-1* regulates PDE polarity, which may share some common elements with the mechanism by which *dsh-1* regulates VC4/5 polarity.

SUPPLEMENTARY DATA

Polyclonal antibodies to DSH-1.

We generated two peptide antibodies to DSH-1 and one to full length recombinant his-tagged DSH-1 protein. Supplementary Figure IV-1B displays the ability of two peptide antibodies to recognize full length recombinant His-tagged DSH-1 immobilized in an ELISA plate. However, these antibodies did not immunostain wild type nematodes. Hence, they will need to be optimized for immunohistochemistry assays and other purposes.

Supplemental Figure IV-1. Polyclonal antibodies to DSH-1. **A)** Schematic representation of the DSH-1 protein and position of peptides used to raise rabbit polyclonal antibodies. Antibodies to the following peptide sequences were produced by Sigma, N-terminal: RLRDQTEENGKEDDFDNKSC and MID: KKKKNKRNFRKPSRC. B) ELISA results of bleed #3. Plates were coated with either 10ug/mL of each peptide or 20ug/mL full length recombinant DSH-1. Goat antirabbit-HRP (BIORAD) was used as secondary antibody and soluble TMB, as substrate. To assess the specificity of the antisera and whether the antibody is capable of recognizing immobilized full length DSH-1, a competitive assay was performed using 10 µg/ml peptide in solution with the serum dilution.

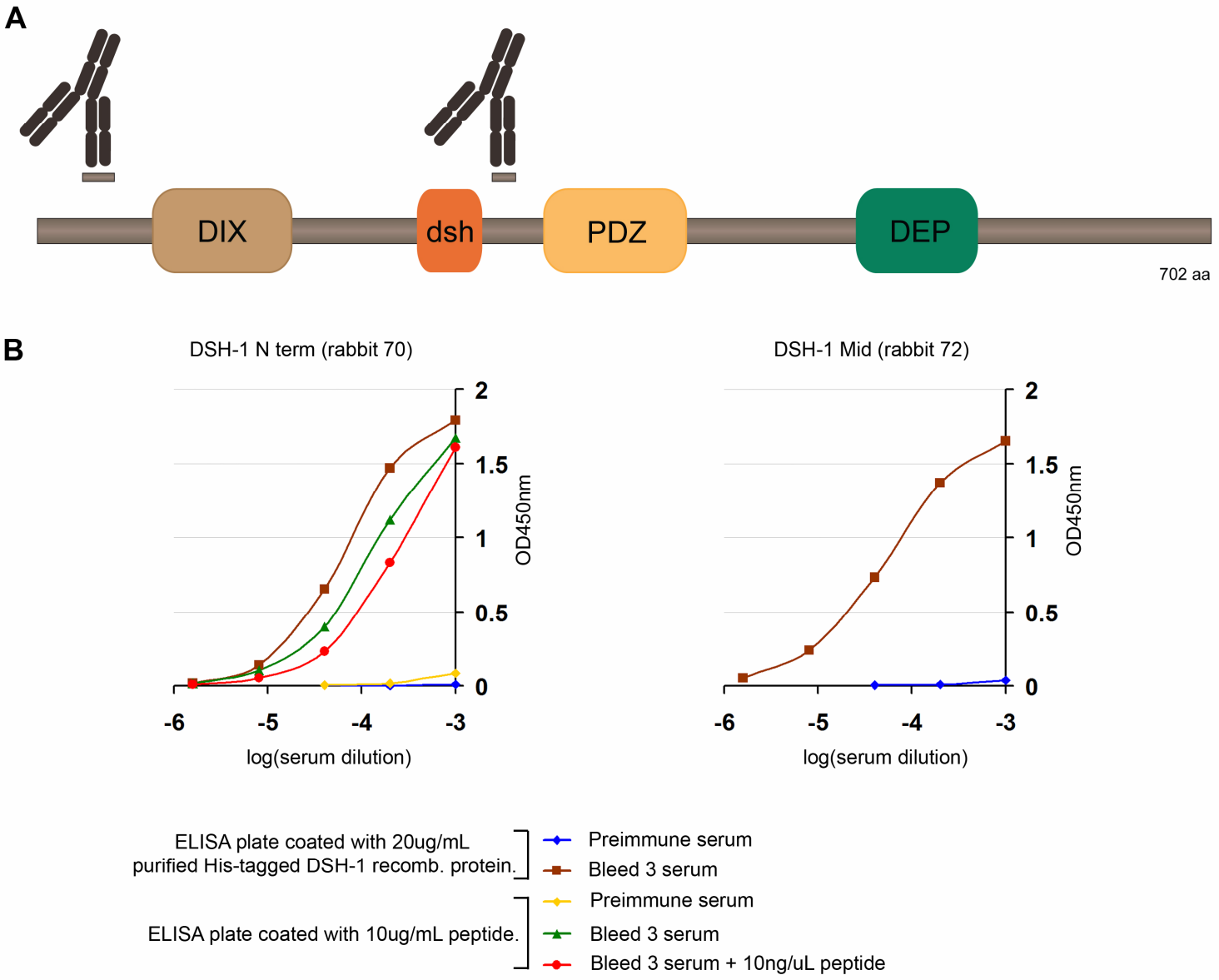
A
DIX
dsh
PDZ
DEP
702 aa
B
DSH-1 N term (rabbit 70)
DSH-1 Mid (rabbit 72)
OD450nm
log(serum dilution)
ELISA plate coated with 20ug/mL purified His-tagged DSH-1 recomb. protein.
Preimmune serum
Bleed 3 serum
ELISA plate coated with 10ug/mL peptide.
Preimmune serum
Bleed 3 serum
Bleed 3 serum + 10ng/uL peptide

CHAPTER V - GENERAL DISCUSSION, FUTURE DIRECTIONS & CONCLUSION.

The focus of my PhD research was to gain insight into how neurons reach and maintain their polarity *in vivo*. My work mostly addressed the role of PCP genes *prkl-1* and *dsh-1* in the morphology of VC4 and VC5 *C. elegans* motorneurons. I have accomplished this using a variety of approaches including forward and reverse genetics, molecular biology, generation of transgenic worms, and confocal and fluorescence microscopy. I have taken advantage of the genetic amenability of *C. elegans* as a model organism to draw answers into this largely unexplored area of research. Our work is among the first to address the role of PCP signalling in regulating neuronal polarity *in vivo*.

The term Planar Cell Polarity was first used in *Drosophila* studies to describe the coordinated orientation of cellular structures (trichomes, a.k.a. hairs) along an axis which is orthogonal to the plane of the epithelial surface (Fanto and McNeill, 2004). The PCP pathway is phylogenetically conserved and important for a plethora of developmental processes, from invertebrates to mammals, including the organized arrangement of ommatidia in the compound eye, vertebrate gastrulation, neural tube closure, polarization of cilia in the organ of corti (Fanto and McNeill, 2004). Although, VC4 and VC5 are two individual neurons and not a tissue *per se*, they clearly exhibit polarity defective phenotypes in PCP mutant backgrounds. In *prkl-1*, *dsh-1* and *vang-1* mutants VC4/5 extend ectopic axons along the AP axis, which transform normal neurons with left-right bipolar morphologies into tripolar neurons. The importance of studying the expression, regulation and function of *prkl-1*, *dsh-1* and *vang-1* in neurons is highlighted by recent findings linking

mutations in human PCP genes to nervous system disease, specifically the linkage of mutations in human *prkl* gene to epilepsy (Bassuk et al., 2008).

The Fz/PCP non-canonical pathway shares common genes with the *Wnt* canonical pathway, including players *Wnt*, *Fz, Vang* and *Dsh*; whereas other genes such as *prkl-1* are unique to the PCP pathway. At the beginning of this project, there was no *prkl-1* allele available to study *prkl-1* role in neuronal polarity. As such, the first objective was to isolate polarity defective mutant nematodes. This initial project yielded four alleles of *prkl-1*, one allele of *dsh-1*, and six alleles of *fntb-1*; all of which display VC4/5 with ectopic AP-oriented axons.

5.1 The *prkl-1* and *vang-1* genes act in a common PCP-like pathway to regulate VC4/5 neuron morphology/polarity, and *dsh-1* acts in a parallel pathway to *prkl-1,vang-1*.

Genetic analysis of *prkl-1* and *vang-1* single and double mutants revealed that the penetrance of the double mutants was not significantly increased, suggesting that these core PCP genes act in a common pathway to suppress AP axon growth. The phenotype of double mutants with *dsh-1*, however, resulted in worsening of the phenotype compared to *prkl-1*, *dsh-1* and *vang-1* single mutants, with about 100% of neurons displaying AP axons, the majority of which (60 % in *dsh-1* and 69 % in *vang-1*) displayed bipolar AP morphologies, reminiscent of vulvaless nematodes (Li and Chalfie, 1990) (Figure V-1). These data suggest that *dsh-1* may act in a parallel pathway to *prkl-1/vang-1* to suppress AP axon growth and to promote the formation of VC4/5 primary axons.

Figure V-1. PCP-like signalling regulates neuron polarity by preventing AP axon growth and promoting ML axon growth. PCP genes *prkl-1*, *dsh-1* and *vang-1* block formation of neurites along the AP axis. Analysis of genetic interactions revealed that *prkl-1* and *vang-1* act in the same pathway to regulate VC4/5 polarity, and *dsh-1* acts in a parallel genetic pathway and may also act in a common pathway with *prkl-1/vang-1*. Simultaneous loss of two PCP genes results in an AP bipolar morphology that is reminiscent of vulvaless mutants, suggestive of a relationship neurons-vulva-PCP. Red gradient in the neuron's cell bodies indicates non-permissive axon growth zone in the AP axis.

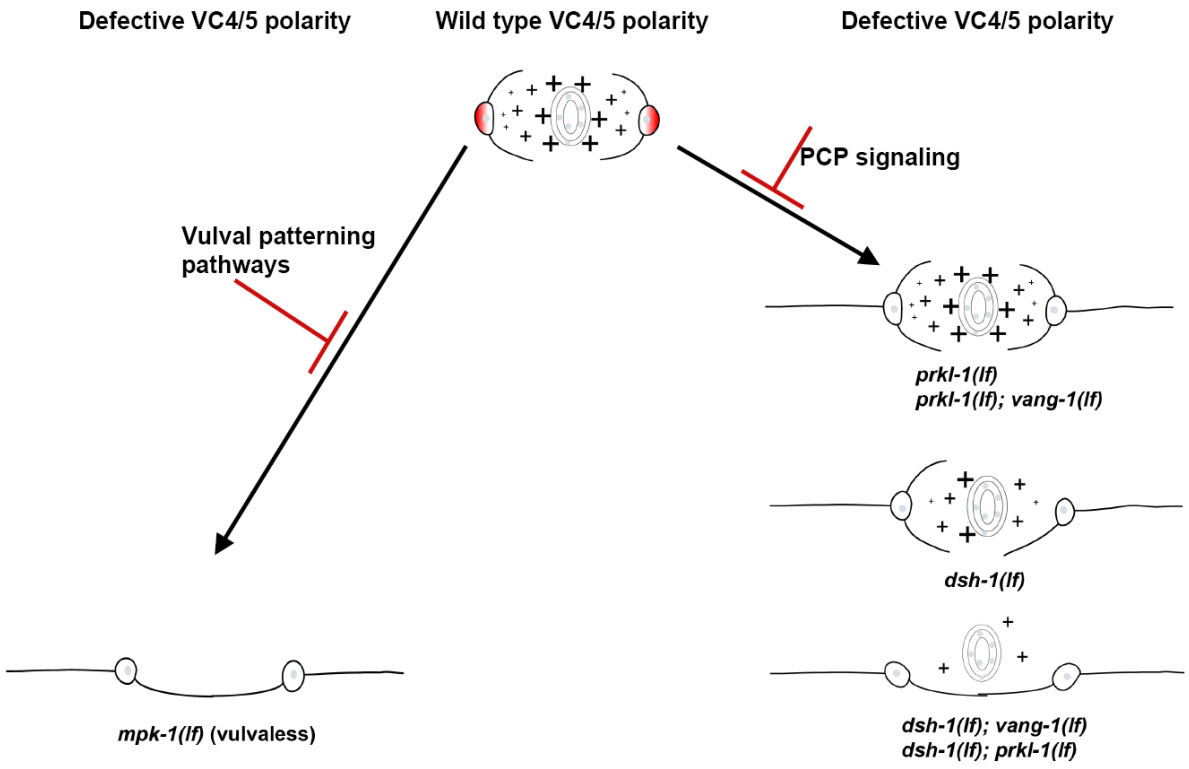

5.2 PRKL-1 functions cell autonomously in VC4/5, whereas DSH-1 and VANG-1 act both cell autonomously, and cell non-autonomously in the epithelium.

Cell-specific rescue experiments revealed that PRKL-1, DSH-1 and VANG-1 act cell autonomously in VC4/5 neurons to prevent AP axon outgrowth (Sanchez-Alvarez et al., 2011). However, DSH-1 and VANG-1 expressed in VC neurons only partially rescued VC4/5 polarity defects, suggesting that the activity of both genes is also required non-neuronally (Sanchez-Alvarez et al., 2011). Accordingly, we found that DSH-1 and VANG-1 act cell non-autonomously in the epithelium to regulate VC4/5 morphology (Sanchez-Alvarez et al., 2011). Core PCP genes have been shown to function cell autonomously and/or cell non-autonomously in different contexts (Vladar et al., 2009; Wu and Mlodzik, 2009). For instance, mosaic analysis in the *Drosophila* wing revealed that neighbouring cells to a PCP mutant patch also display a PCP defective phenotype consisting of disoriented hairs and multiple hairs per cell (Adler et al., 2000). These findings support the notion that cell-cell communication is of essence for PCP establishment and maintenance.

In contrast with the planar polarity of a tightly compacted sheet of epithelial cells in the fly wing or with the polarized migration of mesenchimal cells during embryogenesis, where multiple cells in close contact are synchronically undergoing a common polarization program, our model system consists of two individual motorneurons (VC4/5) flanking the vulva epithelium. Yet, in an analogous manner, the environment provided by the vulva epithelium, and the cellular interactions between VPCs and neurons are critical to the polarity of VC4/5; with the epithelium producing directional cues for polarized axon growth and orientation (Li and Chalfie, 1990).

Furthermore, vulva development is regulated by multiple Wnt/FZ pathways, both canonical and non-canonical (Green et al., 2008). For instance, VANG-1 is required in a PCP pathway for the asymmetric VPC divisions during vulva morphogenesis. In this pathway VANG-1 functions downstream of Wnt/EGL-20 (Green et al., 2008). It is hypothesized that VANG acts as co-receptor, to EGL-20, with cell-autonomously-acting CAM-1 (Ror receptor tyrosine kinase) (Green et al., 2008). Concomitant with the PCP pathway, a canonical mechanism involving Wnts LIN-44 and MOM-2, signalling through FZ/LIN-17 and RYK/LIN-18, respectively, controls β catenin localization, and activates gene transcription in VPCs; regulating the mirror-image cell divisions that take place on opposite ends of the developing vulva (Green et al., 2008). Similarly, multiple mechanisms could be in place to coordinate VC4/5 neuron polarity/orientation in vulva morphogenesis. It is plausible that *vang-1* and *prkl-1* cooperate cell autonomously in VC4/5 neurons in a PCP-like signalling pathway to prevent AP axon growth, while a parallel mechanism involving the function of *vang-1* and/or *dsh-1* cell non-autonomously in the vulva epithelium, is also required to regulate VC4/5 morphology.

Divergence in the *modus operandi* of a single PCP gene in various tissues of an organism, or between orthologs in different species, largely reflects genome economy and diversity of gene function. Overall, timing and context determine gene expression profile, function and consequently, phenotypic outcomes.

5.3 PRKL-1, DSH-1 and VANG-1 are expressed in symmetrically distributed puncta at the plasma membrane of VC4/5.

GFP::PRKL-1, DSH::GFP and VANG-1::GFP are all expressed in VC4/5 neurons, in discrete membrane sub domains (puncta) (Sanchez-Alvarez et al., 2011). It is unknown if these proteins are co localized at the same puncta. PCP proteins have been shown to localize in similar puncta at the plasma membrane of several tissues undergoing PCP. For instance, zebrafish PK localizes in a punctate pattern at the anterior membrane of mesodermal cells undergoing CE, during gastrulation (Yin et al., 2008); and *Xenopus* DVL-2 is expressed as dynamic puncta on the apical membrane of the mucociliary epithelium during PCP signalling (Park et al., 2008).

Interestingly, the MINK (Misshapen Nck-interacting kinase) ser/thr kinase has been shown to phosphorylate DSH, PRKL and VANG in mesodermal cells undergoing CE, during *Xenopus* gastrulation. This post-translational modification is critical for their clustering into discrete puncta at the plasma membrane (Lee et al., 2007; Daulat et al., 2012). It has been shown that MINK1 interacts genetically and physically with PRKL to regulate PCP establishment in the *Drosophila* eye and CE in *Xenopus* embryos (Daulat et al., 2012). In these contexts, MINK phosphorylates a conserved thr residue which is important for the Rab5-dependent endosomal trafficking and enrichment of PRKL within plasma membrane puncta (Daulat et al., 2012). Accordingly, the recruitment of PRKL, DSH and VANG puncta at the plasma membrane of VC4/5 neurons may also depend on phosphorylation or other post translational modification.

Tissue-wide asymmetric localization of PCP proteins has been well documented from invertebrates to vertebrates (Strutt, 2001; Strutt, 2002; Klein and Mlodzik, 2005; Strutt and Strutt, 2009). For instance, *Drosophila* PRKL is asymmetrically enriched at the apical proximal edge of wing cells (Bastock et al., 2003; Strutt and Strutt, 2009), Mouse PRKL2 is asymmetrically localized in the inner ear sensory epithelium (Deans et al., 2007), Zebrafish PRKL is asymmetrically distributed in mesenchymal cells during CE (Veeman et al., 2003) and in zebrafish presomitic mesoderm undergoing CE during gastrulation, PRKL and DSH are localized to opposite ends of the cells (Yin et al., 2008). In this context, PRKL localizes at the anterior cell edges of the dorsal mesoderm, whereas DSH is enriched posteriorly, which is reminiscent of PRKL and DSH localization in the fly wing cells (Yin et al., 2008). However, asymmetric localization of PCP proteins is not required in all tissues undergoing non canonical PCP/CE signalling. For instance, chicken PRKL1 and DSH are distributed symmetrically in elongating myocytes during their polarized alignment along the AP axis of the embryo (Gros et al., 2009). Mouse VANG2 and DSH2 are symmetrically localized in the neuroepithelium, during neural tube closure (Wang et al., 2006a; Torban et al., 2008). Although PRKL-1 is asymmetrically distributed at the plasma membrane of the *C. elegans* vulva, with PRKL-1 enriched towards the vulval lumen (Chapter III), we did not find consistent evidence for PRKL-1 asymmetric distribution in VC4/5 motorneurons. Similarly, DSH-1 and VANG-1 appear to be symmetrically distributed along VC4/5 plasma membrane (Sanchez-Alvarez et al., 2011). The lack of data for the asymmetric localization of PCP proteins in VC4/5 may be interpreted as 1) asymmetric distribution is not required for PCP signalling in VC4/5; 2) overexpressing arrays interfere with the assessment of significantly transient asymmetries; and 3) asymmetries may be expressed at the functional level, via post

translational modifications such as phosphorylation, which might activate or inactivate PCP protein function, thus affecting donwstream pathways and consequently the outcome. For instance phosphorylated and unphosphorylated PCP proteins may be targeted to distinct submembranous compartments, which could not be detected neither with GFP-tagged proteins nor with polyclonal antibodies.

Additionally, PRKL is expressed in VC4/5 nuclei and DSH is diffusely distributed in the cytosol while excluded from the VC4/5 nuclei. Nuclear PRKL is required for the tangential migration of *Zebrafish* FBMN neurons during hindbrain development (Mapp et al., 2011). Moreover, cytosolic DSH has been shown to be important for its function *in vitro*. For example, studies of cultured DVL transfected cells have revealed that the cytosolic pool of DVL is required to maintain the membrane puncta pool, and that both pools are in dynamic equilibrium with each other (Schwarz-Romond et al., 2005). However, the significance of nuclear PRKL and cytosolic DSH in the context of VC4/5 as well as the mechanism and relevance of the symmetrically distributed membrane puncta needs further addressing.

5.4 The number of axons correlates with *prkl-1* dosage (*i.e.* low → tripolar; high → unipolar), but not with *dsh-1* and *vang-1* dosages (*i.e.* low & high → tripolar).

While *prkl-1 lof* results in supernumerary neurites, overexpression results in too few neurites in a dose-dependent manner; suggesting that the number of processes in VC4/5 is sensitive to *prkl-1* dosage (Figure V-2). This is the first report showing a correlation between *prkl-1* dosage and the number of neurites *in vivo*. This finding contrasts with *dsh-1* and *vang-1*, whose overexpression in VC4/5 result in a *lof* phenotype (Sanchez-Alvarez et al., 2011) (Figure V-2), suggesting that a steady-state level of *vang-1* and *dsh-1* is required to prevent

ectopic AP axon growth. The finding that VC4/5 morphologies in *dsh-1* and *vang-1* mutants are similar in *Punc-4::dsh-1.c* and *Punc-4::vang-1* overexpressing nematodes, suggests that *dsh-1* and *vang-1* may be playing a more permissive role in regulating neuron morphology, contrasting with the instructive polarity role of *prkl-1*. *In vitro* studies using cultured mammalian cells, however, have shown an inverse correlation of neurite number with *prkl* and *dsh* levels. For instance, downregulation of DSH in cultured rodent hippocampal neurons abrogates axon differentiation, whereas overexpression results in multiple axons (Zhang et al., 2007). Similarly, mRNA downregulation of *prickle1* and *prickle2* in a murine neuroblastoma cell line (Neuro2A) significantly reduced the number of neurite-bearing cells (Okuda et al., 2007). In C1300 murine neuroblastoma cells, *prickle1* and *prickle2* were found to promote neurite outgrowth in a *dsh* dependent manner (Fujimura et al., 2009).

Both, hairs and axons are cytoskeleton filled structures, yet hairs are actin-based while axons are mainly supported by MTs. Analogous to the role of PCP in VC4/5, *lof* and overexpression of PCP genes in the fly wing not only disrupts hair orientation but also the number of hairs per cell (Fanto and McNeill, 2004). Overall, it seems reasonable to suggests that the downstream role of PCP signalling, be it in a neuron or epithelial cells, is to nucleate and orientate cytoskeleton polymerization.

Interestingly, *prkl-1* dose-dependent effect on the number of VC4/5 neurites bears an interesting resemblance to genes with well known roles in regulating neuron polarity *in vitro* and *in vivo* mouse models, including the protein kinases LKB-1/PAR-4 and cofactor pseudokinase STRAD and SAD/MARK downstream kinases, which regulate the MT cytoskeleton through MAPs (Shelly et al., 2007; Barnes et al., 2007; Shelly and Poo, 2011).

Notably, neuronal response to their gradients results in opposite phenotypes to VC4/5 responses to *prkl-1* manipulations. Thus, while overexpression of LKB-1 & STRAD resulted in multinumerary axons, downregulation impaired axon formation (Shelly et al., 2007; Barnes et al., 2007). Would there be a connection between PRKL-1 and these downstream kinases in the remodelling of VC4/5 cytoskeleton to prevent AP axon growth?

Figure V-2. Number of neurites in VC4/5 correlates with *prkl-1* dosage, but not with *dsh-1* or *vang-1* dosages. Schematic representation of VC4 morphology in distinct genetic backgrounds. While *prkl-1 lof* results in neurons with supernumerary axons (tripolar), *prkl-1* overexpression results in an opposite *gof* phenotype (unipolar). However, both *lof* and overexpression of *dsh-1* and *vang-1* render tripolar neurons.

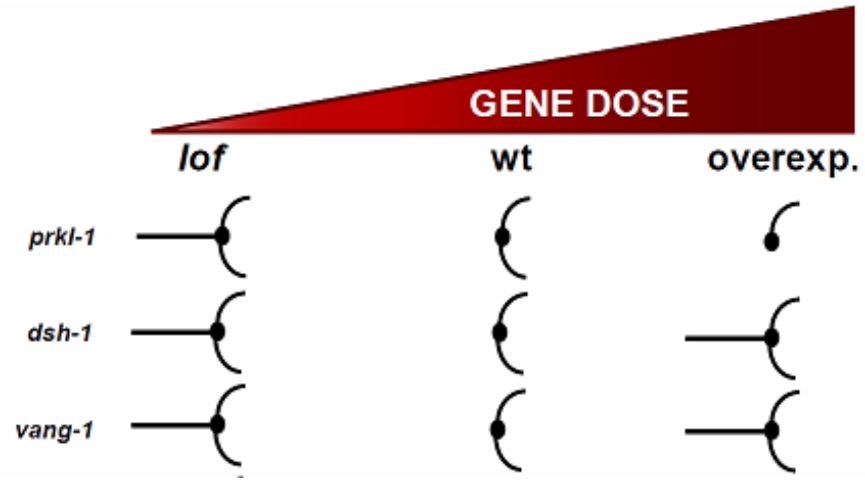

5.5 PRKL-1 acts downstream of VANG-1 and DSH-1 to regulate VC4/5 polarity. A model for the role of non canonical PCP signalling in VC4/5 neuronal polarity.

PRKL-1, DSH-1 and VANG-1 prevent AP axon growth in VC4/5 neurons. PRKL-1 and VANG-1 act in a common PCP-like pathway to regulate the polarity of VC/5, while DSH-1 appears to act in a parallel pathway. The PCP pathway regulating VC4/5 polarity shares several features with classic PCP signalling; including cell autonomous and non-autonomous gene activity, similar *lof* and *gof* phenotypes, and complex genetic interactions (Strutt and Strutt, 2009; Wu and Mlodzik, 2009). In Figure V-3, I present a hypothetical model to explain some of this thesis' results, specifically depicting the cell autonomous components of this PCP pathway.

Although PRKL-1, VANG-1 and DSH-1 don't appear to be asymmetrically distributed, it is plausible they interact with a downstream cascade involving polarity proteins which may become asymmetrically localized in VC4/5 neurons, for instance GSK-3β and PAR proteins, which may ultimately orient the cytoskeleton in VC4/5. Activated GSK-3β and PAR proteins are asymmetrically distributed in developping mouse neurons *in vivo* (Jiang et al., 2005; Yoshimura et al., 2005; Barnes et al., 2007; Shelly et al., 2007). Such hypothesis would be consistent with the finding that both *lof* and overexpression of *vang-1* and *dsh-1* result in a similar *lof* phenotype. In other words, in the absence of the PCP protein, no positional information is transduced to the downstream players and polarity can't be established. Too much PCP protein would overwhelm and/or disrupt the localization machinery of these downstream players resulting in a similar PCP defective outcome. Both situations would lead

to uniform distribution of the downstream players, and subsequent disorientation of the cytoskeleton with similar loss of neuron polarity.

Notably, the finding that *prkl-1* overexpression rescues VC4/5 polarity defects in *dsh-1* and *vang-1* mutants, suggests that *prkl-1* overexpression overrides the need for functional *dsh-1* and *vang-1* in VC4/5, which tentatively places *prkl-1* as a downstream player (Figure V-3). Additionally, the significant increase in the penetrance of the defective phenotype in *dsh-1* double mutants relative to single mutants suggested that *dsh-1* also acts in a parallel pathway, which may possibly be rooted in its cell non-autonomous function in the vulva epithelium (next section). Moreover, PRKL-1 is also capable of overriding the polarization program of other AP oriented neurons such as PDEs and VC6. These data may indicate that PRKL-1 plays an instructive role in neuronal polarity.

Based on literature reports showing that membrane localized puncta of polarity proteins significantly correlates with their PCP signalling activities, it is reasonable to propose that PRKL-1, DSH-1 and VANG-1 expression puncta at the plasma membrane of VC4/5 are functionally important to prevent AP axon growth, yet we do not exclude the possibility that nuclear PRKL-1 and cytosolic DSH-1 might be important as well (Figure V-3). For instance, zebrafish PRKL1B is required in the nuclei of FBMN neurons for their polarized tangential migration in the vertebrate hindbrain (Mapp et al., 2011)

Importantly, a recent study showed that the cellular pool of functional DVL is limited, therefore the availability of DVL in some subcellular compartments *vs* others (*e.g.* cytosol *vs* plasma membrane) determines pathway specificity (Wu et al., 2004). This observation shed light into how the canonical Wnt/Fz signalling can downregulate/antagonize non canonical

pathways in a single cell, and vice versa (Axelrod et al., 1998; Wu et al., 2004). What if a developmental process (*i.e.* neuron polarity) is regulated by distinct DVL signalling (*i.e.* canonical and PCP) synchronically activated in different interacting cell types? Then, DVL cellular resources wouldn't need splitting up into different branches of the Wnt/Fz pathway if each cell type focuses on one pathway. Let's consider, for instance, a theoretical model in which DVL signals the PCP pathway in VC4/5 neurons (Figure V-3) and the β catenin canonical pathway in the vulva epithelia, with the common goal of preventing AP axon growth, and promoting ML axon formation.

Even though we carried out a candidate gene approach to determine if *C. elegans* orthologs of other core PCP genes played a role in VC4/5 polarity, we did not find evidence for the involvement of *Wnts* and *Fzs* in VC4/5 polarization. However, we have yet to address any redundancy between multiple *Wnts* and *Fzs*, in triple and quadruple mutant's combinations. Nonetheless, based on the well established role of FZ in most PCP model systems, and the new found role for Wnt/CWN-2 in regulating AP neuronal polarity in *C. elegans* via DSH-1 (Song et al., 2010), a WNT/FZ pair has been depicted as potential player in the working model for VC4/5 polarization pathway (Figure V-3), which could be acting upstream of DSH-1. We also assessed whether the atypical cadherin Flamingo (a seven pass transmembrane protein with multiple cadherin domains), played a role in the morphology of VC4/5. Interestingly, *fmi-1(tm306)*, a strong *lof* allele, displays wild type VC4/5 morphology (Chapter II); which at first suggested that FMI was not involved in this pathway. The lack of phenotype in *fmi-1 lof* nematodes contrasts with a clear function in *Drosophila* PCP, especially in the wing cells where it is enriched at the proximal/distal cell borders, forming homophilic protein complexes which connect neighbouring cells (Shimada et al., 2001).

However, from the analysis of double mutants *fmi-1; prkl-1* and *fmi-1; vang-1* our laboratory later found that *fmi* significantly suppressed VC4/5 polarity defects in *prkl-1* and *vang-1* mutants, hinting at a role for FMI in promoting AP axon growth (Sanchez-Alvarez et al., 2011). *C. elegans* FMI-1 is primarily expressed in the nervous system including VC4 and VC5 neurons and other VNC neurons such as DA, VA and VB neurons, and in the HSN neurons (Steimel et al., 2010; Najarro et al., 2012). Considering that 1) FMI appears to be excluded from the vulva epithelium (Steimel et al., 2010) and that 2) *Drosophila* FMI functions cell autonomously and non cell autonomously in well studied PCP models with distinct read outs [*e.g.* to orient trichomes in the fly wing epithelia (Usui et al., 1999; Shimada et al., 2001) and to control pioneer dependent navigation of follower axons in the *C. elegans* ventral cord (Steimel et al., 2010)]; one could hypothesize that FMI functions cell autonomously in VC4/5 and cell non-autonomously in ventral cord motorneurons to promote the formation of and to steer VC AP axons. In other words, FMI expressed in VC4/5 (acting cell autonomously) could form homodimers with FMI in other neurons (acting cell non-autonomously), or heterophilic interactions with different cadherins and/or receptors in other neurons which pioneer the AP axon track.

<u>Figure V-3.</u> Model – PRKL-1, DSH-1 and VANG-1 interact in a PCP signalling pathway to establish and maintain VC4/5 neuronal polarity by preventing AP axon growth. Schematic representation of a VC4 or VC5 neuron, and potential roles of cell-autonomous PCP elements which regulate their morphology.

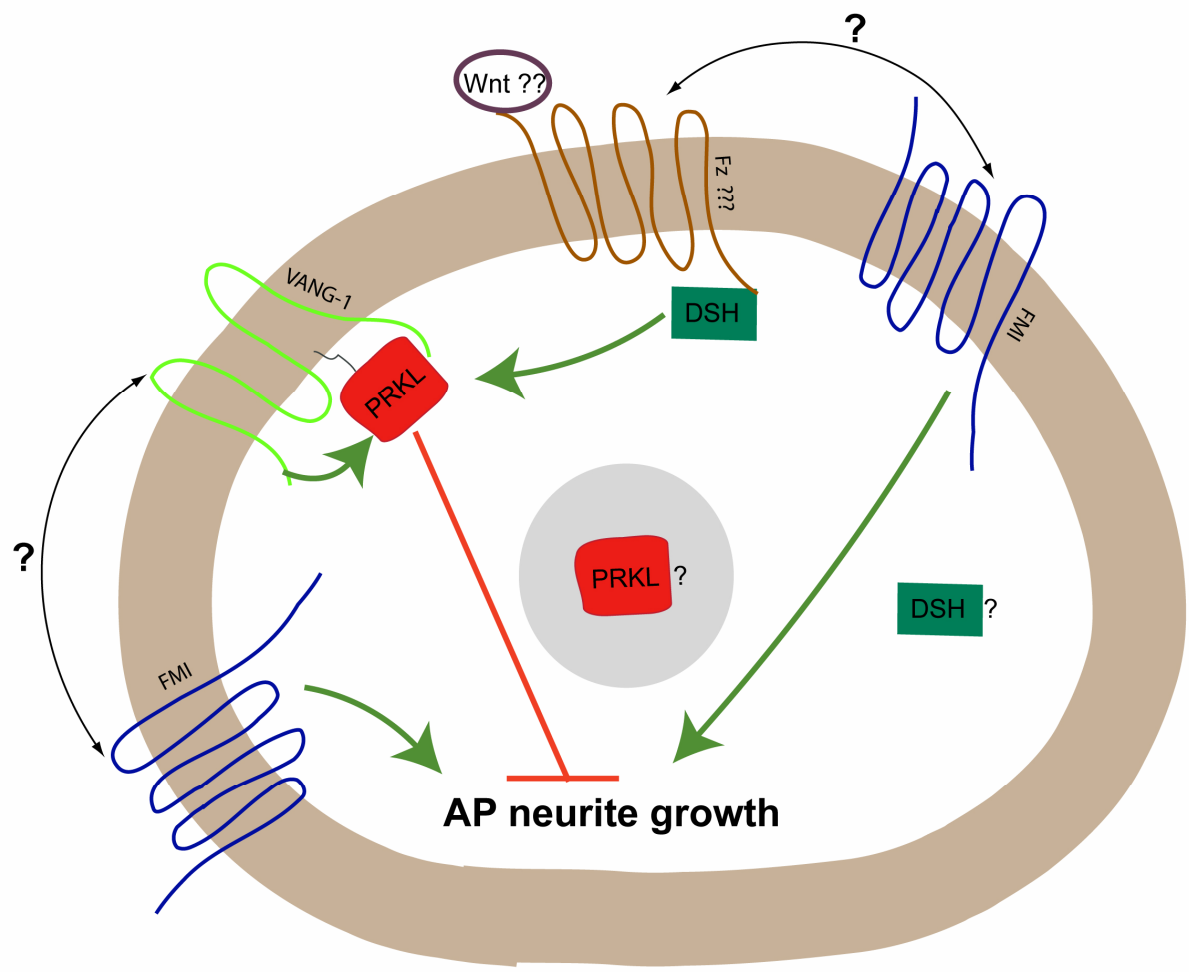

5.6 A parallel non canonical DSH-1 pathway may control VC4/5 polarity.

Vulval-proximal VC4 and VC5 are the only VC motorneurons oriented in the LR axis. In the absence of vulva, VC4 and VC5 are polarized in the AP axis, mimicking the orientation of vulval-distal VCs (Li and Chalfie, 1990). This finding suggested that all six VC neurons are, by default, responsive to AP polarizing cues. This report also indicated that the vulva epithelium is the source of a signal involved in preventing AP axon outgrowth and instructing the vulva-flanking VCs a Left-Right orientation. Altogether, a polarization program for VC4/5 neurons appears to be triggered by the vulva. This could be mediated by direct neuronal contact with guidepost cells in the epithelia and/or a secreted factor produced by the epithelial cells.

It is very interesting how a *dsh-1.c* cDNA expressed from epithelial cells (driven by *Pcol-10*) rescues the polarity defects in VC4/5 neurons of *dsh-1(ok1445)* nematodes (presumably *dsh-1*$^{-/-}$), significantly better than *dsh-1.c* cDNA expressed in the neurons themselves. The level of rescue is comparable to the one attained with the *gfp*-tagged *dsh-1* genomic transgene; that is, rescuing from ~ 67 % VC4/5 with AP axons in *dsh-1(ok1445)* to ~ 13%, with the *dsh-1* genomic array, and to ~ 18 %, with the *Pcol-10::dsh-1.c* array. How can this be explained? Plausibly, this result indicates a parallel pathway for *dsh-1* in regulating VC4/5 polarity. Moreover, in support of a parallel pathway, the double mutants *dsh-1;vang-1* and *dsh-1;prkl-1* display a significantly increased ectopic AP axon phenotype compared to single mutants. An important datum in this puzzle is the finding that the vulva epithelium has the ability to induce *prkl-1* expression in VC4/5 (Figure V-4). This finding may represent the connection between vulva organogenesis and VC4/5 polarization.

Importantly, DSH is known to transduce both canonical or non-canonical Fz signalling (Gao and Chen, 2010). One possibility to explain the role of *dsh-1* activity in the vulva would be that it is implicated in a canonical pathway which controls *prkl-1* expression in VC4/5. Hypothetically, DSH-1 in the epithelia regulates the expression of a factor/morphogen which impacts *prkl-1* expression in VC4/5 neurons. What kind of factor? How would it work? It could be, for instance, a transcription factor (TF) which activates the expression of a transcriptional repressor (TR) controlling *prkl-1* gene activity in VC4/5 (*e.g. dsh-1* → TF → TR ┤ *prkl-1*); which would maintain homeostatic levels of PRKL-1 in the neurons from lateL3/early L4 to adulthood to prevent AP axon growth. This theoretical cascade would explain why *prkl-1* overexpression (using a *prkl-1* genomic array) overrides the need for functional *dsh-1,* as the levels of the putative repressor would be minimal in a *dsh-1*$^{-/-}$ background. In addition this model agrees with the *dsh-1* overexpression phenotype in VC4/5 neurons (using *Punc-4*), whereby the levels of the putative repressor would increase and *prkl-1* transcription would drop, leading to tripolar neurons via the non-canonical PCP pathway. Interestingly, VC4/5 neurons overexpressing *dsh-1* display a purely tripolar morphology similar to *prkl-1 lof*, displaying no other morphological defects such as unipolar neurons or bipolar AP morphologies, which are characteristic of *dsh-1 lof*. The latter also hints at *dsh-1* working canonically in the neurons to control *prkl-1* expression; and/or an independent non-canonical role of *dsh-1* which can be discerned when *dsh-1* levels in the epithelia are not disrupted. This model may be valid to some extent; however VC4/5 polarization can't be explained solely with a linear cascade of events. For instance, this canonical cascade does not explain the *dsh-1 lof* phenotype. In *dsh-1* mutants VC4/5 polarity defects consist of various species, unlike *prkl-1 lof*; ~ 7 % of *dsh-1 lof* neurons are unipolar (phenotype similar to *prkl-*

1 gof), ~ 20 % display an AP bipolar morphology (phenotype similar to double mutants *dsh-1;prkl-1* and *dsh-1;vang-1*) and 50 % are tripolar (phenotype similar to *prkl-1 lof*). Hence, the variability of *dsh-1 lof* phenotypes also points to its involvement in parallel pathways to regulate VC4/5 polarity.

A quick and easy experiment to test the hypothesis that *dsh-1* regulates *prkl-1* expression, would be to assess whether the *Pprkl-1* transcriptional array (described in Chapter III) is ON or OFF in a *dsh-1* mutant background. If OFF, that would indeed suggest that *dsh-1* plays a canonical role regulating *prkl-1* expression. Similarly, *vang-1* could be tested for its ability to induce *prkl-1* expression in VC4/5. The partial applicability of the individual models further suggests that multiple interconnected pathways regulate VC4/5 morphology. Collectively, our findings appear to point at *dsh-1* and *vang-1* playing a permissive role, and *prkl-1* acting instructively to prevent AP axon growth.

Figure V-4. Coupling neuronal polarity to organogenesis. Illustration of epithelia-induced *prkl-1* expression in VC4/5 neurons. The vulva epithelium induces *prkl-1* transcription in VC4/5 motorneurons, where PRKL-1 acts cell autonomously to prevent axon outgrowth along the AP axis. + + + indicates a vulval-derived factor which induces *prkl-1* transcription in VC4/5 neurons.

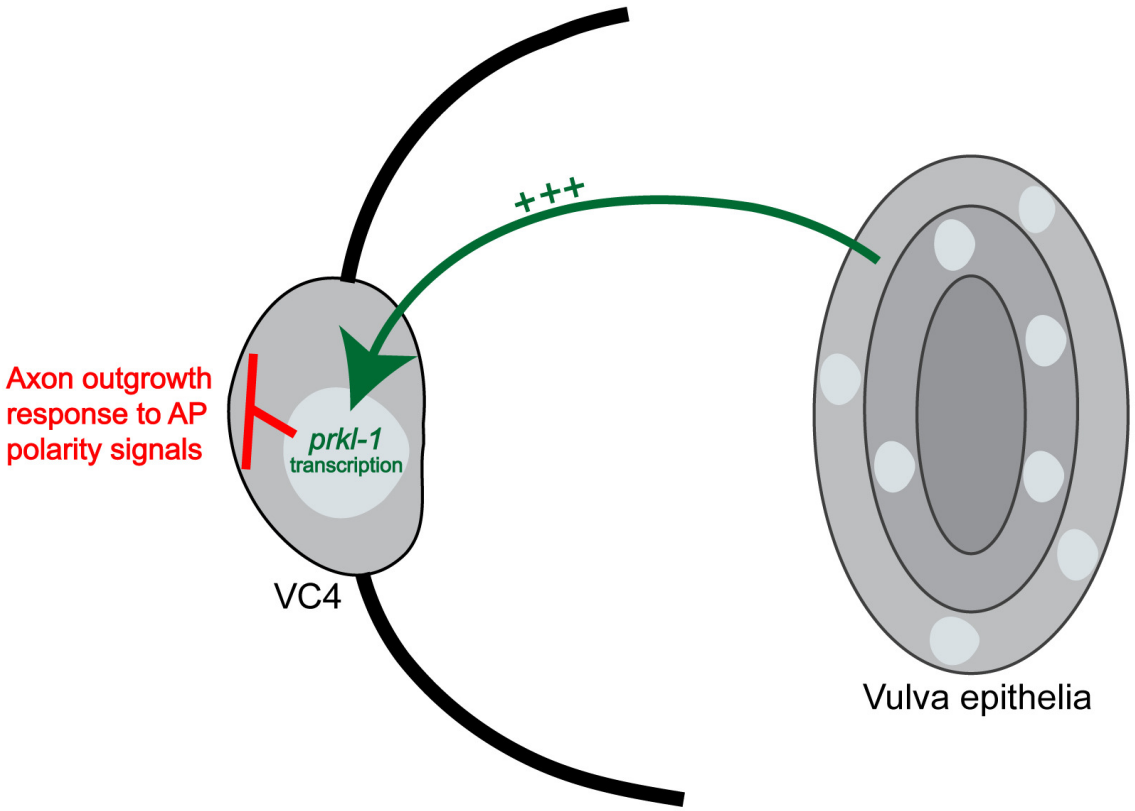

5.7 FUTURE DIRECTIONS

In essence, this thesis has uncovered a new role for the PCP pathway in preventing AP axon growth, particularly by revealing the role of *prkl-1* and *dsh-1* in regulating neuron morphology/orientation. Importantly, there remains significant work to be done before the *in vivo* functions of *prkl-1* and *dsh-1* in neuron polarity/orientation are fully understood. In this section, I will delineate a few questions, some of which are formulated as hypotheses, and propose experiments that may provide further insight into the mechanisms by which *prkl-1* and *dsh-1* regulate neuron morphology/orientation in a PCP-like signalling pathway *in vivo*.

5.7.1 Identity of the upstream factor/morphogen produced by the vulva, which may induce *prkl-1* expression in VC4/5 neurons.

As discussed previously, Li and Chalfie showed that the vulva is a source of polarizing cues for VC4/5 (Li and Chalfie, 1990). In addition, in Chapter III, I showed that the vulva induces *prkl-1* expression in VC4/5 neurons. The combined analysis of these two individual results brings up several questions, such as 1) does the vulva-derived signal, described by Li and Chalfie 1990, induce *prkl-1* expression in VC4/5?, if so 2) is it a secreted or membrane bound signal/morphogen/cue/factor?, and 3) what is the mechanism by which this vulva-derived factor promotes *prkl-1* transcription in VC4/5?

Gene expression changes with time (*i.e.* developmental stage), context (*i.e.* cell type) and very importantly, with environment (*e.g.* effect of developing VPCs in VC4/5 gene expression). One potential approach to uncover the identity of the vulva-derived factor, and the identity of effector genes in VC4/5 neurons, could be to examine gene expression profiles using microarrays of the vulva and VC4/5 at three critical developmental stages: early L3

(prior to axonogenesis), early L4 (during axonogenesis) and young adult (polarity maintenance). It would be more meaningful to study gene expression changes in VC4/5 and in the vulva while changing one parameter at a time. First, we might want to compare the transcription profile of VC4/5, and of vulva cells independently at the three developmental stages mentioned above, in order to discern which genes are differentially expressed during axonogenesis and during polarity maintenance. Second, we might want to study changes in VC4/5 gene expression profile upon ablating the vulva. How does the vulva impact gene expression at times critical for polarity establishment and maintenance? The rationale for this experiment is that VC4/5 genes whose expression is significantly lost upon vulva ablation might depend on a signal from the vulva for expression. In this category, I would expect to find *prkl-1* and also potential upstream components, for instance transcription factors involved in *prkl-1* expression. In addition, genes whose expression is significantly up regulated might require vulva signals for repression. Two methods have been successfully performed to ablate the vulva, genetic and laser micro beams. For a cleaner genetic background, although more labour intensive, laser ablation of the vulva is preferable; which is done by killing the anchor cell in newly malted L3s before vulval precursor cells start to divide, as described previously (Kimble, 1981).

The success of this experiment relies on starting with homogeneous population of cells, synchronized at a specific developmental time, or else meaningful changes from under-represented cells of interested would be lost. Using traditional dissection methods to isolate our cells of interest from our model system is unfeasible, as there is only one VC4 and one VC5 and 22 vulva cells, from about 1000 cells in the adult hermaphrodite. Fortunately, a method known as mRNA tagging can be used to achieve mRNA enrichment from

tissues/cells of interest in small multicellular organisms such as *C.elegans*, where physical dissection is unrealistic (Roy et al., 2002). This method consist in expressing an epitope-tagged mRNA binding protein such as poly-A binding protein (PAB-1) under a promoter which is specific to the cell(s) or tissue(s) of interest, followed by homogenization, immuno-precipitation with an antitag antibody, and microarrays. This approach has been successfully applied to isolate mRNA from a sample as small as two *C. elegans* neurons (Takayama et al., 2010). We would then combine mRNA tagging, to preferentially enrich VC4/5 or vulva cells transcripts at specific developmental times, with microarrays to identify the transcripts that are up and downregulated. The success of this experiment will also depend on selecting the most appropriate promoters for VC4/5 and the vulva. For the vulva there are a few available options such as *Pegl-17* (Burdine et al., 1998). For VC4/5, a promoter which is specifically expressed in VC4/5 and not in other vulval-innervating neurons and or VNC neurons would be preferable.

The approach described above will likely identify new factors involved in VC4/5 neuronal polarity, including components governing the regulation and function of *prkl-1*. Alternatively, a less finicky approach to identify new genes would be to perform modifier genetic screens (see below).

5.7.2 Modifier genetic screens to identify new *prkl-1* interacting genes in a pathway that regulates neuron morphology/polarity.

Modifier genetic screens (suppressor and enhancer) may identify additional components of the PCP signalling pathway involved in the ML orientation of VC4/5 neurons. Since *prkl-1 lof* results in almost complete penetrance of the ectopic AP axon phenotype in VC4/5, a suppressor genetic screen (using *prkl-1(zy11)* as a background strain) seems a viable strategy to identify *prkl-1* interacting genes, key regulators of this signalling cascade. Once mutants are isolated, the most immediate route forward is to clone the mutated locus, test secondary alleles of the gene and study its expression profile and genetic interactions with *prkl-1*, *dsh-1* and *vang-1*. In addition, a partial loss of function allele such as *prkl-1(tm3440)* could be used in an enhancer genetic screen to identify additional components of this pathway or parallel mechanisms involved in VC4/5 morphology/polarity.

5.7.3 Do PRKL-1, DSH-1 and VANG-1 form heteromeric multiprotein polarizing complexes at the plasma membrane of VC4 and VC5 neurons?

Interestingly, PRKL-1, DSH-1, and VANG-1 GFP fusions localize in a punctate pattern at the plasma membrane of VC4/5 neurons (Sanchez-Alvarez et al., 2011). *Drosophila* PRKL, DVL and VANG have been shown to form heteromeric protein complexes *in vitro* (Jenny et al., 2003;Das et al., 2004;Jenny et al., 2005). In addition, these proteins have been shown to regulate each other's localization at opposite ends of the apical membrane in epithelial cells (Jenny et al., 2005). Investigating the interactions of PCP proteins at the plasma membrane and assessing the relevance of these interactions in suppressing AP axon growth would provide important data which will expand the understanding of our model

system; especially because we haven't found evidence for significant changes in PCP protein localization in other PCP mutant backgrounds.

Furthermore, the soma of VC4/5 motor neurons is only 5 µm in diameter which is significantly smaller than that of vertebrate neurons; for instance, the mean soma diameter of cat motorneurons can range from 30-60 µm (Westbury, 1982). The small size of the neurons soma together with the fact that we have used overexpressing arrays may have masked fine changes in localization, which would be difficult to study under such experimental conditions. One appealing alternative to study PCP protein-protein interactions in live VC4/5 neurons would be a technique known as fluorescence resonance energy transfer (FRET). FRET depends on the close proximity (< 10 nm) of a donor-acceptor pair of fluorescent molecules [*e.g.* CFP (donor) and YFP (acceptor), FITC (donor) and Rhodamine (acceptor), BFP (donor) and GFP (acceptor)] (Selvin, 2000). Hence one of the PCP proteins would be tagged with a donor and the other with an acceptor, and co expressed in VC4/5 neurons. A bi-cistronic construct may be used to express equimolar concentrations of the proteins to be examined. This technique may prove invaluable to correlate experimental manipulations of protein-protein interactions to PCP function in VC4/5 motorneurons *in vivo*.

FRET has been successfully used to monitor protein-protein interactions in *C. elegans*. For instance, the functional interaction between presynaptic protein SYD-2/Liprin-α (LAR protein-tyrosine phosphatase-interacting protein) and UNC-104/KIF1A (kinesin-3), was studied in the living worm, by generating trangenic nematodes carrying GFP::SYD-2 and UNC-104::mRFP expressing arrays, or SNB-1::GFP and UNC-104::mRFP arrays for negative control (Wagner et al., 2009).

An alternative approach to study PCP protein interactions at the plasma membrane of VC4/5 neurons, would be to perform bimolecular fluorescent complementation analysis (BiFC) (Kerppola, 2006). This method is based on the association between split fragments of a fluorescent protein, when they are brought together in a macromolecular complex (Kerppola, 2006). This binding reconstitutes a fluorescent complex from non-fluorescent components (Kerppola, 2006). A protocol for BiFC in *C. elegans* has been reported (Shyu et al., 2008a). Importantly, FRET requires close spatial proximity between the donor and acceptor fluorophors, while BiFC not only requires the close proximity between fluorescent protein fragments but also that the split fragments have enough flexibility to associate in a complex (Kerppola, 2006). Interestingly, the combination of BiFC and FRET has been used to study the formation of ternary protein complexes. For instance, a Venus-based BiFC-FRET approach revealed a cross-talk between Fos–Jun heterodimers and the NF-κB nuclear factor in co-transfected COS-1 cells (Shyu et al., 2008b). Such an approach may be extrapolated to our model system in order to assess whether PRKL-1_VANG-1_DSH-1 form ternary protein complexes in the context of life VC4/5 neurons.

5.7.4 Role of PRKL-1 conserved domains in protein localization and neuronal polarity?

PRKL-1 is expressed uniformly in the nuclei and in a punctate pattern at the plasma membrane of VC4/5 neurons (Chapter III). It has been recently shown that *Xenopus* PK-1b is required for the tangential migration of facial branchiomotor neurons (FBMNs) (Mapp et al., 2011). The expression pattern of PK-1b in FBMNs (Mapp et al., 2011) is similar to PRKL-1 in VC4/5. The authors showed that the CAAX motif is required for nuclear but not membrane localization and demonstrated that farnesylation is required for the directed

migration of these neurons (Mapp et al., 2011). Moreover, the authors suggested that the role of PRKL nuclear expression might be PCP independent, whereas the membrane localization is PCP related (Mapp et al., 2011). At the same time they concluded that farnesylation is dispensable for PK-1b plasma membrane localization (Mapp et al., 2011). Consistently, our data suggest that the CAAX motif doesn't seem to be required for PRKL-1 PCP role in VC4/5 (Chapter III). If CAAX/farnesylation is not required for plasma membrane localization and PCP, how does PRKL localize to its functional subcellular compartment? *In vitro* experiments have shown that the PET domain on its own has the ability to bind lipid membranes (Sweede et al., 2008). This finding may help explain why a CAAX-deleted construct rescue VC4/5 polarity defects. An alternative explanation is that in the absence of CAAX, truncated PRKL-1 can be recruited to the membrane through protein-protein interactions with VANG-1. In addition, I have showed that over expressing full length PRKL-1 overrides the need for functional VANG-1. If the notion that ΔCAAX PRKL-1 can be recruited to VC4/5 plasma membrane via VANG-1 is valid, we would expect overexpressing the truncated construct would not be able to rescue VC4/5 defects in *vang-1* mutant nematodes.

Furthermore, we have yet to study whether PRKL-1 localization in the nuclei and/or at the plasma membrane is required for its role in suppressing VC4/5 AP axon growth and what protein domains are involved. This question could be addressed using fluorescent tags such as GFP, which would allow us to correlate the loss of PRKL expression in each compartment to PRKL-1's ability to rescue polarity defects in *prkl-1(zy11)* mutants. To this end, all PRKL-1 deletion constructs used for structure-function studies, in Chapter III, are all GFP-tagged. In order to study how PRKL-1 mutations and deletions affect protein localization, existing

arrays could be outcrossed out of the *cyIs4* background into a reporter-less strain. In addition, in order to identify other important regions more constructs could be generated with smaller deletions and/or point mutated residues.

5.7.5 What is the significance of PRKL-1 nuclear localization to neuronal polarity, and how is it regulated?

One intriguing aspect of PRKL-1 function in VC4/5 is its nuclear localization (Chapter III). Notably, its C-terminal region contains two putative nuclear localization signals (NLSs) (Figure V-5), which may account for PRKL-1 nuclear localization in VC4/5 neurons. Deletion analysis of NLS sequences to assess whether one or both are required to rescue VC4/5 polarity defects in null allele *prkl-1(zy17)*, may provide basic answers. Once the important segment is defined, a reasonable step forward would be to perform a mutational analysis using site-directed mutagenesis. Thus, highly conserved residues could be changed into neutral alanines such as the basic amino acids of the NLSs on the *Punc-4::GFP::prkl-1.c* cDNA rescuing construct. Subsequently, mutated constructs would be injected into null allele *prkl-1(zy17)* nematodes to generate transgenic lines which would be scored for their ability to rescue VC4/5 polarity defects. Is PRKL-1 nuclear localization critical for PCP in VC4/5? To address this and other questions regarding the link between PRKL-1 subcellular localization and function, PRKL-1 deletion constructs were designed as GFP fusions. Hence, these constructs can be used to examine how different truncations/mutations affect PRKL-1 subcellular distribution in VC4/5, and also to uncover to what extent PRKL-1 function depends on nuclear localization and/or membrane localization.

5.7.6 Investigating the role of three polyprolin consensus sequences and two serine-threonine rich motifs within PRKL-1 C-terminal region.

A C-terminal truncated *prkl-1* construct failed to rescue the VC4/5 tripolar phenotype in *prkl-1* mutants (Chapter III). The finding that the C-terminal region is critical for PRKL-1 function in regulating VC4/5 polarity (Figure III-14) warrants more investigation. Thus, to gain further insight into PRKL-1's mechanism, it is critical to identify novel essential domains within the C-terminal region. Provided that the mRNA of the truncated protein is stable and consequently translates into physiological levels of protein expression, potential answers to this question include 1) it is essential to attain functional protein folding and/or 2) the truncated protein acquires close to native 3D structure but is lacking essential elements for PRKL-1 function (*e.g.* region involved in protein-protein interactions). Notably, there are three C-terminal polyproline rich regions, comprising three consensus sequences for Src homology 3 (SH3) binding motifs (Figure V-5), two class I ligands (RxxPxxP), and one class II (PxxPxR) (Park et al., 1997). These sequences might provide the link for PRKL-1 to the cytoskeleton, via SH3-containing adaptor proteins and/or kinases. Importantly, SRC-1 is a member of the Src family of non-receptor tyrosine kinases (SFKs) which are highly conserved proteins consisting of two peptide-binding modules, a Src homology 2 (SH2) and SH3 domains, and a tyrosine kinase domain (Thomas and Brugge, 1997). To test this notion a yeast-2-hybrid assay using SRC-1 as bait and PRKL-1 C-terminal as prey or vice versa; or alternatively GST pull down assays may probe useful to assess their potential physical interaction. This could be followed with mutational analysis of the prolines in the SH3 binding motifs.

Moreover, the PRKL-1 sequence contains two serine/threonine-rich sequences, one located between the LIM2 and LIM3 motifs and the second one located before the NLS sequences (Figure V-5). These fragments may be posttranslationally modified by kinases that could consequently regulate PRKL-1 function. To address the significance of the serine/threonine motifs a deletion/mutational analysis could be performed.

Figure V-5. The PRKL-1 carboxy terminal contains two predicted nuclear localization signals, a potential polyprolin SH3-binding motif, and a CaaX farnesylation motif. Highlighted in red is the PET domain; in yellow, three LIM domains; in black, polyproline sequences (potential SH3-binding ligands), pink residues indicate two consensus polyproline sequences type I (RxxPxxP) and one consensus type II (PxxPxR). Within the C-terminal region, two predicted nuclear localization signals are highlighted in blue, and a conserved CaaX farnesylation motif, in grey, respectively. In addition, orange-coloured residues indicate serine/threonine-rich regions and potential sites of activity regulation by phosphorylation, one in between the second and third LIM domains and the other in the C-terminal domain before the NLSs.

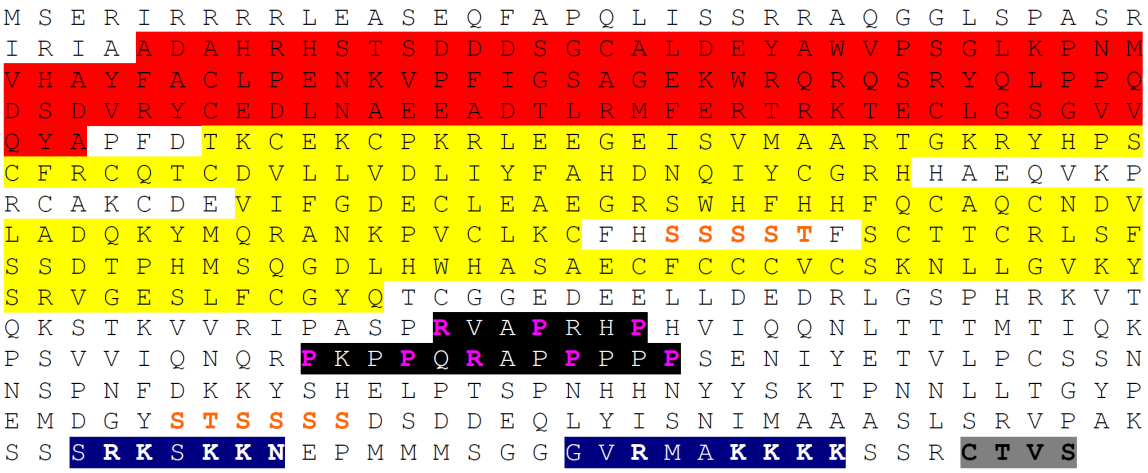

5.7.7 Involvement of PRKL-1B (PET-less) isoform in axon guidance.

While PRKL-1A (long isoform) is implicated in suppressing ectopic AP axon growth, the PRKL-1B (short isoform) appears dispensable for this function, but may instead have other roles in the nervous system. The mutant strain *prkl-1(zy17)* lacks both short and long PRKL-1 isoforms, and is the only *prkl-1* mutant displaying HSN axon guidance defects (Chapter II). This finding suggests that *prkl-1.b* may play a role in axon pathfinding.

Identifying the phenotype-causing DNA lesion in *prkl-1(zy17)* allele is crucial before establishing any definitive links between *prkl-1* short isoform and axon guidance. If sequencing the remaining unsequenced *prkl-1* genomic regions in *zy17* allele doesn't reveal any mutation, then it could be worth considering whole genome sequencing (Sarin et al., 2008). A thorough analysis of *prkl-1(zy17)* phenotypes will reveal if a broader spectrum of neurons are affected by the simultaneous loss of both *prkl-1* isoforms and which other functions in addition to neuron polarity and guidance are affected in this mutant strain. Cell specific rescue experiments will help us understand where and how the *prkl-1* gene is required, and will specifically help establish a connection between the PET-less PRKL-1 isoform and HSN axon guidance. In addition, a candidate genetic analysis will likely reveal other genes that interact with *prkl-1* to regulate HSN axon pathfinding; for instance, by assessing double mutant combinations of *prkl-1(zy17)* with other core PCP mutants, and other genes known to play a role in HSN axon guidance.

The initial polarization and axon pathfinding of HSN neurons has been extensively studied. Briefly, UNC-6/Netrin promotes leading edge formation by inducing the asymmetric distribution of netrin receptor UNC-40 along the ventral membrane of morphologically

unpolarized HSN neurons (Adler et al., 2006). Activation of the UNC-40 receptor leads to the ventral distribution of MIG-10/Lamellipodin, which then recruits the active form of CED-10/Rac (Adler et al., 2006). Ventral localization of MIG-10 contributes to polarize the growth cone by controlling asymmetric F actin assembly (Quinn et al., 2008). MIG-10 and CED-10 also play a role in HSN axon pathfinding (Quinn et al., 2008). In addition to MIG-10, MAX-2 (a PAK family member) also controls the formation of lamellipodia (Frost et al., 1998; Quinn et al., 2006). Growth cone steering in HSNs requires a genetic pathway that involves MIG-10 downstream of CED-10 and MAX-2, with MAX-2 acting in a parallel pathway which is independent of CED-10/Rac (Quinn et al., 2008). Mutations in these three genes result in severe HSN axon guidance defects. It would be interesting to learn if and how *prkl-1* fits in this pathway. Would this signalling cascade be the link for *prkl-1* to cytoskeleton remodelling?

5.7.8 Physiological relevance of AP-oriented VC4/5 axons in PCP mutant nematodes.

Do VC4/5 ectopic AP axons form functional synapses? Our observations indicate that ectopic VC4/5 AP axons remain for the life of the worm; they do not retract or degenerate. This finding may suggest that the ectopic AP axons are making functional synapses with ventral body wall muscles. This notion could be tested by using GFP reconstruction across synaptic partners (GRASP) (Feinberg et al., 2008). A method based on the reconstitution of two complementary GFP fragments expressed on different cells (synaptic partners), as fusions with transmembrane carriers (*e.g.* receptor tyrosine phosphatase PTP-3A, presynaptically; and the human T cell protein CD4, delocalized in the muscle) (Feinberg et al., 2008).

It seems reasonable that if the third axon, oriented at a 90^{o} angle with respect to the primary axons is forming exogenous synapses with body wall muscles, it would have physiological implications for the worm. Hypothetically, putative VC4/5 ectopic synapses with ventral body wall muscles would result in uncoordinated egg laying behaviour. These ectopic synapses would stimulate contractions in a direction perpendicular to the activity of primary VC4/5 axons and result in asynchronous neuron-muscle activity. However, *prkl-1* and *dsh-1* single mutants do not display overt egg-laying defective behaviour. Nonetheless, egg laying defects may not necessary manifest as severe bloating and formation of egg sacs. Instead, the alteration imposed by a third process might be less obvious, such as subtly altered kinetics as previously described in cell-ablation experiments (Waggoner et al., 1998). For instance, it could reflect on the behavioural patterns of the active and/or inactive phases of egg laying; which could be discerned with a careful assessment of the egg laying kinetics, as described (Waggoner et al., 1998).

5.7.9 What is the mechanism by which DSH-1 promotes posterior axon extension in PDE neurons?

Interestingly, both *lof dsh-1* and overexpression result in premature termination of PDE posterior axons, opposed to its role in the VCs. Also, contrary to *dsh-1*, *prkl-1* overexpression affects the anterior and not the posterior axon. These findings suggest that *dsh-1* promotes formation and extension of PDE posterior axons. Do other PCP genes interact with *dsh-1* in the PDEs? This query can be addressed by performing genetic analysis of canonical PCP mutants and genetic screens. How does *dsh-1 lof* and overexpression prevent posterior axon extension in PDEs? In addition, it will be key to assess whether *dsh-1* is acting cell

autonomously or cell non-autonomously, using cell specific rescue experiments. Would overexpressing *prkl-1* in *dsh-1* mutant background result in PDEs with neither anterior nor posterior axons? If so, would the neuron still extend its short ventral process and remain amputated or would it be driven to death from lack of connections? Finally, because kinesin-3-like gene *vab-8 lof* has been reported to display a similar PDE phenotype (Wightman et al., 1996), it would be important to learn if *dsh-1* interacts with *vab-8* in a common or parallel pathway, and also to learn the hierarchy of such a genetic interaction.

5.8 CONCLUSIONS

This thesis has uncovered a novel outcome for the PCP pathway in neuronal polarity. It has provided insight into the genetic pathways and mechanisms by which PRKL-1 and DSH-1 regulate the morphology of *C. elegans* motorneurons. In addition, this thesis has defined a new role for *fntb-1* in suppressing AP axon growth. FNTB-1 is the sole *C. elegans* farnesyl transferase enzyme, a protein of great interest in cancer therapy. Moreover, it has opened new avenues for the study of other neuronal functions requiring the activity of PCP genes *prkl-1* and *dsh-1*.

Studies of biological processes in *C. elegans* have already made important contributions to our understanding of evolutionarily conserved pathways, including those involved in cell death (Horvitz, 2003) and RNA interference (Fire, 2007;Mello, 2007). The high conservation of PCP proteins and PCP signalling mechanisms from invertebrates to mammals encourages further research into this new found read out for the PCP pathway in regulating neuron polarity. Further investigating the functions of *prkl-1*, *dsh-1* and the PCP pathway on neuron polarization in *C. elegans* may shed some light into our understanding of

how neurons polarize in higher organisms, most importantly in humans. To conclude, *prkl* has already been linked to epilepsy and *vang* has been linked to neural tube defects, in humans; hence, it is likely that results obtained from this work will provide insight into how the PCP pathway can be manipulated for axon regeneration after brain and/or spinal cord injury.

REFERENCES

Aberle,H., Bauer,A., Stappert,J., Kispert,A., and Kemler,R. (1997). beta-catenin is a target for the ubiquitin-proteasome pathway. EMBO J. *16*, 3797-3804.

Adler,C.E., Fetter,R.D., and Bargmann,C.I. (2006). UNC-6/Netrin induces neuronal asymmetry and defines the site of axon formation. Nat. Neurosci. *9*, 511-518.

Adler,P.N., Taylor,J., and Charlton,J. (2000). The domineering non-autonomy of frizzled and van Gogh clones in the Drosophila wing is a consequence of a disruption in local signaling. Mech. Dev. *96*, 197-207.

Altun,Z.F., and Hall,D.H. (2011). Nervous system, general description. In Wormatlas.

Andres-Barquin,P. (2001). Ramon y Cajal: a century after the publication of his masterpiece. Endeavour *25*, 13-17.

Arimura,N., and Kaibuchi,K. (2005). Key regulators in neuronal polarity. Neuron *48*, 881-884.

Axelrod,J.D. (2001). Unipolar membrane association of Dishevelled mediates Frizzled planar cell polarity signaling. Genes Dev. *15*, 1182-1187.

Axelrod,J.D. (2009). Progress and challenges in understanding planar cell polarity signaling. Semin. Cell Dev. Biol. *20*, 964-971.

Axelrod,J.D., Miller,J.R., Shulman,J.M., Moon,R.T., and Perrimon,N. (1998). Differential recruitment of Dishevelled provides signaling specificity in the planar cell polarity and Wingless signaling pathways. Genes Dev. *12*, 2610-2622.

Baas,P.W., and Lin,S. (2010). Hooks and comets: The story of microtubule polarity orientation in the neuron. Dev. Neurobiol.

Bach,I. (2000). The LIM domain: regulation by association. Mech. Dev. *91*, 5-17.

Barde,Y.A., Edgar,D., and Thoenen,H. (1982). Purification of a new neurotrophic factor from mammalian brain. EMBO J. *1*, 549-553.

Bargmann,C.I., and Kaplan,J.M. (1998). Signal transduction in the Caenorhabditis elegans nervous system. Annu. Rev. Neurosci. *21*, 279-308.

Barnes,A.P., Lilley,B.N., Pan,Y.A., Plummer,L.J., Powell,A.W., Raines,A.N., Sanes,J.R., and Polleux,F. (2007). LKB1 and SAD kinases define a pathway required for the polarization of cortical neurons. Cell *129*, 549-563.

Bastock,R., Strutt,H., and Strutt,D. (2003). Strabismus is asymmetrically localised and binds to Prickle and Dishevelled during Drosophila planar polarity patterning. Development *130*, 3007-3014.

Beckerle,M.C. (1997). Zyxin: zinc fingers at sites of cell adhesion. Bioessays *19*, 949-957.

Benard,C., Tjoe,N., Boulin,T., Recio,J., and Hobert,O. (2009). The small, secreted immunoglobulin protein ZIG-3 maintains axon position in Caenorhabditis elegans. Genetics *183*, 917-927.

Bigelow,H., Doitsidou,M., Sarin,S., and Hobert,O. (2009). MAQGene: software to facilitate C. elegans mutant genome sequence analysis. Nat. Methods *6*, 549.

Bornens,M. (2008). Organelle positioning and cell polarity. Nat. Rev. Mol. Cell Biol. *9*, 874-886.

Bos,J.L. (1989). ras oncogenes in human cancer: a review. Cancer Res. *49*, 4682-4689.

Brady,S.T. (1993). Motor neurons and neurofilaments in sickness and in health. Cell *73*, 1-3.

Brenner,S. (1974). The genetics of Caenorhabditis elegans. Genetics *77*, 71-94.

Chalfie,M., Tu,Y., Euskirchen,G., Ward,W.W., and Prasher,D.C. (1994). Green fluorescent protein as a marker for gene expression. Science *263*, 802-805.

Chalfie,M., and White,J. (1988). The nervous system. In The nematode Caenorhabditis elegans, (Cold Spring Harbor: Cold Spring Harbor Laboratory Press), pp. 337-391.

Chen,Z., Gore,B.B., Long,H., Ma,L., and Tessier-Lavigne,M. (2008). Alternative splicing of the Robo3 axon guidance receptor governs the midline switch from attraction to repulsion. Neuron *58*, 325-332.

Ciani,L., Krylova,O., Smalley,M.J., Dale,T.C., and Salinas,P.C. (2004). A divergent canonical WNT-signaling pathway regulates microtubule dynamics: dishevelled signals locally to stabilize microtubules. J. Cell Biol. *164*, 243-253.

Ciani,L., and Salinas,P.C. (2005). WNTs in the vertebrate nervous system: from patterning to neuronal connectivity. Nat. Rev. Neurosci. *6*, 351-362.

Cohen,S. (1960). PURIFICATION OF A NERVE-GROWTH PROMOTING PROTEIN FROM THE MOUSE SALIVARY GLAND AND ITS NEURO-CYTOTOXIC ANTISERUM. Proc. Natl. Acad. Sci. U. S. A *46*, 302-311.

Cohen,S., Levi-Montalcini,R., and Hamburger,V. (1954). A NERVE GROWTH-STIMULATING FACTOR ISOLATED FROM SARCOM AS 37 AND 180. Proc. Natl. Acad. Sci. U. S. A *40*, 1014-1018.

Colavita,A., and Culotti,J.G. (1998). Suppressors of ectopic UNC-5 growth cone steering identify eight genes involved in axon guidance in Caenorhabditis elegans. Dev. Biol. *194*, 72-85.

Colavita,A., and Tessier-Lavigne,M. (2003). A Neurexin-related protein, BAM-2, terminates axonal branches in C. elegans. Science *302*, 293-296.

Copp,A.J., Greene,N.D., and Murdoch,J.N. (2003). The genetic basis of mammalian neurulation. Nat. Rev. Genet. *4*, 784-793.

Corsi,A.K. (2006). A biochemist's guide to Caenorhabditis elegans. Anal. Biochem. *359*, 1-17.

Curtin,J.A., Quint,E., Tsipouri,V., Arkell,R.M., Cattanach,B., Copp,A.J., Henderson,D.J., Spurr,N., Stanier,P., Fisher,E.M., Nolan,P.M., Steel,K.P., Brown,S.D., Gray,I.C., and Murdoch,J.N. (2003). Mutation of Celsr1 disrupts planar polarity of inner ear hair cells and causes severe neural tube defects in the mouse. Curr. Biol. *13*, 1129-1133.

Dabdoub,A., Donohue,M.J., Brennan,A., Wolf,V., Montcouquiol,M., Sassoon,D.A., Hseih,J.C., Rubin,J.S., Salinas,P.C., and Kelley,M.W. (2003). Wnt signaling mediates reorientation of outer hair cell stereociliary bundles in the mammalian cochlea. Development *130*, 2375-2384.

Darken,R.S., Scola,A.M., Rakeman,A.S., Das,G., Mlodzik,M., and Wilson,P.A. (2002). The planar polarity gene strabismus regulates convergent extension movements in Xenopus. EMBO J. *21*, 976-985.

Daulat,A.M., Luu,O., Sing,A., Zhang,L., Wrana,J.L., McNeill,H., Winklbauer,R., and Angers,S. (2012). Mink1 regulates beta-catenin-independent Wnt signaling via Prickle phosphorylation. Mol. Cell Biol. *32*, 173-185.

Dawid,I.B., Breen,J.J., and Toyama,R. (1998). LIM domains: multiple roles as adapters and functional modifiers in protein interactions. Trends Genet. *14*, 156-162.

de Anda,F.C., Pollarolo,G., Da Silva,J.S., Camoletto,P.G., Feiguin,F., and Dotti,C.G. (2005). Centrosome localization determines neuronal polarity. Nature *436*, 704-708.

Deans,M.R., Antic,D., Suyama,K., Scott,M.P., Axelrod,J.D., and Goodrich,L.V. (2007). Asymmetric distribution of prickle-like 2 reveals an early underlying polarization of vestibular sensory epithelia in the inner ear. J. Neurosci. *27*, 3139-3147.

Doble,B.W., and Woodgett,J.R. (2003). GSK-3: tricks of the trade for a multi-tasking kinase. J. Cell Sci. *116*, 1175-1186.

Doitsidou,M., Poole,R.J., Sarin,S., Bigelow,H., and Hobert,O. (2010). C. elegans mutant identification with a one-step whole-genome-sequencing and SNP mapping strategy. PLoS. ONE. *5*, e15435.

Duerr,J.S., Frisby,D.L., Gaskin,J., Duke,A., Asermely,K., Huddleston,D., Eiden,L.E., and Rand,J.B. (1999). The cat-1 gene of Caenorhabditis elegans encodes a vesicular monoamine transporter required for specific monoamine-dependent behaviors. J. Neurosci. *19*, 72-84.

Eisenmann,D.M. (2005). Wnt signaling. In Wormbook, I. Greenwald, ed. pp. 1-17.

Etienne-Manneville,S., and Hall,A. (2002). Rho GTPases in cell biology. Nature *420*, 629-635.

Evans,T.C. (2006). Transformation and microinjection. In Wormbook, V. Ambros, ed.

Fahmy,O.G., and Fahmy,M. (1959). New mutant report. Dros. Inf. Serv. ***33***, 85.

Fanto,M., and McNeill,H. (2004). Planar polarity from flies to vertebrates. J. Cell Sci. *117*, 527-533.

Fay,D. (2006). Genetic mapping and manipulation: chapter 6--Mapping with deficiencies and duplications. WormBook. 1-3.

Fay,D., and Bender,A. (2006). Genetic mapping and manipulation: chapter 4--SNPs: introduction and two-point mapping. WormBook. 1-7.

Feinberg,E.H., Vanhoven,M.K., Bendesky,A., Wang,G., Fetter,R.D., Shen,K., and Bargmann,C.I. (2008). GFP Reconstitution Across Synaptic Partners (GRASP) defines cell contacts and synapses in living nervous systems. Neuron *57*, 353-363.

Fire,A. (1986). Integrative transformation of Caenorhabditis elegans. EMBO J. *5*, 2673-2680.

Flames,N., and Hobert,O. (2009). Gene regulatory logic of dopamine neuron differentiation. Nature *458*, 885-889.

Frankel,W.N. (2009). Genetics of complex neurological disease: challenges and opportunities for modeling epilepsy in mice and rats. Trends Genet. *25*, 361-367.

Frost,J.A., Khokhlatchev,A., Stippec,S., White,M.A., and Cobb,M.H. (1998). Differential effects of PAK1-activating mutations reveal activity-dependent and -independent effects on cytoskeletal regulation. J. Biol. Chem. *273*, 28191-28198.

Fujimura,L., Watanabe-Takano,H., Sato,Y., Tokuhisa,T., and Hatano,M. (2009). Prickle promotes neurite outgrowth via the Dishevelled dependent pathway in C1300 cells. Neurosci. Lett. *467*, 6-10.

Gao,C., and Chen,Y.G. (2010). Dishevelled: The hub of Wnt signaling. Cell Signal. *22*, 717-727.

Gao,F.B., Kohwi,M., Brenman,J.E., Jan,L.Y., and Jan,Y.N. (2000). Control of dendritic field formation in Drosophila: the roles of flamingo and competition between homologous neurons. Neuron *28*, 91-101.

Garriga,G., Desai,C., and Horvitz,H.R. (1993). Cell interactions control the direction of outgrowth, branching and fasciculation of the HSN axons of Caenorhabditis elegans. Development *117*, 1071-1087.

Ghosh-Roy,A., and Chisholm,A.D. (2010). Caenorhabditis elegans: a new model organism for studies of axon regeneration. Dev. Dyn. *239*, 1460-1464.

Gleason,J.E., Szyleyko,E.A., and Eisenmann,D.M. (2006). Multiple redundant Wnt signaling components function in two processes during C. elegans vulval development. Dev. Biol. *298*, 442-457.

Goldstein,B., and Macara,I.G. (2007). The PAR proteins: fundamental players in animal cell polarization. Dev. Cell *13*, 609-622.

Goode,B.L., and Eck,M.J. (2007). Mechanism and function of formins in the control of actin assembly. Annu. Rev. Biochem. *76*, 593-627.

Green,J.L., Inoue,T., and Sternberg,P.W. (2008). Opposing Wnt pathways orient cell polarity during organogenesis. Cell *134*, 646-656.

Greenwald,I. (1997). Development of the Vulva. In *C. elegans* II, (Cold Spring Harbor, New York: Cold Spring Harbor Laboratory Press), pp. 519-541.

Gros,J., Serralbo,O., and Marcelle,C. (2009). WNT11 acts as a directional cue to organize the elongation of early muscle fibres. Nature *457*, 589-593.

Gubb,D., and Garcia-Bellido,A. (1982). A genetic analysis of the determination of cuticular polarity during development in Drosophila melanogaster. J. Embryol. Exp. Morphol. *68*, 37-57.

Guo,S.X., Bourgeois,F., Chokshi,T., Durr,N.J., Hilliard,M.A., Chronis,N., and Ben-Yakar,A. (2008). Femtosecond laser nanoaxotomy lab-on-a-chip for in vivo nerve regeneration studies. Nat. Methods *5*, 531-533.

Hamblet,N.S., Lijam,N., Ruiz-Lozano,P., Wang,J., Yang,Y., Luo,Z., Mei,L., Chien,K.R., Sussman,D.J., and Wynshaw-Boris,A. (2002). Dishevelled 2 is essential for cardiac outflow tract development, somite segmentation and neural tube closure. Development *129*, 5827-5838.

Hammarlund,M., Nix,P., Hauth,L., Jorgensen,E.M., and Bastiani,M. (2009). Axon regeneration requires a conserved MAP kinase pathway. Science *323*, 802-806.

Heisenberg,C.P. (2002). Wnt signalling: refocusing on Strabismus. Curr. Biol. *12*, R657-R659.

Heisenberg,C.P., Tada,M., Rauch,G.J., Saude,L., Concha,M.L., Geisler,R., Stemple,D.L., Smith,J.C., and Wilson,S.W. (2000). Silberblick/Wnt11 mediates convergent extension movements during zebrafish gastrulation. Nature *405*, 76-81.

Herculano-Houzel,S. (2009). The human brain in numbers: a linearly scaled-up primate brain. Front Hum. Neurosci. *3*, 31.

Hill,R.J., and Sternberg,P.W. (1992). The gene lin-3 encodes an inductive signal for vulval development in C. elegans. Nature *358*, 470-476.

Hilliard,M.A., and Bargmann,C.I. (2006). Wnt signals and frizzled activity orient anterior-posterior axon outgrowth in C. elegans. Dev. Cell *10*, 379-390.

Hillier,L.W., Coulson,A., Murray,J.I., Bao,Z., Sulston,J.E., and Waterston,R.H. (2005). Genomics in C. elegans: so many genes, such a little worm. Genome Res. *15*, 1651-1660.

Hirokawa,N., and Takemura,R. (2005). Molecular motors and mechanisms of directional transport in neurons. Nat. Rev. Neurosci. *6*, 201-214.

Hobert,O. (2002). PCR fusion-based approach to create reporter gene constructs for expression analysis in transgenic C. elegans. Biotechniques *32*, 728-730.

Hobert,O. (2010a). Neurogenesis in the nematode Caenorhabditis elegans. WormBook. 1-24.

Hobert,O. (2010b). The impact of whole genome sequencing on model system genetics: get ready for the ride. Genetics *184*, 317-319.

Hobert,O., Carrera,I., and Stefanakis,N. (2010). The molecular and gene regulatory signature of a neuron. Trends Neurosci. *33*, 435-445.

Hodgkin,J., Horvitz,H.R., and Brenner,S. (1979). Nondisjunction Mutants of the Nematode CAENORHABDITIS ELEGANS. Genetics *91*, 67-94.

Hoffmann,M., Segbert,C., Helbig,G., and Bossinger,O. (2010). Intestinal tube formation in Caenorhabditis elegans requires vang-1 and egl-15 signaling. Dev. Biol. *339*, 268-279.

Horiguchi,K., Hanada,T., Fukui,Y., and Chishti,A.H. (2006). Transport of PIP3 by GAKIN, a kinesin-3 family protein, regulates neuronal cell polarity. J. Cell Biol. *174*, 425-436.

Horvitz,H.R. (2003). Worms, life, and death (Nobel lecture). Chembiochem. *4*, 697-711.

Inagaki,N., Chihara,K., Arimura,N., Menager,C., Kawano,Y., Matsuo,N., Nishimura,T., Amano,M., and Kaibuchi,K. (2001). CRMP-2 induces axons in cultured hippocampal neurons. Nat. Neurosci. *4*, 781-782.

Insolera,R., Chen,S., and Shi,S.H. (2011). Par proteins and neuronal polarity. Dev. Neurobiol. *71*, 483-494.

Jenny,A., Darken,R.S., Wilson,P.A., and Mlodzik,M. (2003). Prickle and Strabismus form a functional complex to generate a correct axis during planar cell polarity signaling. EMBO J. *22*, 4409-4420.

Jessen,J.R., Topczewski,J., Bingham,S., Sepich,D.S., Marlow,F., Chandrasekhar,A., and Solnica-Krezel,L. (2002). Zebrafish trilobite identifies new roles for Strabismus in gastrulation and neuronal movements. Nat. Cell Biol. *4*, 610-615.

Jiang,H., Guo,W., Liang,X., and Rao,Y. (2005). Both the establishment and the maintenance of neuronal polarity require active mechanisms: critical roles of GSK-3beta and its upstream regulators. Cell *120*, 123-135.

Katanaev,V.L., Ponzielli,R., Semeriva,M., and Tomlinson,A. (2005). Trimeric G protein-dependent frizzled signaling in Drosophila. Cell *120*, 111-122.

Katoh,M. (2002). Strabismus (STB)/Vang-like (VANGL) gene family (Review). Int. J. Mol. Med. *10*, 11-15.

Kemphues,K. (2000). PARsing embryonic polarity. Cell *101*, 345-348.

Kemphues,K.J., Priess,J.R., Morton,D.G., and Cheng,N.S. (1988). Identification of genes required for cytoplasmic localization in early C. elegans embryos. Cell *52*, 311-320.

Kerppola,T.K. (2006). Design and implementation of bimolecular fluorescence complementation (BiFC) assays for the visualization of protein interactions in living cells. Nat. Protoc. *1*, 1278-1286.

Kibar,Z., Torban,E., McDearmid,J.R., Reynolds,A., Berghout,J., Mathieu,M., Kirillova,I., De,M.P., Merello,E., Hayes,J.M., Wallingford,J.B., Drapeau,P., Capra,V., and Gros,P. (2007). Mutations in VANGL1 associated with neural-tube defects. N. Engl. J. Med. *356*, 1432-1437.

Kimble,J. (1981). Alterations in cell lineage following laser ablation of cells in the somatic gonad of Caenorhabditis elegans. Dev. Biol. *87*, 286-300.

Kishi,M., Pan,Y.A., Crump,J.G., and Sanes,J.R. (2005). Mammalian SAD kinases are required for neuronal polarization. Science *307*, 929-932.

Klein,T.J., and Mlodzik,M. (2005). Planar cell polarization: an emerging model points in the right direction. Annu. Rev. Cell Dev. Biol. *21*, 155-176.

Klingensmith,J., Nusse,R., and Perrimon,N. (1994). The Drosophila segment polarity gene dishevelled encodes a novel protein required for response to the wingless signal. Genes Dev. *8*, 118-130.

Krylova,O., Messenger,M.J., and Salinas,P.C. (2000). Dishevelled-1 regulates microtubule stability: a new function mediated by glycogen synthase kinase-3beta. J. Cell Biol. *151*, 83-94.

Kuhl,M., Sheldahl,L.C., Park,M., Miller,J.R., and Moon,R.T. (2000). The Wnt/Ca2+ pathway: a new vertebrate Wnt signaling pathway takes shape. Trends Genet. *16*, 279-283.

Lackner,M.R., and Kim,S.K. (1998). Genetic analysis of the Caenorhabditis elegans MAP kinase gene mpk-1. Genetics *150*, 103-117.

Lee,R.H., Iioka,H., Ohashi,M., Iemura,S., Natsume,T., and Kinoshita,N. (2007). XRab40 and XCullin5 form a ubiquitin ligase complex essential for the noncanonical Wnt pathway. EMBO J. *26*, 3592-3606.

Levi-Montalcini,R. (1952). Effects of mouse tumor transplantation on the nervous system. Ann. N. Y. Acad. Sci. *55*, 330-344.

Levi-Montalcini,R., MEYER,H., and Hamburger,V. (1954). In vitro experiments on the effects of mouse sarcomas 180 and 37 on the spinal and sympathetic ganglia of the chick embryo. Cancer Res. *14*, 49-57.

Li,C., and Chalfie,M. (1990). Organogenesis in C. elegans: positioning of neurons and muscles in the egg-laying system. Neuron *4*, 681-695.

Li,L., Hutchins,B.I., and Kalil,K. (2009). Wnt5a induces simultaneous cortical axon outgrowth and repulsive axon guidance through distinct signaling mechanisms. J. Neurosci. *29*, 5873-5883.

Li,R., and Gundersen,G.G. (2008). Beyond polymer polarity: how the cytoskeleton builds a polarized cell. Nat. Rev. Mol. Cell Biol. *9*, 860-873.

Lickteig,K.M., Duerr,J.S., Frisby,D.L., Hall,D.H., Rand,J.B., and Miller,D.M., III (2001). Regulation of neurotransmitter vesicles by the homeodomain protein UNC-4 and its transcriptional corepressor UNC-37/groucho in Caenorhabditis elegans cholinergic motor neurons. J. Neurosci. *21*, 2001-2014.

Lindsay,R.M., Thoenen,H., and Barde,Y.A. (1985). Placode and neural crest-derived sensory neurons are responsive at early developmental stages to brain-derived neurotrophic factor. Dev. Biol. *112*, 319-328.

Liu,W., Sato,A., Khadka,D., Bharti,R., Diaz,H., Runnels,L.W., and Habas,R. (2008). Mechanism of activation of the Formin protein Daam1. Proc. Natl. Acad. Sci. U. S. A *105*, 210-215.

Liu,Z., Kirch,S., and Ambros,V. (1995). The Caenorhabditis elegans heterochronic gene pathway controls stage-specific transcription of collagen genes. Development *121*, 2471-2478.

Long,S.B., Casey,P.J., and Beese,L.S. (1998). Cocrystal structure of protein farnesyltransferase complexed with a farnesyl diphosphate substrate. Biochemistry *37*, 9612-9618.

Maehama,T., and Dixon,J.E. (1998). The tumor suppressor, PTEN/MMAC1, dephosphorylates the lipid second messenger, phosphatidylinositol 3,4,5-trisphosphate. J. Biol. Chem. *273*, 13375-13378.

Mandell,J.W., and Banker,G.A. (1995). The microtubule cytoskeleton and the development of neuronal polarity. Neurobiol. Aging *16*, 229-237.

Mapp,O.M., Walsh,G.S., Moens,C.B., Tada,M., and Prince,V.E. (2011). Zebrafish Prickle1b mediates facial branchiomotor neuron migration via a farnesylation-dependent nuclear activity. Development *138*, 2121-2132.

Maung,S.M., and Jenny,A. (2011). Planar cell polarity in Drosophila. Organogenesis. *7*, 165-179.

McNeill,H. (2010). Planar cell polarity: keeping hairs straight is not so simple. Cold Spring Harb. Perspect. Biol. *2*, a003376.

McTaggart,S.J. (2006). Isoprenylated proteins. Cell Mol. Life Sci. *63*, 255-267.

Mello,C., and Fire,A. (1995). DNA transformation. Methods Cell Biol. *48*, 451-482.

Montalcini,R.-L. Nobel Lecture. The nerve growth factor thirty-five years later. 1986.

Ref Type: Online Source

Murdoch,J.N., Doudney,K., Paternotte,C., Copp,A.J., and Stanier,P. (2001). Severe neural tube defects in the loop-tail mouse result from mutation of Lpp1, a novel gene involved in floor plate specification. Hum. Mol. Genet. *10*, 2593-2601.

Najarro,E.H., Wong,L., Zhen,M., Carpio,E.P., Goncharov,A., Garriga,G., Lundquist,E.A., Jin,Y., and Ackley,B.D. (2012). Caenorhabditis elegans flamingo cadherin fmi-1 regulates GABAergic neuronal development. J. Neurosci. *32*, 4196-4211.

Nance,J., and Zallen,J.A. (2011). Elaborating polarity: PAR proteins and the cytoskeleton. Development *138*, 799-809.

Nelson,W.J. (2003). Adaptation of core mechanisms to generate cell polarity. Nature *422*, 766-774.

Ng,J. (2012). Wnt/PCP proteins regulate stereotyped axon branch extension in Drosophila. Development *139*, 165-177.

Nishimura,T., Kato,K., Yamaguchi,T., Fukata,Y., Ohno,S., and Kaibuchi,K. (2004). Role of the PAR-3-KIF3 complex in the establishment of neuronal polarity. Nat. Cell Biol. *6*, 328-334.

O'Brien,R.J., Lau,L.F., and Huganir,R.L. (1998). Molecular mechanisms of glutamate receptor clustering at excitatory synapses. Curr. Opin. Neurobiol. *8*, 364-369.

Okuda,H., Miyata,S., Mori,Y., and Tohyama,M. (2007). Mouse Prickle1 and Prickle2 are expressed in postmitotic neurons and promote neurite outgrowth. FEBS Lett. *581*, 4754-4760.

Park,H.W., Boduluri,S.R., Moomaw,J.F., Casey,P.J., and Beese,L.S. (1997). Crystal structure of protein farnesyltransferase at 2.25 angstrom resolution. Science *275*, 1800-1804.

Park,M., and Moon,R.T. (2002). The planar cell-polarity gene stbm regulates cell behaviour and cell fate in vertebrate embryos. Nat. Cell Biol. *4*, 20-25.

Qadota,H., Inoue,M., Hikita,T., Koppen,M., Hardin,J.D., Amano,M., Moerman,D.G., and Kaibuchi,K. (2007). Establishment of a tissue-specific RNAi system in C. elegans. Gene *400*, 166-173.

Quinn,C.C., Pfeil,D.S., Chen,E., Stovall,E.L., Harden,M.V., Gavin,M.K., Forrester,W.C., Ryder,E.F., Soto,M.C., and Wadsworth,W.G. (2006). UNC-6/netrin and SLT-1/slit guidance cues orient axon outgrowth mediated by MIG-10/RIAM/lamellipodin. Curr. Biol. *16*, 845-853.

Quinn,C.C., Pfeil,D.S., and Wadsworth,W.G. (2008). CED-10/Rac1 mediates axon guidance by regulating the asymmetric distribution of MIG-10/lamellipodin. Curr. Biol. *18*, 808-813.

Rawls,A.S., and Wolff,T. (2003). Strabismus requires Flamingo and Prickle function to regulate tissue polarity in the Drosophila eye. Development *130*, 1877-1887.

Rodriguez-Viciana,P., Warne,P.H., Dhand,R., Vanhaesebroeck,B., Gout,I., Fry,M.J., Waterfield,M.D., and Downward,J. (1994). Phosphatidylinositol-3-OH kinase as a direct target of Ras. Nature *370*, 527-532.

Rohrschneider,M.R., Elsen,G.E., and Prince,V.E. (2007). Zebrafish Hoxb1a regulates multiple downstream genes including prickle1b. Dev. Biol. *309*, 358-372.

Roy,P.J., Stuart,J.M., Lund,J., and Kim,S.K. (2002). Chromosomal clustering of muscle-expressed genes in Caenorhabditis elegans. Nature *418*, 975-979.

Saburi,S., and McNeill,H. (2005). Organising cells into tissues: new roles for cell adhesion molecules in planar cell polarity. Curr. Opin. Cell Biol. *17*, 482-488.

Sanchez-Alvarez,L., Visanuvimol,J., McEwan,A., Su,A., Imai,J.H., and Colavita,A. (2011). VANG-1 and PRKL-1 cooperate to negatively regulate neurite formation in Caenorhabditis elegans. PLoS. Genet. *7*, e1002257.

Sarin,S., Prabhu,S., O'Meara,M.M., Pe'er,I., and Hobert,O. (2008). Caenorhabditis elegans mutant allele identification by whole-genome sequencing. Nat. Methods *5*, 865-867.

Schafer,W.F. (2006). Genetics of egg-laying in worms. Annu. Rev. Genet. *40*, 487-509.

Schafer,W.R. (2005). Egg-laying. WormBook. 1-7.

Schwarz-Romond,T., Merrifield,C., Nichols,B.J., and Bienz,M. (2005). The Wnt signalling effector Dishevelled forms dynamic protein assemblies rather than stable associations with cytoplasmic vesicles. J. Cell Sci. *118*, 5269-5277.

Seifert,J.R., and Mlodzik,M. (2007). Frizzled/PCP signalling: a conserved mechanism regulating cell polarity and directed motility. Nat. Rev. Genet. *8*, 126-138.

Selvin,P.R. (2000). The renaissance of fluorescence resonance energy transfer. Nat. Struct. Biol. *7*, 730-734.

Sharma-Kishore,R., White,J.G., Southgate,E., and Podbilewicz,B. (1999). Formation of the vulva in Caenorhabditis elegans: a paradigm for organogenesis. Development *126*, 691-699.

Sheldahl,L.C., Slusarski,D.C., Pandur,P., Miller,J.R., Kuhl,M., and Moon,R.T. (2003). Dishevelled activates Ca2+ flux, PKC, and CamKII in vertebrate embryos. J. Cell Biol. *161*, 769-777.

Shelly,M., Cancedda,L., Heilshorn,S., Sumbre,G., and Poo,M.M. (2007). LKB1/STRAD promotes axon initiation during neuronal polarization. Cell *129*, 565-577.

Shelly,M., and Poo,M.M. (2011). Role of LKB1-SAD/MARK pathway in neuronal polarization. Dev. Neurobiol. *71*, 508-527.

Sherwood,D.R., and Sternberg,P.W. (2003). Anchor cell invasion into the vulval epithelium in C. elegans. Dev. Cell *5*, 21-31.

Shi,S.H., Jan,L.Y., and Jan,Y.N. (2003). Hippocampal neuronal polarity specified by spatially localized mPar3/mPar6 and PI 3-kinase activity. Cell *112*, 63-75.

Shimada,Y., Usui,T., Yanagawa,S., Takeichi,M., and Uemura,T. (2001). Asymmetric colocalization of Flamingo, a seven-pass transmembrane cadherin, and Dishevelled in planar cell polarization. Curr. Biol. *11*, 859-863.

Shyu,Y.J., Hiatt,S.M., Duren,H.M., Ellis,R.E., Kerppola,T.K., and Hu,C.D. (2008a). Visualization of protein interactions in living Caenorhabditis elegans using bimolecular fluorescence complementation analysis. Nat. Protoc. *3*, 588-596.

Shyu,Y.J., Suarez,C.D., and Hu,C.D. (2008b). Visualization of AP-1 NF-kappaB ternary complexes in living cells by using a BiFC-based FRET. Proc. Natl. Acad. Sci. U. S. A *105*, 151-156.

Simons,M., and Mlodzik,M. (2008). Planar cell polarity signaling: from fly development to human disease. Annu. Rev. Genet. *42*, 517-540.

Song,S., Zhang,B., Sun,H., Li,X., Xiang,Y., Liu,Z., Huang,X., and Ding,M. (2010). A Wnt-Frz/Ror-Dsh pathway regulates neurite outgrowth in Caenorhabditis elegans. PLoS. Genet. *6*.

Steimel,A., Wong,L., Najarro,E.H., Ackley,B.D., Garriga,G., and Hutter,H. (2010). The Flamingo ortholog FMI-1 controls pioneer-dependent navigation of follower axons in C. elegans. Development *137*, 3663-3673.

Steinert,P.M., and Roop,D.R. (1988). Molecular and cellular biology of intermediate filaments. Annu. Rev. Biochem. *57*, 593-625.

Strutt,D., and Strutt,H. (2007). Differential activities of the core planar polarity proteins during Drosophila wing patterning. Dev. Biol. *302*, 181-194.

Strutt,D.I. (2001). Asymmetric localization of frizzled and the establishment of cell polarity in the Drosophila wing. Mol. Cell *7*, 367-375.

Strutt,D.I. (2002). The asymmetric subcellular localisation of components of the planar polarity pathway. Semin. Cell Dev. Biol. *13*, 225-231.

Strutt,H., and Strutt,D. (2009). Asymmetric localisation of planar polarity proteins: Mechanisms and consequences. Semin. Cell Dev. Biol. *20*, 957-963.

Sulston,J., Dew,M., and Brenner,S. (1975). Dopaminergic neurons in the nematode Caenorhabditis elegans. J. Comp Neurol. *163*, 215-226.

Sulston,J.E., and Brenner,S. (1974). The DNA of Caenorhabditis elegans. Genetics *77*, 95-104.

Sulston,J.E., and Horvitz,H.R. (1977). Post-embryonic cell lineages of the nematode, Caenorhabditis elegans. Dev. Biol. *56*, 110-156.

Sulston,J.E., and White,J.G. (1980). Regulation and cell autonomy during postembryonic development of Caenorhabditis elegans. Dev. Biol. *78*, 577-597.

Sweede,M., Ankem,G., Chutvirasakul,B., Azurmendi,H.F., Chbeir,S., Watkins,J., Helm,R.F., Finkielstein,C.V., and Capelluto,D.G. (2008). Structural and membrane binding properties of the prickle PET domain. Biochemistry *47*, 13524-13536.

Szu-Yu,H.T., and Rasband,M.N. (2011). Maintenance of neuronal polarity. Dev. Neurobiol. *71*, 474-482.

Tahirovic,S., and Bradke,F. (2009). Neuronal polarity. Cold Spring Harb. Perspect. Biol. *1*, a001644.

Takayama,J., Faumont,S., Kunitomo,H., Lockery,S.R., and Iino,Y. (2010). Single-cell transcriptional analysis of taste sensory neuron pair in Caenorhabditis elegans. Nucleic Acids Res. *38*, 131-142.

Theisen,H., Purcell,J., Bennett,M., Kansagara,D., Syed,A., and Marsh,J.L. (1994). dishevelled is required during wingless signaling to establish both cell polarity and cell identity. Development *120*, 347-360.

Thomas,J.H., Stern,M.J., and Horvitz,H.R. (1990). Cell interactions coordinate the development of the C. elegans egg-laying system. Cell *62*, 1041-1052.

Thomas,S.M., and Brugge,J.S. (1997). Cellular functions regulated by Src family kinases. Annu. Rev. Cell Dev. Biol. *13*, 513-609.

Tissir,F., and Goffinet,A.M. (2006). Expression of planar cell polarity genes during development of the mouse CNS. Eur. J. Neurosci. *23*, 597-607.

Torban,E., Patenaude,A.M., Leclerc,S., Rakowiecki,S., Gauthier,S., Andelfinger,G., Epstein,D.J., and Gros,P. (2008). Genetic interaction between members of the Vangl family causes neural tube defects in mice. Proc. Natl. Acad. Sci. U. S. A *105*, 3449-3454.

Uemura,T., and Shimada,Y. (2003). Breaking cellular symmetry along planar axes in Drosophila and vertebrates. J. Biochem. (Tokyo) *134*, 625-630.

Usui,T., Shima,Y., Shimada,Y., Hirano,S., Burgess,R.W., Schwarz,T.L., Takeichi,M., and Uemura,T. (1999). Flamingo, a seven-pass transmembrane cadherin, regulates planar cell polarity under the control of Frizzled. Cell *98*, 585-595.

van der Wouden,J.M., Maier,O., van Ijzendoorn,S.C., and Hoekstra,D. (2003). Membrane dynamics and the regulation of epithelial cell polarity. Int. Rev. Cytol. *226*, 127-164.

Veeman,M.T., Slusarski,D.C., Kaykas,A., Louie,S.H., and Moon,R.T. (2003). Zebrafish prickle, a modulator of noncanonical Wnt/Fz signaling, regulates gastrulation movements. Curr. Biol. *13*, 680-685.

Vinson,C.R., Conover,S., and Adler,P.N. (1989). A Drosophila tissue polarity locus encodes a protein containing seven potential transmembrane domains. Nature *338*, 263-264.

Vladar,E.K., Antic,D., and Axelrod,J.D. (2009). Planar cell polarity signaling: the developing cell's compass. Cold Spring Harb. Perspect. Biol. *1*, a002964.

Waggoner,L.E., Zhou,G.T., Schafer,R.W., and Schafer,W.R. (1998). Control of alternative behavioral states by serotonin in Caenorhabditis elegans. Neuron *21*, 203-214.

Wallingford,J.B., Fraser,S.E., and Harland,R.M. (2002). Convergent extension: the molecular control of polarized cell movement during embryonic development. Dev. Cell *2*, 695-706.

Wallingford,J.B., and Habas,R. (2005). The developmental biology of Dishevelled: an enigmatic protein governing cell fate and cell polarity. Development *132*, 4421-4436.

Wallingford,J.B., and Harland,R.M. (2001). Xenopus Dishevelled signaling regulates both neural and mesodermal convergent extension: parallel forces elongating the body axis. Development *128*, 2581-2592.

Wallingford,J.B., Rowning,B.A., Vogeli,K.M., Rothbacher,U., Fraser,S.E., and Harland,R.M. (2000). Dishevelled controls cell polarity during Xenopus gastrulation. Nature *405*, 81-85.

Wang,J., Hamblet,N.S., Mark,S., Dickinson,M.E., Brinkman,B.C., Segil,N., Fraser,S.E., Chen,P., Wallingford,J.B., and Wynshaw-Boris,A. (2006a). Dishevelled genes mediate a conserved mammalian PCP pathway to regulate convergent extension during neurulation. Development *133*, 1767-1778.

Wang,J., and Wynshaw-Boris,A. (2004). The canonical Wnt pathway in early mammalian embryogenesis and stem cell maintenance/differentiation. Curr. Opin. Genet. Dev. *14*, 533-539.

Wang,Y., Guo,N., and Nathans,J. (2006b). The role of Frizzled3 and Frizzled6 in neural tube closure and in the planar polarity of inner-ear sensory hair cells. J. Neurosci. *26*, 2147-2156.

Wang,Y., and Nathans,J. (2007). Tissue/planar cell polarity in vertebrates: new insights and new questions. Development *134*, 647-658.

Weiner,J. (2012). Time, Love, Memory. A Great Biologist and his Quest for the Origins of Behaviors Vintage).

Westbury,D.R. (1982). A comparison of the structures of alpha and gamma-spinal motoneurones of the cat. J. Physiol *325*, 79-91.

White,J.G., Southgate,E., Thompson,J.N., and Brenner,S. (1986). The Structure of the Nervous System of the Nematode Caenorhabditis elegans. Philos Trans R Soc Lond B Biol Sci. *314*, 1-340.

Wicks,S.R., Yeh,R.T., Gish,W.R., Waterston,R.H., and Plasterk,R.H. (2001). Rapid gene mapping in Caenorhabditis elegans using a high density polymorphism map. Nat. Genet. *28*, 160-164.

Wiggin,G.R., Fawcett,J.P., and Pawson,T. (2005). Polarity proteins in axon specification and synaptogenesis. Dev. Cell *8*, 803-816.

Wightman,B., Baran,R., and Garriga,G. (1997). Genes that guide growth cones along the C. elegans ventral nerve cord. Development *124*, 2571-2580.

Wightman,B., Clark,S.G., Taskar,A.M., Forrester,W.C., Maricq,A.V., Bargmann,C.I., and Garriga,G. (1996). The C. elegans gene vab-8 guides posteriorly directed axon outgrowth and cell migration. Development *122*, 671-682.

Wu,J., Klein,T.J., and Mlodzik,M. (2004). Subcellular localization of frizzled receptors, mediated by their cytoplasmic tails, regulates signaling pathway specificity. PLoS. Biol. *2*, E158.

Wu,J., and Mlodzik,M. (2009). A quest for the mechanism regulating global planar cell polarity of tissues. Trends Cell Biol. *19*, 295-305.

Yanik,M.F., Cinar,H., Cinar,H.N., Chisholm,A.D., Jin,Y., and Ben-Yakar,A. (2004). Neurosurgery: functional regeneration after laser axotomy. Nature *432*, 822.

Yin,C., Kiskowski,M., Pouille,P.A., Farge,E., and Solnica-Krezel,L. (2008). Cooperation of polarized cell intercalations drives convergence and extension of presomitic mesoderm during zebrafish gastrulation. J. Cell Biol. *180*, 221-232.

Yook,K. (2005). Complementation. WormBook. 1-17.

Yoshimura,T., Arimura,N., and Kaibuchi,K. (2006). Molecular mechanisms of axon specification and neuronal disorders. Ann. N. Y. Acad. Sci. *1086*, 116-125.

Yoshimura,T., Kawano,Y., Arimura,N., Kawabata,S., Kikuchi,A., and Kaibuchi,K. (2005). GSK-3beta regulates phosphorylation of CRMP-2 and neuronal polarity. Cell *120*, 137-149.

Zahler,A.M. (2005). Alternative splicing in C. elegans. WormBook. 1-13.

Zhang,F.L., and Casey,P.J. (1996). Protein prenylation: molecular mechanisms and functional consequences. Annu. Rev. Biochem. *65*, 241-269.

Zhang,X., Zhu,J., Yang,G.Y., Wang,Q.J., Qian,L., Chen,Y.M., Chen,F., Tao,Y., Hu,H.S., Wang,T., and Luo,Z.G. (2007). Dishevelled promotes axon differentiation by regulating atypical protein kinase C. Nat. Cell Biol. *9*, 743-754.